Technische Universität München

TUM School of Engineering and Design

Cell-cell interaction in a synthetic co-culture: PHA production from sunlight and CO_2 co-cultivating *Synechococcus elongatus* and *Pseudomonas putida*

Franziska Pia Kratzl

Vollständiger Abdruck der von der TUM School of Engineering and Design der Technischen Universität München zur Erlangung einer

Doktorin der Ingenieurwissenschaften (Dr.-Ing.)

genehmigten Dissertation.

Vorsitz:	Prof. Dr. rer. nat. Sonja Berensmeier
Prüfende der Dissertation:	1. Prof. Dr.-Ing. Andreas Kremling
	2. Prof. Dr. Karl Forchhammer
	3. Dr. Daniel Volke, Ph.D.

Die Dissertation wurde am 13.09.2023 bei der Technischen Universität München eingereicht und durch die TUM School of Engineering and Design am 22.11.2023 angenommen.

Abstract

In laboratories, microbes are primarily cultured as single species, so-called axenic cultures, due to their easier controllability and handling. However, in nature, microbes rarely exist in isolation; instead, they thrive in consortia where diverse interactions occur. The combination of the positive aspects of axenic cultures and the potential synergistic effects of complex communities can be merged into defined (synthetic) co-cultures. In times of a rising atmospheric CO_2 concentration, a special co-culture brings together carbon-fixing bacteria with those that enhance the metabolic capacity of the co-culture. Therefore, this thesis investigates a synthetic co-culture of the cyanobacterium *Synechococcus elongatus* PCC 7942 *cscB*, which feeds a heterotrophic derivative of *Pseudomonas putida* KT2440 with sucrose.

First, a systematic screening of both existing and one newly designed heterotrophic co-culture partner was conducted to evaluate medium chain length polyhydroxyalkanoate (mcl-PHA) productivity. Mcl-PHA is a biodegradable bioplastic and holds promise to substitute petroleum-based polyesters. Carrying the operon *cscRABY* enabled not only higher metabolic activity towards sucrose in the axenic culture of *P. putida*, as previously described, but also in the co-culture at a 1.8 L scale. The process resulted in a 1.7-fold increase of PHA accumulation in the co-culture. Furthermore, by employing the *P. putida cscRABY* Δ*nasT* derivative, which is incapable of metabolizing nitrate for growth, a complete separation of the nitrogen sources between the co-culture partners could be achieved. The nitrogen separation enabled precise and individual control over the growth rates. Further, it facilitated the calculation and adjustment of the $\frac{C}{N}$-ratio, a key value for PHA accumulation, to the optimal ratio of 26. Ultimately, a maximum PHA titer of 393 mg L^{-1} was accumulated, representing the physiological maximum of PHA accumulation per cell in *P. putida* KT2440. Finally, experiments underlined that sucrose uptake through the *cscRABY* operon bypasses the glucose oxidation in the periplasm in *P. putida*. This conclusion was drawn by utilizing the *P. putida* Δ*gcd* derivative equipped with the sucrose operon. In comparison to *P. putida cscRABY*, no further increase in PHA accumulation could be observed.

Next, potential feedback or interaction between *S. elongatus cscB* and *P. putida cscRABY* were investigated. A remarkable growth-promoting effect brought about by the presence of the heterotrophic partner on the cyanobacterium was observed, leading to a growth rate increase of up to 80% (compared to the induced strain) and increased photosynthetic capacity. After detailed characterization of the effect on the physiological growth, the co-culture was investigated on a transcriptional, proteomic and metabolomic level. This multi-OMICs approach revealed several moderate changes, including alterations in the metabolism, transportation, and stress response in both microbes, indicating multi-level interactions. In particular, the up-regulation of transport processes for amino acids and degradation of aromatic compounds in *P. putida cscRABY* suggests the exchange of molecules between the partners. The present study brings the controllability of the co-culture process at a 1.8 L scale to the next level and provides an advanced understanding of the versatile interaction between the co-culture partners.

Zusammenfassung

In Laboratorien werden Mikroorganismen in erster Linie als Kulturen von einzelnen Spezien, so genannte axenische Kulturen, untersucht, da diese methodisch leichter zu handhaben sind. Wirft man jedoch einen Blick in die natürlich Umgebung von Mikroorganismen, existieren diese nur selten isoliert, stattdessen gedeihen sie besonders in Konsortien und Co-Kulturen, in denen vielseitige Interaktionen stattfinden können. Die positiven Aspekte von axenischen Kulturen können mit denen aus komplexen Konsortien verbunden werden, zum Beispiel in sogenannten definierten (synthetischen) Co-Kulturen. In Zeiten steigender CO_2-Konzentration in unserer Atmosphäre bekommen spezielle Co-Kulturen besonders viel Aufmerksamkeit. Diese Co-Kulturen verbinden kohlenstofffixierende Bakterien mit solchen, die die Stoffwechselkapazität von Co-Kultur erhöhen. Daher wird in dieser Arbeit eine synthetische Co-Kultur bestehend aus dem Cyanobakterium *Synechococcus elongatus* PCC 7942 *cscB* und verschiedenen Derivaten von *P. putida* untersucht. Das Cyanobakterium stellt dabei die Kohlenstoffquelle Saccharose für den genetisch modifizierten Partner zur Verfügung.
Zunächst wurde eine systematische Untersuchung von sowohl bestehenden als auch von einem neu entwickelten heterotrophen Co-Kulturpartner durchgeführt. Ziel war die Akkumulierung von Polyhydroxyalkanoat mit mittlerer Kettenlänge (mcl-PHA) zu bewerten. PHA ist ein biologisch abbaubarer Biokunststoff, der als vielversprechenden Ersatz für erdölbasierte Polyester in Frage kommt. Die genomische Integration des Operons *cscRABY* ermöglichte nicht nur eine höhere Stoffwechselaktivität mit Saccharose in der axenischen Kultur von *P. putida*, sondern erhöhte auch das heterotrophe Wachstum in der Co-Kultur im Maßstab von 1,8 L. Dies führte letzendlich zu einem Anstieg der PHA-Akkumulation um das 1,7-fache. Darüber hinaus konnte durch den Einsatz von *P. putida cscRABY* Δ*nasT*, welcher Nitrat nicht mehr verstoffwechseln kann, eine vollständige Trennung der Stickstoffquellen zwischen den Co-Kulturpartnern erreicht werden. Dies ermöglichte eine präzise und individuelle Kontrolle der Wachstumsraten. Weiter erleichterte dies die Berechnung, sowie die Einstellung des Kohlenstoff-zu-Stickstoff $\frac{C}{N}$-Verhältnisses, ein Schlüsselwert für die PHA-Akkumulation. Das $\frac{C}{N}$-Verhältnis konnte auf den in der Literatur beschriebenen optimalen Wert von 26 eingestellt werden, was einen maximalen PHA-Titer von 393 mg L^{-1} ermöglichte. Dies stellt bereits das physiologische Maximum der PHA-Anreicherung in *P. putida* dar. Weiter konnten Hinweise gefunden werden, dass die Aufnahme von Saccharose durch das *cscRABY*-Operon die Glukoseoxidation im Periplasma von *P. putida* umgeht. Dies konnte mit dem *P. putida* Δ*gcd*-Derivat nachgewiesen werden, das im Vergleich zu *P. putida cscRABY* keine Steigerung der PHA Akkumulation aufwies.
Weitergehend wurden mögliche Interaktionen zwischen *S. elongatus cscB* und *P. putida cscRABY* untersucht. In der Anwesenheit des heterotrophen Partners konnte ein bemerkenswerter wachstumsfördernder Effekt beobachtet werden. Dieser Effekt manifestierte sich in einer Steigung der Wachstumsrate um bis zu 80 % im Vergleich zum induzierten *S. elongatus* cscB, sowie in einer erhöhten Photosynthesekapazität. Aufgrund dieser phänomeologischen Beobachtung wurde die Co-Kultur anschließend auf Transkript-, Protein- und Metabolit-Ebene untersucht. Dieser Multi-OMIC-Ansatz zeigte viele moderate Unterschiede auf, welche Veränderungen im Stoffwechsel, im Transport, und in der Stressantwort beider Mikroorganismen beinhaltete. Die transkriptionelle Hochregulierung von Transportprozessen, insbesondere für Aminosäuren, und der Abbau von aromatischen Verbindungen in *P. putida cscRABY*, deutet auf den Austausch von Komponenten

zwischen den Partnern hin.

Die vorgestellte Arbeit überschreitet die bisher erreichte Kontrollierbarkeit in den Co-Kulturprozesses im 1,8-Liter-Maßstab und ermöglicht zusätzlich ein besseres Verständnis der vielseitigen Interaktion zwischen den Co-Kulturpartnern.

Acknowledgements

I would like to thank

- Andreas Kremling, for giving very good lectures were I learned a lot of new things and for offering me the PhD-position to work with the co-culture.
- All team members of SBT. I'll begin with Kathi, who introduced me to the topic and patiently answered numerous questions related to the co-culture. Whenever I needed assistance, she was just one Zoom call away. I also thank Hannes Löwe for patiently answer all my questions at the beginning of the project. I learned a lot from you. Alberto Marin-Sanguino, you have been an exceptional role model, showcasing unmatched passion for our work. Thank you for teaching Thi and me skiing in just one day! A special shout-out goes to Dieu Thi Doan, my "office" partner. Our quick breaks and stretching sessions in the office made lab work feel like a breeze. We spent joyful evenings at various locations with the other team members, and Thi's organizing skills always made it a success. Martina Cantone, your presence in the office during the challenging times of corona meant a lot. Our walks and ice cream breaks together with Ana were refreshing, and your advice on handling transcriptomic data was invaluable. I thank Ana-Sofia Ortega and Marleen Beentjes for being my lab partners! Your constant support in the lab, whether it was locating missing pipettes or ordering new lab supplies, was invaluable. You are both not only good biotechnologists but also really good team players. José García Lima, thank you for joining the group at the perfect time and rekindle my passion for biotech. We had many stimulating science related discussion but also talked a lot over current news or political stuff. You were so motivated that we set up a great practical course for the students. You will do great in your project. Further, I like to thank our new PhD student, Carina Meiners, for bringing fresh and intriguing perspectives into the group. Carina, along with Lucas Hermann and Luisa Klein, fit perfectly into the team, and I am really looking forward to their upcoming projects! I consider myself very fortunate to have found not only dedicated colleagues but also wonderful friends among SBT.
- Stefan Darchinger for always having my back when it came to shipping samples and sorting out all the behind-the-scenes stuff. I thank Lucia Abarca-Cabrera for being my lab partner on weekends! I also thank all STT members for hustling hard to make the lab work despite the crazy corona situation and all the restrictions possible. Those lab shifts weren't easy, but we made it work together!
- All team members of BVT. A special mention goes to Anton Rückel, Irina Schwarz, Ingmar Polte, and Anne Oppelt for their support. I thank Irina for being my "study" partner since our bachelor. I thank Ingmar Polte for never stopping to be my supervisor and who taught me the best phrase for live: Wir lernen ja noch. Anton, thanks for being the go-to person for

engineering questions and for those fun chats about games, anime and shows. I want to thank Anne for sparking my interest for gas fermentation. To everyone, thanks for the great discussions, working together through weekends, having holidays together (Irina!), bicycling tours, game nights and the great (emotional) support throughout the years.

- All the students I've had the privilege of teaching, who, in turn, have taught me so much. This incredible group includes Luisa Klein, Franz Zettl, Marlene Urban, Martin Biechl, Carina Eisebraun, Elias Bruss, Ivan Lizat, and Florian Hasenkopf. Our time together in the lab (or infront of the computer) has been an absolute blast, and your enthusiasm and drive have constantly motivated me to learn and explore new things.
- All cooperation partners. Science thrives on communication and asking challenging questions. I consider myself fortunate to have collaborated with exceptional researchers like Jagroop Pandhal and Mengxun Shi.
- The DFG Priority Program InterZell, which I had the privilege to be a part of. A heartfelt thank you goes out to every member of the group for the discussions and addressing the topic of imposter syndrome in science at different bars in Koblenz.
- The team around Andre Richter that provided the LaTeX template at GitHub on which this document is based on (https://github.com/TUM-LIS/tum-dissertation-latex).
- Anna Königer for consistently being an amazing friend to me and for always understanding my circumstances. Whether it was cooking, watching shows, skating, hiking, or any activity we did, we always had a great time together. Magdalena and Ludwig Kratzl for always having my back (e.g. with food or running) and being amazing siblings.
- Finally, I thank Simon Hollerith. Your passion for your research and dedication have been a constant source of inspiration for me. We truly had an amazing time so far and I am looking forward to what follows.

Contents

List of abbreviations

Table 1: The most important abbreviation used in this thesis.

Abbreviation	Specification
3-HA	3-hydroxyalkanoate (a PHA monomer)
Acetyl-CoA	Acetyl coenzyme A
AcoA	Pyruvate dehyrogenase subunit E1
ADP	Adenosine diphosphate
ATP	Adenosine triphosphate
***att*Tn7**	Attachement site for Tn7-transposon in *P. putida* KT2440
bp	Base pair
C	Carbon
CO_2	Carbon dioxide
CscA	Sucrose-6-phosphate hydrolase
CscB	Sucrose permease
CscR	Negative transcription regulator of *cscA*, *cscB* and *cscY*
CscY	Sucrose porin
DNA	Deoxyribonucleic acid
DIW	Deionized water
DEG	Differentially regulated gene
EDEMP cycle	Metabolic cycle combining activities of the EMP- and ED-pathwayy as well as the PP-pathway
ED Pathway	Entner-Doudoroff pathway
EMP Pathway	Embden-Meyerhof-Parnas pathway
EPS	Exopolysaccharides
FSC	Forward scatter
H^+	Proton
HILIC	Hydrophilic Interaction Liquid Chromatography
HPLC	High-Performance Liquid Chromatography
IPTG	Isopropylthio-β-galactoside
MS	Mass spectrometry
N	Nitrogen
NaCl	Sodium chloride
NADH	Reduced from of nicotinamide adenine dinucleotide
NADPH	Reduced from of nicotinamide adenine dinucleotide phosphate
PAR	Photosynthetically active ratioation
PCR	Polymerase chain reaction
PFD	Photon flux density
PHAs	Polyhydroxyalkanoates
PHBs	Polyhydroxybutyrates
PhaZ	PHA depolymerase
PP	Pentose phosphate pathway
RNA	Ribonucleic acid
ROS	Reactive oxidative species
RP	Reverse phase chromatography
SEVA	Standard European Vector Architecture
TCA	Tricarboxylic acid cycle
QC	Quality control

Symbols

Table 2: The most important symbols used in this thesis.

Abbreviation	Specification	Dimensions
$\frac{C}{N}$-ratio	Carbon to nitrogen ratio	-
r_{mol_C}	Molar carbon uptake rate	mol · h $^{-1}$
r_{mol_X}	Molar nutrient uptake rate	mol · h $^{-1}$
r_{mol_N}	Molar nitrogen uptake rate	mol · h $^{-1}$
μ	Growth rate	h^{-1}
μ_{max}	Maximal growth rate	h^{-1}
C_S	Substrate concentration	g · L^{-1}
C_{suc}	Sucrose concentration	g · L^{-1}
C_X	Biomass concentration	g · L^{-1}
C_{Xcdw}	Biomass - cell dry weight	g · L^{-1}
$Y_{C_{xsuc}}$	Biomass yield for sucrose as carbon source	-
E_{Photon}	Energy of one photon	J
λ	Wavelength	nm
λ_{max}	Maximum wavelength	nm
λ_{min}	Minimum wavelength	nm
$p-value$	p-value	-
$log_2(FC)$	Logarithmic fold change between a case and a control	
$OD_{wavelength}$	Optical density of the sample at a given wavelength	-
t	Time	s, min, h, d
T	Temperature	℃
V_R	Reactor volume	L
V_S	Sample volume	µL or mL
(v/v)	Volume percent	%
(w/v)	Weight percent	%
Constants		
N_A	Avogadro constant	6.022 ·10^{23} mol $^{-1}$
c	Speed of light	2.99 · 10^8 m·s^{-1}
h	Boltzmann constant	1.38 · 10^{23} J· K^{-1}

1 Introduction

Antonie van Leeuwenhoek revealed the world of microorganisms in the 17th century, terming the small inhabitants *"animalcules"* and changed together with fellow scientists such as Robert Hook the view on the world through microscopy [1]. Since then, our understanding of microbes and their impact on human health as well as our environment has drastically evolved. Building upon the microscope invention, Robert Koch developed methods to better distinguish cells and bacteria by using dyes and different fixation techniques, and he was the first to connect certain diseases to the causing microbe, launching the field of (medical) bacteriology. Koch also strongly influenced today's standard cultivation techniques of pure bacterial cultures by studying, among others, the pathogen *Mycobacterium tuberculosis* responsible for the tuberculosis disease. In his postulates, he manifested how to connect a microbe with a disease, which included isolating bacterial species to investigate them separately and deduce their potential pathogenicity [2], [3], [4].
Today we have conscience control over microbes and their components, such as enzymes, allowing us to manipulate microbial behavior and traits. Even the step out of the laboratory scale towards targeted processes and defined applications is possible. A beautiful example of red biotechnology is the recombinant human insulin production in the model organism *Eschericha coli*. With estimated 510.8 million people suffering from diabetes type II in 2030, further optimizing production routes and application forms are ongoing and essential tasks [5], [6], [7]. Several milestones had to be met in multidisciplinary research to come this far. First, it was necessary to decipher the multiple tasks cell components, such as deoxyribonucleic acid (DNA), ribonucleic acid (RNA), and proteins, have. In 1928, Griffith's experiment showed that bacterial cells can exchange genetic information and, with it, certain characteristics. The three-dimensional structure of DNA was solved in 1953 [8]. However, it should take several more decades until the DNA sequence can be read. The *Dogma of molecular biology*, which states that the genetic information is directed from DNA over mRNA to proteins unilateral by Francis Crick [9], was another breakthrough in understanding living matter. In 1977, Sanger et al. developed one of the first techniques to decipher DNA sequence, today called first-generation DNA-sequencing [10]. Sequencing technologies further received a significant boost through the human genome project launched in 1990 and finalized by 2003 [11]. Another indispensable technique in (molecular) biology is the polymerase chain reaction (PCR), which allows for amplifying any DNA fragment wanted and was introduced in the 1980s [12]. All these discoveries and many more revolutionized the efficiency of studying microbes and how we can employ them in biotechnology. With increasing computational power, mathematical models for describing microbes e.g. by reconstructing the (nearly) whole metabolism can be solved in seconds through linear optimization programming. Further, handling high-throughput data for example of Omics experiments with millions of sequence reads or thousand of protein counts became much easier and less time-consuming. Additionally, predicting protein folds from the amino acid sequence has

become easier than ever before thanks to the tool AlphaFold, enabling faster and more accurate predictions [13], [14]. Nowadays, the digital transformation of the lab is a hot topic, with the buzzword laboratory 4.0 derived from industry. Here, automatization of operations and digital processing of all data, at best in real-time, should be achieved [15], [16].

We all have witnessed the most recent and outstanding example of how scientific progress can change our lives. The handling of the COVID-19 pandemic caused by the virus SARS-Cov-2. Through the outstanding cooperation of different pharmaceutical companies, supported by multiple governments and organizations, a safe and effective vaccine was produced in less than a year. Notably, the Pfizer–BioNTech COVID-19 vaccine was the first ever authorized mRNA-based vaccine [17]. The scientific success achieved in battling the COVID-19 pandemic should serve as an inspiration for another pressing one: The human-caused climate change. CO_2 concentrations are steadily rising and reached a global average of 417 ppm in 2022 [18]. To put this number into context: The CO_2 concentration in the atmosphere as Robert Koch was working on the tuberculosis pathogen in 1884 was 293 ppm! With the wold's commitment to limit the temperature rise to 1.5 °C, we should act now (The Paris Agreement, 2015 [19]). To tackle this problem, advanced CO_2 fixing technologies and serious efforts to reduce CO_2-emissions and other greenhouse gases are needed. Pathways for CO_2 fixation are intensely studied in organisms naturally performing photosynthesis, such as algae and cyanobacteria, as well as artificially, for example with the Crotonyl-(CoA)/ethylmalonyl-CoA/ hydroxybutyryl-CoA (CETCH)-cycle [20].

Another problem of the modern world is the steadily increasing plastic pollution. Due to slow degradation or even non-degradability in the environment, plastic accumulates everywhere, including in the gastrointestinal system of animals and eventually in our food chain. Over the years, awareness and political actions have risen, but we still need to cope with plastics already accumulated in nature. Researchers are studying various microbes, such as the fungi *Aspergillus nidulans* [21] or insects that can naturally metabolize plastics[1]. As a new subclass of hydrolases, the PETases are a group of enzymes that can degrade polyethylene terephthalate (PET), which is among the materials most used as containers for drinks and food [21], [22]. Finding enzymes naturally able to degrade plastic can build the base for enzyme engineering to increase their substrate spectrum or activity. In some cases, the release of very small plastic particles, so-called micro-plastics, is unpreventable, for instance, the abrasion of car wheels in everyday usage. In these cases, biodegradable plastics could step in, which are plastics that allow complete microbial digestion. The global annual production of entirely bio-based plastics is approx. 2 million tonnes, with a share of two-thirds being biodegradable polymers [23]. Many microbes can produce polymers that can fulfill the properties of traditional petroleum-based plastics. One example are polyhydroxyalkanoates, a broad group of polyesters with different physical and chemical properties.

To unlock new microbial products, for example, new polyesters, a shift in traditional one-species cultivation introduced by Robert Koch and colleagues towards controllable co-cultures consisting of two or more species has been started. Today we know that microbes rarely exist as isolated species, and they seem to thrive the most in partnerships with others. Consequentially, the next step is to investigate co-cultures and manipulate them to our desire. That is only possible through the great achievements and solid groundwork of the mothers and fathers of biotechnology.

[1] (Company Beworm, https://www.beworm.org/)

Motivation

A light-driven synthetic co-culture was designed, in which the modified cyanobacterium *Synechococcus elongatus* PCC 7942 *cscB* provides the feedstock for the heterotrophic partner, a genetically engineered derivative of the gram-negative *Pseudomonas putida* EM178 [24], [25]. In the presence of elevated salt concentration, *S. elongatus* naturally converts a part of the photosynthetically fixed CO_2 into sucrose, which serves as a compatible solute. By the action of the heterologously expressed CscB sucrose permease originated from *E. coli* EDL933, sucrose is secreted into the culture supernatant. Here, it serves as sole carbon source for *P. putida* derivatives to generate biomass and potential production of targeted compounds. As *P. putida* is naturally unable to metabolize sucrose, it was genetically modified to enable sucrose uptake and subsequent metabolization. Thus, Löwe et al. generated a *P. putida* variant able to grow on sucrose caring the *cscAB* gene randomly integrated into the genome and derived from *E. coli* W [26]. The resulting *P. putida* strain was used to set up the a co-culture with *S. elongatus cscB* [25]. The cyanobacterium was able to support the heterotrophic growth in the co-culture over 2-3 weeks. As a proof of concept, nitrate limitation was applied to the co-culture, which naturally induces the accumulation of the biopolymer medium-chain-length (mcl) polyhydroxyalkanoate (PHA) in pseudomonads. The maximal achieved PHA-titer was 0.15 g L^{-1} with a production rate of 23 mg L^{-1} d^{-1} in a co-cultivation process at a scale of 1.8 L [25]. However, the heterotrophic partner showed fluctuating growth behavior, which was reflected by high standard deviations of *P. putida cscAB's* cell count. Additionally, the produced PHA was metabolized from the heterotrophic partner at the end of the process. Considering that the growth rate of *P. putida cscAB* reached only 50% of the maximum growth rate compared to growth on a glucose/fructose mixture, it was concluded that the heterotrophic partner deals with insufficient sucrose uptake. Therefore, a newly identified sucrose gene cluster *cscRABY* from *Pseudomonas protegens* Pf-5, a close relative of the used strain, was genomically integrated into *P. putida* EM178 leading to a very potent sucrose metabolizing strain [27].

The newly designed *P. putida cscRABY* derivative should be used to improve the co-cultivation process in terms of controllability and efficiently producing the bioplastic mcl-PHA. PHA is accumulated in unbalanced nutrient conditions. The best results for pseudomonads growing on PHA structurally non-similar substrates are achieved in a state of carbon excess combined with a limitation of essential nutrients, for example, nitrogen or sulfur [28]. For *P. putida* KT2440, a nitrogen limitation with an optimal carbon-to-nitrogen ratio of 26 was described in literature [29]. Therefore, the optimal $\frac{C}{N}$-ratio ratio should be implemented in the co-culture process to increase PHA accumulation. To adjust and control the nitrogen supply for the heterotrophic partner, a separation of the nitrogen source of the co-culture partners should be investigated by using a second derivative *P. putida cscRABY* Δ*nasT* in co-culture processes [30]. This *P. putida* derivative is unable to metabolize nitrate due to the deletion of the *nasT* gene, a part of the two-component response regulator NasT/NasS for recognizing nitrate.

Microbial interactions in co-cultures are omnipresent, and especially the connection between phototrophic and heterotrophic organisms is widespread in nature [31]. Cyanobacteria are handled as potential substitutes for traditional feedstocks due to their carbohydrate accumulation ability. As they fix atmospheric CO_2 in photosynthesis and can be cultured in ponds at or on the ocean, cyanobacteria additionally offer less conflict with arable land. Natural communities of microbes are highly complex and have multi-layered interaction, which can be reduced by employing only hand-picked partner organisms in defined (synthetic)

co-cultures, as the one investigated in this thesis. Thus, sucrose-secreting cyanobacteria, such as *S. elongatus cscB* are connected to heterotrophs with high metabolic production capacities. Different co-cultures of *S. elongatus cscB* with heterotrophic bacteria and yeast indicate versatile forms of interaction besides the synthetic interaction over the sucrose feed [32]. For instance, *Escherichia coli* showed a positive effect on the growth of the phototrophic partner, but *Bacillus subtilis* was negatively affected when co-cultivated with *S. elongatus cscB* through the production of reactive oxidative species (ROS) [32]. Thus, potential interaction or feedback between the two co-culture partners *S. elongatus cscB* and *P. putida cscRABY* should be investigated. For this, the co-culture should be compared to the respective axenic cultures in terms of growth and sucrose secretion in different scales and conditions. On the one hand, the growth should be investigated on a phenomenological level, including the lag phase, exponential growth (growth rate), and behavior in the stationary phase, which correlates with the stability of the culture. On the other hand, as not all interactions have a direct impact on the growth behavior, the co-culture should be compared to the axenic cultures on a transcriptional, proteomic, and metabolomic level. For example, it was found that relief of oxidative stress and increase in CO_2 availability for the cyanobacterium is present in the co-culture with 3-hydroxypropionic acid (3-HP) producing *E. coli* ABKm [33]. Further, a positive response of *E. coli* BL21(DE3) to the cyanobacterium was recorded while producing isoprene [34]. Thus, to study the potential interaction on a holistic level between *P. putida cscRABY* and *S. elongatus cscB* a suitable co-culture reference process should be set up allowing parallelization and reproducible growth of the co-culture partners.

Outline of the thesis

This section presents the organisation of the dissertation. Chapter 2 provides a theoretical discussion on co-cultures, examining the concept from various perspectives. It concludes with a detailed summary of the characteristics of the used co-culture partners, highlighting their relevant features and potential industrial applications. Chapter 3 provides a comprehensive overview of the experimental techniques used in the study, emphasizing their theoretical foundations for better understanding. Chapter 4 is divided into three parts. The first part discusses the establishment of a co-cultivation process specifically set up for polyhydroxyalkanoate (PHA) production. It outlines the steps taken to optimize PHA accumulation with the synthetic co-culture. The second part of Chapter 4 investigates potential interactions between the co-culture partners on a physiological level. It ends with the set up of a reference process to investigate the co-culture on a transcriptional, proteomic and metabolomic level. The third part of Chapter 4 presents a detailed discussion of the Omics results obtained. The thesis closes with a concise summary and outlook (see Chapter 5) on the investigated co-culture. Furthermore, a summary of the effect of physical contact between the co-culture partners is presented in section A.1. Lastly, section A.2 briefly explores the potential expansion of the product spectrum in the co-culture system, aiming to diversify the range of products synthesized by the heterotrophic partner *P. putida*.

2 Theoretical Background

This chapter provides a theoretical overview of microbial consortia and a condensed review of the bacterial co-culture investigated in this thesis. Over the last two decades, a paradigm shift has been initiated to expand the traditionally one-species biotechnology with controllable co-cultures consisting of two or more species in the same reaction vessel. Understanding the natural lifestyle of microbes can lead to discovering new metabolic routes for producing biological products and identifying new scientific targets for fundamental research [35], [36].

2.1 Microbial consortia in nature

Microbial consortia or communities are formed of at least two different species living in the same habitat and interacting with each other in various forms and they are omnipresent [37]. Diverse communities are studied in terrestrial or aquatic ecosystems and are investigated in association with fermented food, such as dairy products or beer [38], [39]. Further, they are analyzed as pathogens that can trigger inflammation, for example, in the intestine of humans [40]. Most consortia exist as biofilms where different microbes frequently are embedded in an exopolysaccharide network (EPS) secreted by community members. It is a widespread mode of living for microbes because biofilms offer a mature coping mechanism to low nutrient availability, mechanical loads, and desiccation [41]. These advantages can be transferred to all consortia because individual species can hardly survive in nature except as highly specialized niche tenants.
Early "biotechnology" commonly applied undefined co-cultures to preserve food. Mixtures of yeast strains were used to ferment sugar to alcohol, or bacterial mixed-cultures were applied to produce vinegar. Both alcohol and vinegar reduce microbial growth and can protect valuable nutrients. Back then, it was mostly a trial-and-error approach, and of course, reasons behind the longer durability of food were not yet understood. But these early processes enabled today's biotechnology in multiple fields, such as the biofuel production or the food processing sector where cell-free enzymes, pure-cultures, or defined mixed-cultures are applied equally [42], [43].

2.1.1 Investigating natural microbial communities

Native microbial communities are highly complex as they can consist of many species or phyla and show fluctuating functional capacities, which are, among others, determinated by their multilevel interactions. Adequately analyzing communities, or the microbiome, is only possible due to breakthrough progress in sequencing technologies, proteomics, and metabolomics [44]. A holistic description of consortia in their

natural environment identifies the members of the respective community and their metabolic or ecological functionality. For analyzing natural communities, the first step is the taxonomic identification of these multi-species systems. Here, 16S ribosomal RNA (16S rRNA) analysis allows genus or even species-specific identification of microbes because 16S rRNA is strongly conserved in structure and sequence as a part of the prokaryotic ribosome [45]. The second and more difficult step is the structure-function mapping of the investigated microbiome, as the composition of a consortium can determine pathogenicity, the capability of digesting specific organic matter, or whether respiration takes place anaerobically or aerobically [46]. One approach is to divide the members of a community into functional groups, which not only reduces the complexity, but allows connecting the community composition with an associated ecosystem function. This division is possible because the species of a functional group covary only weakly or negatively with one another, which means that species with similar functions are unlikely to be found in the same consortium [47]. A new aspect of microbial communities is the concept of *social niches*, which reflect how likely one species is observed in a community of other microbes. Species can either thrive in compositionally dissimilar communities or need a stable combination of partner microbes. Over the social niche breadth (SNB), defined as the mean of the pairwise compositional dissimilarity between an ecological sample in which a taxon is found, taxons can be divided into social specialists or social generalists. That strongly correlates with the capability of species to cope with a broader spectrum of environmental conditions. For instance, the taxon *Pseudomonas* was found to have a positive and high SNB, which means it includes representatives growing in different communities [48].

Nowadays, the human microbiome is one of the most intensely studied consortia, which represents all microbes living in and on human bodies. The oral microbiome, which includes teeth and other areas such as the tongue, cheek, palate, throat, or tonsils, represents the second largest consortium after the human gut system. The average person harbors $\sim$ 250 species from a pool of approx. 700 documented species [49]. Some species belong to the core microbiome that all (healthy) individuals have, and others to the variable microbiome, which is unique to individuals depending on the host's lifestyle and environmental factors. Most recent studies have shown that the oral microbiome composition strongly differs between the parts of the oral cavity. Further, it was reported that the host's physiological state, for example pregnancy, can influence the oral microbiome compilation. A universal composition-disease relationship has not yet been found, but scientists agree that imbalanced compositions or *"dysbiosis"* can cause inflammatory disease [50], [51].

2.1.2 Natural mixed cultures of phototrophs and heterotrophs

Very prominent examples of consortia are those consisting of photoautotrophs and chemoheterotrophs. Photoautotrophic organism are organisms which convert light energy into chemical energy and use CO_2 as a carbon source. In contrast, chemoheterotrophic organisms rely on (organic) carbon sources other than CO_2, using these compounds for their energy generation and as building blocks. Evidence of photosynthetic organisms dates back over 3.4 billion years [52]. It started with various different electron donors like hydrogen H_2 or hydrogen sulfide H_2S. This form of photosynthesis can still be found in strict anaerobic bacteria as purple sulfur or purple non-sulfur bacteria. They often live in highly specialized niches like hot springs or

black smokers. Billions of years later, oxygenic photosynthesis occurred for the first time, which uses water as electron donor and produces oxygen as a side product:

$$n\,CO_2 + n\,H_2O + h\nu \longrightarrow (CH_2O)_n + n\,O_2$$

This event caused a remarkable change in earth's atmosphere and was, as far as research knows, a single evolutionary step in microbes, so-called cyanobacteria [53], [54]. But the worlds oxygenation was a slow process and early life evolved to live within an oxidizing environment. One ancient evidence for this can be found in microbial mats. They consist of several layers of functional groups of microbes and can be regarded as a closed ecosystem since they are self-sufficient in their carbon supply by using photosynthesis. Here, phototrophs and heterotrophs live closely together and are in a constant exchange of gasses and nutrients. That created the best environment to train ancient bacteria to cope with different concentrations of oxygen. The top layer of today's microbial mats are phototropic microorganisms such as cyanobacteria or algae, which are essential for all other microbes in the mat since they fix CO_2 into organic carbon compounds (see Figure 2.1, **A**). This carbon may be glycolate excreted during photorespiration, fermentation products such as acetate or ethanol produced during the night or carbohydrates e.g. sucrose or threhalose which may be excreted due to salinity downshock [31]. Microbes with different lifestyles colonize the mat in different areas. Chemoorgano(hetero)trophs, which use organic compounds as carbon and chemical energy source, metabolize carbon products from the photothrophs. In the top zones of microbial mats, organism may perform aerobic respiration and species which occur in deeper layers of the mat ferment the organic substrates. In deeper layers, chemolithotrophs can derive energy from inorganic electron donors such as nitrogen or sulfur compounds and provide minerals such as reduced sulfate to the other microbes in the mat [55]. Another example of natural consortia consisting of heterotrophic and phototrophic organisms can be found between plants and various bacteria. Plant growth-promoting (PGP) bacteria increase plant growth, accelerate germination and offer additional protection against phytopathogens [56]. Most PGP bacteria occur in the rhizosphere and secrete a variety of metabolites such as phytohormones or provide nitrogen for their host plants. Further, the fixation of atmospheric nitrogen N_2 is a multilayered interaction between various bacteria, fungi and plants. The nitrogen fixing bacteria can be separated in free-living bacteria as the cyanobacterium *Nostoc* and in bacteria which live in root nodules of plants such as leguminosa. Both fix nitrogen into ammonia NH_4^+ catalysed by nitrogenases. The production of ammonia is an activity that rhizophere-located PGP bacteria perform as well. Nitrifying bacteria oxidize ammonia first into nitrite NO_2^-, which is subsequently converted to nitrate NO_3^- (see Figure 2.1 **B**). Nitrate is the most common uptake form of nitrogen in plants. To close the nitrogen cycle of our ecosystem, denitrifying bacteria carry out denitrification to convert nitrate to free atmospheric nitrogen.

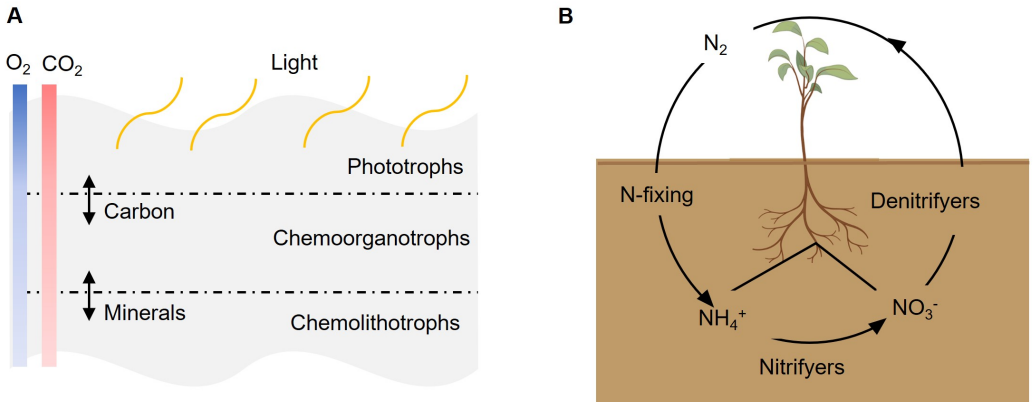

Figure 2.1: **(A)** Schematic visualisation of microbial mats consisting of layers of phototrophs, chemoorganotrophs and chemolithotrophs. Phototrophic organisms provide carbon and oxygen for other community members. Oxygen (O_2) and carbon dioxide (CO_2) concentration decreases with the mats thickness, which is indicated through the blue and red gradient (dark blue equals a high concentration of oxygen and light blue a low concentration of oxygen; dark red equals a high CO_2 concentration and light red indicates a low concentration). **(B)** Simplified nitrogen cycle in our environment, with nitrogen (N)-fixing bacteria forming ammonia NH_4^+, nitrifyers forming nitrate NO_3^-, and denitrifyers which form atmospheric nitrogen N_2. The Figure was created with the help of BioRender (http://www.BioRender.com).

2.1.3 Interaction in natural mixed cultures

Interaction is usually considered as the exchange of information in the form of molecules or physical contact. For the sake of simplicity, the interplay between two individual cells, or two uniformly behaving species, can be used to determine the dynamic of a community. Taking a closer look at the exchange of molecules as a form of interaction: It means a signal(-molecule) gets emitted from one species or individual cell (input), and the receiver, which needs to be equipped with a suitable receptor for subsequent processing of the input, forms a response (output) to the signal. When members of the same species interact, it is called intra-species interaction. The most prominent example is quorum sensing type I (QSI), which is the regulation of gene expression in response to the cell population density [57]. In some cases, gene expression only makes sense when most of the population performs it, for instance, to switch on genes for virulence or biofilm formation. The minimal quorum sensing circuit contains a:

- synthase for biosynthesis of a signal molecule (also called autoiducer (AI))
- receptor for sensing the signal molecule and to pass the signal on
- response (change in gene transcription) after processing the signal through a regulatory chain (e.g. two-component system or conformation change of proteins)

QSI was first identified in the gram-negative bacterium *Aliivibrio fischeri*, which lives as a symbiont in the light-producing organ of the Hawaiian bobtail squid. The protein LuxI synthesizes the signal molecule N-acyl homoserine lactone (AHL, autoinducer). This autoinducer freely diffuses through the membrane and activates LuxR, a transcriptional activator for the bacterial bioluminescence *luxCDABE*-operon (see Figure 2.2 **A**). Other gram-negative bacteria such as *Pseudomonas aeruginosa* or *Agrobacterium tumefaciens* mediate the communication of their cell density with similar systems containing at least LuxI and LuxR homologs [57], [58]. In contrast to the symbiont *Aliivibrio fischeri*, both species switch on pathogenicity

against their respective host. In gram-positive bacteria, the signal molecules are small peptides that induce a phosphorylation/dephosphorylation cascade in a two-component regulatory response when cell density is high enough (see Figure 2.2 **B**). Aside from intra-species interaction, the interplay can occur between different species in communities and is accordingly called inter-species interaction. Remaining with the example of quorum sensing, a version of inter-species interaction was found in *Vibrio harveyi*. It uses QSI for cell density-depending induction of bioluminescence gene expression and a second system belonging to the QS type II (see Figure 2.2 **C**). This form of QS responds to signal molecules that are chemically furanosyl borate diesters, termed autoinducer type II (AI-2). The signal molecule is synthesized through the synthase LuxS and binds to a receptor/sensor complex. That induces a phosphorylation/dephosphorylation cascade which deactivates the transcriptional repressor LuxO and allows the activator LuxR (not homolog to LuxR of *A. fischeri*) to enhance transcription of the bioluminescence genes. To summarize, this QS-type forms a hybrid of both model QS systems from gram-negative and gram-positive bacteria. Interestingly, many bacteria contain highly conserved LuxS homologs. For example, it was shown that autoinducers from type AI-2 of at least 75 other species induce the bioluminescence genes in *V. harveyi*. As a results, QS-II is handled as an inter-species communication system [59], [60].

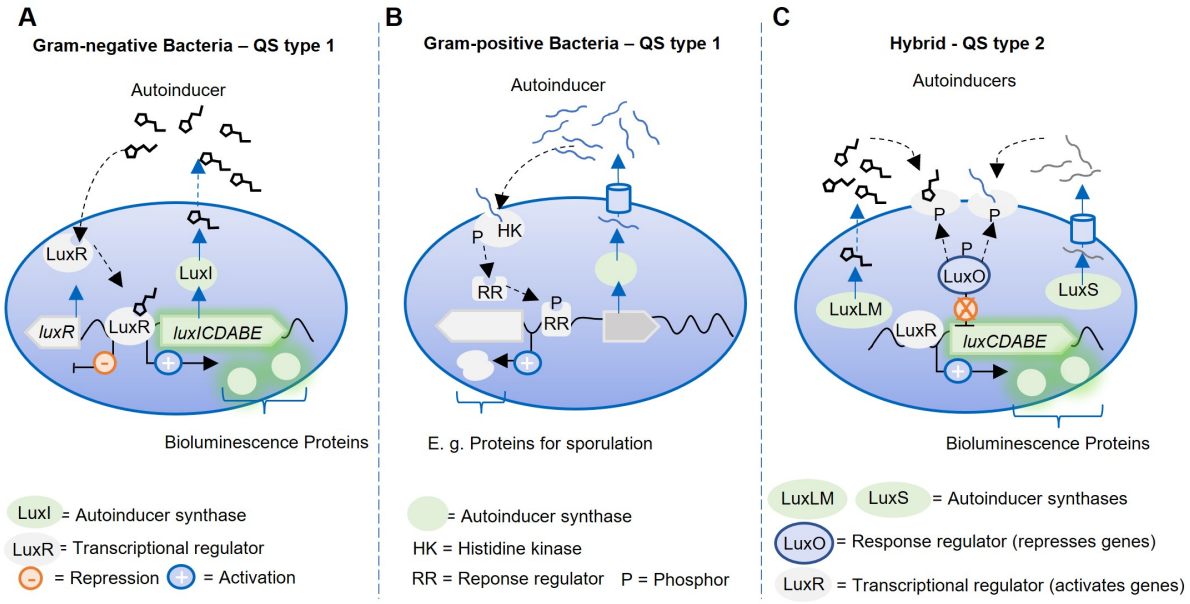

Figure 2.2: Three types of quorum sensing in bacteria. **(A)** Gram-negative Bacteria - QS type 1: Visualisation of the quorum sensing in *Aliivibrio fischeri*. The autoinducer N-acyl homoserine lactone is synthesized from the synthase LuxI. The binding of the autoinducer activates the transcriptional regulator LuxR, which in turn activates (+) bioluminescence genes but represses its own transcription (-). **(B)** Gram-positive Bacteria - QS type 2: Depicted is an overview of peptide-mediated quorum sensing. A high enough peptide autoinducer signal induces a phosphorylation cascade, which allows conformational change of the response regulator, DNA-binding, and activation or repression. **(C)** Hybrid-QS type 2: Depicted is the simplified hybrid quorum sensing circuit of *Vibrio harveyi*. Two autoinducers are produced: A homoserine lactone type autoinducer (AI-1) and a furanosyl borate diester type autoinducer (AI-2). Both have a cognate two-component sensor kinase. When bound, the complex can induce a phosphorylation/dephosphorylation cascade. The dephosphorylation of the response regulator LuxO, which act as a repressor for the *luxCDABE*-operon, allows the transcriptional regulator LuxR to activate the bioluminescence genes. All figures were adapted from [57].

Most interaction models are based on the pairwise interplay of two entities that define the globally combined behavior of a community, also called ecological interaction. Recent developments try to include the interplay

of more cells, termed higher-order interaction. An example of this higher-order interaction can easily be found: A toxin-degrading microbe, which protects other toxin-sensitive community members from the producing species promotes, in the end, the co-existence of more than two strains [61]. In this example, the pairwise comparison does not lead to the same result as the degrading microbe has a positive effect on the toxin-sensitive community members but a negative effect on the toxin producer. Another example of modeling communities or co-cultures is realized through the combination of stoichiometric genome-scale models and forming so-called community models. This approach can be extended by incorporating not only a time component by simulating uptake rates with simple kinetics but also a spatial component [62]. Due to the complexity of multi-species communities, their versatile interactions within the community, the interplay with the environment, and/or the host, a detailed in-depth characterization of their interaction is still challenging. Nevertheless interaction of natural communities as for example between phototrophs and heterotrophs are targets in biotechnology. For instance, microalgae can be used for biofuel production due to their biomass composition, lipid and fatty acid accumulation. To decrease down-stream processing cost, usually strains with high sedimentation rates are applied. It was found that some heterotrophic bacteria induce floc-forming within the microalgae *Chlorella sorokiniana* KNUA114, which increases sedimentation rates and consequently makes harvesting microalgae biomass cheaper [63].

2.2 Easier to investigate: Defined synthetic co-cultures

In the last century, monocultures or axenic (*"free from foreign life"*) cultures have been the state of the art for microbiological studies as well as for biomanufacturing due to a simpler handling and safety-control [64]. This view on the microbial world does not reflect the actual lifestyle of microorganisms, nor does it consider the complex interaction and communication in inter-phylum consortia [35]. The high complexity of natural co-cultures can be reduced by employing only a few hand-picked partner organisms. This is called a defined co-culture. Interactions, such as cell-cell communication, can be selected or more easily investigated, and the co-culture partners can be controlled to carry out defined processes. A further step is to use genetically modified bacterial strains to build up or enhance the dependency of the co-culture partners either for a fundamental research approach or to exploit certain traits in bioproduction. An example of non-natural or synthetic defined co-cultures would be one-another complementing "synthetic" auxotrophic microbes (see Table 2.1). For instance, adaptive laboratory evolutionary experiments resulted in amino acid auxotrophs from *E. coli*, which were able to perform metabolic cooperation between the different strains. In the end, both partners evolved to produce significantly more of the respective amino acid compared to the wild-type strains [65].This common form of division of labor was recently also shown in synthetic bacterial cross-feeding of amino acids in *Corynebacterium glutamicum* carrying one or more auxotrophies [66]. That means employing defined synthetic co-cultures combines the advantages of undefined (natural) mixed cultures e.g. division of labor, robustness against contamination, and extended product spectrum with the ones of axenic cultures e.g. high controllability and an easier handling [67], [68]. The progress in synthetic biology, improvements in metabolic models, and analysis techniques becoming more affordable helps to create a repertoire of customized co-culture partners. Interactions may be programmed by implementing genetic feedback loops or exploiting natural strategies such as quorum sensing [69], [70]. In a study in 2008, a synthetic *E. coli* predator-prey co-culture was constructed based on quorum sensing. Here, one population produces a cell density-dependent antidote for the otherwise not surviving *E. coli*-predator population. The predator population produces a toxin, which kills in sufficiently high concentration the *E. coli*-prey population [71]. The opportunity to match different consortia partners together with customized traits might be used as a "plug-and-produce" similar to puzzle pieces in synthetic co-cultures, which finally accelerate the biomanufacturing of chemicals, proteins or nucleic acid (see Figure 2.3 **A**) [72].

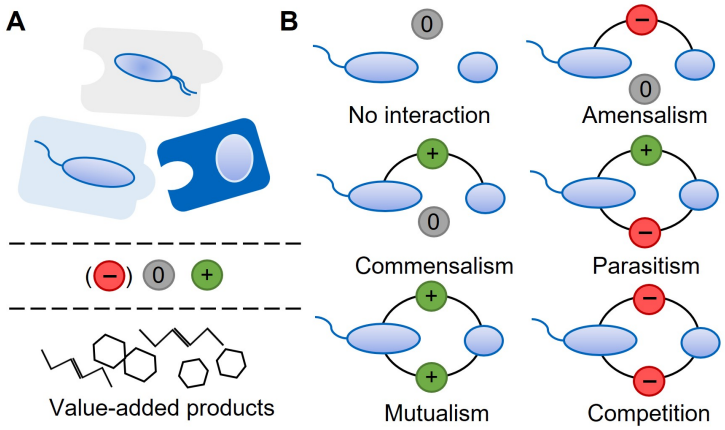

Figure 2.3: **(A)** In defined synthetic co-culture, the partners can be connected in a "plug-and-produce" manner, where wanted interaction and metabolic traits can be chosen to produce the desired value-added product such as puzzle-pieces [72]. **(B)** Categories of bidirectional microbial interactions: no interaction (neutralism) (0/0), competition (-/-) , amensalism (-/0), parasitism (+/-), commensalism (+/0) and mutualism (+/+) (Figure part B was adapted from [73]).

Table 2.1: Types of co-cultures and examples.

Type of co-cultures	**Examples and references**
Natural (undefined) co-cultures	The human intestine microbiome [40]; Conversion of biowaste to biogas (methane) [74].
Defined co-cultures	Targeted use of natural synergistic effects for better degradation of hard to access substrates e.g. cellulose [75].
Defined co-cultures with GMO[1]	Targeted use of natural synergistic effects but engineered strains, e. g. to better accumulate a intercellular product. This is a special case of defined co-cultures.
Synthetic defined co-cultures	Auxotrophic bacterial strains supplying one another with the missing nutrient [65], [66].

2.2.1 Types of interaction in co-cultures of two members

Interactions between community members are omnipresent and can occur within and between species or even among different phyla. Considering only two interacting microbes, each of them can have a positive, neutral, or negative effect on the other one, which results in six global interaction types (see Figure 2.3 **B**) [73]. In rare cases, no interaction, also termed neutralism (0/0), between the microbes exists. At a metabolic level, it can be translated into no shared metabolites [73], which may be the case in highly specialized bacteria. A more common form of interaction is commensalism, where one microbe exerts a positive effect on the co-culture partner, whereby the other one shows a neutral form of interaction. This type of interaction can be found in food chains in the nitrogen cycle of our ecosystem (see Section 2.1.2) or, to name a more specific example, in the co-culture between *Bacillus subtilis* and *Cupriavidus necator*. The first co-culture partner feeds the second with propionate, and there is at least no apparent feedback from the latter one [76]. In

[1] GMO = genetically modified organism

contrast, syntrophy or cross-feeding is the most prominent example of mutualistic interactions (+/+). Here, one co-culture microbe partially metabolizes a complex substrate, which is in turn accessible to another partner. This partner might remove toxins or harmful gases, which creates the environment needed for both partners. The boundary between commensalism and mutualism is often ambiguous, since apparently "no interaction" can indeed only be a hidden one (not yet measured one). Notably, there is an evolutionary drive to positive interaction, as it is likely that redundant metabolic pathways get lost over time [77]. Additionally, complementary metabolic pathways create stable and long-lasting communities. Thus, auxotrophy is a common example of division of labor in complex communities [78]. A negative effect on community members or direct co-culture partners can occur due to the production of, for other microbes, harmful by-products or due to the synthesis of targeted toxins. When only one species performs this negative interaction and the other species affects its partner neutrally, it is called amensalism (-/0). This form of interaction is unstable and leads, in the end, to the extinction of at least one partner species [79]. A predator-prey relationship, or parasitism (-/+), is a form of interaction where one microorganism takes advantage of the partner. That can be seen in the live cycle of *Bdellovibrio* genus, which can prey on gram-negative bacteria [80]. Another example is the predator *Myxococcus xanthus*, which has an advanced life cycle including preying on *E. coli* [81]. A pronounced competition over a shared substrate or space is a negative interaction in both directions (-/-). It is assessed as a fundamental reason for evolutionary developments in co-cultures [82].

2.2.2 Modelling of co-cultures and their dynamics

To model the behaviour of microbes, a set of kinetic equations have been developed. These can be used to investigate the dynamic of a defined co-culture and their different relationships as well. Most ideas date back to the last century and usually are integrated into a mass equation for growth:

$$\frac{dm_X}{dt} = \mu \cdot m_X \tag{2.1}$$

with m_X (g) as the mass of the cell and μ (h^{-1}) as the growth rate of the cell. The growth rate can be further described with the Monod-equation (2.2) [83], which explains the quantitative relation between cell growth and a limiting nutrient:

$$\mu = \mu_{max} \cdot \frac{c_s}{c_s + K_s} \tag{2.2}$$

Here, μ_{max} (h^{-1}) represents the maximal growth rate, c_s (g L^{-1}) is the limiting substrate concentration and K_s (g L^{-1}) the half-saturation constant for the limiting substrate. Equation 2.3 can be extended to multiple limiting substrates c_{si} (g L^{-1}):

$$\mu = \mu_{max} \cdot \prod_i \frac{c_{si}}{c_{si} + K_{si}} \tag{2.3}$$

There are various further extensions to the Monod-equation, which include substrate or product limitation to better describe the dependency between microbial growth and substrates [84]. Coupling a set of kinetic equations was recently used to describe a co-culture of *S. elongatus cscB* carrying plasmid-based the

sucrose phosphate synthase (*sps*) with *E. coli* as heterotrophic partner bacterium. The dynamics dependent on the ratio of phototroph to heterotroph in the co-culture, can be successfully described with this model approach [85].

Other modeling approaches where used when ecological microbial consortia are described. One of the most prominent examples is the Lotka–Volterra predator-prey model. In its most simple form it takes two entities into account: The prey $N(t)$ and the predator $P(t)$. The prey grows αN and dies through the act of the predator $-\beta PN$. The predator can only grow and produce offspring in the presence of the prey γPN otherwise it dies $-\delta P$. Whereby α, β, γ and δ are parameters. This leads to the coupled differential equations:

$$\frac{dN}{dt} = \alpha N - \beta PN \tag{2.4}$$

$$\frac{dP}{dt} = \gamma PN - \delta P. \tag{2.5}$$

Its solution shows a phase drifted oscillating behaviour between the two populations. A drawback is that the model shows an exponential growth of the prey in absence of the predators. Therefore the equations were modified to

$$\frac{dN}{dt} = \alpha N(1 - \frac{N}{K}) - \beta PN \tag{2.6}$$

$$\frac{dP}{dt} = \gamma PN - \delta P \tag{2.7}$$

with an logistic growth term for the prey $1 - \frac{N}{K}$. Here, K is termed the *"carrying capacity"* and describes the maximum of organisms which the environment can sustain [86] and, further, this system is stable (has a Lyapunov function). The basic model has various further extension such as prey immigrants. Today, hybrid models of the Monod-equation and logistic models were set up, too [79].

Constraint-based metabolic modeling

Metabolic models are reconstructions of cellular networks which includes *all* (Genome-scale models) or some (core-models) metabolic reactions within a cell [87], [88]. Stoichiometric coefficients of all the reactions of interest are written in a stoichiometric matrix S, so that each row corresponds to a compound and each column to a reaction. To describe the change of the metabolites over time $\dot{\underline{C}}$ in the metabolic network, their uptake and consumption are considered ($S \cdot \underline{r}$) [89]. Further, the dilution of the metabolites due to cell growth is represented through $\mu \cdot \underline{C}$. In combinations it leads to:

$$\dot{\underline{C}} = S \cdot \underline{r} - \mu \cdot \underline{C}. \tag{2.8}$$

By assuming a quasi-steady state and neglecting the dilution term due to fast turnover of metabolites by enzyme-catalysed reactions, Equation 2.8 can be simplified to

$$\underline{\dot{C}} = S \cdot \underline{r} = 0. \tag{2.9}$$

Because S contains usually more columns than rows, the given problem is underdetermined and has infinite mathematical solutions. For quantitatively analyzing biological meaningful solutions of a metabolic network through flux balance analysis (FBA), the solution space can be constrained by biological criteria or (reaction) measurements. FBA solves a linear optimization problem with an objective function (ϕ). Most problems are formulated in a way that the growth rate of the microbe gets maximized, constrained by reaction boundaries [90]. Since simple metabolic models disregard proteins, DNA, and other macromolecules, the cell‘s biomass is regarded to be formed out of atoms that incorporate into macromolecules. The resulting stoichiometric biomass production reaction $r_{Biomass}$ is included in the model for optimization [91]. It should be noted that the biomass composition is assumed to be constant in the steady state [92]. Constraining models with additional information, such as gene regulation and enzyme turnover, or expanding models with basic thermodynamics can further improve simulations [90]. The intensely studied metabolic network of *E. coli* K-12 advanced to the gold standard of metabolic modeling, with its most recent model iML1515 [93], [87]. For example, metabolic model-driven analyses allowed targeted genetic engineering of a *E. coli* L-trypthophan producer strain [94]. For co-cultures and large consortia one question is if interaction can be predicted based only on intracellular circuits. Recently, new community metabolic models combined the phototrophic model of *S. elongatus* (IJB792, [95]) with different models of heterotrophs, e.g. a metabolic model from gram-positive bacterium *B. subtilis* (iYO844, [96]). Community growth simulations were calculated by maximizing the growth of both community members in this study. Overflow metabolites were particularly analyzed in the community model as they can be exchanged in the co-culture [97].

2.2.3 Synthetic co-cultures of phototrophs and heterotrophs

The design of synthetic co-cultures is a careful venture as multiple aspects and parameters need to be assessed and results should go along with sustainable biotechnology in the best-case scenario. In most cases, processes are designed such that the microbes live under the premise of the division of labor, which allows different wanted traits of microbes to complement each other profitably. One example of doing so is pairing heterotrophs with phototrophs. This composition of microbes is, as described above, prominent in nature (see Chapter 2.1.2), and some phototrophs are not axenically culturable due to their strong heterotrophic dependency [68]. For example, a study conducted genome-wide high-throughput screening and identify 32 genes in *E. coli* K-12 that promote the growth of the companion microalgae *Chlorella vulgaris* [98].
In co-cultures of phototrophs and heterotrophs, the photoautotrophic member, such as cyanobacteria or algae, uses solar power to fix CO_2 into carbon, accessible for heterotrophic members of the community, which in the case of synthetic co-cultures convert it to value-added products due to cooperating metabolic pathways. The model organism *Synechococcus elongatus* PCC 7942 naturally accumulates sucrose when exposed to elevated NaCl concentration [99]. The genomic integration of an H^+/sucrose symporter *cscB* in the neutral site 3 (NS3) enabled sucrose secretion with a rate of up to 36 mg L^{-1} hr^{-1}. It was calculated that

with this $\sim$ 85% of its photosynthetically fixed carbon is channeled into sucrose when the cyanobacterium carries additionally the sucrose phosphate synthase gene *sps* [24], [100]. To this day, several robust synthetic co-cultures were set up with the *S. elongatus cscB* derivative, and valuable compounds such as α-amylase, polyhydroxybutyrate (PHB), polyhydroxyalkanoates (PHA) or isoprene were successfully produced. The metabolic capacity of the synthetic co-cultures was increased because of model heterotrophic partners such as *E. coli*, *Pseudomonas putida*, *Bacillus subtilis*, and *Saccharomyces cerevisiae* [32], [25]. The study by Hays et al. used firstly only microbes that are naturally able to take up and subsequent metabolize sucrose. However, the heterotrophic partners *E. coli* W and *S. cerevisia* W303 showed reduced or no growth due to metabolite repression at low sucrose concentrations in axenic cultures. Not until applying a mutant of *S. cerevisia* W303, derived by laboratory directed evolution, and an *E. coli* W derivative without the catabolite repressor *cscR*, was it possible to set up stable co-cultures with *S. elongatus cscB* over 6 or 18 days, respectively [32]. In 2020, a study reported the production of 3-hydroxypropionic acid (3-HP) with a co-culture consisting of the fast-growing cyanobacterium *S. elongatus* UTEX 2973 carrying the *cscB* gene for sucrose secretion and a genetically derivative of *E. coli* BL21 (DE3) from light and CO_2. The heterotrophic partner was equipped with a sucrose catabolic pathway (*cscB*, *cscA* and *cscK*) as well a malonyl-CoA reductase-coding gene for 3-HP synthesis (*mcr*) to achieve a final production of approx. 68.3 mg L^{-1} of the product [60]. These co-cultures are some examples of how research attempts to unlock CO_2 as a feedstock for heterotrophs to produce value-added products.

2.3 Synthetic Co-culture of *Pseudomonas putida* and *Synechococcus elongatus*

This section focuses on describing the co-culture studied in this thesis and provides more details about the co-culture partners. First, the general properties of each microbe are explained, including it's metabolism. Additionally, for the heterotrophic partner, the accumulation of the polymer polyhydroxyalkanoate (PHA) is described. The section on each co-culture partner ends with the potential applications in the industry.

Löwe at al. designed a light-driven synthetic co-culture, in which the cyanobacterium *Synechococcus elongatus* PCC 7942 *cscB* provides the feedstock for the heterotrophic partner, a genetically engineered derivative of the gram-negative *Pseudomonas putida* KT2440 [25], [26]. In the presence of elevated salt concentrations, *S. elongatus* converts part of the photosynthetically fixed CO_2 into sucrose, which serves as a compatible solute [99]. By the action of the heterologously expressed CscB sucrose permease from *E. coli* EDL933, sucrose is secreted into the culture supernatant. It serves as the sole carbon source for a modified *P. putida* to generate biomass and supports the production of biotechnological target compounds (see Figure 2.5) [24].

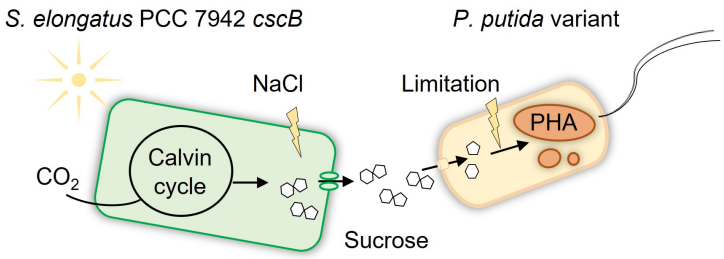

Figure 2.4: Synthetic co-culture of *S. elongatus* PCC7942 *cscB* and a sucrose metabolising *P. putida* variant. CO_2 is photosynthetically fixed in the Calvin cycle to 3-phosphoglycerate, which is subsequently converted to sucrose. Through the CscB symporter, sucrose is secreted from cyanobacterial cells into the medium. Here, it serves as the sole carbon source for the heterotrophic partner. *P. putida* can naturally accumulate polyhydroxyalkanoates (PHA) in the cytoplasm when, for instance, carbon excess is combined with a limitation of essential nutrients.

P. putida EM178 is a prophage free derivative of *P. putida* KT2440. It was genetically modified to expand its substrate spectrum towards sucrose [26]. As described in the literature, the expression of *cscA*, encoding a sucrose hydrolase, and *cscB*, which encodes a sucrose/proton symporter, achieved a stable sucrose consuming *E. coli* derivative [101]. Therefore, Löwe et al. transferred this principle to *P. putida*, generating a variant able to grow on sucrose caring the *cscAB* genes derived from *E. coli* W, randomly integrated into the genome via a vector based on a mini Tn5 transposon plasmid [26], [102]. The observed growth rate for the constructed strain called *P. putida* PP_3398::*cscAB* with sucrose as a carbon source was 0.27 h^{-1}, that is approximately half the growth rate reached with a fructose-glucose mixture as a carbon source [26].
The resulting *P. putida* strain was used to set up the first co-culture with *S. elongatus cscB* [25]. The cyanobacterium had maximum productivity of 0.35 g sucrose L^{-1} d^{-1} at 150 mM NaCl grown axenically and could support the heterotrophic growth in the co-culture. As a proof of concept, nitrate limitation was applied to the co-culture, which naturally induces the accumulation of the biopolymer medium-chain-length

(mcl) polyhydroxyalkanoate (PHA) in *P. putida cscAB*. The maximum achieved PHA-titer was 0.15 g L^{-1} with a production rate of 23 mg L^{-1} d^{-1} [25]. However, the heterotrophic partner showed fluctuating growth behavior, reflected by high standard deviations of *P. putida cscAB's* cell count. Additionally, the produced PHA was metabolized again by the *P. putida cscAB* at the end of the process. Considering that the growth rate of *P. putida cscAB* reached only 50 % of the maximum growth rate compared to the growth on a glucose/fructose mixture, it was concluded that the heterotrophic partner faces challenges with the sucrose uptake. Further, it became more evident that the outer cell membranes of *P. putida* and *E. coli* have major differences in their composition in terms of permeability towards carbohydrates. This leads to the hypothesis that the CscB symporter is redundant when expressed in *P. putida* and the apparent sucrose uptake derives only from some secreted CscA hydrolase proteins. Therefore, a more efficient sucrose uptake and metabolization system for *P. putida* was searched and found through *in silico* homology studies of different sucrose gene clusters. This new sucrose gene cluster was identified in *Pseudomonas protegens* Pf-5, a close relative of the used strain, was identified and termed *cscRABY* [27]. The cluster encodes a LacI-like regulator CscR, the invertase CscA, the transporter CscB and the porin CscY (see Figure 2.5 **A**) [27]. In complementation experiments, it was shown that the porin enabled sucrose uptake when cells were grown in LB pre-cultures and subsequently transferred to a minimal medium with the carbohydrate. That highlights the importance of porins, especially without the previous adapting phase of the metabolism to sugar uptake and degradation. Figure 2.5 **B** depicts the sucrose uptake and metabolization schematically. Sucrose crosses the outer cell membrane over the porin CscY and is then transported from the periplasm into the cytoplasm with the symporter CscB. Within the cell, the hydrolase CscA splits the disaccharide into glucose and fructose. The latter most likely be re-imported by the fructose-PTS system for phosphorylation and mobilization for the core metabolism [103]. Glucose can be intracellularly phosphorylated and directly integrated into the metabolism.

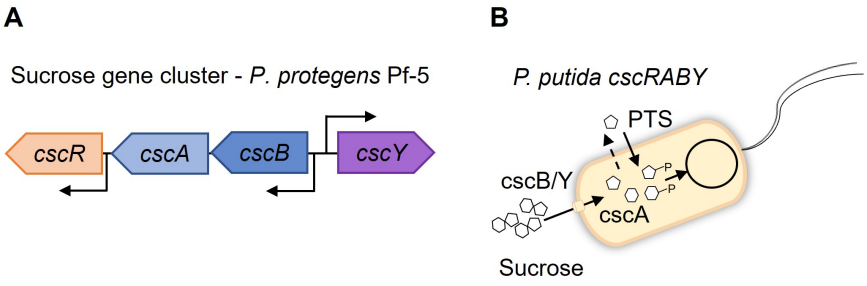

Figure 2.5: **(A)** The native sucrose gene cluster of *P. protengens* Pf-5 consists of a regulator CscR, the invertase CscA, the transporter CscB and the porin CscY. The arrangement on the chromosome is indicated through the arrow direction of the genes. The *in-silico* identified native promoters of the genes are marked with black arrows. This part of the Figure was adapted from [27]. **(B)** Current model of sucrose uptake and metabolisation of *P. putida cscRABY*. The disaccharide sucrose is taken up through the porin CscY in the outer membrane. With the help of the CscB transporter, sucrose enters the cytoplasm, where CscA splits the disaccharide into the two monosaccharides, glucose and fructose. Glucose can directly be phosphorylated and subsequently integrated into the carbon core metabolism. Fructose might be tken up again via the fructose-phosphotransferase system (PTS^{Fru}).

2.3.1 The heterotrophic partner: *Pseudomonas putida*

The rod-shaped γ-proteobacterium *P. putida* is strictly aerobic and omnipresent in nature. It is a versatile microorganism that adapts easily to changes in environmental conditions. Furthermore, it can cope with challenging milieus like harsh pH, toxins, and xenobiotics due to specific drug efflux systems [104].
P. putida KT2440 has a 6.1 kbp genome which is fully sequenced. Gene annotation can be, for example, found in the database Pseudomonas.com (https://www.pseudomonas.com/), which includes links to other commonly used databases such as the National Library of Medicine (NCBI, https://www.nlm.nih.gov/) or String Database (https://string-db.org/). Metabolic engineering often starts with a plasmid or cloning vector. Most of them have been developed in and with *E. coli* and might not be suitable for other organisms. To face this problem, the Standard European Vector Architecture (SEVA) database was developed with its most updated version SEVA 4.0 [105]. It provides a modular arrangement of elements to create customized plasmids for wanted requirements (https://seva-plasmids.com/). The SEVA-plasmids are strongly utilized for genetic engineering in *P. putida*. Various other tools facilitate the genetic manipulation of the microbe. Genome editing can be performed transposon-based (most prominent Tn5 and Tn7 [106]), [107] and the newest developments are CRISPR interference-mediated gene regulation strategies [108]. To further advance the understanding and increase bioproduction capacity with *P. putida* as a cell factory, metabolic models as whole genome-scale models (most updated model iJN1462) [109], and many smaller core models have been successfully established. Core models have been used, e.g. for identifying targets for metabolic engineering to increase the polyhydroxyalkanoate (PHA) yield in *P. putida* [110] or to investigate how *P. putida* responses to oxidative stresses [111], [112]. A further example is the analysis of the gradual consumption of the LB medium components from *P. putida* with the metabolic model iJN1411 [113].

P. putida is handled as a direct bio-control agent, as it thrives in the soil and, especially, in the rhizosphere. It can be utilized for bioremediation as *P. putida* can cope with contaminated soil environments [111]. Further, it is known to have plant growth-promoting effects due to competition and inhibition against plant pathogens (see Chapter 2.1.2). Plants can produce high levels of reactive oxygen species (ROS) as an immune response to pathogens [114], which is why *P. putida* is equipped with advanced ROS coping mechanisms, such as efflux pumps, various catalases, and a metabolism able to produce more reducing equivalents when necessary. *P. putida* has a core metabolism that differs from other gram-negative bacteria, which allows it to grow in difficult areas [115].

Metabolic peculiarities of P. putida

P. putida harbors a special combination of the Emden-Meyerhof-Parnas (EMP, glycolysis) pathway and the Entner–Doudoroff (ED) pathway, which was deciphered by isotope labeling experiments first in 2015 by Nikel et al. [116]. Both pathways catabolize glucose to pyruvate in a series of enzyme-catalyzed steps. However, in *P. putida* it became evident that it does not use a linear form of the ED pathway for glucose catabolism but an interlinkage of an incomplete EMP pathway and the ED pathway itself in a cyclic manner, called the EDEMP-pathway (see Figure 2.6) [116]. Further, the Pentose Phosphate (PP) pathway provides pentose intermediates for the EMP pathway, which lacks the crucial enzyme 6-phosphofructo-1-kinase (Pfk). The absence of this enzyme, which catalyzes the ATP-dependent conversion of fructose-6-phosphate into fructose-1,6-bisphosphate, forces the upper EMP pathway in a gluconeogenic direction. This unusual

combination allows *P. putida* to produce an excess of reducing power in the form of nicotinamide adenine dinucleotide phosphate (NADPH), which is supposed to help the organism in harsh conditions [116], [117].

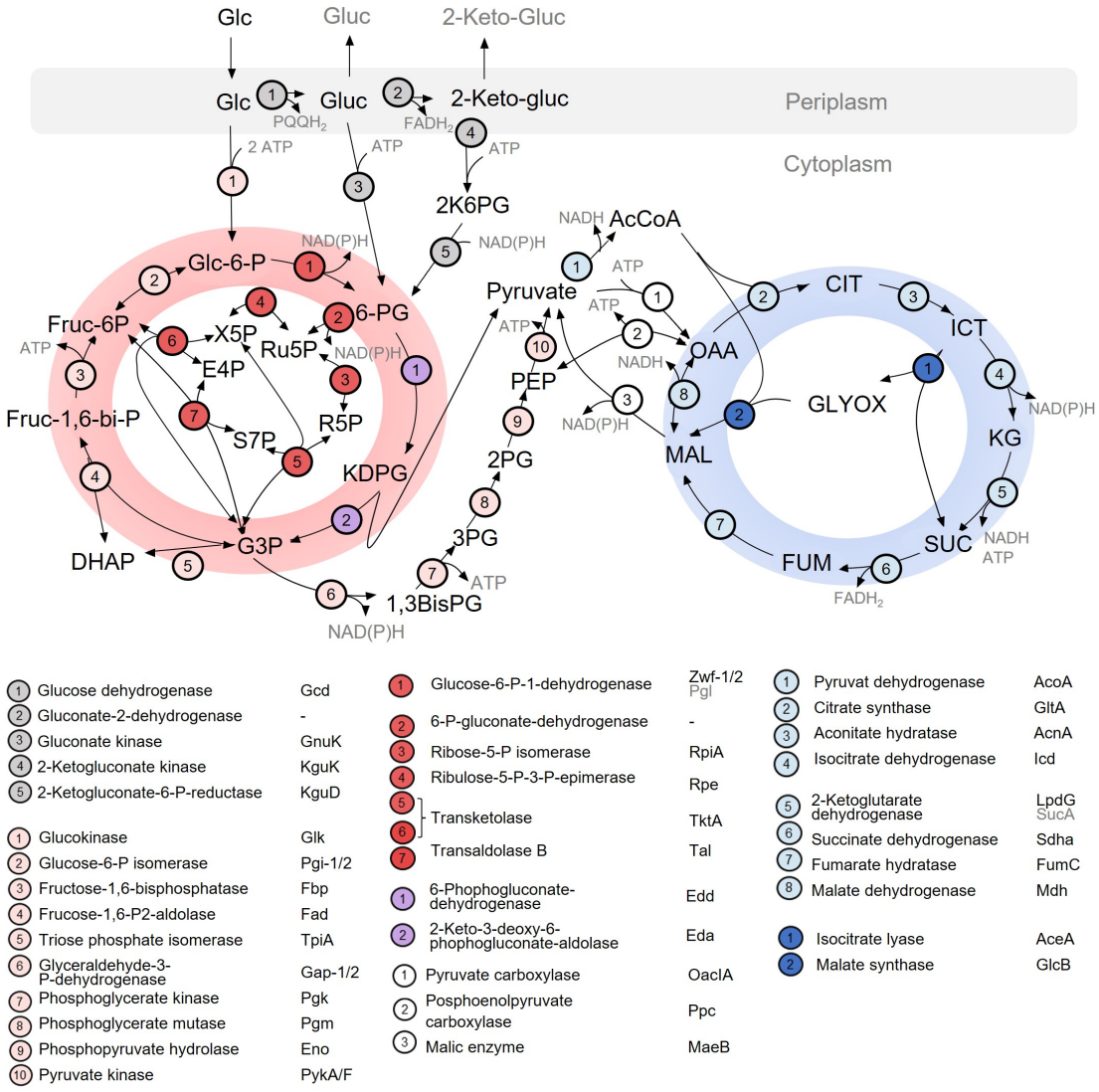

Figure 2.6: Core metabolism of *P. putida* KT2440. Gray: Glucose oxidation in the periplasm to gluconate and subsequently to 2-keto-gluconate. Both are common overflow metabolites in *P. putida* and can be transported out of the periplasm. Red: The Emden-Meyerhof-Parnas (EDEMP) pathway is a combination of the Entner–Doudoroff (ED)-pathway, an incomplete EMP-pathway, and the connecting Pentose-Phosphate (PP)-pathway. Blue: Tricarboxylic acid cycle (TCA) pathway with glyoxylate shunt. Glc = glucose, Gluc = gluconate, 2-Keto-Gluc = 2-keto-gluconate, Glc-6-P = glucose-6-phosphate, 6-PG = 6-Phosphogluconate, KDPG = 2-Keto-3-desoxy-phosphogluconat , G3P = glycerinaldehyd-3-phosphate, DHAP = dihydroxyacetone phosphate, Fruc-1-6,bi-P = fructose-1-6-bis-phosphate, Fruc-6P = fructose-6-phosphate, 1,3BisPG = 1,3-Bisphosphoglyceric acid, 3PG = 3-Phosphoglyceric acid, 2PG = 2-Phosphoglyceric acid, PEP = phosphoenolpyruvate, AcCoA = acetyl-coenzyme A, CIT = citric acid, ICT = iso-citric acid, KG = ketoglutarate, SUC = succinate, FUM = fumarate, MAL = malate, OAA = oxaloacetate GLYOX = glyoxylate. The Figure was adapted from [116] and [104].

With the EDEMP-pathway, also the glucose uptake differs in *P. putida* [116]: In the periplasm, glucose can be oxidized to gluconate (gluc) or keto-gluconate (2-keto-gluc) and subsequently channeled into the cytoplasm while converted to 6-phosphogluconate (6-PG). The other option is the direct uptake via an ABC-transporter (GtsABCD) and phosphorylation by glucokinases, such as Glk, to glucose-6-phosphate (Glc-6-P) in the cytoplasm. The periplasmatic oxidation enables *P. putida* to circumvent this direct ATP-costly glucose uptake via an ABC-transporter and is, therefore, the preferred route [104]. That means that the periplasmatic route is a shortcut to the ED pathway (see Figure 2.6) which applies the two unique enzymes, a 6-PG-dehydratase (Edd) and a 2-keto-3-desoxy-phosphogluconate (KDPG)-aldolase (Eda). Eda catalyzes the second reaction to form one glycerin-3-aldehyde (G3P) and one pyruvate, reducing drastically resource-demanding enzymes. The G3P is recycled back to Glc-6-P, which completes the EDEMP cycle (see 2.6) [116]. The textbook balance for the ED pathway is depicted in the chemical formula below [115]:

$$\text{Glucose} + \text{ADP} + \text{Pi} + \text{NAD}^+ + \text{NADP}^+ \longrightarrow 2\,\text{ATP} + 2\,\text{H}_2\text{O} + 2\,\text{NADH} + 2\,\text{H}^+ + 2\,\text{Pyruvate}$$

For *P. putida*, the additional energy demanding ABC-transport of glucose needs to be taken into account. In most metabolic models, the glucose uptake is considered with one additional ATP dephosphorylation, which shifts the reaction to no direct net gain of the energy molecule [109]. Only the reducing-equivalent NADH can be transformed into $\sim$ 2.5 ATP (BioNumbers ID 114728). The balance differs when the preferred route over glucose oxidation in the periplasm is regarded. Here, the uptake and phosphorylation for oxidized glucose costs only one ATP, leading to one direct net gain of the energy molecule (compare Figure 2.6). For the $FADH_2$ produced in the periplasm $\sim$ 1.5 ATP per molecule can be estimated (BioNumbers ID 110682).

The merged PP-pathway forms as in other microbes pentose-sugar precursors such as ribose 5-phosphate or erythrose 4-phosphate, which are necessary for cell maintenance (see Figure 2.6). The tricarboxylic acid cycle (TCA) is prepared by the decarboxylation from pyruvate to acetyl-CoA (AcCoA). The next step is then the entry reaction catalyzed by the citrate synthase, which merges acetyl-CoA (C2 molecule) with oxaloacetate (OAA, C4 molecule) to citric acid (CIT, C6 molecule). In the following steps, citric acid is oxidized to recycle the oxaloacetate (OAA). Intermediates of the TCA cycle act as precursors for amino acids, hemes, and lipids[2][3]:

- Oxaloacetate is the precursor of aspartate, which is involved in the biosynthesis of other amino acids, such as lysine.
- The intermediate α-ketoglutarate (KG) is the precursor for glutamate, which acts as starting point for the biosynthesis of other amino acids and purines.
- Succinyl-CoA is a precursor for hemes, lysine, and methionine.

The glyoxylate shunt bypasses the reaction catalyzed by the isocitrate dehydrogenase and α-ketoglutarate dehydrogenase of the TCA (see Figure 2.6). The first enzyme of the glyoxylate shunt is AceA, which catalyzes the formation of glyoxylate (GLYOX) and succinate (SUC) from isocitrate (ICT). Subsequently, glyoxylate is converted to malate (MAL) and integrated into the TCA catalyzed through the enzyme GlcB [118]. Different metabolic states can shut down the TCA or the glyoxylate cycle respectively in *P. putida* [119]. For more detailed reactions in the EDEMP, PP, and TCA pathway, see Figure 2.6.

[3] (see KEGG database; https://www.genome.jp/pathway/map01230)

A promising substitute for conventional plastics - PHA

As mentioned above, *P. putida* can, among many other bacterial species, naturally accumulate polyhydroxyalkanoates, short PHAs. These are storage polyesters produced in unbalanced nutrient conditions, e.g., carbon excess and limitation of essential nutrients such as nitrogen, sulfur, or phosphor. PHA is handled as a promising bioplastic as it is biodegradable, biocompatible, and might be able to substitute some of the petroleum-based plastics [120]. PHAs are accumulated in so-called carbonosomes, which are insoluble hydrophobic granules. On their surface, proteins for polymerization, hydrolysis, and regulation are located, as well as structure-giving proteins can be found associated with the granules.

PHA can be divided into three main classes depending on the 3-(R)-hydroxyacyl (HA)-monomer length integrated into the polymer (see Table 2.2). A polymer consisting of monomers smaller than six carbons are termed short-chain-length (scl)-PHA. The homopolymer polyhydroxybutyrate (PHB) produced by *Cupriavidus necator* is the most prominent example. PHA built up of C6-C14 3-HA monomers, and are consequentially called medium-chain-length (mcl)-PHA, and polymers, which include even longer monomers, are termed long-chain-length (lcl)-PHA. The latter is rarely found in nature [121], [28].

Table 2.2: Overview of different PHA classes and example for microorganisms producing them.

Polymer class	**3-HA length**	**Examples**
Small chain length (scl)-PHA	< C6	Polyhydroxybutyrate (PHB, homopolymer); e.g. produced by *Cupriavidus necator*; poly(3-hyxdroxybutyrate-co-3-hydroxyvalerate) PHBV produced by *Haloferax mediterranei* with highest cell content of 47% [122].
Medium chain length (mcl)-PHA	C6 - C14	Usually different heteropolymers produced e.g. by Pseudomonads [123].
Long chain length (lcl)-PHA	> C14	No natural examples.
Aromatic PHAs	e.g. phenyl or benzoyl monomers	P(3H5PhV) produced by *P. oleovorans*; P(3HA-3H4BzB) *Pseudomonas cichorii* YN2 [124].
Other PHAs	mixed scl/mcl-PHA C4 and C6	Poly(3-hydroxybutyrate-co-3-hydroxyhexanoate) synthesized by *Aeromonas caviae* [125].

The accumulation of mcl-PHAs is highly conserved that in pseudomonads it can even function as a phylogenetic marker [28]. The first report of mcl-PHA production was with *P. putida* GPo1, formerly known as *P. oleovorans*, grown on n-octane [28]. *P. putida* KT2440 naturally accumulates mcl-PHA with a variable monomer composition of C6 to C14, depending on the substrate and reaction conditions. The incorporation of different monomers defines the physicochemical properties of the mcl-PHA polymer. *P. putida* carries two clusters of PHA-genes: The first operon consists of two mcl-PHA polymerases termed PhaC1 (PP_5003) and PhaC2 (PP_5005), a depolymerase called PhaZ (PP_5004) and a transcriptional activator (PP_5006), which acts on both PHA clusters as an activator. The second operon encodes the phasins PhaF (PP_5007) and PhaI (PP_5008), which are the proteins responsible for the regulation and structure of the PHA granules [28] (see Figure 2.7). The synthesis of PHA starts with integrating an (R)-3-hydroxyacyl-CoA unit into the existing polymer catalyzed by PhaC1 (or C2). The resulting polymer can, under carbon demand, be degraded into free (R)-HA monomers. Firstly, an (R)-3-hydroxy-acid molecule is split from the polymer via hydrolysis

catalyzed by PhaZ. It is subsequently activated with co-enzyme-A to an (R)-3-hydroxy-acyl-CoA over an acetyl(acyl)-CoA-synthetase (Acs). This mobilized monomer can enter the central metabolism or starts the PHA cycle once again (see Figure 2.7). In *P. putida* KT2440 more than six enzymes obtain CoA ligase activity necessary to mobilize the monomers. In contrast to *P. putida* GPo1, in *P. putida* KT2440 it is not completely revealed which enzymes act directly on the PHA polymer [28], [121].

The polymer can be synthesized from intermediates of the β-oxidation or through precursors derived from the fatty acid *de novo* synthesis. The fatty acids that are structurally similar to PHA are the preferred substrates for intracellular accumulation of mcl-PHA in *P. putida*. With octanoate, PHA accumulates up to 80 % of the bacterial cell dry weight [126]. An explanation for this is that fatty acids of 6 - 12 carbons are either directly incorporated in the polymer or just shortened by C2, C4, or C6 units [28]. However, carbon retrieved from sugars or aromatic compounds is directed to the fatty acid *de novo* synthesis to generate monomers. All those structurally non-related substrates to PHA are guided over the key intermediate acetyl-CoA (see Figure 2.7). Since FabA activity is restricted to 3-hydroxyacyl-ACP with ten carbons as substrates [127], a high content of 3-hydroxydecanoic acid is incorporated into PHA polymer [110] [128], when *P. putida* growths on PHA non-related substrates.

As far as current research indicates, the *de novo* synthesis of fatty acids is only linked to the PHA metabolism through the 3-hydroxyacyl-ACP-CoA transacylase (PhaG). For the β-oxidation, a conversion from 3-ketoacyl-CoA and an isomerization from (S)-3-hydroxyacyl-CoA to (R)-3-hydroxyacyl-CoA should be possible. However, the only experimentally verified connection to the PHA cycle is through trans-2-enoyl-CoA, catalyzed by PhaJ.

The PHA metabolism is overall a delicate cycle, tightly connected to the routes for fatty acid synthesis or degradation and even more embedded into the core carbon metabolism as the $\frac{NADPH}{NADP}$ ratio influences polymer synthesis as well [126]. PHAs are mostly produced under nutrient-imbalanced conditions resulting in a carbon excess combined with a nutrient limitation that results in high $\frac{C}{N}$, $\frac{C}{P}$, or $\frac{C}{S}$ ratios. When the sole carbon source is structurally non-related to PHA, a limitation significantly improves the accumulation of the corresponding polymer. Accumulation of mcl-PHA in *P. putida* KT2440 grown on sugars was found when imbalanced $\frac{C}{N}$ ratios were applied [29]. In literature, an optimal $\frac{C}{N}$ ratio of 26 is described when glucose is used as a sole substrate of *P. putida* KT2440 [29]. It leads to mcl-PHA accumulated up to 25% of cell dry weight [29]. The carbon to nutrient ratio $\frac{C}{X}$ can be defined as the carbon uptake r_{mol_C} [mol · h^{-1}] rate divided by nutrient uptake rate r_{mol_X} [mol · h^{-1}] [129]:

$$\frac{C}{X} = \frac{r_{mol_C}}{r_{mol_X}} \tag{2.10}$$

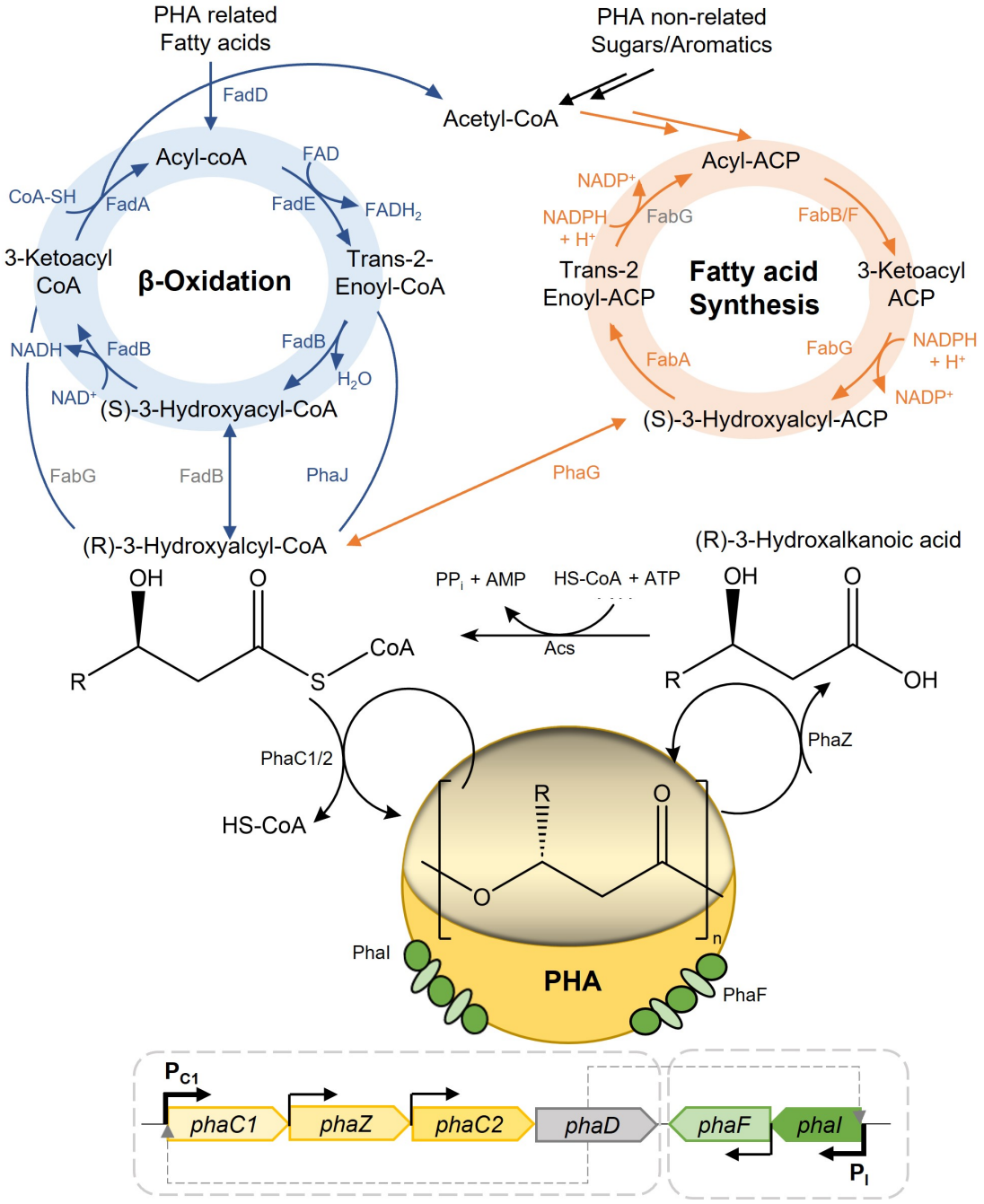

Figure 2.7: The two operons for PHA accumulation in *P. putida* KT2440 and the PHA-metabolism embedded in the central carbon metabolism. The first PHA-operon consists of *phaC1* and *phaC2*, which both encode PHA-polymerases, *phaZ* is the PHA-depolymerase, and *phaD* which encodes a transcriptional regulator activating transcription via interaction on main promoters (thick black arrow, P_{C1} and P_I) of both operons. The second operon (green) consists of *PhaF* and *phaI* encoding for phasins, which are responsible for the regulation and structure of the PHA granules. The surface of the PHA granule is the acting point of polymerization and depolymerization (hydrolysis). The polymer can be synthesized from different carbons sources. Substrates, structurally similar to PHA, such as fatty acids, are processed in the β-oxidation (blue reactions). The initial step of the β-oxidation is catalyzed through FadD, which activates free fatty acids into an acyl-coA. In subsequent reactions, fatty acids are degraded, and $FADH_2$ and NADH are formed (participating enzymes FadE, FadB, and FadA). Structurally non-similar substrates to PHA, such as sugars, come from the fatty acid *de novo* synthesis (orange) to from PHA monomers (participating enzymes FabB/F, FabG, and FabA). When enzymes are depicted in gray, it means that the reaction is not yet experimentally verified (FabG and FadB). AMP = adenosine monophosphate; ATP = adenosine triphosphate; CoA = coenzyme A; ACP = acyl carrier protein. The Figure was adapted from [28].

P. putida as chassis in biotechnology

As described above, *P. putida* is a highly capable microorganism and is thus suitable to function as a chassis in biotechnology. Since a chassis enables straightforward reconfiguration of its core metabolism to align with industry demands, it should further exhibit robust growth on various substrate classes used as feedstocks, while also demonstrating versatile capabilities in product production. The overall handling of the microbe should be easy and reproducible with high biomass accumulation and low by-product formation in processes [104]. All these points are tangible for *P. putida* due to its intrinsic metabolic properties and progress in synthetic biology approaches:

- *P. putida* can use a broad range of substrate classes, including lignin and octanoate [130], [131]. Further, due to its adaptable metabolism, it can thrive on waste streams, such as industrial oil.
- Through different genetic engineering strategies, the substrate spectrum could be expanded towards other substrates such as sucrose [27], D-cellobiose, or xylose [132].
- It is equipped with a high-stress resistance, which includes an advanced coping mechanism against oxidative stresses and degradation or adaption to solvents such as phenol [133].

Next to the intensely studied degradation of xenobiotics as efficient bioremediation microbe and the accumulation of mcl-PHA (see above), *P. putida* is capable of degrading lignin-derived aromatics [134]. In soil-associated bacteria, aromatic compound degradation takes place in the β-ketoadipate pathway. In *P. putida* ortho-cleavage route of the β-ketoadipate pathway is encoded on the chromosome, which enables the bacterium to grow on benzoate as the sole carbon and energy source [135]. That opens the possibility for new feedstocks in processes with *P. putida* (see Figure 2.8).

The product spectrum of *P. putida* KT2440 can be increased through a whole set of genome-modifying tools. For example, the production of terpenoids, such as the yellow-colored carotenoid zeaxanthin, was achieved by introducing the carotenoid biosynthesis genes from *Pantoea ananatis* DSM30080 and over-expression of three genes from the methyl-D-erythritol phosphate (MEP) pathway [134]. Recently, *P. putida* was engineered to produce l-theanine, a taste-enhancing free amino acid, normally found in green tea [136]. Another product which paves the way for *P. putida* as chassis in the industry is 2-quinoxalinecarboxylic acid, which can be produced with *P. putida* ATCC 33015 as whole cell biocatalyst [137].

High cell-density cultivation is one of the keys to industrial processes. It was possible to produce a final cell dry weight of 120 g L^{-1} in 33 h with *P. putida* without the supply of oxygen [138]. At the industrial scale, stresses such as substrate gradients due to inhomogeneous mixing can occur. As a result, the bioreactor builds up regions of nutrient starvation. To investigate how *P. putida* can handle such an environment, a stirred-tank bioreactor was combined with a plug-flow reactor in which the stress condition of glucose (or carbon) starvation were simulated [139]. The cells reacted quickly upon starvation with an accumulation of PHA, glycogen, and a supply of amino acids from proteins. Another stress situation might be uneven oxygen distribution in industrial-scale bioreactors. Recently, a study showed that *P. putida* can cope with short anoxygenic phases despite being a strict aerobic microbe. Further, a lack of oxygen confined little changes in the proteome of the microbe [140].

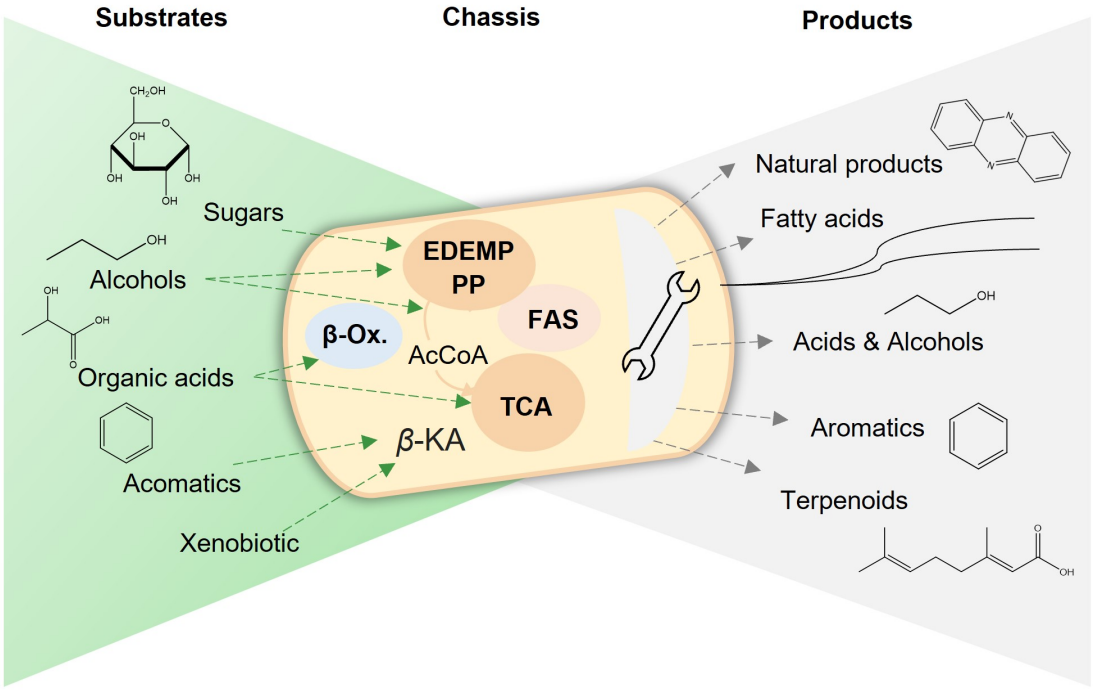

Figure 2.8: *P. putida* as a chassis in bioproduction of value-added products. It grow on various substrate classes such as sugars, aromatics or xenobiotics and its inherent metabolism can convert it to valuable precursors. These precursors can be directly used or easily transformed into required products through genetic manipulations. Common product classes are alcohols, organic acids, terpenoids or natural products, e.g. phenanzine. EDEMP = combination of Enter-Doudoroff pathway and Emden-Meyerhof-Parnas pathway, PP = Pentose phosphate pathway, TCA = tricarboxylic acid cycle, β-Ox. = β-oxidation, FAS = fatty acid *de-novo* synthesis, β-KA = β-ketoadipate, AcCoA = acetyl-coenzyme-A. The Figure was adapted according to Weimer et al. [104].

2.3.2 The phototrophic partner: *Synechococcus elongatus*

The gram-negative in freshwater living *S. elongatus* PCC 7942 has a small and fully sequenced genome of 2.7 Mbp. It is naturally competent, and various tools have been established to genetically modify the cyanobacterium over the last few decades [141]. It is, next to *Synechocistis*, handled as a model cyanobacterium for research on the circadian clock [142], [143], understanding prokaryotic photosynthesis and is a promising candidate to serve as a platform organism for bioproduction [144], [145]. Today, models for metabolic engineering are available, and recently a condensed version of the genome-scale model iJB792 was developed for the *in-silico* analysis of omega-3-fatty acid production (iMS837) [146], [95]. Latest transcriptomic and proteomics studies, e.g., concerning the nitrogen starvation of the cyanobacterium [147], can complement models or provide new hypothesis.

Cyanobacteria and their photosynthetic efficiency

With climate change gaining ground and with ever-so-rising CO_2 concentration, organisms able to remove the greenhouse gas from the atmosphere are handled as one promising building block to face it. Cyanobacteria are prokaryotes that are capable of performing oxygenic photosynthesis, which means they use H_2O as an electron donor and produce O_2 as a side-product. This first step absorbs energy from light to produce NADPH and ATP, which can be considered energy molecules and are spent in the second step. Here, CO_2 is fixed into 3-phosphoglycerate and subsequently used to build up higher carbohydrates or biomass (see Figure 2.9)

[54]. The Calvin cycle can be divided into carboxylation, reduction and regeneration: The anorganic carbon fixation is performed from a 1,5-bisphosphate carboxlase/oxygenase (RubisCO). RubisCO, developed in an oxygen-free atmosphere and therefore, has a low affinity towards CO_2. It can unspecifically react with O_2 producing 2-phosphoglycolate. In principle, carbon is a valuable resource, and microbes that turn a share of it into value-added products such as alcohols, lipids, or carbohydrates could reduce traditional, often CO_2-emitting production routes. Cyanobacteria offer several advantages compared to algae or terrestrial plants. For example, they tend to have slightly higher photosynthetic efficiency compared to plants (cyanobacteria 5% compared to C3 $\sim$ 3.5% and C4 $\sim$ 4.3%) when grown under optimal conditions [52]. Another definition of photosynthetic efficiency considers the annually obtained biomass per area used. In this case, crop plant photosynthetic efficiency drops below 1%, whereby cyanobacteria can reach an efficiency of 3% [52]. The reasons for higher efficiency are that cyanobacteria can be cultivated in brackish or seawater, so they do not compete with agricultural land or freshwater, and they do not maintain photosynthetically inactive components such as stems or roots. Further, some cyanobacteria can accumulate more biomass compared to plants [53], [148].

Carbohydrate synthesis in S. elongatus

Cyanobacteria mostly accumulate polysaccharides such as glycogen or as lipids when nutrient limitation or variation in light occurs. Glycogen is a branched α-polyglucan and is derived from the synthesis of glucose (see Figure 2.9) [149]. Further, it is handled as a carbon sink among cyanobacteria. Recently the genetic regulation of the glycogen metabolism and content was successfully deciphered in *S. elonatus* PCC 7942 [150]. It was observed that a mutant of *Synechocystis* sp. PCC 6803, which is unable to accumulate glycogen, balances its excess energy with other overflow metabolites such as pyruvate [151]. The most abundant stress factor cyanobacteria have to cope with is varying salinity levels [99]. That induces two forms of stress: 1) high osmotic pressure and 2) high ionic strength. At high salt concentration, the salt-out strategy, which involves the active export of ions (Na^+, Cl^-) as well as the production of osmoprotectants, is induced. These osmotic active substances are organic compounds of low molecular weight, such as sucrose or trehalose [99], [152]. The accumulation of these compounds balances the osmotic gradient between the cytoplasm and the surrounding and further prevents the loss of internal water. For cyanobacteria with low salt tolerance, as *S. elongatus*, it is common to synthesize sucrose *de novo* as a compatible solute. Sucrose is a disaccharide of glucose and fructose connected by a α,β- 1 $\rightarrow$ 2 glycosidic bond.

The biosynthesis of sucrose is directly connected to the Calvin cycle and thus connected to the light-independent phase of photosynthesis, see Figure 2.9. For the sucrose production, after the CO_2-fixation in the Calvin cycle, two key enzymes are necessary: The sucrose phosphate synthase (SPS), which connects activated nucleotide-glucose (NDP-glc) with fructose-6-phosphate (F6P) to sucrose-6-phosphate (S6P) and then the subsequent sucrose phosphate phosphatase (SPP) dephosphorylates S6P to sucrose (see Figure 2.9) [152]. The first step of sucrose synthesis is reversible, and the rate-limiting reaction is catalyzed by SPS, which transfers the glycosyl group from an activated sugar such as UDP or ADP-glucose to the acceptor fructose-6-phosphate. The second step is irreversible hydrolysis of the phosphate moiety from S6P of the phosphatase SPP, which acts highly specifically [152]. The small genome of *S. elongatus* encodes only a fused protein for sucrose synthesis, with a domain that has an SPS and SPP functionality. It was showen that the SPS domain is activated by ions, which matches the finding that the ionic strength had

more influence on sucrose accumulation than the osmotic pressure [99]. The regulation on a transcriptional level of sucrose synthesis is poorly understood in *S. elongatus* PCC 7942. In *Nostoc* sp. PCC 7120, a two-component regulator OrrA was described, which might repress the expression of *sps* at low salinity levels [53]. Further, the degradation of comparable solutes and the delicate balancing of synthesis/degradation is not completely understood. In *S. elongatus*, the sucrose invertase encoded by Synpcc7942_0397 was recently discovered as the sole sucrose degradation enzyme [99]. As mentioned above, genetic modification of different *Synechococcus* species allowed secretion of sucrose into the medium in the presence of salt stress through the genomic introduction of sucrose-transporter [152], [153]. *S. elongatus* PCC 7942 has a medium salinity resistance of about 0.9% ($\sim$ 150 mM NaCl; brackish water has up to 3% salinity) [24]. The induction of the integrated CscB sucrose H^+-symporter reduces the biomass accumulation and glycogen formation by redirecting the carbon flow towards sucrose secretion of *S. elongatus cscB* but increases the total carbon fixation in the cyanobacterium [24]. With over-expression of *sps*, an improvement of sucrose secretion in the close-relative *S. elongatus* UTEX 2973 [154] without salt stress was achieved.

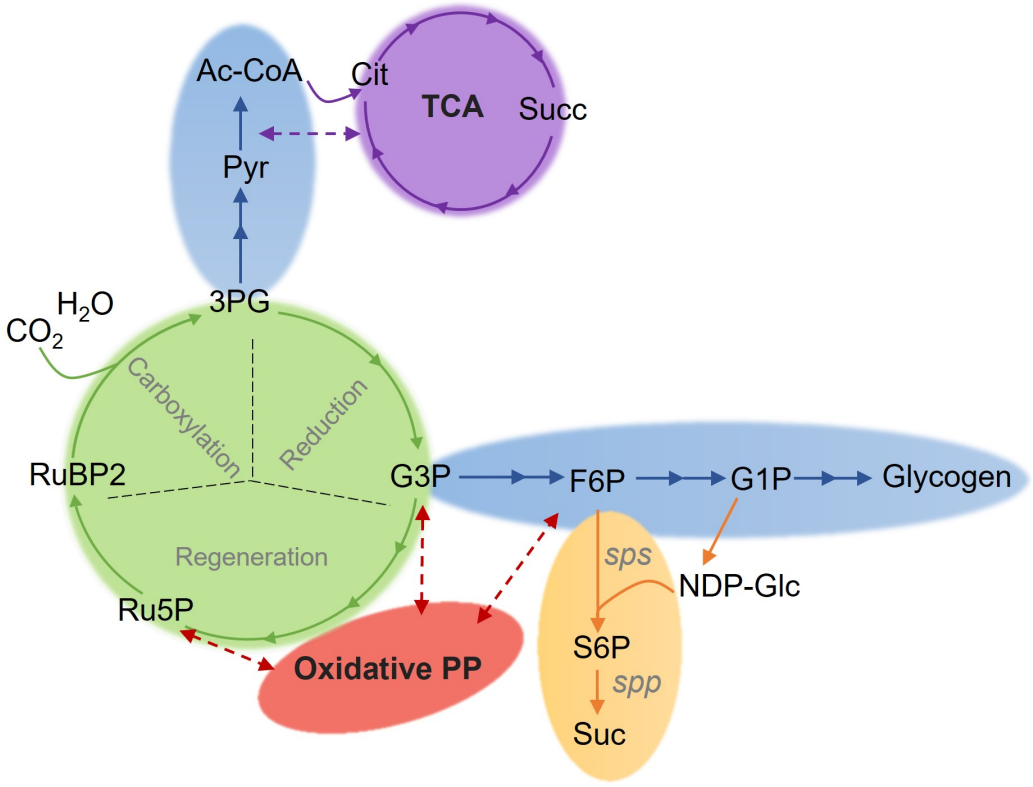

Figure 2.9: Schematic visualisation of the carbon core metabolism of *S. elongatus*. Green cycle represents the Calvin cycle consisting of three major steps: carboxylation, reduction of 3-phosphorglycerate (3PG) to glycerinaldehyde-3-phosphate (G3P), and regeneration of ribulose-1,5-bisphosphate (RuBP2) over multiple steps as ribulose-5-phosphate (Ru5P). Blue areas mark reactions connected to gluconeogenesis; one starting from G3P forming among others fructose-6-phosphate (F6P) and glucose-1-phosphate (G1P) and is connected to the carbon storage molecule glycogen. Over F6P and a nucleoside diphosphate (NDP = nucleoside diphosphates) activated glucose (NDP-Glc), sucrose-6-phosphate can be synthesised and subsequently sucrose (Suc) is formed. The key enzymes for sucrose *de novo* synthesis are the sucrose phosphate synthase (SPS) which catalyses the reaction to S6P and sucrose phosphate phosphatase (SPP) which catalysis the dephosphorylation to sucrose. The other metabolic path connected to gluconeogenesis or pyruvate oxidation starts from 3-PG forming pyruvate (Pyr) or acetyl-CoA (Ac-CoA), which forms a connection to the tricarboxylic acid cycle (TCA, purple cycle) with many intermediates such as citrate (Cit) and succinate (Succ). Further connections are indicated through a purple dashed arrow. The connection of the Calvin cylcle to the oxidative pentose phosphate (PP) cycle is indicated through red dashed arrows.

Light-driven bioproduction with Cyanobacteria

Cyanobacteria are hold as promising factories for generating alternative feedstocks, as they can accumulate and secrete carbohydrates from light and CO_2. Likewise, cyanobacteria are considered as new sustainable platform organisms which can produce various chemicals, such as biofuels. Due to the search for alternatives to petrol-based fuels, hydrogen is handled as a promising clean fuel. Recent progress in genetically modifying *Anabeaena* sp. PCC 7120 led to the production of 6 times more hydrogen than with the wild type. Other biofuels produced by cyanobacteria are ethanol (0.23 g L^{-1} *S. elongatus* PCC 7942, 5.5 g L^{-1} *Synechocystis* sp. PCC 6803), isobutyraldehyde and isobutanol produced with *S. elongatus* PCC 7942. In Synechocystis PCC 6803, L-lactic acid, a building block for various other industries, was produced with a titer of 1.8 g L^{-1}. Some cyanobacteria can accumulate poly-3-hydroxybutyrate (PHB) under unbalanced nutrient conditions. However, accumulation in un-engineered strains, as *Synechocystis* sp. PCC 6803 is low,

and some cyanobacteria, as *S. elognatus* PCC 7942, are reported not to accumulate PHB [155]. Further, the physiological reasons for cyanobacteria to produce PHB are not completely understood. For example, PHB accumulation under various abiotic stresses, such as nitrogen starvation, did not result in improved fitness compared to PHB-free mutants of *Synechocystis* Δ*phaEC* [156]. Recent studies have enhanced the accumulation of PHB by metabolically engineered cyanobacteria and/or via improved culture conditions and medium composition. Phototrophic biotechnological processes are not yet economically feasible because of problems such as lacking scalability of bioreactors or biomass accumulation limitation due to shading effects [53].

3 Material and Methods

3.1 Bacterial strains

Table 3.1: Used heterotrophic and phototrophic bacterial strains.

Strain name	Description	Function and reference
P. putida EM178	Prophage-free derivative of *P. putida* KT2440 ΔPP3849-PP3920 (prophage 1), ΔPP3026-PP3066 (prophage 2), ΔPP2266-PP2297 (prophage 3), ΔPP1532-PP1586 (prophage 4)	Reference strain in growth experiments [157].
P. putida EM178 *att*Tn7::*cscRABY*	*P. putida* EM178 with genomic integrated *cscRABY*-operon from *Pseudomonas protegens* Pf-5	Strain used as heterotrophic co-culture partner [27].
P. putida EM178 *att*Tn7::*cscRABY* ΔnasT	Derivative of *P. putida* EM178 *att*Tn7::*cscRABY* with deletion of the *nasT* gene (PP_2093) encoding a response regulator receiver protein	Strain used as heterotrophic co-culture partner [30].
P. putida KT2440 Δ*gcd*	Derivative of *P. putida* KT2440 with deletion of *gcd* gene (PP_1444), which encodes for a quinoprotein glucose dehydrogenase	Reference strain in growth experiments or recipient strain for conjugation [126].
P. putida KT2440 Δ*gcd* attTn7:: *cscRABY*	Derivative of *P. putida* KT2440 Δ*gcd* with genomic integration of the sucrose operon *cscRABY* from *P. protegens*	Analyzed for mcl-PHA accumulation derived from this study.
E. coli HB101 (pRK600)	F$^-$ λ hsdS20(rB^- mB^-) recA13 leuB6(Am) araC14 Δ(gpt-proA)62 lacY1 galK2(Oc) xyl-5 mtl-1 thiE1 rpsL20(Sm^R) glnX44(AS)	Strain for quarto parental mating; Contains helper plasmid [158].
E. coli DH5α λpir (pTnS1)	Derivative of *E. coli* DH5α λpir, contains a mini Tn7 encoding transposase	Strain for quatro parental mating [159].
E. coli DH5α λpir (pTnS1 pTn7-M(*cscRABY*))	Derivative of *E. coli* DH5α λpir, carrying the plasmid with the sucrose-operon *cscRABY*	Donor strain for quatro parental mating [27].
S. elongatus PCC 7942 *cscB*	Derivative of *S. elongatus* PCC 7942 with gnomic integrated *cscB* gene in neutral site 3 (ns3) from *E. coli* EDL933	Strain used as phototrophic co-culture partner [24].

3.2 Media

LB-Medium - (Lysogeny Broth): For pre-cultures or undefined growth conditions, LB-Medium was used. The medium was made in advance. The LB agar plates were prepared by adding 15 g L^{-1} agar-agar to the liquid medium.

Table 3.2: LB-Medium and LB-Agar.

Medium component	**Concentration, g L^{-1}**
NaCl	10
Typtone/Peptone	10
Yeast extract	5
Agar-agar	15

Minimal media for the heterotrophic partner: For defined cultivation conditions, the minimal medium M9 was used with different carbon sources depending on the metabolic characteristics of the *P. putida* derivative used. The medium was freshly prepared from the separately steam sterilized stock solutions (see Table 3.3). For M9-agar plates, 15 g L^{-1} agar-agar was added to the medium. For experiments with different nitrogen sources, a nitrogen-free M9 10X salt solution was prepared (see Table 3.4).

Table 3.3: M9 minimal medium and M9 agar-plates with different carbon source.

Medium Component	**Volume, mL L^{-1}**
M9 salt stock solution (10 X)	100
$MgSO_4$	2
Carbon-source (100 g L^{-1})	30
Agar-agar	15 g L^{-1}

Table 3.4: 10X salt stock solution for M9 medium.

Medium component	**Concentration, mM**
$Na_2HPO_4 \cdot 2\,H_2O$ I	420
KH_2PO_4	220
NaCl	86
NH_4Cl	187

Minimal media for the phototropic partner and the co-culture: For defined cultivation conditions in axenic cultures of *S. elongatus cscB* and the co-culture, a modified version of the BG11 medium was used. The medium stock solutions were separately steam sterilized, except for stock solution II, which was sterile filtrated (cut-off 0.2 µm), aliquoted into 2 mL tubes, and frozen at -20 °C. The medium was freshly prepared when needed and sterile filtrated after the components were mixed together. For $BG11^+$ plates 2X-$BG11^+$ was prepared and mixed with heated water-agar solution (30 g L^{-1} agar-agar in H_2O).

Table 3.5: BG11$^+$-Medium and BG11$^+$-Agar modified after Löwe et al. [25].

Medium component	Volume per L, mL^{-1}
Stock solution I	1
Stock solution II	1
$NaNO_3$ (3.53 M)	5
K_2HPO_4 (1.72 M)	1
$MgSO_4 \cdot 7\,H_2O$ (1 M)	2.74
DIW	add to 1 L
Agar-agar	15 g L^{-1}

Table 3.6: Stock solution I for BG11$^+$-medium [25].

Medium component	Concentration, g L^{-1}
$Co(NO_3)_2 \cdot 6\,H_2O$ I	0.049
$CuSO_4 \cdot 5\,H_2O$	0.079
H_3BO_3	2.86
$MnCl_2 \cdot 4\,H_2O$	1.81
$Na_2MoO_4 \cdot 2\,H_2O$	0.39
$ZnSO_4 \cdot 7\,H_2O$	0.22

Table 3.7: Stock solution II for BG11$^+$-medium [25].

Medium component	Concentration, g L^{-1}
Ammonium iron(II) citrate (14 - 18 % iron content)	6
$CaCl_2 \cdot 2\,H_2O$	0.079
Citric acid	5
$MgSO_4 \cdot 7\,H_2O$	75
$Na-EDTA \cdot 2\,H_2O$	1.1
DIW	add to 1 L

3.3 Buffer and solutions

Table 3.8: NaCl-solution for flow cytometry.

Medium component	Concentration, g L^{-1}
NaCl	8.5
DIW	add to 1 L

Table 3.9: 1-propanol-HCl solution for propanolysis.

Medium component	Concentration, ml (100 mL)$^{-1}$
HCl	20
1-propanol	80

Table 3.10: PBS buffer for dilution series.

Medium component	Concentration, g L^{-1}
NaCl	0.8
KCl	0.2
$Na_2HPO_4 \cdot 2H_2O$	1.78
KH_2PO_4	0.27
DIW	add to 1 L

3.4 Small-scale cultivation of axenic and co-cultures

3.4.1 Preservation and maintenance of microbes

S. elongatus cscB

First, a liquid stationary culture was streaked out onto $BG11^+$ plates to achieve single colonies of the cyanobacterium. The plate was illuminated at 22 µmol m^{-2} s^{-1} and incubated at 30 °C. After colonies had formed, a single colony was transferred into a 100 mL shake flask without baffles, filled with 10 mL $BG11^+$ and incubated at 30 °C, 22 µmol m^{-2} s^{-1}, and 120 rpm in an orbital shaker (Multitron Pro from Infors HT, Switzerland) without additional aeration. After cells reached the stationary phase, they were harvested by centrifugation for 5 min. at 4,000 g and 4 °C. Then the cells were resuspended in 5 mL $BG11^+$ supplemented with 3% (v/v) dimethyl sulfoxide (DMSO) for cryopreservation and subsequently aliquoted into cooled (-80 °C) 1 mL cryo-preservation tubes. For long-term storage, cells were kept at -80 °C.

P. putida derivatives

For long-term storage of *P. putida* derivative cells, a 3 mL LB-medium culture was prepared overnight. The next day, the cells were centrifuged for 1 min. at 8,000 g, 4 °C, and were subsequently resuspended in 3 mL fresh LB-medium. After this, 500 µL of the bacterial culture was mixed with an equal volume of a sterile glycerol:water solution (50% v/v) and filled in a 1 mL cryopreservation tube. Long-term storage was at -80 °C, and short-term storage was at -20 °C.

3.4.2 Pre-cultures of *S. elongatus cscB*

Pre-cultures for cultivation in the flat-panel photobioreactor

Firstly, the cryoperseved *S. elongatus cscB* cell were defrosted and subsequently washed with freshly prepared $BG11^+$ medium. For this, cells were centrifuged at 6,500 g for 5 min. at room temperature, the supernatant was discarded, and the remaining pellet was resuspended in 1 mL of the medium. The procedure was repeated twice, and in the end, cells were resuspended in 3 mL $BG11^+$ medium in a 50 mL falcon. For light-acclimatization, cells were kept at low illumination for 1-2 days. After this, the cyanobacteria were transferred into an unbaffled 100 mL shake flask and filled with medium to a final volume of 20 mL. These cultivation flasks were capped with cellulose plugs to decrease water loss due to illumination. The cyanobacteria were cultivated until they reached the stationary phase after 7-10 days. The conditions were: 25-30 °C, a constant photon flux density of 20-22 µmol m^{-2} s^{-1} and 120 rpm in an orbital shaker (Multitron Pro from Infors HT, Switzerland), without additional aeration of CO_2. After cells reached the stationary phase, they were harvested and used as a starter culture in different experiments.

Pre-cultures for cultivation in a parallelized membrane reactor system

S. elongatus pre-cultures were first grown in BG11$^+$ medium under the conditions described above. After reaching the stationary phase, the cultures were transferred to BG11$^+$ medium supplemented with 150 mM NaCl, inoculated in a 1:20 (v/v) ratio, and grown under the same conditions. The salt-acclimatized phototropic cultures were used to investigate potential interactions of the co-culture partner.

3.4.3 Pre-cultures of *P. putida* derivatives

The pre-cultures of the different *P. putida* derivatives always started with an LB culture of 3-5 mL. After this, cells were transferred to the minimal medium either BG11$^+$ or M9-medium supplemented with a carbon source. In some cases, a third pre-culture followed where BG11$^+$ supplemented with a carbon source and an additional 150 mM NaCl was used to adapt the cells to the salt stress.

Pre-cultures of P. putida derivatives for cultivation in a flat-panel photobioreactor

Heterotrophic pre-cultures of *P. putida* derivatives were grown in 5 mL LB-medium overnight at 30 °C and 220 rpm (MaxQ 8000 from Thermo Scientific, USA). 100 µL of the culture were transferred to 5 mL BG11$^+$ medium supplemented with 1-3 g L^{-1} sucrose and in the case of *P. putida cscRABY* Δ*nasT* growth was supported with addition of 1 g L^{-1} urea. After this, the cells were transferred to a third pre-culture with a defined inoculation ratio of 1:1000 (% v/v) in 250 ml shake flasks filled with 10 mL BG11$^+$ medium supplemented with 150 mM NaCl. The cultures were cultivated under the same conditions as the pre-cultures.

Pre-cultures of P. putida cscRABY for cultivation in a parallelized membrane reactor system

Pre-cultures of *P. putida* were grown in 3 mL LB-medium at 30 °C and 220 rpm (MaxQ 8000 from Thermo Scientific, USA). Subsequently 100 µL were transferred to a second pre-culture consisting of 3 mL BG11$^+$ medium with 3 g L^{-1} sucrose and grown overnight. For the interaction reference experiment, the stationary *P. putida cscRABY* cultures were transferred into BG11$^+$ medium supplemented with 150 mM NaCl and 1-3 g L^{-1} sucrose in 100 mL shake flasks without baffles and grown under the same conditions as the pre-cultures. The cultures were centrifuged (4,000 g, 5 min.) and then resuspended in fresh 5 mL BG11$^+$ supplemented with 150 mM NaCl before being added to the membrane reactors.

3.4.4 Growth experiment of *P. putida* derivatives

For growth experiments with *P. putida* derivatives, an LB pre-culture was inoculated by transferring an individual colony from an LB plate or by transferring a small amount of frozen cells from a cryopreserved tube (see cryopreservation in Section 3.4.1). After cultivation overnight, a second pre-culture in M9-medium supplemented with an appropriate carbon source was inoculated from this LB pre-culture. The resulting pre-culture was then used to inoculate the main culture with a start OD_{600} of 0.05-0.1. Growth experiments were usually performed in 250 mL shake flasks and filled with 20% M9-medium to guarantee optimal oxygen supply. Experiments consisted of at least biological triplicates. In the exponential phase, samples for OD_{600} or flow cytometry were taken every 1-2 h. OD_{600} was measured with a plate reader photometer (Tecan plate reader Infinite 200 PRO). Depending on the metabolic properties of the derivatives, different carbon and nitrogen sources were used.

3.4.5 Co-cultivation in 12-well plates

Experiments were performed in 12-well plates (Brand, Germany) at a 1.6 mL scale to investigate potential interactions between the co-culture partners. *S. elongatus cscB* was inoculated to an OD_{750} of 0.05 in $BG11^+$ medium supplemented with 150 mM NaCl and cells were acclimated for two days to salt and other conditions (25–30 °C, 120 rpm, 20 µmol photons m^{-2} s^{-1}, incubator Multitron Pro from Infors HT from Switzerland). No additional aeration was provided, and the plates were sealed with laboratory film (Parafilm M, United States) to prevent water evaporation. Water loss was considered by verifying the volume left in the wells at the end of the experiment. Gene expression of the sucrose transporter CscB in cyanobacterial cultures was induced with 0.1 mM Isopropyl ß-D-1-thiogalactopyranoside (IPTG). For analysing the interaction independently of the sucrose feed an extra batch of sucrose of 1 g L^{-1} was added to support heterotrophic growth at the beginning of the experiment. Co-cultures were started with different cell counts of *P. putida cscRABY* to achieve different phototroph:heterotroph ratios. For experiments in darkness, the plates were covered in tinfoil. To check for (cross)-contamination of the induced axenic growing cyanobacteria, regular streaks on LB plates and subsequent incubation at 30 °C for heterotrophic growth were performed.

3.4.6 Co-cultivation in shake flasks

The pre-cultures of *S. elongatus cscB* and *P. putida* derivatives were performed as described in Sections 3.4.2 and 3.4.3. For co-cultivation, two scales of shake flasks (100 mL or 250 mL) were used and filled with 20% (v/v) $BG11^+$ medium supplemented with 150 mM NaCl. The phototrophic partner was either induced with 0.1 mM IPTG, or a batch sucrose of 1-3 g L^{-1} was added to the cultures to support heterotrophic growth. Normally, an acclimatization phase of 1-2 days for the phototrophic partner to the reaction condition preceded the co-culture phase (30 °C, 22 µmol photons m^{-2} s^{-1}, and 120 rpm without additional aeration). The co-cultivation was started by adding a *P. putida* derivative in different inoculation ratios (e.g. 1:1). Samples were taken once a day and optical density, cell count, and sucrose concentration were determined (details in Section 3.6.5 and 3.6.3).

3.5 Co-cultivation in a flat-panel photobioreactor

Liter-scale cultivations of the synthetic co-culture of *S. elongatus cscB* and different *P. putida* derivatives were performed in an airlift flat-panel photobioreactor (PBR) Labfors Lux 5 (Infors HT, Switzerland) with an working-volume of 1.8 L. It consists of the reactor station, which is connected to an external computer and a cultivation vessel.

Reactor station

The process conditions, such as temperature, pH, and dissolved oxygen (DO), can be tightly controlled and monitored with the software Iris 6.0. Furthermore, the reactor station offers connection ports for four peristaltic pumps, which can be used for substrate feed, supply with anti-foam, or to adjust the pH with acid or base. On the other side of the station a water-cooled white light-emitting diode (LED) panel, which can reach a maximum photon flux density of up to 3,000 µmol m^{-2} s^{-1}, is attached. A gas mixing station allows defining a gas mixture of air (or O_2) and CO_2

Cultivation vessel

The photobioreactor has two chambers separated through a glass panel, both are embedded in a stainless steel case. The cultivation chamber, which is placed in front of the LED, offers the microbes a place to grow, and a subsequent cooling chamber helps temper the vessel as wished. A temperature probe can be inserted into the cultivation chamber from the top of the reactor. The reactor station (for heating) and an external chiller allow controlling the temperature of the process. The cultivation chamber has a 2 cm thickness and within it, a 25.3 cm long and 1.93 cm wide baffle is attached to a perforated metal tube where gassing takes place (sparger). This allows the supply with gasses, such as CO_2 (or O_2), and homogenization of the culture broth. The mixing in the flat-panel photobioreactor follows the gas lift principle. The aeration induces circulation of the culture broth between the gassed liquid with lower density and the other side of the baffle, where the liquid sinks due to a higher density [160]. The stainless steel frame of the cultivation chamber is equipped with multiple ports. In the used setup of the reactor, four of these ports were equipped with a pH-probe, pO_2-probe, exhaust gas cooler, and the *super safe sampler* as an aseptic sampling system (Infors, HT). Additionally, a septum was integrated for inoculation of the bioreactor with bacterial cells. Furthermore, two couplings were fixed on the top of the reactor to connect a feed or refill the cultivation vessel with the medium. On the bottom of the reactor, a drain valve was connected for discharging liquids from the cultivation vessel. See Figure 3.1 **A** for a schematic visualisation of the PBR and Figure 3.1 **B** for the bioreactor during a process in the lab.

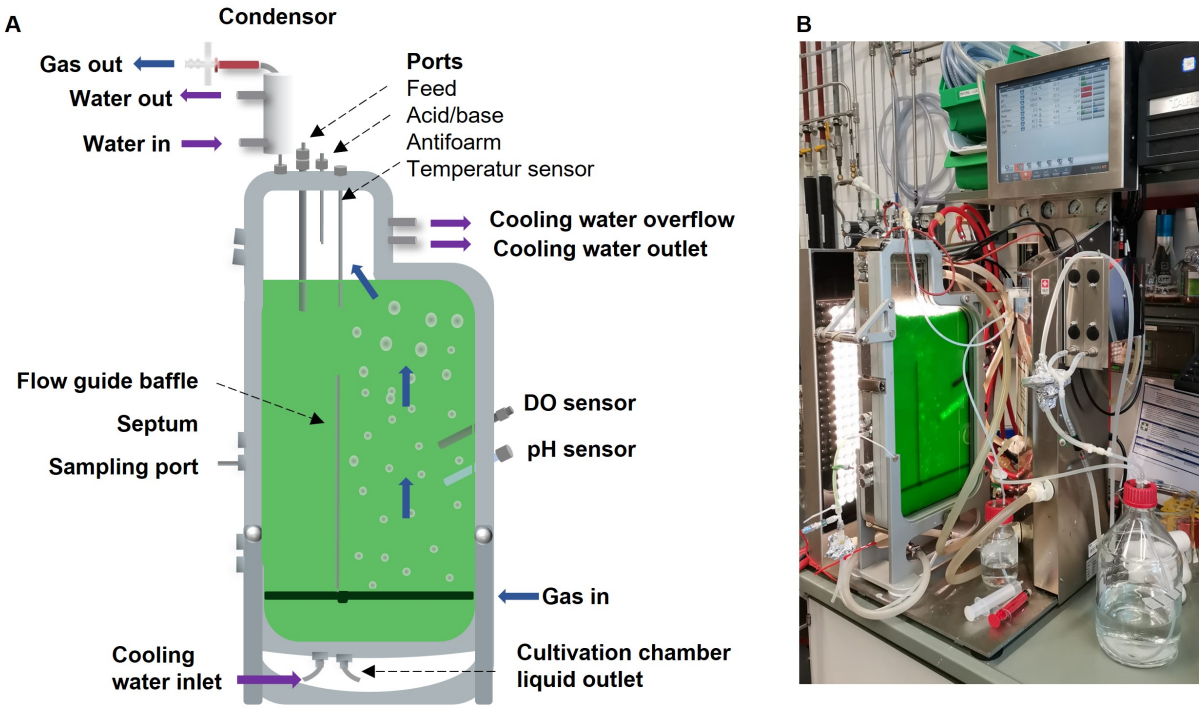

Figure 3.1: **(A)** Shows a schematic visualization of the airlift photobioreactor Lux 5 from Labfors (Infors HT, Switzerland). → (Blue arrow) shows the path of the gas from the dispenser to the gas outlet. The gas induces a circulation of the culture broth guided by a flow guide baffle. The flow of cooling water in the cooling chamber, located behind the cultivation chamber, is indicated by (violet arrows) →. Ports for the antifoam, temperature sensor, and other optional components are positioned at the top of the reactor vessel. At the opposite side from the sensors, the sampling port and septum can be integrated. The Figure was adapted from Infors[1]. **(B)** Shows a co-cultivation process with the photobioreactor in the lab.

Before a process was started, the PBR was steam-sterilized completely filled with 30 mM KCl solution to protect the pH-probe at 121 ℃ for 20 min. After cooling the reactor to ∼ 70 ℃, it was connected to the reactor station. The KCl solution was subsequently sterile discharged over the drain valve at the bottom of the vessel. In the meantime, sterile 1.8 L of $BG11^+$ medium supplemented with 150 mM NaCl was prepared and filled into the reactor with a peristaltic pump over a coupling at the top of the PBR. Simultaneously, the airflow was switched on to 1.96 L min^{-1} enriched with 2% CO_2 (40 mNL min^{-1}). The gas flow was saturated with water in a pressure stable 2 L bottle connected to a sterile filter to prevent the concentration of the culture broth due to drying effects. At the beginning of each process, the pH was adjusted to 7.4 with 1 M NaOH, except for the nitrate unlimited process where 1 M HNO_3 was used (see Section 4.1.2). After reaching the pH equilibrium, the reactor was inoculated with 10-20 mL of a stationary *S. elongatus cscB* culture to reach a start OD_{750} between 0.05 and 0.1 (see Section 3.4.2). For this, cells were harvested by centrifugation at 3,200 g for 3 min. at room temperature and washed once with 5 mL $BG11^+$ medium supplemented with 150 mM NaCl. After the second centrifugation under the same conditions, cells were suspended in 2-3 mL $BG11^+$ medium supplemented with 150 mM NaCl and injected into the reactor over the lateral implemented septum with a sterile cannula. This resulted in an optical density of approx. 0.1 at 750 nm (Eppendorf Biospectrometer basic photometer). In the case of nitrite-limited processes, nitrogen-free $BG11^+$ medium was used to wash and resuspend the cells. After inoculation, the light (PFD = photon flux density) was set to ∼ 240 µmol m^{-2} s^{-1}, which was adjusted applying the Equation (3.1) (∼10 %, see Figure 3.2). Usually, a substrate

[1](https://www.infors-ht.com/de/)

unlimited and axenic acclimatization phase to light and salt for the cyanobacterium followed. During the whole process, the temperature was controlled to 30 °C. Sucrose secretion was induced by adding 180 µL (0.1 mM) IPTG to the reaction vessel over the septum. The co-culture phase of the process was started after approx. two days with the inoculation of a *P. putida* derivative. *P. putida* pre-cultures were prepared as described in Section 3.4.3 and washed twice with $BG11^{+}$ medium supplemented with NaCl under the same condition as *S. elongatus cscB* pre-cultures. 1 mL sterile polypropylene glycol (10% antifoam) was added to the bioreactor through the septum when needed. Samples of 5-10 mL were taken once a day using the super-safe sampler. The optical density and cell count were measured. Further, carbohydrates, PHA, and nitrogen were analyzed (see Sections 3.6.1-3.6.4). The process volume was approximately constant during the process, as the gas was saturated with sterile water, the cooling of the exhaust was adapted to the process, and samples were taken. The process was shut down when the stationary phase of the co-culture partners was reached. After completion of the process, the culture broth was drained through the reactor's bottom valve, and the cultivation chamber was filled with fresh water after removing the probes. Then the reactor was sterilized at 120 °C, 1 bar over-pressure for 20 minutes, and subsequently disassembled and cleaned with water and 80% ethanol.

$$PFD = 19.75 \cdot I_{set} + 42.62 \tag{3.1}$$

The Equation (3.1) describes the PFD in µmol m^{-2} s^{-1}, when the set light intensity is given in %.

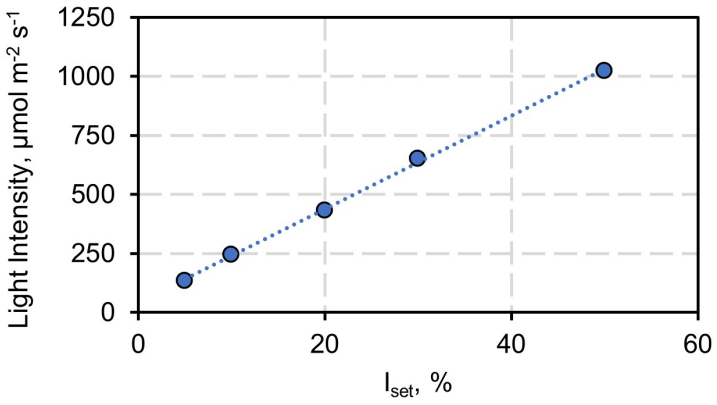

Figure 3.2: Correlation of adjusted light intensity I_{set} in % at the reactor station and light intensity in µmol m^{-2} s^{-1}.

For PHA accumulation, nitrogen limitation for the heterotrophic partner needed to be implemented. Therefore, co-culture processes either had urea, nitrate, or both feeds to achieve nitrogen separation of the co-culture partners and PHA accumulation within the heterotroph (see Figure 3.3 **A**-**C**).

Processes with nitrate limitation and batch urea:

After consumption of an initial batch nitrate of 50 mg L^{-1}, a 1 M HNO_3-feed was connected to the process. Here, the peristaltic pump integrated into the station was calibrated and used to set different feeding rates for the co-culture or the cyanobacterium in the axenic culture phase (see Table 3.11). The container with the HNO_3 solution was weighted before the start of the process and after the shut down to re-evaluate the provided nitrogen. For additional support of the heterotrophic biomass production 0.36 g L^{-1} urea batch was

added simultaneously with the inoculation of the *P. putida* derivative.

Processes with additional urea-feed:

For the separation of the co-culture partner's nitrogen supply, an additional constant urea-feed with different feeding rates was applied (see Table 3.12). The integrated peristaltic pump of the reactor station was calibrated and used for this purpose (see Figure 3.3 **B**).

Table 3.11: Adjusted nitrate feed rates during different processes.

Urea feed	**mg L^{-1} d^{-1}**
Process with *P. putida cscRABY*	
Axenic culture phase	74
Co-culture phase	110
Process 2 with *P. putida cscRABY ΔnasT*	
Feeding-rate	105
Process 3 with *P. putida cscRABY ΔnasT*	
Feeding-rate	105

Table 3.12: Urea feeding rates in processes with *P. putida cscRABY ΔnasT*.

Urea feed	**mg L^{-1} d^{-1}**
Process 1 with *P. putida cscRABY ΔnasT*	
Feeding-rate I	13.3
Feeding-rate II	6.7
Feeding rate III	2.2
Process 2 with *P. putida cscRABY ΔnasT*	
Feeding-rate I	40
Feeding-rate II	20
Feeding rate III	2.2
Process 3 with *P. putida cscRABY ΔnasT*	
Feeding-rate I	40
Feeding-rate II	25

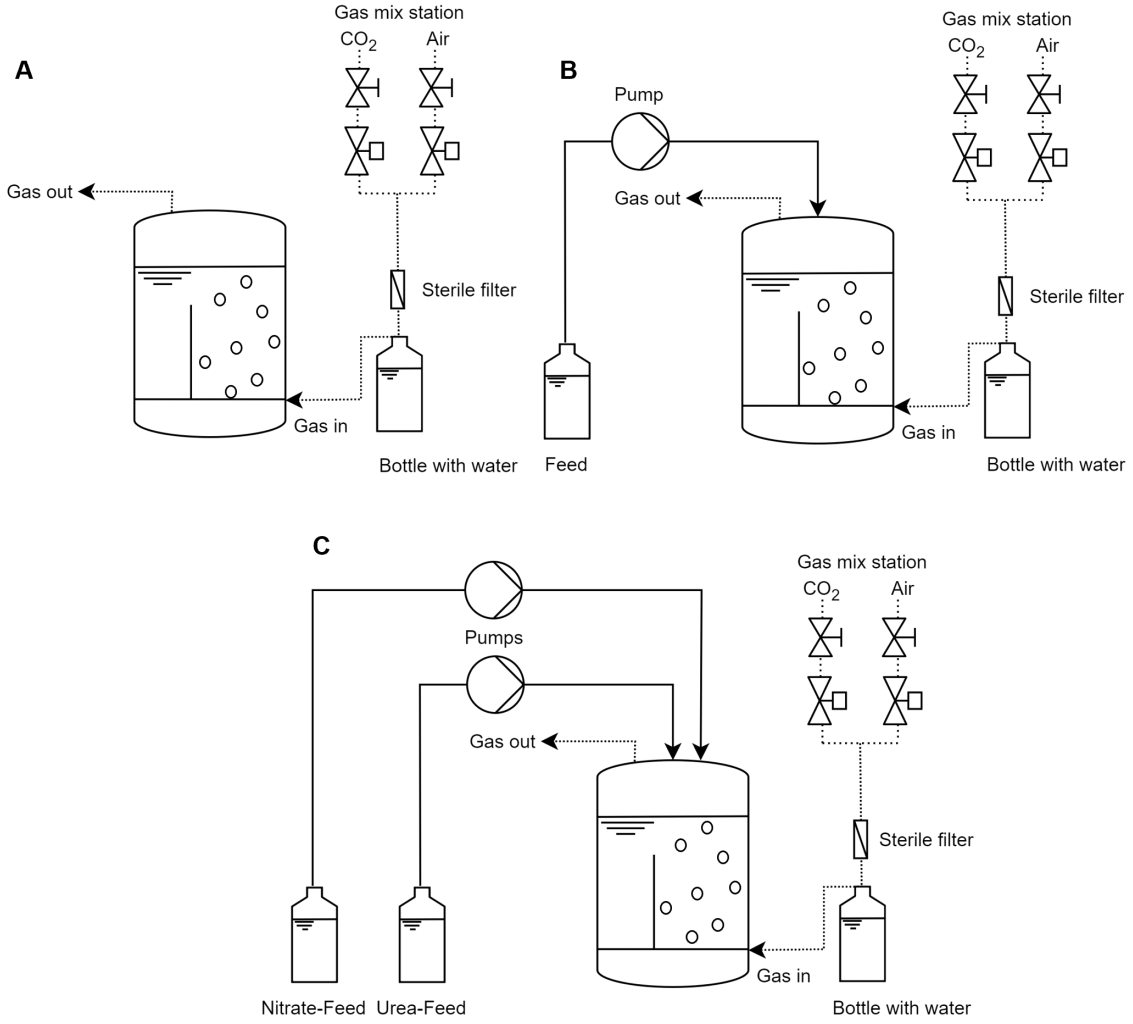

Figure 3.3: **(A)** Process scheme for the co-cultivation process in the photobioreactor (bubble column) without additional feeds. The gas mix station combines 2% CO_2 and air, which is subsequently directed through a sterile filter to a pressure-stable bottle filled with sterile water. In this process, the airflow is saturated with water to prevent water loss during cultivation. The saturated gas mixture is then directed into the bioreactor and exits through the gas outlet. **(B)** Shows a process scheme for the co-cultivation process with one feed (nitrogen source: urea or nitrate) connected to the bioreactor with a peristaltic pump and **(C)** visualizes a process with two parallel feeds (nitrogen sources: urea and nitrate). The scheme was created with the help of https://www.drawio.com/.

3.5.1 Describing microbial growth

When cell division and growth are proportional then the specific growth rate (h^{-1}) is defined as:

$$\mu = \frac{1}{m_X} \cdot \frac{dm_X}{dt} \tag{3.2}$$

with m_x representing the biomass of the cells in g and $\frac{dm_X}{dt}$ the change of the bacterial biomass per time [84]. Equation (3.2) describes microbial growth in the exponential phase, where μ is regarded as constant. For other growth phases extensions are necessary. Cyanobacterial growth often transitions from exponential to linear due to self-shading effects [161]. For determination of the maximal growth rate, the early exponential phase can be used [161], otherwise growth can be described by the unspecific growth rate:

$$\mu' = \frac{dC_X}{dt} = \mu \cdot C_X = const. \tag{3.3}$$

The unspecific growth rate was calculated using the simple linear model $C_X = p1 \cdot t + p_2$. The parameters p_1, p_2 were estimated by the least square method, which minimizes the difference between the data and the model.

Bacterial growth is often described to be connected to at least one limited substrate (see Section 2.2.2). In the co-culture the main limited substrate for the heterotrophic partner is sucrose in g L^{-1}, which is produced by the phototrophic partner. The sucrose concentration per time in g L^{-1} h^{-1} is, therefore, a balance between sucrose production r_{sec_suc} and sucrose uptake r_{up_suc}.

$$\frac{dC_{suc}}{dt} = r_{sec\_suc} - r_{up\_suc} \tag{3.4}$$

Further, the biomass yield $Y_{C_{XS}}$ in (g g^{-1}) was experimentally determined to be [27]:

$$Y_{C_{XS}} = \frac{dC_X}{dC_S} \approx 0.23 \tag{3.5}$$

with C_X being the formed biomass in g L^{-1} and C_S the substrate metabolised in g L^{-1}.

3.6 Analytical methods

3.6.1 Optical density

The Lambert-Beer-law relates the attenuation of light with the properties of a medium when it gets transmitted. Cells in a medium can, for instance, be the attenuating species of light.

$$E_\lambda = log(\frac{I}{I_0}) = \epsilon \cdot c \cdot L \tag{3.6}$$

With E_λ being the molar attenuation or absorbance at a given wavelength, I_0 the intensity of the incoming light, and I the intensity of the transmitting light, ϵ is the molar attenuation coefficient, c gives the concentration of the measured solution, and L is the optical path length. To determine the optical density, two devices were available: The Eppendorf Biospectrometer basic and the Tecan microplate reader (Plate reader Infinite 200 PRO). For the biospectrometer, a cuvette with a light path of 1 cm was used, and optical densities were measured at 600 nm (heterotroph) or 750 nm (phototroph or co-culture). When the OD or absorbance was measured with the plate reader, a volume of 200 µL per well was used.

3.6.2 Flow cytometry

To assess the growth of the cells in the co-culture, each partner's growth had to be determined separately. Flow cytometry provides a rapid analysis of single cells based on their physical or chemical properties and is, therefore, suitable for detecting the individual cell growth of the co-culture partner. In principle, flow cytometry consists of three main components: a fluidic system, an optical module, and detectors, which are connected to a computer to record and evaluate the results (see Figure 3.4) [162]. The fluid system of a flow cytometer is critical to precisely align cells for passing the laser beam one by one. The sample is injected into the center of a laminar flowing sheath fluid (isotonic solution) stream. The sample steam has a lower velocity than the surrounding sheath fluid stream. Both streams do not mix under laminar flow conditions and are then accelerated due to the narrowing of the flow cuvette. That accelerates the cells and forces them to travel at the same speed through the laser beam (see Figure 3.4). This principle is called hydrodynamic focusing [163]. At the analysis point, a focused and coherent laser (e.g. λ_{Ex} = 488 nm) meets the fluid stream with the aligned cell. The incoming light of the laser is then scattered through the cell. The FCS detector is placed behind an obscuration bar to prevent direct illumination from the laser (see Figure 3.4). Cells or particles induce forward scattering (FSC), which is proportional to the cell or particle size. Further, various side scatter (SSC) occur when the laser beam hits a particle. Often, the light which is scattered at a 90 ° angle to FSC is recorded in flow cytometry. The SSC is proportional to the granularity or complexity of the cells passing the laser beam. Next to scattering, fluorescence, which means the emission of light caused by a specific excitation wavelength, can be detected through photodetectors. Fluorescence can have a natural cause through fluorescence pigments or excitable chromophores or can be genetically introduced by the expression of fluorescence proteins, such as the green fluorescent protein (GFP). Another option to separate cells in a mixed sample, for instance blood cells, can be achieved using specific fluorescence dyes or fluorescently conjugated antibodies, such as CD3 FITC. For each specific photodetector, different types of filters are

implemented. They only allow the transmission of light with a specific wavelength or range. For instance, a bandpass filter 525/40 allows the detection wavelength in the range of 525 ± 20 nm. The photodetectors (photodiodes) convert the photon flux (photons per time) into an electrical signal [164], [163]. Data analysis provides the separation of a mixture of cells, cell counting, or visualization of biological effects. Defined biologically meaningful sections, so-called gates, are chosen which are used to separate cells according to their properties.

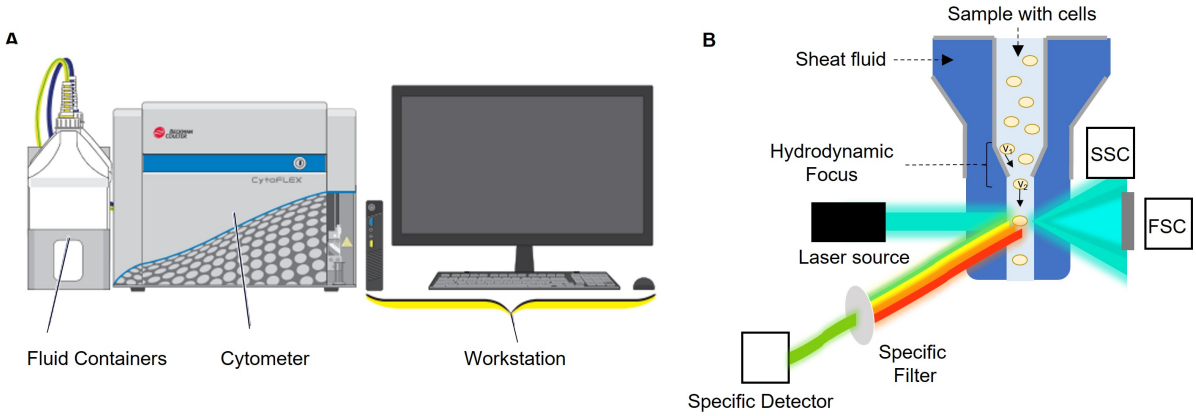

Figure 3.4: **(A)** Visualization of the flow cytometer workstation with the fluid containers (waste and fresh sheath fluid), the cytometer, and the connected computer for evaluation (Figure modified from Beckman Coulter[2]. **(B)** Schematic representation of the flow cuvette in a flow cytometer. Cells and particles are forced through the hydrodynamic focus to adapt their velocity. Cells have a lower velocity v_1 at the sides and a higher velocity in the middle of the nozzle v_2. When a cell passes the laser beam, the light gets scattered, or specific fluorescence dyes (proteins) emit light with a higher wavelength after excitation from the laser. The scattered light can be detected from an SSC = side scatter detector or an FSC = forward scatter. The forward scatter is behind an obscuration bar (gray bar). The emitted light from different dyes gets filtered through specific filters and is converted into an electrical signal in specific detectors. Figure part B was adapted from [165].

To differentiate the co-culture partner *S. elongatus cscB* from different *P. putida* derivatives, the flow cytometer CytoFLEX from Beckman Coulter was used. The device is equipped with two lasers (488 nm and 638 nm) and eight fluorescence channels. To get an optimal resolution of the co-culture partners, samples were diluted until ∼100-500 events (cells) per µL were recorded into the set gate "*cells*". The gate was defined over the cell granularity of the two cell species. Cells were diluted with filtered (cut-off: 0.2 µm) 8.5 g L^{-1} NaCl. Every dilution step and the final samples were mixed directly before being measured. When co-culture samples or *P. putida* axenic samples were measured a non-specific fluorescent dye was used N-(3-Triethylammoniumpropyl)-4-(4-(4-(diethylamino)phenyl)butadienyl)pyridinium dibromide (rh414 solved in DMSO, final concentration 3 µM) to separate the heterotrophic population from the noise of the device. The used device settings can be found in Table 3.13, and the default adjustment of the flow rate was "*medium*" at 30 µL s^{-1}. Usually, the measurement was stopped after recording 200,000 events. Measurements were usually conducted in triplicates. The cyanobacteria were recorded in the channel 640-660 nm or 488-780 nm, and the heterotrophs were recorded in the channel 488-585 nm. For data examinations, the software CytoFlex 2.1 was used. Individual cell counts of different populations were gated and analyzed according to their cell count, size, or fluorescence.

[2](https://www.beckman.com/flow-cytometry/research-flow-cytometers/cytoflex)

Maintenance of the devices: Before starting measurements, filtered water or NaCl (8.5 g L^{-1}) was injected into the device starting with the maximum flow (240 µL s^{-1}) and slowly decreased to the default flow rate. After each measurement session, the device was cleaned according to the *daily cleaning* program of the manufacturer. At least every month, the *deep clean* procedure was carried out, usually with overnight incubation of the cleaning solution and subsequent priming.

Table 3.13: Used settings for determining the cell count and the emission at different wavelenght.

Channel	Gain
FSC	165
SSC	500
488-585_50 nm	400
640-660_20 nm	100
488-780_60 nm	400

3.6.3 High performance liquid chromotography - HPLC

HPLC is used to separate mixtures due to their interaction between a mobile phase (a solvent) and a stationary phase (the functional groups on a matrix packed into a column) defined through specific physio-chemical properties of an analyte. Carbohydrates (sucrose, glucose and fructose) were quantified using high pressure liquid chromatography from Agilent (1100 series, Waldbronn, Germany) with a Shodex SH 1011 column. Samples were first centrifuged at 8,000 g for 1 min. (Centrifuge 5418 R, Eppendorf) and subsequently the supernatant was particle size exclusion filtered (cut-off = 0.2 µm). After this, the supernatant was mixed with an equal volume of 0.2 g L^{-1} ethylene diamine tetra-acetic acid disodiumsalt (Na_2-EDTA) in HPLC-vials to stabilize the sugar, except when concentrations were expected to be less than 0.3 g L^{-1}, then only 10% (v/v) were added. Sample that were not directly used were stored short term at 4 °C and long term at -20 °C. As a standard, a solution with sucrose, glucose and fructose, or only sucrose was prepared in a concentration range between 2-0.1 g L^{-1}. The device was prepared by opening the purge valve and washing the system with the solvent used during the measurements with a flow rate of 0.5 mL min^{-1}. After 15 min. the flow rate was switched off and the valve was shut. Then, the column was carefully equilibrated by setting the flow rate incrementally from 0.05 mL min^{-1} to 0.45 mL min^{-1}, at which the method started. After a constant pressure of $\sim$ 35 bar was reached the measurements were started. The method was either 60 min. or 30 min. long and further setting can be found in Table 3.14.

Table 3.14: Used HPLC settings for quantifying carbohydrates.

Channel	Adjustment
Flow rate	0.45 mL min^{-1}
Solvent	Sulfuric acid 0.5 mM
Column temperature	30 °C
Refractive index detector (RID) temperature	50 °C
Column	Shodex SH 1100
Injection volume	1 µL

Other substances as citrate, phosphate and ethanol were quantified using a Shimadzu LC2030C Plus HPLC with a Bio Rad aminex HPX-87H column. Samples were particle size exclusion filtered (cut-off =

0.2 µm) and subsequently 100 µL transferred into HPLC vials with inlets (see Table 3.15). Concentrations of the carbohydrates or other substances were calculated by integration of the peak area of each peak and correlated to the corresponding standard.

Table 3.15: Used settings for quantifying the other metabolites.

Channel	Adjustment
Flow rate	0.6 mL min^{-1}
Solvent	Sulfuric acid 0.5 mM
Column temperature	30 °C
Refractive index detector (RID) temperature	40 °C
UV-detector temperature	60 °C
Column	HPX-87H
Injection volume	1 µL

3.6.4 Polyhydroxyalkanoate - PHA analytic

PHA is a polyester accumulated as an intracellular storage compound from bacteria. Mcl-PHA comprises (R)-3-hydroxyalkanoic acid monomers with different chain lengths. In the *P. putida* derivatives, these monomers consist of C6-C12 carbon length, inheriting different physical-chemical properties (for details on PHA see Chapter 2.7) [28].

To quantify the intracellular polymer PHA two main steps are necessary: Firstly, it needs to be extracted from the cells, and secondly, converted into its monomers for measurements. The most accurate method for quantifying PHA is gas chromatography since other approaches, such as staining with Nile red or HPLC have their limits. Default approaches use a one-pot extraction combined with base- or acid-catalyzed lysis of the polymer into its monomers. Common protocols use methanolysis or propanolysis, which both are chemically transesterification reaction as can be seen in the reaction below [166].

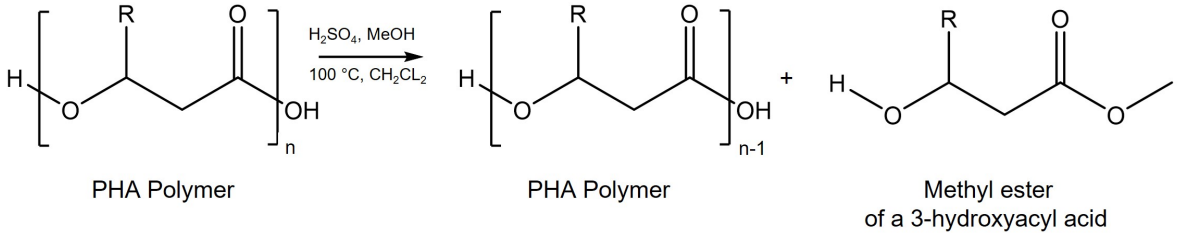

Figure 3.5: An example of acid-catalyzed methanolysis or transesterification of a PHA polymer (n). In this process, the polymer undergoes cleavage, resulting in the formation of one methyl esters 3-hydroxyacyl acid monomer and the polymer shortened by one monomer (n-1).

Sample preparation

Samples were stored at -80 °C for at least 14 h and were subsequently lyophilized at -60 °C and 0.08 mbar to completely dispose of leftover liquids. From here on, work was conducted under a fume hood. The freeze-dried pellets were resolved in acidified 1-propanol (80% to 20% hydrogen chloride HCL, v/v) for propanolysis of the 3-HA monomers. Then the solution was transferred to pressure-stable tubes, and chloroform was added in equal volumes. The volumes used were adjusted throughout the experiments but were in the range of 300-400 µL. Additionally, 20 µL PHB and 3-methylbenzoate (3-MB) were added as internal standards with

different but known concentrations. Both standards were beforehand dissolved in chloroform using a water bath heated to 80 °C. The 3-hydroxybutyric acid (C4, PHB) standard was added in a range of 1-5 mg L^{-1}, with 5 mg L^{-1} being the solubility limit. The 3-MB standard was added in a concentration range of 1-10 mg. As external standards 3-hydroxyoctanoate (C8) and 3-hydroxydecanoate (C10) were used. The esterification of the samples and the standard was allowed for at least 8 h in an 80 °C water bath. Samples were then transferred to safe-lock Eppendorf tubes to avoid the release of volatile chloroform. To remove salts from the sample, 800 µL DIW was added. The samples were mixed in a ball mill (Retch MM 200 ball mill 25 Hz, 3 min., Retch GmbH Germany) and subsequently centrifuged at 8,000 g for 3 minutes. From the extracted organic phase, approx. 300 µL were taken for final sample preparation. Ultimately, each sample was dried of excess water using solid $NaCO_3$ and neutralized with solid $NaSO_4$ into the samples. For the measurement, 100 µL of the liquid supernatant was transferred into GC vials with inlets.

Gas chromatography (GC)-method

The samples were separated with a ZB-WAX column (Phenomenex, USA, length: 30 m, ID 0.32, film 0.25 µm) and measured with a flame ionization detector heated to 245 °C. The injection volume was 1 µL with a split ratio of 1:10, and the injector temperature was set to 240 °C (AOC-20i autoinjector SHIMADZU, Japan). Hydrogen gas was used as carrier gas at a flow rate of 3 mL min^{-1}. The different PHA-monomers were separated by applying a temperature gradient, starting at 80 °C for 1 min., afterward linearly increasing the temperature by 5 °C every minute, stopping at 240 °C with a holding time of 5 min. The analytic was carried out in the laboratories of Werner Siemens-Chair of Synthetic Biotechnology (WSSB).

Peak identification and calculations

Through previous verification with mass spectra analysis and measurements of standards, the monomers could be identified (see Figure A.3) [27]. The retention time of the different monomer-propyl esters can be found in Table 3.16.

Table 3.16: Monomer propyl-esters and their retention time.

Monomer-propylester	Composition: C - O - H	Retention time, min.	Molar mass, g mol^{-1}
3-Hydroxybutyrate	7 - 3 - 14	7.2	146.109
3-Hydroxyhexanoate	9 - 3 - 18	10.66	174.141
3-Hydroxyoctanoate	11 - 3 - 22	14.36	202.173
3-Hydroxydecanoate	13 - 3 - 26	18.26	230.205
3-Hydroxydodecanoate	15 - 3 - 30	22.6	258.237
3-Hydroxydodecanoate (12:1) [a]	15 - 3 - 28	22.9	256.237
3-Methylbenzoate	9 - 2 - 10	12.16	136.15

[a] The cis and trans monomer of 3-hydroxydodecanoate were usually calculated together

In chromatography, the ratio between a signal (area) and the concentration or quantity of the analyte, which is responsible for the signal, is called the molar response factor:

$$MRF_i = \frac{A_i \cdot M_{st}}{A_{st} \cdot M_i} \cdot MRF_{st} \tag{3.7}$$

A_i is the signal, usually the peak area or the integrated signal. A_{st} is the signal of a standard (reference substance). Whereby M_i and M_{st} are the molar masses for the signal of interest and the standard. The response factor MRF_{st} of the standard is assigned an arbitrary factor (e.g. 1).

A study in 2010 showed the prediction of response factors from the molecular structure using combustion enthalpies. The monomers consist of three elements: carbon, oxygen, and hydrogen. Thus, the combustion of a monomer with the structure $C_{n_C}H_{n_H}O_{n_O}$ is expected to form n molecules of CO_2 and H_2O in the flame ionization detector (FID). De Saint Laumer et al. expressed the enthalpy formation of oxygen and the combustion production as a linear combination, resulting in the following formula when only the three elements are considered [167]:

$$H_{comb}^{MF} = 11.06 + 103.57 \cdot n_C + 21.85 \cdot n_H - 48.18 \cdot n_O \tag{3.8}$$

H_{comb}^{MF} is the absolute value of the combustion enthalpy (expressed in kcal mol^{-1}) for the respective monomer. $n_C/_O/_H$ is the number of carbon, oxygen or hydrogen found in the respective monomer.

The predicted molar response factor was expressed by the following formula [168]:

$$MRF = -0.0708 + 8.57 \cdot 10^{-4} \cdot H_{comb}^{MF} \tag{3.9}$$

Here, MRF [-] stands for the molar response factor and H_{comb}^{MF} is the absolute value of the combustion enthalpy. In Table 3.17 the calculated MRF values are depicted.

Table 3.17: Calculated of $\Delta H_{comb.}$ and MRF for the monomer-propylesters.

Monomer-propylester	$\Delta H_{comb.}$	**MRF**
3-Hydroxybutyrate	879.41	0.698
3-Hydroxyhexanoate	1191.95	0.951
3-Hydroxyoctanoate	1486.5	1.20
3-Hydroxydecanoate	1781.03	1.46
3-Hydroxydodecanoate	2075.57	1.77
3-Hydroxydodecanoate (12:1)	2031.87	1.67

Next to the determination with the MRF values, a correlation deriving from the standards curves of PHB, 3-Hydroxyoctanoate and 3-Hydroxydodecanoate could be determined (see example in Figure A.4):

$$\text{Conc. [mg mL}^{-1}] = 2.25 \cdot 10^{-8} \cdot No_{carbon} + 2.15 \cdot 10^{-7} \tag{3.10}$$

3.6.5 Analytical assays

Nitrogen assay

For nitrate determination, the NO_2/NO_3—assay from ENZO (Enzo life science, USA) was used, and the user manual was strictly followed.

Urea assay

The urea concentration of the culture supernatant was determined using the urea/ammonia-assay Kit of Megazyme (NEOGEN, Megazyme, USA), which is based on the enzymatic oxidation of NADH to NAD^+ at a wavelength of 340 nm and was scaled down (factor 10) for photometric measurement with a microplate reader (Tecan plate reader Infinite 200 PRO). Otherwise, the user manual was strictly followed.

Carbohydrate assay

Sucrose, glucose, and fructose were also quantified by using a sucrose assay kit sca20-1kt (Sigma-Aldrich, St. Louis, USA). The sucrose was first hydrolyzed to glucose and fructose using an invertase (sucrose assay reagent). The resulting monosaccharides were phosphorylated to fructose-6-phosphate (glucose assay reagent), which reacted with NAD^+ to 6-phosphogluconate and NADH. The concentration of NADH was directly proportional to the quantity of fructose-6-phosphate and, thus, sucrose. NADH was again quantified using a microplate reader at 340 nm (Tecan plate reader Infinite 200 PRO). The user manual was strictly followed.

Iron assay

For iron determination, the iron—assay-kit from Sigma-Aldrich (MAK025-1KT) was used, and the user manual was strictly followed.

3.7 Cultivation in parallelized membrane reactors

For parallel cultivation, the platform CellDEG HDC 9.100 Universal Platform (CellDEG GmbH, Germany) was used. The setup consists of three main components: A cultivation platform, an LED lamp (400-RX LED), and a growth control unit (GCU) (see Figure 3.6). Maximal nine membrane reactors (HD100 Cultivator) can be mounted to the hollow cultivation platform with fixation rings. The platform is placed onto an orbital shaker (compact shaker KS15 A, Edmund Bühler GmbH, Germany) to guarantee the mixing of the cells during the process. CO_2 supply of photosynthetic organisms is controlled over the GCU. For this, the half-spherical reactors have a membrane on the bottom where CO_2 diffusion can take place from the space underneath (see Figure 3.7). The partial pressure pCO_2 can be set with the GCU, which forms a closed loop between the platform, a condensate trap, and itself. Illumination conditions can be set, and the temperature can be monitored with four temperature sensors (see Figure 3.6). Temperature control can only be achieved over the LED growth lamp (energy input), four ventilators, which are mounted behind the GCU, and ventilation slots above the LED lamp.

Membrane reactors

The reactors used in the study have a half-spherical shape, with a permeable membrane fixed at the bottom. The CO_2-enriched air is supplied over the membrane via gas diffusion which occurs from the gas phase below. At the top of the membrane reactor, a cap with a membrane allows for gas exchange. The reactors were reused multiple times (approximately 10 times) in the experiments. Prior to each use, they were sterilized according to the manufacturer's protocol using 10% hydrogen peroxide (H_2O_2). Additionally, the reactors were washed three times with sterile DIW and rinsed again with sterile DIW before the start of each process. The reactors had a volume range of 50-100 mL, with a typical volume of 95 mL used for the processes.

Growth control unit

The GCU (Gas Control Unit) allows for customized profiles for CO_2 and illumination. Users can choose between constant, linear, or exponential progressions for these parameters. Additionally, day and night cycles can be programmed for the light parameter. The current settings of the device, as well as the system status (including temperature and relative humidity of the gas in the loop), are displayed on a plot panel. The default CO_2 injection pulse time of 20 ms, set by the device factory, proved sufficient to supply the cyanobacteria growth at a CO_2-partial pressure of 2%.

Maintenance of the device

After each process, all tubes were disconnected and dried. If needed, the condensate water trap was emptied and washed with water, followed by rinsing with 80% ethanol, and finally dried. The device was kept in standby mode for approximately 1 hour after shutting down the processes to allow the gas loop and the CO_2 sensor to dry. The cultivation platform was washed with DIW and wiped with an 80% solution of 2-propanol.

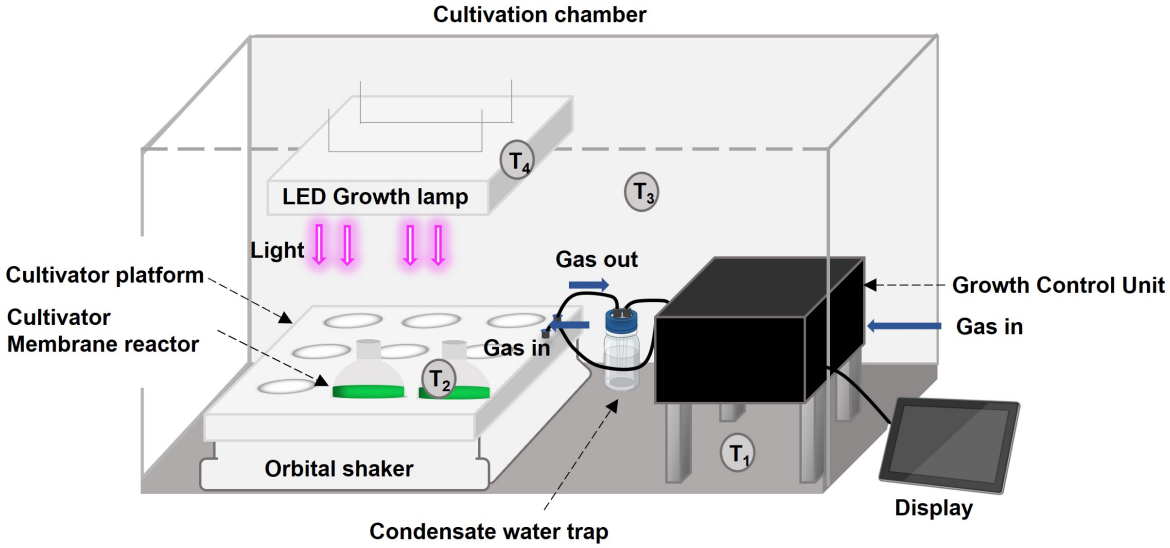

Figure 3.6: Schematic depiction of the parallelized cultivation setup from CellDEG GmbH, Germany. The set consists of a cultivation chamber, in which the LED growth lamp, the cultivator platform, and the growth control unit (GCU) are placed. The cultivator platform has nine ports to connect cultivators, or the membrane reactors, from the CellDEG GmbH. From the hollow space below the membrane reactors, cells are supplied with CO_2. The gas mixture is defined through the GCU, which is connected to an external CO_2- supply and forms a gas loop between the cultivation platform, the connected reactors, a reservoir for condensate, and itself. The four temperature sensors are indicated through T_1 - T_4. T_1= temperature of the internal gas mixing chamber. T_2= temperature of the culture, T_3= temperature of the cultivation chamber, T_4= temperature of the lamp. From an external attached display, cultivation conditions can be monitored or set. The blue arrows → indicate where the gas supply takes place. The Figure was partially created with the help of BioRender (http://www.BioRender.com).

Light from the LED panel for phototrophic growth

In general the energy of a photon with a given frequency or wavelength can be described as:

$$E_{Photon} = h \cdot \nu = \frac{h \cdot c}{\lambda} \tag{3.11}$$

The energy of a photon is solely determined by two constants, namely Planck's constant (h = 6.63 · 10^{-34} J s) and the speed of light (c = 3 · 10^{8} m s^{-1}), as well as the frequency (ν) or wavelength (λ) of the photon. To quantify the light intensity of a light source for biological systems, different terms have been established. The photon flux density (PFD, Φ^m) is usually expressed in µmol photons m^{-2} s^{-1} when using SI units and working with photosynthetic organisms. Sometimes the outdated unit µE *"mikroeinstein"* m^{-2} s^{-1} can still be found. The PFD represents the number of photons, passing through a specific area in a given time. When working with phototropic organisms, the expression PPFD can often be found, which stands for photosynthetic photon flux density. This expression focuses on the photosynthetically active radiation (PAR) in the range of 400-700 nm, which is used by photosynthetically active organisms at a particular area and time [169], [170].

With the PDF (Φ^m) and the energy of one photon, the power density can be calculated with Equation (3.12) [170]:

$$H = \phi^m \cdot E_{Photon} = \phi^m \cdot \frac{h \cdot c}{\lambda} \tag{3.12}$$

Used light sources for boosting phototrophic growth have a spectrum of photons of different wavelengths. It is often described as the spectral irradiance (I(λ)), which describes the power density divided by the wavelength. The integral of the spectral irradiance within the wavelength band of interest gives the total power density. Both can be expressed in quantum units or energy units (see Table 3.18).

Table 3.18: Spectral irradiance and total power density function in quantum units or engergy units.

Irradiance	Symbol	Unit	Note
Spectral irradiance in quantum units	$I^Q(\lambda)$	µmol m^{-2} nm^{-1} s^{-1}	Power density at a given wavelength
Spectral irradiance in energy units	$I^E(\lambda)$	W m^{-2} nm^{-1}	Power density at a given wavelength
Integral spectral irradiance in quantum units	H_T^Q	µmol m^{-2} s^{-1}	Total power density
Integral spectral irradiance in energy units	H_T^E	W m^{-2}	Total power density

Via integration of the spectrum from the used light source, the total power density can be calculated from its spectral irradiance. A simple conversion from energy in quantum units is not possible because photons decrease in energy with increasing wavelength, which also means that more photons are necessary to achieve the same power. A conversion from quantum units (µmol m^{-2} s^{-1}) to energy units (W m^{-2} nm^{-1}) is necessary because many devices measure the light in energy units. Calculations, which can be found in detail in Section A.4, led to the conversion Equation (3.13) [169], which applies specifically to the LED (400-RX LED) employed:

$$H_T^Q(PAR) = H_T^E(PAR) \cdot 5.05 \tag{3.13}$$

Here, $H_T^E(PAR)$ is measured in W m^{-2}. Light calibration was carried out from the manufacturer and was checked with a miniature spectrometer (Flame-T, Ocean Optics Inc., Florida, USA) with the software OceanView.

3.7.1 Co-cultivation in a parallelized membrane reactor

For ensuring high reproducibility and parallelizability, the CellDEG HDC 9.100 Universal Platform (CellDEG GmbH, Germany) was used. In all processes, a CO_2 partial pressure of 2% was set. Different light profiles for the high-power LED light sources (RX-400 LED light Source from Valoya) were implemented (e. g. constant light of 50 photons s^{-1} m^{-2} or exponential light of 120–600 µmol photons s^{-1} m^{-2}). Cells were grown in co-culture optimized BG11$^+$ medium supplemented with 150 mM NaCl [25], and 0.1 mM IPTG was added to induce the sucrose permease CscB of *S. elognatus cscB*. In all co-culture processes, the heterotrophic partner was *P. putida cscRABY*. At the beginning of each process, the pH was set to 7.5 and was not further controlled. For this, the prepared BG11$^+$ medium was aliquoted into the membrane reactors, resulting in an overall volume of 950 mL, then 0.350 mL of a 3 M NaOH solution was added to each reactor. After that, the reactors were placed onto the cultivation platform, and CO_2 supply was turned on. After approx. 3 h the pH equilibrium of the medium was reached, and the process was started by the inoculation of cyanobacteria from a salt-acclimated permanent culture to an OD_{750} in a range of 0.1-0.2 (see Section 3.4.2). Water

loss through condensation was considered by monitoring the weight of the membrane reactors during the processes. The co-culture was started by adding *P. putida cscRABY* cultures (see Section 3.4.3) after an axenic culture phase. Experiments with different inoculation time points and densities were performed. During the processes, the cell count, optical density, and sucrose concentration were determined by daily sampling of 1-2 mL of the culture broth as described in Sections 3.6.2 and 3.6.3. The cultures were regularly checked for contaminations by streaking on LB agar plates, which were incubated for at least three days at 30 °C.

3.7.2 Reference experiment in a parallelized membrane reactor

The reference experiment consisted of biological triplicates of axenic cultures (*S. elongatus* or *P. putida*, respectively) and co-cultures, thus all nine places on the cultivation platform were used. The process started with an acclimatization phase for the phototrophic partner (Starting with an OD_{750} of 0.1–0.2) under constant light at 150 µmol s^{-1} m^{-2} and 2% CO_2. After 14-18 h, the co-culture was started by the inoculation of *P. putida cscRABY* to an OD_{600} of 0.05. Heterotrophic axenic cultures were supplied with external carbon by a sucrose feed. Thus, a cap had to be designed to enable feeding and *in situ* sampling of cells in the membrane reactor provided by the CellDeg company (see Figure 3.7). The cap consists of two cylinders: the broader has a height of 12.4 nm, starts with a diameter of 50 mm, and narrows at the top to a diameter of 38.7 mm. That is also the diameter of the smaller cylinder, which has a height of 9.59 nm. The cap can be placed on the reactor lid resulting in an overall height of 22 mm. The cap serves as a bracket for two cannulas, one enabling feeding of the heterotrophic partner and the other one serving as a sampling port (see Figure A.6 for more details). The ports for the cannulas narrow conical to fix them on top of the membrane reactor. It was further assured with a 6.5 mm width hole that the membrane for aeration on the reactor top was not closed. The sucrose secretion rate by the phototrophic partner grown in co-cultures was estimated and used to define the sucrose feeding rate for the axenic cultures of *P. putida cscRABY*. Beforehand a peristaltic pump was calibrated and a sucrose solution of 100 g L^{-1} was prepared. The resulting feeding rates can be found in the respective Chapter 4.2.4. Batch sucrose of 0.1 g L^{-1} was provided into the axenic *P. putida cscRABY* cultures at the beginning, mimicking the initial sucrose production of the phototrophic partner. Sampling was carried out as usual. After approx. 60 h samples for multi-OMICS analysis were taken, centrifuged at 4,000 rpm for 5 min. (10 mL proteomics) or 13,000 rpm, 1 min. (centrifuge 5418 R, Eppendorf) (1 mL for metabolomics and transcriptomics) at 4 °C and subsequently stored at –80 °C.

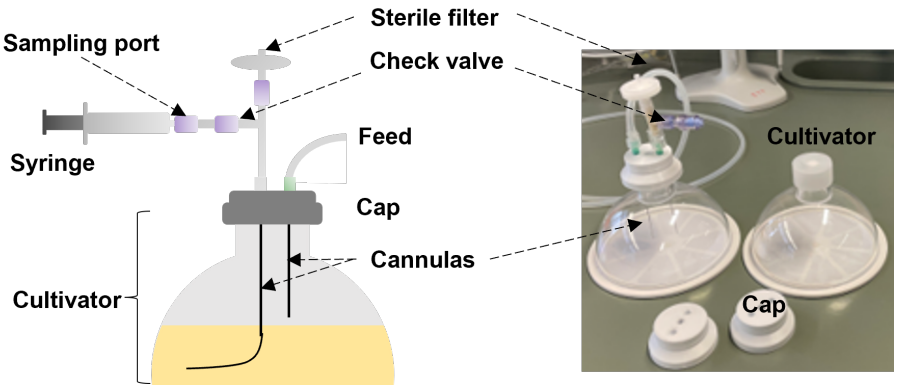

Figure 3.7: Left: Schematic depiction of the cultivator from CellDeg GmbH, Germany and a designed cap for sampling and feeding of the heterotrophic partner. Right: Cultivator equipped with the cap carrying the feeding tube and the sampling port.

3.7.3 Axenic cultivation of *P. putida cscRABY* with sucrose-feed

In axenic cultures of *P. putida cscRABY* carbon was either added as a batch, intermitted feed, or feed. For the reference experiment, the sucrose feed was calculated based on beforehand performed co-culture processes to adjust the growth rates of the axenically grown heterotrophs with those grown in co-culture. An explicit example calculation is provided appendix (see A.13). With the correlation shown in Equation (3.14) between the optical density at 600 nm and the cell count C_x [cell mL^{-1}] for *P. putida*, a connection to the cell dry weight C_{Xcdw} was determined in Equation (3.15).

$$C_X = 2.2 \cdot 10^9 \cdot OD_{600} \tag{3.14}$$

The optical density for this correlation was measured with the plate reader photometer (Plate reader Infinite 200 PRO). Further, a correlation between the cell dry weight C_{Xcdw} [g L^{-1}] and the cell count can be find:

$$C_{Xcdw} = \frac{C_X}{2.2 \cdot 10^9} \cdot 0.256. \tag{3.15}$$

Löwe et al. determined the biomass yield reached of *P. putida cscRABY* growing on sucrose to $Y_{Xsuc} = 0.23 \frac{g}{g}$ [27]. That means with the Equation (3.16) the available sucrose for the heterotrophic partner during growth in a given time period Δt in [g L^{-1} d^{-1}] can be estimated.

$$\frac{\Delta C_{suc}}{\Delta t} = \frac{\Delta C_{Xcdw}}{Y_{Xsuc} \cdot \Delta t} \tag{3.16}$$

The biomass yield is considered constant, and the term $\frac{\Delta C_{Xcdw}}{\Delta t}$ was calculated with linear regression of the cell count of *P. putida cscRABY*.

3.7.4 Sample preparation for OMIC analysis

The term *"OMIC"* summarizes studies dealing with research objects ending with *"ome"*, such as the transcriptome, proteome, and metabolome. In transcriptomics, a set of mRNAs, or transcripts, of cells are investigated. Consequentially, in proteomics a collection of proteins, and in metabolomics, a collection of metabolites are studied. Usually, these techniques are comparative approaches, which means a biological entity is treated, e. g. by exposing it to a drug, and compared to the biological entity not treated. For the co-culture between *S. elongatus cscB* and *P. putida cscRABY* it signifies that the co-culture (case) is compared with the respective axenically grown cultures (control). The resulting difference between case and control is usually expressed in a logarithmic fold change, which can be seen exemplary with an observed transcript A in Equation (3.17).

$$log_2(FC) = log_2(\frac{\text{Number of transcript A in case}}{\text{Number of transcript A in control}}) \quad (3.17)$$

To investigate the potential interaction between the co-culture partners not only at a physiological level, samples for transcriptomic, proteomic, and metabolomics were also taken in the reference experiments (see Chapter 3.7). In Table 3.19 basic characteristics of the co-culture partner's genomes are summarized.

Table 3.19: Characteristics of the co-culture partners' genomes.

***S. elognatus* PCC 7942**	**Characteristics**	***P. putida* KT2440**
2.74	Length in Mbp	6.20
55.4	GC-content in %	61.5
2762	Number of genes	5483
Can be diploid	Note	-

General handling of the samples

Tubes and falcons were labeled and cooled before taking the samples. The sampling point for transcriptomics and proteomics was 67.5 hours in reference Experiment II and 53.5 hours in reference Experiment I for metabolomics. All samples were kept on dried ice at -60 °C. Except during centrifugation, which was performed for 1 min. at 8,000 g and 4 °C for the metabolomic and transcriptomic samples and 3 min. at 4,000 g and 4 °C for the proteome sample. The samples were snap frozen and stored after removal of the supernatant at -80 °C before shipping or performing the metabolite extraction. For the techniques described below, each of the two axenic cultures — *S. elongatus cscB* and *P. puitda cscRABY* — as well as the non-separated co-culture of both partners, was treated as a single sample.

Transcriptomic and untargeted proteomic

RNA isolation, transcriptome measurements, and basic bioinformatic analysis were performed from Eurofins in Konstanz, Germany. Samples for proteomics were cooled and shipped to the University of Sheffield, Department of Chemical and Biological Engineering, where protein extraction and mass spectrometry (MS)-analytic and bioinformatic analysis were carried out. Briefly, proteins were extracted, trypsin-digested and desalted using Bond Elut OMIX C18 tips (Aligent Technologis). After this Liquid chromatography-tandem mass spectrometry (LC-MS/MS) proteome analysis was performed using reverse-phase LC on a Dionex Ultimate 3000 RSLC nano 2 system coupled online to a Q Exactive HF mass spectrometer (Thermo Scientific). Statistical analysis of protein identification was performed using the LFQ-Analyst website (https://bioinformatics.erc.monash.edu/apps/LFQ-Analyst/).

Metabolite extraction and separation for untargeted metabolomics

Samples for metabolomic analysis were snap frozen and stored at –80 °C after centrifugation. For extraction of the metabolites, the frozen pellets were resuspended in 1 mL cooled MetOH (-80 °C, 80% (v/v MetOH:H_2O)) and incubated at -80 °C for 20 min. Then, samples were centrifuged at 8,000 g for 5 min. at 4-8 °C, and the metabolite-containing supernatant was transferred to a tube on dry ice. This process was repeated with 0.5 mL of 80% MetOH, and the supernatant was transferred to the same tube on dry ice. After this, the samples were lyophilized in a SpeedVac provided by the BioBayMS center in Freising. The BioBayMS center

was also responsible for HPLC and MS measurement for untargeted metabolomics analysis. Briefly, samples were separated using two types of columns. A UPLC BEH Amide 2.1×100 mm, 1.7 μm analytic column (Waters, Eschborn Germany) with a 400 μL min^{-1} flow rate for Hydrophilic Interaction Liquid Chromatography (HILIC) and a Kinetex XB18 2.1 x 100 mm, 1.7 μm (Phenomenex, Aschaffenburg Germany) for Reverse Phase Chromatography (RP) with a 300 μL min^{-1} flow rate. Mass spectrometer (MS) settings in the positive mode were as follows: Gas 1 55, Gas 2 65, Curtain gas 35, temperature 500 ℃, Ion Spray Voltage 5500, declustering potential 80. The mass range of the TOF MS and MS/MS scans were 50–2000 m/z and the collision energy was ramped from 15–55V. MS settings in the negative mode were as follows: Gas 1 55, Gas 2 65, Cur 35, temperature 500 ℃, Ion Spray Voltage –4500, declustering potential –80. The mass range of the TOF MS and MS/MS scans were 50–2000 m/z and the collision energy was ramped from –15–55V.

3.8 Molecular methods

3.8.1 Quadrupole mating

The *cscRABY* operon provides the ability to metabolize sucrose and was previously cloned in the vector pTn7-M [27]. This vector allows side-specific integration into the *att*Tn7 side in the genome of *P. putida*, which is localized approx. 25 bp downstream of the *glmS* gene. Two helper strains are necessary for a successful genomic integration of the operon into *P. putida*: The strain *E. coli* HB101 (pRK600), which contains the genes for the conjugal transfer of the pTn7-M-*cscRABY* plasmid and *E. coli* DH5α (pTns1) carring the transposase genes for genomic integration (see Table 3.10). The donor strain was *E. coli* DH5α λpir, which carries the pTn7-M vector with the *cscRABY* operon integrated into the multiple cloning side. The acceptor strain was *P. putida* KT2440 Δ*gcd*. The bacterial strains were streaked out on LB-agar plates with the corresponding antibiotics and incubated overnight at 30 ℃ (*P. putida*) or 37 ℃ (*E. coli*), then a single colony was picked and transferred into 3 mL LB with the corresponding antibiotic. The cultures were grown overnight, then 200 μL of each culture were mixed and centrifuged at 8,000 g for 5 min. at room temperature. After this, 750 μL of the medium was discarded, and the cells were resuspended in the leftover medium. The remaining droplet was then put in the middle of an LB plate without antibiotics and incubated for 8 h at 30 ℃. Then cells were transferred to M9-citrate plates with gentamicin (10 μg mL^{-1}). After colonies had formed, a single colony was transferred to M9-sucrose plates without additional antibiotics.

Table 3.20: Strains and their antibiotic resistance.

Strain	**Anibiotic, μg mL^{-1}**
E. coli HB101 (pRK600)	Chloramphenicol - 35
E. coli DH5α (pTns1)	Ampicillin - 100
E. coli DH5α λpir (pTn7-M-*cscRABY*)	Kanamycin - 50
P. putida KT2440 Δ*gcd*	no

3.8.2 Validation of the genomic integration

To check the successful integration on a genomic level, a colony polymerase chain reaction (PCR) with following conditions was performed.

Table 3.21: Colony PCR components.

Component	**Volume, µL**
FastGene 2x Ready Mix	8
Primer *Pput Tn7l* (ATT AGC TTA CGA CGC TAC ACC C)	2
Primer *Pputt glmS* UP (AGT CAG AGT TAC GGA ATT GTA GG)	2
DIW	Add to 20
DNA	One colony per tube

Table 3.22: Cycler program for the colony PCR.

Step	**Temperature, °C**	**Time, s**	**Cycles**
Initial Denaturation	94	30	1
Denaturation	94	20	30
Primer Annealing	50	30	30
Elongation	68	30	30
Final Elongation	68	5 min.	1
Hold	16	∞	1

Visualisation of the results of the colony PCR was achieved through 1% agarose gel electrophoresis (Rotiphorese Gelchamber, Roth GmbH, Germany). As DNA-size marker a 100 bp ladder from NEB (New England Biolabs, USA) was used.

4 Results and Discussion

4.1 Optimizing the synthetic co-culture process of *S. elongatus cscB* and different *P. putida* derivatives

The following chapters focus on arranging a highly controllable process with the synthetic co-culture of *S. elongatus cscB* and different *P. putida* derivatives to produce medium chain length polyhydroxyalkanoate (mcl-PHA) from light and CO_2. Therefore, a stepwise streamlining towards a targeted nutrient limitation for the heterotrophic partner, employing the broad toolbox of process engineering, was performed. At the end of each section, the results are discussed and put into context with the state-of-the-art in the respective biotechnological field [1].

4.1.1 Co-cultivation with the strain *P. putida cscRABY*

To improve the synthetic co-culture of *S. elongatus cscB* and *P. putida* as a heterotrophic partner, the recently constructed strain *P. putida cscRABY* was employed in the co-cultivation process [27]. In contrast to *P. putida cscAB* used in the previous setup of co-culture processes [25], the 'new' co-culture partner strain possesses an increased capability for sucrose uptake and subsequent consumption (see Chapter 2). It was achieved by chromosomal integration (*att*Tn7) of the complete sucrose utilization operon *cscRABY* derived from *Pseudomonas protegens* Pf-5. It encodes the permease CscB, the sucrose-splitting invertase CscA, as well as the regulator CscR and the porin CscY. Especially the latter one was shown to be crucial for a stable sucrose consumption phenotype, when *P. putida* could not acclimatize to carbohydrate uptake and subsequent metabolization [27].

The first step was to develop an effective method for growth quantification of both co-culture partners since counting colony-forming units (cfu) is only reasonably possible for the heterotrophic partner and remains an erroneous method. A suitable approach could be implemented by using flow cytometry because different cell sizes and emissions between 600-700 nm of the co-culture partners facilitate the separation of the partners' cell populations (see Figure 4.1 **A**). So the remaining challenge was to differentiate between the smaller *P. putida* and the unspecific signal of the device (noise), which was accomplished by using an unspecific hydrophobic dye called RH414 (N-(3-triethylammoniumpropyl)-4-(4-4-(diethylamino) phenyl) butadienyl) pyridinium dibromide) (see Figure 4.1 **B**). Its fluorescence within 488-585 nm range allowed for a clean separation of *P. putida*, *S. elongatus* and the unspecific signal (see Section 3.6.2 for the detailed method explanation).

[1] Some of the presented results in this chapter have already been published in [129]

In the context of intercellular PHA accumulation, the presence of limited essential nutrients becomes advantageous, particularly when utilizing a structurally non-similar PHA substrate like sucrose (further details provided in Chapter 2). In the previous co-culture process, nitrogen in the form of nitrate was used as a limiting substrate. By applying a limiting nitrate-feed, a maximum PHA titer of 156 ± 40 mg L^{-1} after 16 days with a maximal production rate of 23.8 ± 6 mg L^{-1} d^{-1} was recorded [25]. One drawback was that it could not be differentiated between the share of nitrogen metabolized by each co-culture partner. In consequence, the process conditions chosen were a trade-off between providing enough nitrogen for the cyanobacterium to grow and produce sucrose while having sufficiently low nitrogen to induce a PHA accumulation regime in *P. putida*. Thus, an alternative nitrogen source for the heterotrophic partner, the carbamide urea, was investigated as a second step toward an improved co-culture production process. *S. elongatus* does not have genes for urea degradation in contrast to *P. putida* (result of database search). Therefore, using urea as an additional nitrogen source separates the nitrogen supply unilaterally. As expected, *P. putida* KT2440 was able to grow similarly with both nitrogen sources (see Figure 4.1 **C**). Initial experiments demonstrated the anticipated response in *S. elongatus cscB*; it exhibited comparable growth patterns in cases where either no nitrogen or 0.83 g L^{-1} urea was introduced. An undisturbed growth was observed when 2.35 g L^{-1} nitrate was used as the sole nitrogen source for the cyanobacterium. As the chlorophyll synthesis is connected to the nitrogen supply, the cultures without nitrate turned yellow-green, starting chlorosis or, in other words losing chlorophyll (see Figure 4.1 **D**) [147]. This specific urea metabolization allows the separation of the supplied nitrogen from the cyanobacterium and specifically boosts the growth of the heterotrophic partner. Consequently, a co-cultivation process with *S. elongatus cscB* and *P. putida cscRABY* for PHA production was established, with urea as an additional nitrogen source.

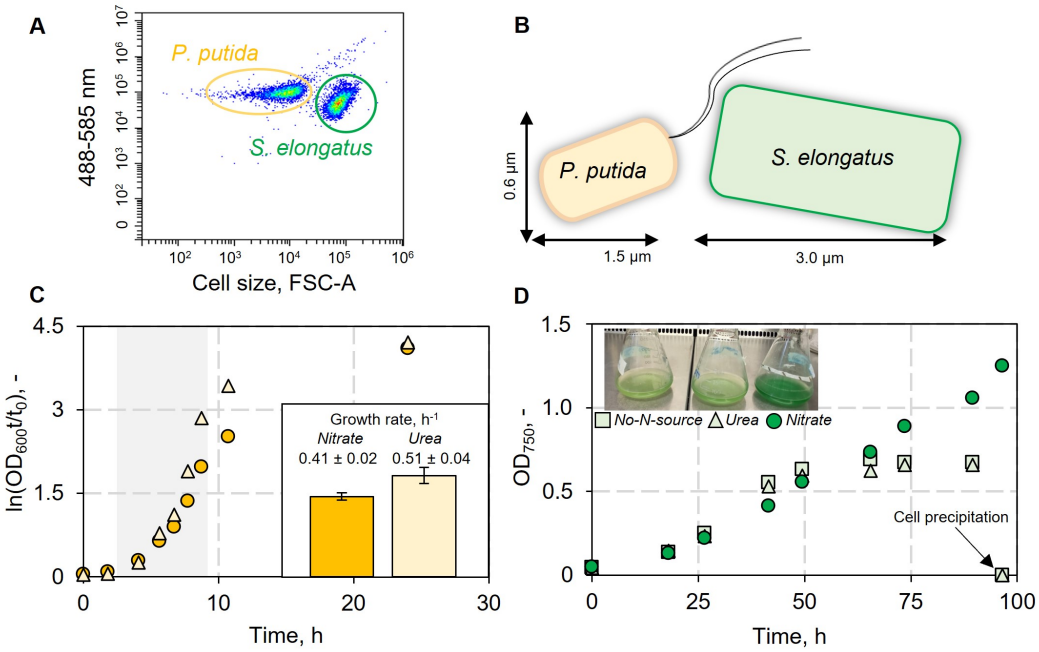

Figure 4.1: **(A)** Example of population separation of *P. putida cscRABY* and *S. elongatus cscB* over the cell size (correlated with forward scattering (FSC-A)) and the flourescene between 488-585 nm achieved by flow cytometry. **(B)** Schematic depiction of cell size of the co-culture partners. **(C)** Growth of *P. putida* KT2440 with urea (triangles) and nitrate (circles) as nitrogen sources in M9 medium. Experimental condition: Shake flask experiment with 10 mL M9 medium with 27.7 mmol nitrate or 13.8 mmol urea as nitrogen sources and glucose (5 g L^{-1}) as a carbon source at 30 °C, 220 rpm in an orbital shaker MaxQ 8000 from Thermo Scientific. **(D)** Growth of *S. elongatus cscB* with no nitrogen (squares), urea (triangles), and nitrate (circles). After 50 h, a loss of chlorophyll was observed when grown with no nitrogen or urea, and after 75 h, cell precipitation was observed. Experimental condition: Shake flask experiment with 20 mL $BG11^+$ medium supplemented with nitrate 27.7 mmol or urea 13.8 mmol at 25 °C, 120 rpm, 20 µmol photons s^{-1} m^{-2} in an orbital shaker (Multitron Pro from Infors HT).

The co-cultivation process was separated into two phases, a first axenic culture phase, in which *S. elongatus cscB* was cultivated axenically, and a subsequent co-cultivation phase. This phase was started by the addition of *P. putida cscRABY* to the process vessel (see Figure 4.2 **A**). During the whole process, the optical density was determined at 750 nm, reflecting the cell density of both strains in the co-culture phase. Additionally, the cell count of each strain was monitored by flow cytometry, which enables recording the co-culture partners' respective growth (see 4.2 **B**). The nitrogen-free $BG11^+$ medium was supplemented with an initial amount of 50 mg L^{-1} nitrate, which served for biomass production and adaptation phase to light and salt of the cyanobacterium. After the batch nitrate was completely metabolized, marked by a drop in the pO_2, a constant nitrate feed of 74 mg L^{-1} d^{-1} was set, resulting in linear growth of *S. elongatus cscB* (see Figure 4.2 **B**). After an OD_{750} of 0.6 was reached, sucrose secretion was switched on by inducing the expression of the heterologous *cscB* symporter in *S. elongatus cscB*, and cells were grown for another 30 h to increase the extracellular sucrose concentration for the supply of the heterotrophic partner. In the subsequent co-cultivation phase, the nitrate feed was raised to 110 mg L^{-1} d^{-1}, and a batch of urea in a concentration of 36 mg L^{-1} was added. As a result, the co-cultivation phase is further divided into a biomass production phase of *P. putida cscRABY* in which urea is available to enhance the heterotrophic growth and a PHA-production phase, where nitrogen is limited by the overall applied nitrate feed (see Figure 4.2 **A**). Through the nitrogen limitation, linear growth of the cyanobacterial partner with a non-specific growth

rate of $23.8 \cdot 10^7 \pm 1.62 \cdot 10^7$ cell mL^{-1} d^{-1} settled. *P. putida cscRABY* growth slowed down after urea was completely metabolized to a rate of $5.52 \cdot 10^7 \pm 1.26 \cdot 10^7$ cells mL^{-1} d^{-1} (calculated from process time 150 to 330 h). Simultaneously, sucrose started to accumulate in the supernatant, reaching a maximum titer of 1.1 g L^{-1}. These conditions of carbon overflow and nitrogen limitation are favorable for the accumulation of the naturally produced storage compound mcl-PHA in *P. putida*. Therefore, with the depletion of the urea, *P. putida cscRABY* entered the PHA production phase. The intracellular PHA was quantified after one pot extraction and propanolysis from the cells by gas chromatography (for detailed method description, see Chapter 3.6.4). In the overall process, a maximum titer of 256 ± 2 mg L^{-1} was reached, which corresponds to an average of 0.12 pg PHA $cell^{-1}$ (see Figure 4.2 **C**). A production rate of PHA of 9 ± 2.13 mg L^{-1} d^{-1} (calculated between 10.2–26 days) was reached. As expected, the composition of the accumulated polymer did not change, with 3-hydroxydecanoic acid (∼ 62%) being the most abundant and 3-hydroxyoctanoic acid (∼ 23 %) the second most abundant (see Appendix A.7 Table A.5).

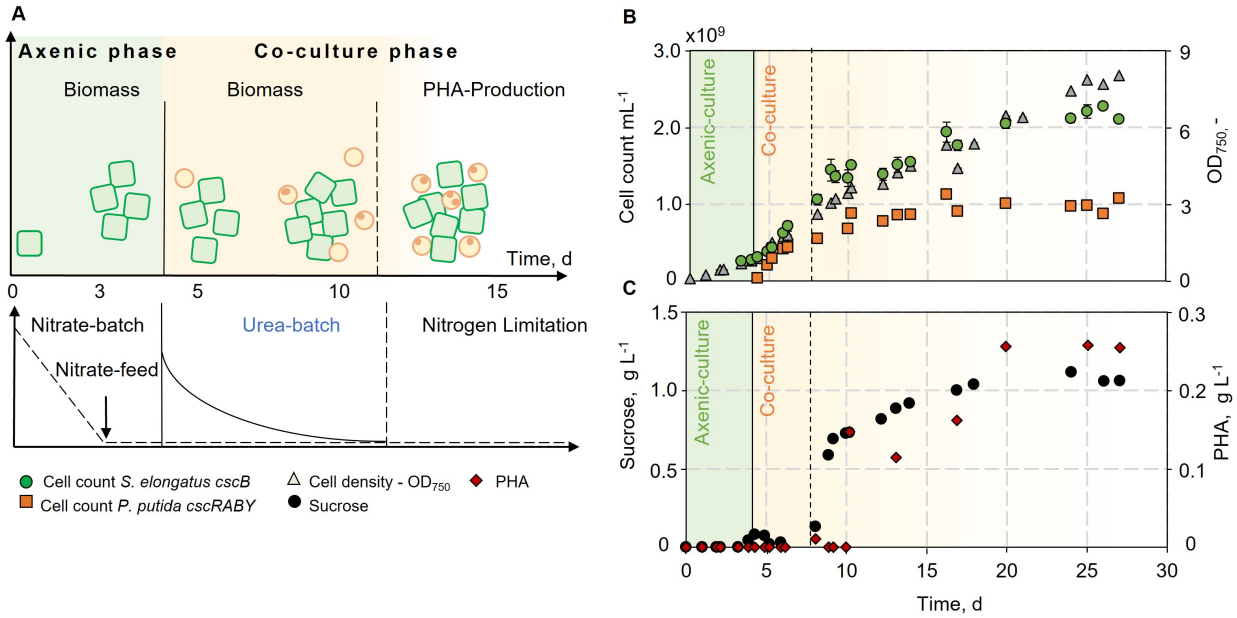

Figure 4.2: Co-culture of *S. elongatus cscB* and *P. putida cscRABY* with nitrate limitation in a flat panel photobioreactor with a working volume of 1.8 L. The process was divided into two phases: Axenic-culture of *S. elongatus cscB* with a nitrate batch of 50 mg L^{-1} and a nitrate feed of 74 mg L^{-1} d^{-1} (green area) for acclimatisation and biomass production. The co-culture phase started with inoculation (vertical line) of *P. putida cscRABY* and the medium was supplementation of a urea batch concentration of 36 mg L^{-1}. Simultaneously, the nitrate feed was adjusted to 110 mg L^{-1} d^{-1} (yellow area). The co-culture phase can be subdivided into a biomass accumulation phase for the heterotrophic partner and a PHA-production phase in which nitrogen is limiting. **(A)** Graphical overview of the co-culture process; green = phototrophic partner and yellow = heterotrophic partner. **(B)** Growth of the co-culture partners is represented in cell count and shared OD_{750}. Values given are the mean of technical triplicates, and the error bars represent the standard deviation. **(C)** Sucrose and PHA concentrations were determined in single measurements. Process conditions: $BG11^+$ supplemented with 150 mM NaCl at 30 °C and pH 7.4 (not controlled); Aeration: 1.96 NL min^{-1} air with 2 % CO_2; Illumination: constant at 240 µmol photons s^{-1} m^{-2}; Induction of the sucrose permease CscB was conducted with 0.1 mM IPTG simultaneously when the nitrate feed was started.

Discussion

The application of the sucrose metabolizing strain *P. putida cscRABY* led to a stable co-culture with *S. elongatus cscB* by more than three weeks. The implemented nitrogen limitation over a shared nitrate feed allowed for a maximum titer of 256 ± 2 mg L^{-1} of PHA, which is 1.5 times more than with the previously used co-culture partner *P. putida cscAB* [27]. Adding urea enabled a biomass production phase of *P. putida* preceding the PHA accumulation phase. Since PHA is accumulated in hydrophobic inclusions, the carbonosomes, higher biomass production of the heterotrophic partner allows for higher PHA titer. The cell counts in the previous processes with *P. putida cscAB* came from counting colony-forming units (cfu) and can not be compared to the measured cell count from the flow cytometer. It should be noted that cfu counting usually underestimates cell counts, which corresponds to an overestimated PHA yield per cell.

Although *S. elongatus cscB* is not capable of metabolizing urea, *P. putida cscRABY* can metabolize both nitrogen sources, making it difficult to accurately calculate the nitrogen available for the heterotrophic partner and, consequently, for PHA accumulation. Thus, it was not possible to estimate the limitation for *P. putida*, which was set by the implemented nitrate feed.

At this point, it should be further noticed, that a stabilizing effect on *S. elongatus cscB* did occur when the cyanobacterium was grown in co-culture with urea as the sole nitrogen source. The axenic cultures showed chlorosis after 2-3 days, and in the end cell precipitation. The cyanobacterial cells in co-culture with *P. putida cscRABY*, even though not growing, remained green over more than two weeks (see Figure A.7 **A**). However, the growth of *S. elongatus cscB* was not positively effect by just adding urea, as it was confirmed in co-cultures supplemented with both nitrate and urea (see Figure A.7 **B**).

4.1.2 Growth control: *P. putida cscRABY* △*nasT* and individual N-sources

The optimal carbon-to-nitrogen ratio for PHA accumulation in *P. putida* is approximately 26 [29]. In the synthetic co-culture, the carbon supply is limited by the sucrose production of *S. elongatus cscB* and the supplemented nitrate is shared between the two organisms. To precisely adjust the needed nitrogen for the heterotrophic partner, further separation and controllability of the process are necessary. Therefore, another recently constructed strain, *P. putida cscRABY* △*nasT*, employed in the co-culture. This strain is no longer able to metabolize nitrate due to the deletion of the NasT response regulator protein of the two-component system NasS/NasT [30]. Consequently, nitrate is exclusively available for *S. elongatus cscB*. To enable and control the growth of *P. putida cscRABY* △*nasT* and to set the PHA-producing condition, urea was used as a nitrogen source for this organism. First, the individual tunability of the growth of *P. putida cscRABY* △*nasT* by different urea feeds in the co-culture was investigated. For this, a co-culture process (Process 1) with three different urea feeding rates (see Table 4.1) and a non-limiting nitrate batch (2.35 g L^{-1}) was set up. The co-culture consisted of the phototrophic partner *S. elongatus cscB* and the most recently constructed *P. putida cscRABY* △*nasT* (see Figure 4.3 **A**).

As in the process described before, a first axenic phase for acclimatization of the cyanobacterium was conducted in which, upon induction of sucrose secretion, up to 1.6 ± 0.13 g L^{-1} of sucrose was detectable in the supernatant. During the process *S. elongatus cscB* showed a sigmoidal growth behavior because of non-limited nitrogen conditions implemented (see Figure 4.3 **B**). The change from exponential to linear

growth occurs most likely due to light limitation caused by self-shading effects. The subsequent co-culture phase was again started by inoculation of *P. putida cscRABY* Δ*nasT* and the accumulated sucrose was immediately metabolized. The first urea feeding rate of 13.3 mg L^{-1} d^{-1} resulted in linear growth of the heterotroph with a rate of around $2 \cdot 10^{11}$ cells mL^{-1} d^{-1}. Throughout this first phase, *P. putida cscRABY* Δ*nasT* experienced both carbon and nitrogen limitation as sucrose concentration stayed at low levels. In total, 36 mg L^{-1} of urea were supplied in this first feeding phase which equals the amount of urea that served as a batch in the process described above with *P. putida cscRABY* (see 4.1.1). After this heterotrophic biomass generation phase, a cell count of $0.5 \cdot 10^9$ cells mL^{-1} was reached, which compared very well to the one reached in the process described in Section 4.1.1 after the supplied urea batch was consumed. Now, the PHA production phase was initiated by generating a stronger nitrogen limitation due to a reduction of the urea feeding rate by two to 6.7 mg L^{-1} d^{-1}, which likewise resulted in half of the non-specific growth rate of *P. putida cscRABY* Δ*nasT* of around $1.1 \cdot 10^{11}$ cells mL^{-1} d^{-1} (see Table 4.1). To test the effect of a further reduction of the urea supply on the growth of *P. putida cscRABY* Δ*nasT*, in a third phase 2.2 mg L^{-1} d^{-1} urea were fed. This led to a constant cell count of $1 \cdot 10^9$ cells per ml, which might be a result of a strong nitrogen limitation (see Figure 4.3 **C**).

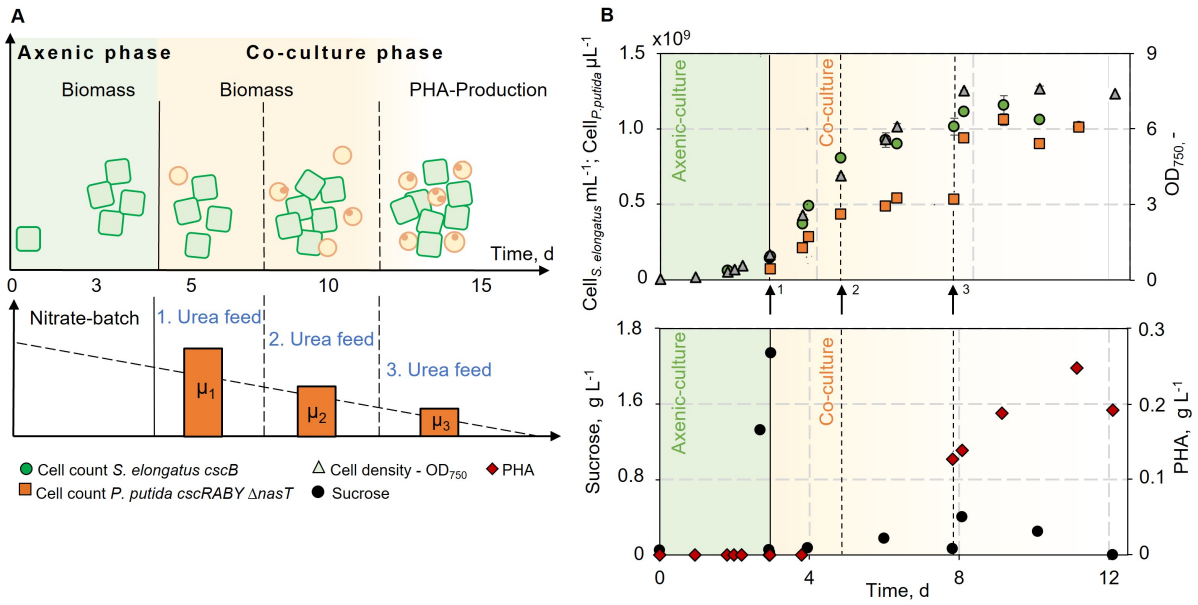

Figure 4.3: Co-culture of *S. elongatus cscB* with *P. putida cscRABY* Δ*nasT* in a 1.8 L scale (Process 1). The process was divided into two phases: Axenic culture of *S. elongatus cscB* with non-limited nitrate supply (green area) and a co-culture phase (yellow area), which started with the inoculation (vertical line) of *P. putida cscRABY* Δ*nasT*. The co-culture phase comprised three different urea-feeding rates indicated by arrows 13.3 mg L^{-1} d^{-1} ($\uparrow^1$), 6.7 mg L^{-1} d^{-1} ($\uparrow^2$) and 2.2 mg L^{-1} d^{-1} ($\uparrow^3$). The co-cultivation phase can be subdivided into a biomass production phase of the heterotrophic partner and a PHA-accumulation phase. The PHA-production phase was initiated by nitrogen limitation (dashed lines). **(A)** Graphical overview of the process with three different urea feeds; μ_1-μ_3 indicate the growth rates of *P. putida cscRABY* Δ*nasT* with the respective urea feed. **(B)** Growth of the co-culture partners represented in cell count and OD_{750}. The numbers given are the mean of technical triplicates, and the error bars represent the standard deviation. **(C)** Sucrose and PHA concentrations during the process. PHA data represent the results of single or duplicate measurements. Process conditions: $BG11^+$ supplemented with 150 mM NaCl at 30 °C and pH 7.4 (controlled with HNO_3); Aeration: 1.96 NL min^{-1} air with 2% CO_2; Illumination: constant at 240 µmol photons s^{-1} m^{-2}; Induction of CscB permease with 0.1 mM IPTG.

Analysis of the PHA concentration revealed, that the polymer was accumulated primarily in the second and third feeding phases (see Figure 4.3 **C**). Here, growth was reduced to an extent that allowed sucrose to accumulate in the medium, which created a regime of carbon overflow and nitrogen limitation. In the overall process, a maximum titer of 209 ± 33 mg PHA L^{-1} was reached with a maximal PHA production rate of 33 ± 4.4 mg L^{-1} d^{-1}. The maximum titer compares well to the process described in Section 4.1.1. But due to the considerably reduced process time, the maximum PHA production rate was about twice as high. At the end of the process (after around 12 days), when sucrose was no longer detectable anymore, PHA levels slightly decreased again, presumably due to metabolization by *P. putida cscRABY* Δ*nasT* itself.

Process with limited nitrate and urea-feeds

The next logical step was to combine the two processes described to gain more control over the growth and sucrose secretion of the cyanobacterium with a nitrate feed and adjust *P. putida's* growth with an urea-feed. This differential feeding strategy allows setting and controlling the growth rates of both partner strains individually. The volumetric PHA yield of the overall process should be increased by raising the cell number of *P. putida cscRABY* Δ*nasT* through more available nitrogen (see Table 4.1). The processes (Process 2) had the same phases as before (see Figure 4.4 **A**) and the acclimatization phase of *S. elongatus cscB* compared well to the approach with *P. putida cscRABY* (see 4.1.1). In contrast to the first process, a nitrate feed of 105 mg L^{-1} d^{-1} was implemented, which resulted in a higher growth rate of the cyanobacterium ($33.4 \cdot 10^7$ cell mL^{-1} d^{-1}) in comparison to the process described in Section 4.1.1. Furthermore, the final cell count reached was around $2.6 \cdot 10^9$ cells ml^{-1}, which is more than twice as high as observed in the previous processes (see Figure 4.4). As in the previous process three different urea-feeding rates were applied for *P. putida cscRABY* Δ*nasT* (see Table 4.1). They were chosen to provide different ratios of carbon to nitrogen, as PHA accumulation is known to be dependent on the carbon to nitrogen $\frac{r_{mol_C}}{r_{mol_N}}$ ratio [28], [126]. The first feeding rate was set to 40 mg L^{-1} d^{-1}, which is three times higher than in the first process with *P. putida cscRABY* Δ*nasT* described above. This resulted in a growth rate of about $4.9 \cdot 10^8$ cells mL^{-1} d^{-1} and a final cell count of $8.5 \cdot 10^8$ cells mL^{-1} at the end of this phase (see Figure 4.4 **B**). In this phase, a slight accumulation of sucrose of ∼ 0.2 g L^{-1} was detectable, suggesting that growth was still limited by the nitrogen source (see Figure 4.4 **C**). The second and third feeding rates were 20 and 2.2 mg L^{-1} d^{-1} and should provide conditions for PHA production with medium and high nitrogen limitation. In total, 2.3 times more urea was fed than in the previous process with *P. putida cscRABY* Δ*nasT*. The second feeding rate, which was half of the first feeding rate, resulted in a growth rate of around $2.3 \cdot 10^8$ cells mL^{-1} d^{-1}, which is about half of the growth rate observed in the first feeding phase. With the third feeding rate, which was approximately nine times lower than the second, the growth rate consequently was also reduced by a factor of nine, remaining nearly constant (see Table 4.1). With this, the non-specific growth rate of *P. putida cscRABY* Δ*nasT* could predictably be set by adjusting the urea feeding rate, while the growth of *S. elongatus cscB* was not influenced.

The adjusted urea-feeding rate had a direct influence on the PHA accumulation. In the first feeding phase, the $\frac{r_{mol_C}}{r_{mol_N}}$ ratio was the lowest, so no PHA accumulation could be detected. However, in the second feeding phase in which less urea was supplied, a higher $\frac{r_{mol_C}}{r_{mol_N}}$ ratio is expected when the sucrose-secretion remains

constant. PHA started to accumulate with a rate of 33 ± 1.1 mg L^{-1} d^{-1}. Sucrose accumulated in the medium, clearly indicating that the growth of *P. putida cscRABY ΔnasT* was limited by the nitrogen source. In the third feeding phase, where the $\frac{r_{mol_C}}{r_{mol_N}}$ ratio is expected to be even higher by a strong reduction of the urea concentration in the feed, no further increase in the amount of PHA accumulation could be observed, except for the sample point directly after the change to the third feeding rate, suggesting a too strong limitation. The highest achieved titer with this method was 292 ± 10 mg L^{-1}. The sucrose concentration remained stable at a constant level of around 1 g L^{-1} until day 13, after which it started to decline along with the accumulated PHA.

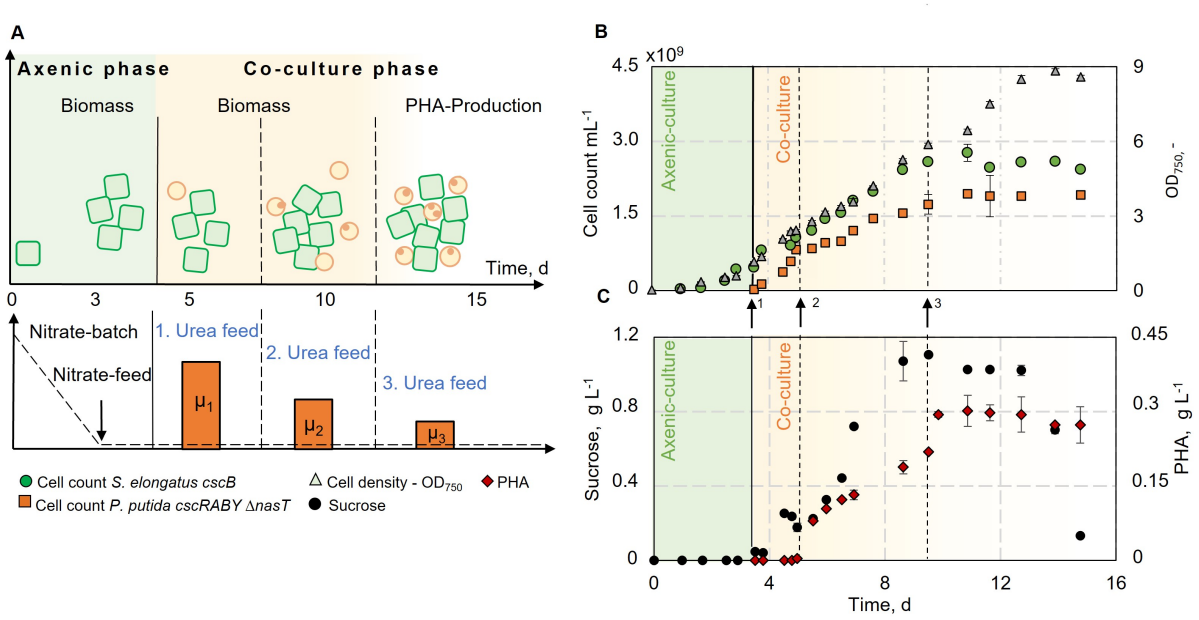

Figure 4.4: Co-culture of *S. elongatus cscB* with *P. putida cscRABY ΔnasT* with N-limitation for both co-culture partners in a 1.8 L scale process (Process 2). The overall process was divided into two main phases: Axenic culture phase of *S. elongatus cscB* with a batch nitrate supply of 50 mg L^{-1} (green area) and after biomass generation a constant nitrate feed of 105 mg L^{-1} d^{-1}; A co-culture phase (yellow area) started with the inoculation (vertical line) of *P. putida cscRABY ΔnasT* and comprised two different urea-feeding rates indicated by arrows: 40 mg L^{-1} d^{-1} ($\uparrow^1$) and 20 mg L^{-1} d^{-1} ($\uparrow^2$). The co-cultivation phase can be subdivided into a biomass production phase of the heterorophic partner and a PHA-accumulation phase. The PHA-production phase was initiated by nitrogen limitation (dashed lines). **(A)** Graphical overview of the process with two different urea feeds; μ_1- μ_3 indicate the growth rates of *P. putida cscRABY ΔnasT* with the respective urea feed. **(B)** Growth of the co-culture partners is represented in cell count and OD_{750}. The numbers given are the mean of technical triplicates, and the error bars represent the standard deviation. **(C)** Sucrose and PHA concentrations during the process. PHA measurements were performed in duplicates. Process conditions: $BG11^+$ supplemented with 150 mM NaCl at 30 °C and pH 7.4 (controlled with HNO_3); Aeration: 1.96 NL min^{-1} air with 2% CO_2; Illumination: constant at 240 µmol photons s^{-1} m^{-2}; Induction of CscB permease with 0.1 mM IPTG simultaneously when the nitrate feed was started.

Table 4.1: Urea feeding rates and non-specific growth rate of *P. putida cscRABY* Δ*nasT* in process.

Urea feed, mg L^{-1} d^{-1}	Growth rate, cells mL^{-1} d^{-1}	Nitrogen concentration
Process 1 with *P. putida cscRABY* Δ*nasT*		
Feeding-rate I - 13.3	$2.0 \cdot 10^{11} \pm 1.6 \cdot 10^{10}$	High
Feeding-rate II - 6.7	$1.1 \cdot 10^{11} \pm 5.8 \cdot 10^{10}$	Medium
Feeding rate III - 2.2	$5.8 \cdot 10^{10} \pm 3.9 \cdot 10^{10}$	Low
Process 2 with *P. putida cscRABY* Δ*nasT*		
Feeding-rate I - 40	$4.9 \cdot 10^{8} \pm 0.8 \cdot 10^{8}$	High
Feeding-rate II - 20	$2.3 \cdot 10^{8} \pm 0.2 \cdot 10^{8}$	Medium
Feeding rate III - 2.2	$2.7 \cdot 10^{7} \pm 0.2 \cdot 10^{8}$	Low

Estimation of the settled $\frac{C}{N}$-ratio

A molar ratio of the concentration of carbon to nitrogen $\frac{r_{mol_C}}{r_{mol_N}}$ in the medium of approximately 26 was described to be optimal for PHA accumulation in *P. putida* KT2440 [29]. Through control of both co-culture partners' growth rates, the adjusted ratio in each urea-feeding phase can be estimated and put into context with the literature.

Whereas the nitrogen concentration is known through the defined urea feed, the exact carbon concentration in the medium cannot be directly measured. The reason for this is that a share of the sucrose secreted by *S. elongatus cscB* is directly consumed by heterotrophic partner and converted to cell mass, PHA, or utilized for cell maintenance. Therefore, a good estimation of the amount of sucrose, or carbon secreted by *S. elongatus cscB* had to be found. The time-dependent sucrose concentration in the bioreactor ($\frac{dc_{suc}}{dt}$) is described by the differential Equation (4.1). It considers, the sucrose secretion by *S. elongatus cscB* (r_{sec_suc}) and the sucrose uptake of *P. putida cscRABY* Δ*nasT* ($q_{up\_suc} \cdot c_{P.puitda}$). This apparent sucrose accumulation rate (r_{acc_suc}) can be described as:

$$\frac{dc_{suc}}{dt} = r_{acc\_suc} = r_{sec\_suc} - q_{up\_suc} \cdot c_{P.putida} \tag{4.1}$$

whereby $c_{P.puitda}$ (g L^{-1}) represents the cell dry weight of *P. putida cscRABY* and the sucrose specific uptake rate is given by q_{up_suc} (h^{-1}). The cyanobacterial sucrose secretion rate is described by r_{sec_suc} (g L^{-1} h^{-1}). The sucrose secretion rate is, therefore:

$$r_{sec\_suc} = r_{acc\_suc} + q_{up\_suc} \cdot c_{P.putida} \tag{4.2}$$

The sucrose specific uptake rate by *P. putida* can be defined as follows:

$$q_{up\_suc} = \frac{\mu_{P.putida}}{Y_{C_{X\,suc}}} + q_{PHA} \tag{4.3}$$

With $\mu_{P.putida}$ being the specific growth rate and $Y_{C_{X\,suc}}$ the biomass yield of *P. putida* with sucrose. q_{PHA} (h^{-1}) defines the specific product formation rate of PHA. Insertion of (4.3) in Equation (4.2) leads to:

$$r_{sec\_suc} = r_{acc\_suc} + \left(\frac{\mu_{P.puitda}}{Y_{C_{X\,suc}}} + q_{PHA}\right) \cdot c_{P.puitda} \tag{4.4}$$

The growth rate $\mu_{P.putida} = \frac{r_{P.puitda}}{c_{P.puitda}} \approx$ constant, and the PHA production rate $q_{PHA} = \frac{r_{PHA}}{c_{P.puitda}} \approx$ constant could be extracted from linear regression of the experimental data in the respective time period. The same procedure was used for calculating the sucrose accumulation rate (r_{acc_suc}). The biomass yield from sucrose of *P. putida cscRABY* was determined previously to be 0.23 ± 0.02 g g^{-1} and was considered constant [27] (see Section 3.5.1). Finally, the sucrose secretion r_{sec_suc} rate can be transformed into a molar carbon secretion rate r_{mol_c} which is represented in Equation (4.5):

$$r_{mol_c}[mol \cdot h^{-1}] = (r_{acc\_suc} + \frac{r_{P.puitda}}{Y_{C_{Xsuc}}}) \cdot \frac{12 \cdot V_R}{M_{suc}} + r_{PHA,mol} \cdot 9.63 \tag{4.5}$$

whereby V_R (L) represents the reactor volume, M_{suc} (g mol^{-1}) the molar mass of sucrose and $r_{PHA,mol}$ the molar PHA production rate. The number 9.63 represents the weighted average number of carbon atoms in the heteropolymer mcl-PHA accumulated in *P. putida cscRABY* grown on sucrose. With an estimation of the supplied carbon in the process the $\frac{mol_C}{mol_N}$ ratio can be calculated with Equation (4.6):

$$\frac{mol_C}{mol_N}[-] = \frac{r_{mol_C}}{r_{mol_N}} \tag{4.6}$$

The so obtained $\frac{r_{mol_C}}{r_{mol_N}}$ ratios can be found in Table 4.2. The ratio in the first urea feeding-phase was ≈ 20.1, and for the second phase a ratio of ≈ 31 can be calculated. Both ratios are close to 26, which is regarded as optimal for PHA accumulation in pseudomonads, but PHA accumulation was only observed in the second phase with a ratio of 31. For the last implemented feeding rate, the ratio could not be calculated since the growth of the heterotrophic partner was nearly constant, and no further increase in sucrose concentration was measured. Regarding this, a r_{mol_C} of zero would lead to a ratio of zero, which might explain no further PHA accumulation at the end of the process.

Table 4.2: Estimated $\frac{r_{mol_C}}{r_{mol_N}}$ ratio for second process with *P. putida cscRABY ΔnasT*

Urea feed	**Estimated $\frac{r_{mol_C}}{r_{mol_N}}$ ratio, -**
Feeding-rate I	20.1
Feeding-rate II	31
Feeding rate III	n. a.[2]

4.1.3 Optimization of the C/N-ratio for PHA production in the co-culture

In Process 3, the PHA accumulation phase was designed in a way to reach a $\frac{r_{mol_C}}{r_{mol_N}} \approx 26$. By assuming that the molar carbon secretion rate r_{mol_C}, which is equivalent to the sucrose secretion rate of *S. elongatus cscB*, is constant, an increase of the nitrogen feed should lower the $\frac{r_{mol_C}}{r_{mol_N}}$ ratio. Hence, in order to lower the $\frac{r_{mol_C}}{r_{mol_N}}$ ratio from 31 to 26 during the PHA accumulation phase, the urea-feeding rate needs to be increased by 25%. To achieve this, the urea-feeding rate was set to 25 mg L^{-1} d^{-1} as can be seen in Table 4.3. Otherwise the process was conducted as before (see Figure 4.5 **A**). The axenic phase compared well to the ones of the processes before, and sucrose was readily accumulated and reached a maximum of 0.54 g L^{-1}. The first

[2] n. a.= not applicable

urea-feeding phase served, as in the prior processes, as the biomass production phase of *P. putida cscRABY* Δ*nasT* with the same urea feed being supplied as in the process described in Section 4.1.2. This led to a comparable growth rate of about $10^8 \pm 1.5 \cdot 10^8$ cells mL^{-1} d^{-1} (see Figure 4.5 **B**). In the subsequent PHA production phase, the growth rate of *P. putida cscRABY* Δ*nasT* declined due to N-limitation, but it remained higher than in the process described in Section 4.1.2, as more nitrogen was available due to the decreased $\frac{r_{mol_C}}{r_{mol_N}}$ ratio (compare Table 4.3). The accelerated growth also led to a higher sucrose consumption rate, leading to lower sucrose levels in the medium compared to the processes previously described.
Taking the experimental data of the designed process into account, the $\frac{r_{mol_C}}{r_{mol_N}}$ ratio was calculated to be 25.8, which closely matches the desired target of 26. The PHA accumulation rate was determined to be 42.1 mg L^{-1} d^{-1}. However, it is worth noting that PHA accumulation already started in the biomass production phase suggesting that the heterotrophic cells were stressed and/or perceived signals of limitation. Furthermore, the ratio in the first phase could not be estimated due to decreasing sucrose concentrations. The cell count of *P. putida cscRABY* Δ*nasT* was higher than in the other processes because more carbon was available for biomass production and maintenance. This is also reflected by the higher maximum PHA titer of 393 ± 53 mg L^{-1} (see Figure 4.5 **C**). By the end of the process, almost all sucrose was consumed by *P. putida cscRABY* Δ*nasT*. This suggests that the cell count of *P. putida cscRABY* Δ*nasT* already was in the maximum range possible, as there is an inherent limitation due to the amount of sucrose produced by *S. elongatus cscB* in the co-culture.

Table 4.3: Urea feeding rate, non-specific growth rate and the $\frac{mol_C}{mol_N}$-ratio of *P. putida cscRABY* Δ*nasT*.

Urea feed, mg L^{-1} d^{-1}	**Growth rate, cells mL^{-1} d^{-1}**	**Estimated $\frac{mol_C}{mol_N}$ ratio, -**
Feeding-rate I - 40	$5.1 \cdot 10^8 \pm 1.5 \cdot 10^8$	n.a.[3]
Feeding-rate II - 25	$3.5 \cdot 10^8 \pm 1.2 \cdot 10^8$	25.8

[3] n. a.= not applicable

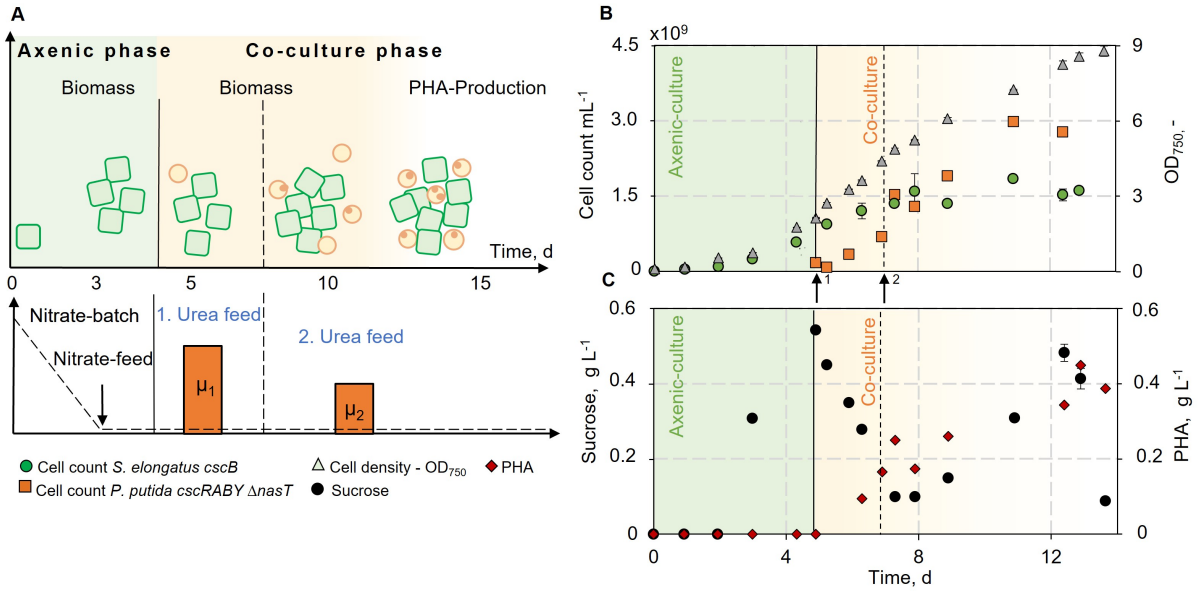

Figure 4.5: Co-culture of *S. elongatus cscB* with *P. putida cscRABY* Δ *nasT* with an optimized $\frac{mol_C}{mol_N}$ ratio in a 1.8 L scale process (Process 3). The process was divided into two phases: Axenic-culture of *S. elongatus cscB* with a nitrate batch of 50 mg L^{-1} and a nitrate feed of 105 mg $L^{-1}d^{-1}$ (green area). Co-culture phase (yellow area) started with inoculation (vertical line) of *P. putida cscRABY* Δ*nasT*. Two different urea feed rates were applied, indicated by arrows: 40 mg $L^{-1}d^{-1}$ ($\uparrow^1$) and 25 mg $L^{-1}d^{-1}$ ($\uparrow^2$). The PHA-production phase by nitrogen limitation is indicated with a dashed line. **(A)** Graphical overview of the process. μ_1 and μ_2 represent the growth rates of *P. putida cscRABY* Δ*nasT* with the respective urea feed. **(B)** Growth of the co-culture partners represented in cell count and OD_{750}. The numbers given are the mean of technical triplicates, and the error bars represent the standard deviation. **(C)** Sucrose and PHA concentrations in the process. Sucrose and PHA measurements were performed in single or double measurements. Process conditions: $BG11^+$ supplemented with 150 mM NaCl at 30 °C and pH 7.4 (controlled with HNO_3); Aeration: 1.96 NL min^{-1} air with 2% CO_2; Illumination: constant at 240 μ mol photons s^{-1} m^{-2}; Induction of CscB permease with 0.1 mM IPTG.

Discussion

Medium chain length polyhydroxyalkanoates (Mcl-PHAs) are industrially valuable polymers combining similar properties of petroleum-based plastics with biocompatibility and -degradability. *P. putida* accumulates mcl-PHA from different carbon sources, such as fatty acids and glucose [28]. Through the introduction of the *cscRABY*-operon, a stable sucrose consuming co-culture partner was generated [27]. Utilizing this engineered strain in a co-culture process for PHA production resulted in a 60% higher PHA titer compared to the previously employed *P. putida cscAB* strain. It is advantageous to apply a limitation for PHA accumulation in pseudomonads, especially when grown on PHA non-related substrates. Thus, the applications of *P. putida cscRABY* Δ*nasT* [30], which is unable to grow on nitrate due to a deletion of the gene *nasT* was only reasonable to adjust a defined $\frac{mol_C}{mol_N}$ ratio and, therefore, implement PHA-producing conditions over nitrogen limitation.

The $\frac{mol_C}{mol_N}$ ratio adjusted in the co-culture represents a trade-off between the carbon produced by the cyanobacterium and availability of nitrogen in the medium. In Process 1, the non-limiting condition for the phototropic partner led to a uncontrolled release of sucrose, which was not synchronized with the nitrogen availability and, consequently, PHA production. Thus, individual and independent nitrogen supply was an option to meet the specific conditions of the co-culture for the production of PHA.

Different fed-batch strategies ($V_R \approx$ const.) allowed to adjust a defined $\frac{mol_C}{mol_N}$ ratio of 25.8 and in the final process (Process 3) a PHA titer of 393 mg L^{-1} with a rate of 42.1 mg $L^{-1}d^{-1}$ was produced. However, no increase in the PHA content could be achieved on the single-cell level, suggesting that a physiological optimum was already reached. Further improvement of the synthetic consortium in terms of PHA production, therefore, relies on other strategies, as working with high cell densities by employing other cyanobacterial strains with higher sucrose production rates. This might be achieved by applying the fast-growing *S. elongatus* UTEX 2973, which was recently equipped with *cscB* for sucrose secretion [154]. Another strategy would be to apply *P. putida* derivatives, metabolically engineered for an increased PHA production particularly with substrates structurally not related to PHA [110]. Many endeavors to increase the PHA accumulation in *P. putida* have been made. To just name a few: deletion of the PhaZ depolymerase or over-expression of PhaC polymerase. The deletion of *phaZ* gene increased mcl-PHA production when *P. putida* is cultured with sodium octanoate as the sole carbon source [28]. However, most other genetic manipulations had a negative effect on the delicate PHA metabolism [28]. In 2013, a significant improvement in PHA accumulation from glucose as carbon source was achieved by deleting the glucose dehydrogenase *gcd* and optimizing the production process [110]. The advancements in understanding the peculiarities in the core metabolism of *P. putida* are integrated into well-working metabolic core models of the bacterium, enabling more targeted metabolic engineering approaches [116].

As PHA is accumulated intracellularly, the costs of polymer recovery should be considered. This problem can be reduced by a well-controlled bio-process with defined biomass and production phases. A study demonstrated that well-designed extraction techniques for PHA can significantly reduce the cost per unit of PHA, thereby attributing the primary expenses to the input carbon sources in bio-production [171]. In a future co-culture process carbon from the atmosphere could contribute to lower costs. Another option is to focus on the 3-HA monomer production, which leave the cell due to their chemical properties [172]. These monomers could be customized polymerised after purification, so that, it meets the physical and chemical properties

needed.

Although *P. putida* has the ability to metabolize urea, the complete characterization of its urea metabolism is still ongoing. The urea degrading genes are located in an urease encoding operon (PP_2842 - PP_2849) controlled by NtrC [173]. However, disrupting genes in this operon using random barcode transposon sequencing did not lead to fitness decreased phenotypes when grown with urea as sole nitrogen source [173]. Despite that, it was shown that *S. elongatus cscB* is not affected by adding urea in axenic cultures, it could still use the side product HCO_3^- in the co-culture. As the air flow in the described processes was saturated with 2% carbon the small share of carbon introduced through urea (approx. 0.36 g L^{-1}) can assumingly be neglected. However, the co-culture should be, at least in future, a carbon neutral process, which might not be possible with urea as additional nitrogen source. Current industrial urea production is decidedly not environmentally friendly, as it's production, together with ammonium, has a high energy demand and CO_2 emissions. However, there is ongoing research to make ammonium and urea production more sustainable [174]. Moreover, *P. putida* might be able to use urea from waste-streams. To determine the suitability of urea as a nitrogen source in the future, processes involving the investigation of carbon balance can be implemented.

4.1.4 Co-cultivation with *P. putida cscRABY* Δ*gcd*

The *P. putida* KT2440 derivative *P. putida* KT2440 Δ*gcd* was described to double the PHA accumulation when grown on glucose. The reason behind this is that the deletion of the gene *gcd* prevents the bypass of periplasmatic glucose oxidation to gluconate. Further, the higher PHA accumulation was attributed to a shifted $\frac{NADPH}{NADP^+}$-ratio after analyzing the derivative with a metabolic core model [110]. Therefore, the strain should be enabled to metabolize sucrose via introducing the *cscRABY*-operon and investigated in terms of mcl-PHA accumulation as axenic culture and in the co-culture.

After successful side-specific integration of the *cscRABY* operon (see Section 3.8.1 for details), the growth of the new derivative *P. putida att*Tn7::*cscRABY* Δ*gcd* was investigated in M9 minimal medium with sucrose and compared to the wildtype *P. putida* KT2440 and the predecessor strain, grown on an equimolar glucose-fructose mixture. The resulting strain's growth behaved similarly to the predecessor *P. putida* KT2440 Δ*gcd* with similar growth rates of 0.44 ± 0.03 h^{-1} and 0.45 ± 0.01 h^{-1} (see Table 4.4). This is approx. 20% less than the growth rate of *P. putida* KT2440 when grown on a glucose-fructose solution. The growth reduction is in line with what is described in literature (see Figure 4.6 **A**) [110], [175]. The growth behavior of the predecessor strain with a glucose-fructose solution was precisely the same as observed for the new derivative and is therefore not shown in the diagram.

In batch experiments, an increase of PHA of approx. 20% was achieved when *P. putida* Δ*gcd* was grown on glucose according to literature [110]. After 24 h of PHA accumulating conditions, no significant difference between *P. putida cscRABY* and *P. putida cscRABY* Δ*gcd* was observed in shake flasks when grown on sucrose, but a slight but not significant increase in PHA accumulation was recorded when an equimolar mixture of fructose and glucose was used for both strains (see Figure 4.6 **B**). Even though no increase in PHA accumulation with sucrose as a carbon source was observed, a co-culture process at a scale of 1.8 L with similar conditions as described in Section 4.1.1 was set up to investigate PHA production under

co-culture and controlled conditions. *P. putida cscRABY* Δ*gcd* reached a maximal titer of ∼ 208 mg L^{-1} after 380 h of process time (end sample point OD_{750} = 6.62), which is in the range of what was accumulated in *P. putida cscRABY* and confirms the results in shake flasks with sucrose as the sole carbon source (see Appendix A.9).

Table 4.4: Growth rate of new derivative *P. putida* attTn7::*cscRABY* Δ*gcd* in comparison to predecessor strains.

***P. putida*-derivative**	**growth rate, h^{-1}**
P. putida KT2440	0.57 ± 0.03 h^{-1}
*P. putida att*Tn7::*cscRABY* Δ*gcd*	0.44 ± 0.03 h^{-1}
P. putida KT2440 Δ*gcd*	0.45 ± 0.01 h^{-1}

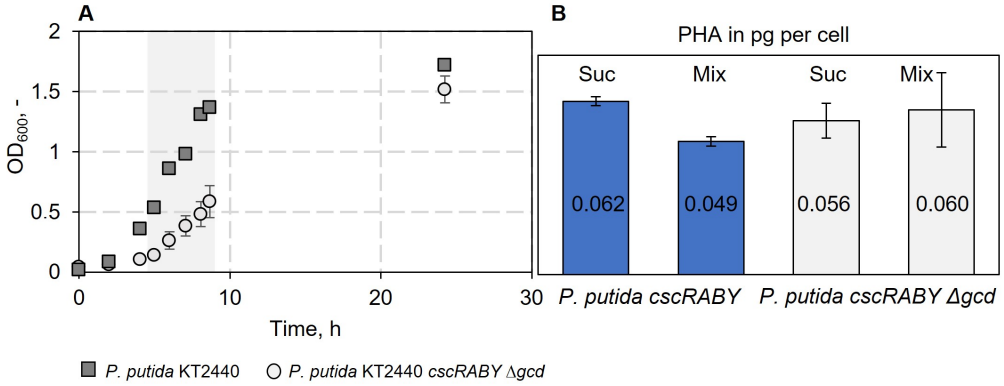

Figure 4.6: **(A)** Growth of *P. putida* KT2440 in comparison to the new strain *P. putida* KT2440 *cscRABY* Δ*gcd*. The gray area marks the region for calculating the growth rates. Experimental conditions: M9 medium supplemented with 2 g L^{-1}, 30 °C, 220 rpm. Single measurements were conducted for the wildtype culture *P. putida* KT2440 and biological triplicates were monitored for the *P. putida* KT2440 *cscRABY* Δ*gcd*. **(B)** PHA accumulation (in pg per cell) with sucrose or an equimolar mixture of glucose and fructose after 24 h. Blue = PHA accumulation for *P. putida cscRABY*; Gray = accumulation in *P. putida cscRABY* Δ*gcd*. Experimental conditions: M9 medium with nitrogen-limited conditions of 8 g L^{-1} sucrose or mixed carbon solution (equimolar fructose-glucose solution) and with 0.1 g L^{-1} NH_4Cl as nitrogen source, 30 °C, 220 rpm orbital shaker (MaxQ 8000 from Thermo Scientific, USA). The cultures were conducted in biological duplicates.

Discussion

The most likely explanation for no increase in PHA accumulation with sucrose in *P. putida cscRABY* Δ*gcd* in defined conditions lie at a metabolic level. The metabolic route of glucose oxidation to gluconate is assumingly already bypassed through the *cscRABY* operon, with the integration of the porin CscY in combination with the H^+/sucrose symporter CscB. The integration, therefore, seems to at least partially evade the oxidation of glucose in the periplasm and channels the glucose into the cytoplasm, where it is directly phosphorylated. This hypothesis is affirmed through the results obtained with the new derivative *P. putida cscRABY* Δ*gcd*. The two strains might be investigated in terms of gluconate production in limited and unlimited process conditions. Furthermore, the two strains should be investigated in terms of $\frac{ATP}{ADP}$ and $\frac{NADPH}{NADP^+}$, as the uptake with the GTS transport system might be more ATP costly in the *P. putida* Δ*gcd* strain than the uptake with the CscB transporter and subsequent phosphorylation in the cytoplasm. The metabolic properties of *P. putida cscRABY* might be a reason for the in general higher PHA accumulation of approx. 30% of the cell dry weight. Further, investigations of PHA accumulation in axenic *P. putida cscRABY* Δ*gcd* with the different carbon sources such as glucose, sucrose, or citrate are necessary to confirm the results described above. The use of a

transfer plasmid in the co-culture system could facilitate other genetic improvements (see Section A.2). Given the absence of antibiotics in the current co-culture processes, the sucrose operon *cscRABY* could serve as a potential selection marker. To further advance PHA accumulation in the co-culture process, a gene of interest could be *acoA*, which encodes a pyruvate dehydrogenase subunit. Overexpression of this gene has been shown to increase the PHA content in *P. putida* even more [126] (see Section A.2).

4.2 Exploring interaction in the synthetic co-culture of *S. elongatus cscB* and *P. putida cscRABY*

This chapter presents first physiological observations made during the co-cultivation of *S. elongatus cscB* and *P. putida cscRABY*. It provides an overview of the experimental setup used to investigate potential interactions between the two organisms in a parallel membrane reactor. Furthermore, the chapter concludes with a comprehensive presentation of transcriptional, proteomic, and metabolic obtained[4].

4.2.1 Physiologic interactions in focus

It was frequently observed that cyanobacteria grow more efficiently in co-cultivation with heterotrophic bacteria in both natural and synthetic co-cultures [176], [32]. As physiological changes in the growth behavior can manifest themselves in a reduced lag phase, a higher growth rate, or a more stable stationary phase, different scaled growth experiments were carried out. In the following experiments, the bacterial growth was compared between the co-culture and the respective axenic cultures.

Influence on initial growth

To analyse the influence of *P. putida cscRABY* on the initial growth of the co-culture partner *S. elongatus cscB* experiments were performed in 12-well plates at a scale of 1.6 mL. The cell count of the cyanobacterium was determined in the axenic-cultures and the co-culture after 24 h. It was differentiated between an “ON-” and an “OFF-status” of the synthetic connection. In the ON-mode, the sucrose secretion by *S. elongatus cscB* was induced, which was not the case in the OFF-mode where an additional batch of sucrose of 1 g L^{-1} was added to support heterotrophic growth (see Figure 4.7). As interaction may depend on the inoculation ratio (phototroph:heterotroph), different starting cell counts of *P. putida cscRABY* were used, which resulted in *S. elongatus cscB* to *P. putida* ratios of 1:1, 1:10^{-3}, and 1:10^{-5}. As shown in Figure 4.7 **A** & **B**, the presence of *P. putida* promotes the initial growth of *S. elongatus cscB* in every case, as cell counts of the cyanobacterium were higher in all co-cultures after 24 h compared to the axenic culture. This effect was independent of whether the synthetic connection between both partners via the sucrose feed was ON or OFF. In the ON-situation, no difference was observed with increasing inoculation ratios. whereas in the OFF-status with an inoculation ratio of 1:1, the positive effect on the cyanobacterial initial growth was slightly less pronounced. A possible explanation could be stronger shading effects on *S. elongatus cscB* due to higher cell densities of *P. putida cscRABY* reached within this first 24 h.

[4] Some of the presented results in this chapter have been summarized in a manuscript with the title "*Pseudomonas putida* as saviour for troubled *Synechococcus elongatus* in a synthetic co-culture – interaction studies based on a multi-OMICs approach" for publication.

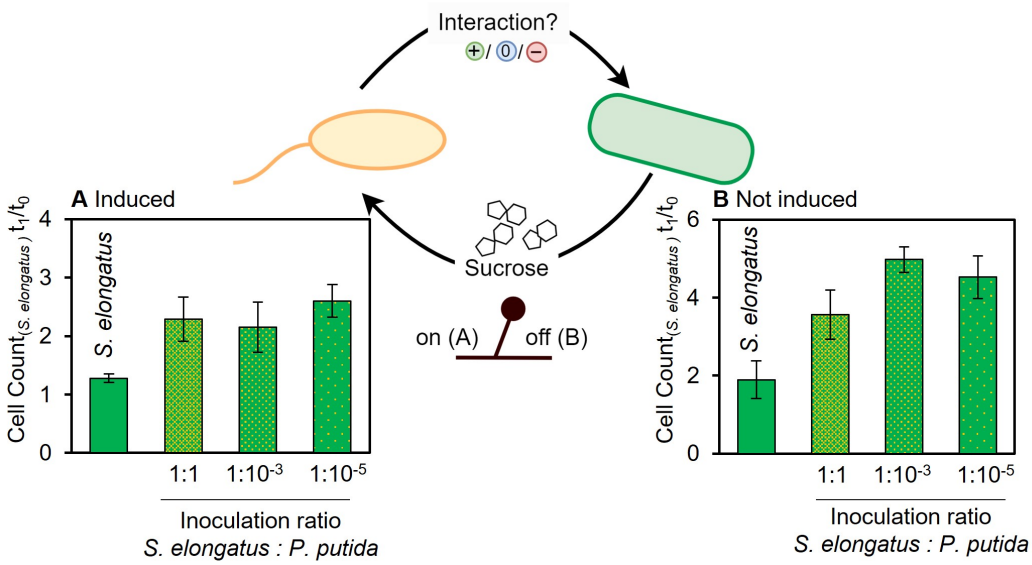

Figure 4.7: Influence from the heterotrophic partner on the initial growth of *S. elongatus cscB*. Depicted is the cell count of *S. elongatus cscB* in axenic culture and three co-cultures with decreasing initial *P. putida cscRABY* inoculation concentrations after 24 h. Data is normalized to the start cell count (t0). **(A)** "On-status" of the synthetic connection - IPTG-induced sucrose production. **(B)** "Off-status" - External support of heterotrophic growth by a sucrose batch. Experimental condition: 12-well plate, 1.6 ml $BG11^{+}$ supplemented with 150 mM NaCl, 25 °C, 120 rpm, 22 µmol m^{-2} s^{-1}, and no additional aeration. In the case of **(A)** 0.1 mM IPTG and in the case of **(B)** 1 g L^{-1} sucrose was added. Error bars derive from at least three biological triplicates.

Influence on the growth rate and long-term stability

To investigate influences on the growth rate and long-term stability, experiments were transferred to shake flasks at a scale of 20 mL. The decision to change the scale was primarily motivated by the challenge of water loss in the 12-well plates. This challenge could not be effectively prevented and would have resulted in substantial fluctuations of the cell count during prolonged experiments. In Figure 4.8 **A**, an example growth curve of axenic *S. elongatus cscB* induced (0.1 mM IPTG) and two co-cultures with an inoculation ratio of 1:1 and $1{:}10^{-4}$ are depicted. As can be seen, the progression of the different cultures' optical density is very similar. The slightly higher OD_{750} values for the co-culture are owed to the addition of *P. putida cscRABY*. The growth rate of *S. elongatus cscB* grown as an axenic culture determined from 12 biological replicates (see Figure 4.8 **B** and **C**) is statistically not different from the cyanobacterial growth rate in the co-culture (determined from 9 biological replicates). Furthermore, the cell count of *S. elongatus cscB* was the same after the cultures reached the stationary phase (120.5 h) when comparing the axenic culture to the co-cultures (see Figure 4.8 **D**). The observations from the shake flask experiments indicated a relatively neutral influence of *P. putida cscRABY* on the growth rate and stationary phase of *S. elongatus cscB*. In the axenic cultures sucrose accumulated to 0.253 ± 0.06 g L^{-1} (after 165 h) and 0.48 ± 0.03 g L^{-1} (after 303 h) (see Figure 4.8 **E**), whereby sucrose could not be measured in the co-cultures as it was metabolised by the heterotroph. Initial growth of *S. elongatus cscB* between 22-48 h was also influenced rather neutral in shake flasks, even though an inoculation ratio of 1:1 showed a slightly positive effect. Therefore, the positive effect of the heterotroph on the phototrophic initial growth could not be transferred to the shake flasks.

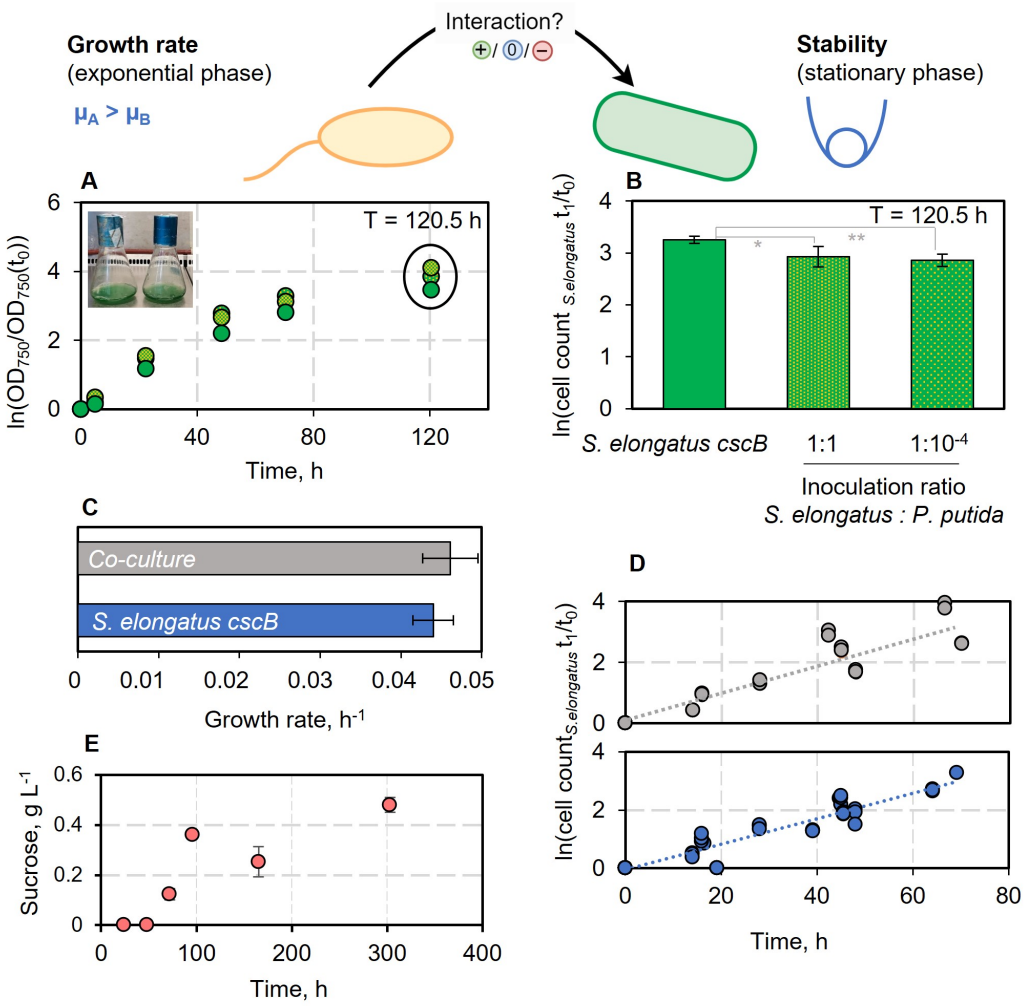

Figure 4.8: **(A)** Optical density of *S. elongatus cscB* (green circle) and two co-cultures with different inocultaion ratios of *P. putida cscRABY* (1:1 yellow-green circle and $1{:}10^{-4}$ light yellow-green circle) **(B)** Shows the cell count normalized to the start cell count of *S. elongatus cscB* for the axenic culture (green bar) and the two co-culture with different inoculation ratios (1:1 yellow-green bar and $1{:}10^{-4}$ light yellow-green bar) after 120.5 h. **(C)** Calculated growth rate of *S. elongatus cscB* shown for co-culture (gray) and axenic culture (blue) conditions. **(D)** Cell counts for Calculation of the growth rates. The co-culture growth rate is based on 9 biological replicates from three separate experiments conducted under identical conditions. Axenic culture growth rate is based on 12 biological replicates from four distinct experiments. **(E)** Sucrose concentration in induced axenic cultures demonstrated by using data from six biological replicates. Experimental conditions: IPTG 0.1 mM, 20 mL shake flask, 22 µmol m^{-2} s^{-1}, 30 °C, 120 rpm, no additional aeration carried out in an orbital shaker Multitron Pro form Infors HT. Statistical evaluation: unpaired T-test with α = 0.05. Statistical evaluation: unpaired T-test with α = 0.05. *,** not statistically significant.

Next, the influence of the phototroph on *P. putida cscRABY* was investigated. Here, differentiating between various growth phases in induced and non-induced scenarios was not feasible, as a valid comparison of the co-cultures would only be accurate if the sucrose secretion was mimicked by an external feed. Nevertheless, the influence of adding the cyanobacterium while *P. putida cscRABY* grew on a batch sucrose of 1 g L^{-1} was investigated in 12-well plates. In the diverse co-cultures examined by Hays et al., a notable negative impact of *S. elongatus cscB* on various heterotrophic partners, with a pronounced effect on the gram-positive bacterium *Bacillus subtilis*, was documented [32]. This clear effect of high densities of *S. elongatus cscB* on the growth of *P. putida cscRABY* could not be confirmed, as can be seen in Figure 4.9 **A**. Even though not statistically

significant, a tendency towards weaker growth of *P. putida* when inoculated with less of cyanobacterial cells might be the case (compare Figure 4.9). In previous studies, reactive oxidative species (e.g. $O_2^{-\bullet}$, $OH^{\bullet}$, H_2O_2) produced by *S. elongatus cscB* was shown to be the most invasive substance for heterotrophic growth. Therefore, as ROS are side-products of photosynthesis, co-cultivations were performed with or without light in 12-well plates and compared to axenic cultures of *P. putida cscRABY* grown under equal conditions (see Chapter 3 for details). Two different cyanobacterial cell densities were used for inoculation in the co-culture as shown in Figure 4.9 **B**, but no statistically significant difference (unpaired T-test, $\alpha = 0.05$) in heterotrophic growth could be detected. The formation of ROS through photosynthesis had no detectable influence on the growth of *P. putida cscRABY* under the conditions tested.

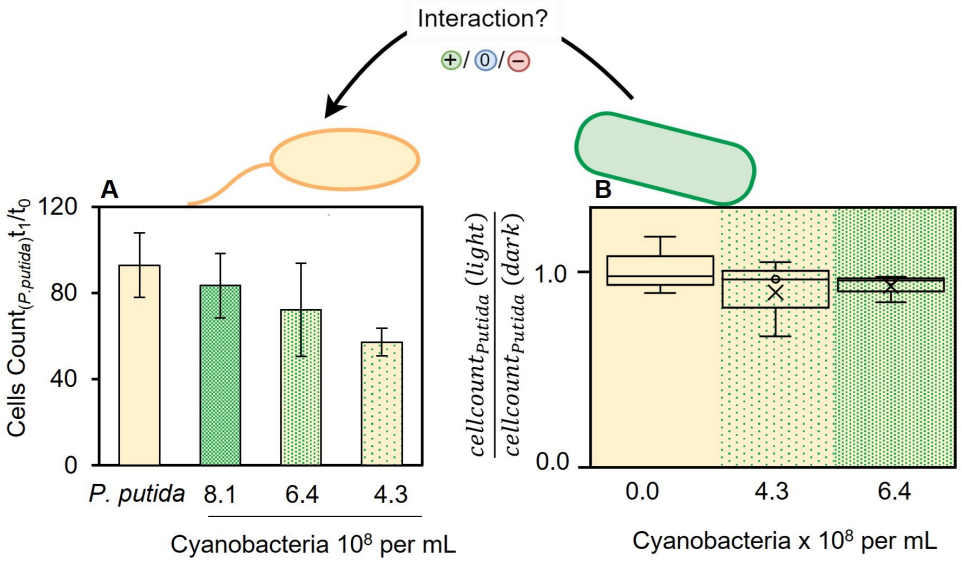

Figure 4.9: Influence of the phototrophic partner on the growth of *P. putida cscRABY*. **(A)** shows the cell count of *P. putida cscRABY* after 24 h of growth in axenic culture or in three co-cultures with decreasing initial *S. elongatus cscB* inoculation concentrations. Data is normalized to the start cell count (t_0). **(B)** Comparison of *P. putida* cell count grown in light and dark, as axenic-culture and in two co-cultures with different cyanobacterial inoculation cell counts. Experimental condition: 12-well plates, 1.6 ml $BG11^+$ supplemented with 150 mM NaCl, 25 °C, 120 rpm, 22 µmol m^{-2} s^{-1} and no additional aeration. 1 g L^{-1} sucrose was added to support heterotrophic growth. At least three biological triplicates were performed.

Discussion

The physiological influence of the co-culture partner on each other was investigated at different scales. Initially, the growth of *S. elongatus cscB* was found to be positively affected when grown in co-cultures in 12-well plates. However, no significant differences were observed in the growth rates or stability during the stationary phase in shake flasks for the cyanobacterium. Further, the influence on the initial growth in the shake flask was neutral too. Discrepancies in outcomes across experiments conducted at different scales are expected, given that factors such as mixing and aeration play important roles in governing the distribution of CO_2 and O_2 within the cultures. These dynamics, in turn, can significantly impact bacterial growth. Particularly at smaller scales, a limitation of CO_2 for the cyanobacterium could explain the observed positive effect when *P. putida cscRABY* is added. It should be noted that no induction and induction with 0.1 mM or 1 mM IPTG had no measurable influence on the cyanobacterial growth in shake flasks, which

stands in contrast to results from other groups and findings made in different scale during this thesis [24]. One reason could be the long adaptation phase cyanobacteria had in the shake flasks, as the pre-cultures are grown at the same conditions as the experiments were conducted (see Section 3.4.2 for details).
The influence of *S. elongatus cscB* on *P. putida cscRABY* was only investigated in 12-well plates using a batch culture with a sucrose concentration of 1 g L^{-1}, and without inducing the synthetic connection between the two partners. This experimental setup was chosen to minimize the reliance of *P. putida cscRABY* on the sucrose feed by the cyanobacterium. Interestingly, the previously observed negative effect on heterotrophic growth could not be confirmed when *P. putida cscRABY* was used as a co-culture partner. Pseudomonads are well known for their excellent resistance against oxidative stress, which might contribute to the fact that *P. putida cscRABY* shows no difference in terms of growth. Furthermore, it should be noted that in co-cultures with higher cell counts of *P. putida cscRABY* compared to *S. elongatus cscB*, clusters of assumingly from cells of both organisms were frequently observed. These clusters normally formed at the beginning of the cultivation and dissolved toward the end (see Figure A.8 in A.8). As a quantification of the cell count was not possible during cluster formation these experiments are not shown in the above section. As mentioned in the theoretical background section, biofilm formation is an important survival strategy employed by various microbes to withstand harsh environmental conditions. However, it is worth noting that the observed clusters were not attached to any surface and therefore cannot be directly termed as a biofilm. The laboratory strain of *S. elongatus* PCC 7942 is not able to form biofilm due to self-suppression of the responsible genes, whereas freshly obtained samples from the strain do not carry the mutations to repress biofilm synthesis [177]. The strain of *P. putida* used in this study has the ability to produce biofilms [178], thus its likely that the clusters are formed due to adding heterotrophic partner. In future optimized co-cultures, it may be beneficial using the strain *P. putida* EM371, which is unable to produce biofilm because of deletion of all pili and flagella ("naked strain") on the bacterial surface [179].

4.2.2 *S. elongatus cscB* experiments using a 9-fold membrane reactor

To analyze the interaction between the co-culture partners in more detail, cultivations were carried out in the HD-9.100 CellDeg platform system, which permits parallel co-cultivations under comparable conditions and guarantees high reproducibility. To find suitable cultivation conditions for the co-culture, the effect of different reaction conditions on the axenic growth behavior and sucrose secretion of the cyanobacterium *S. elongatus cscB* was investigated. As frequently reported induction of the CscB symporter reduces the biomass and glycogen accumulation of the engineered *S. elongatus cscB* but increases the total carbon fixation [24]. As shown in Figure 4.10 **A**, a similar influence of IPTG-induced sucrose export on the growth of *S. elongatus cscB* was observed. With constant illumination of 150 µmol m^{-2} s^{-1} and without induction, *S. elongatus cscB* grew with a rate of 0.064 h^{-1}. The presence of 0.1 mM IPTG in the culture, however, nearly halved the growth rate to 0.038 h^{-1} (compare Table 4.5). This outcome was not due to a negative effect of the sucrose accumulated in the medium along growth (see Figure A.10), but as frequently described in the literature, an effect of re-channeling the carbon flux in the heterologous sink of sucrose secretion. Next, the influence of the time point of induction and an exponential light profile was investigated in respect to the cyanobacterial growth (see Figure 4.10 **B**). Thereby, it was observed that induction from the beginning

resulted in a decrease in the growth rate as observed in the constant light profile (see Figure 4.10 **C**). However, the effect was way more severe in conditions of exponential light (t_d = 52 h), where cultures did not just have reduced growth rates but also went into a state of photobleaching after 80 h (light of approx. 300 µmol m^{-2} s^{-1}; cultures were shutdown). In contrast, this photobleaching effect was not observed when cultures were induced after two days (∼ 40 h) of cultivation or grown with constant light. Moreover, the growth rates of non-induced and induced cultures after two days were comparable (initially induced: 0.038 ± 0.004 h^{-1} and induction after two days: 0.040 ± 0.001 h^{-1}). The later induced cultures performed also better in the sucrose accumulation. After 63.5 hours, the initially induced cultures had accumulated 0.10 ± 0.019 g L^{-1} of sucrose, while the cultures induced on the second day had already 0.34 ± 0.085 g L^{-1} accumulated of the carbohydrate. This trend continued, and by 87.5 hours, the cultures inoculated on the second day had reached a sucrose titer of 0.75 ± 0.38 g L^{-1}, whereas the sucrose concentration in the initially induced cultures remained constant. Thus, the interplay of the time point of induction and the illumination profile showed to be an important factor for the growth behavior of the cyanobacterium. A longer non-induced phase could help *S. elongatus cscB* to adapt to the environmental conditions. This photoacclimatisation, in turn, could lead to notable differences in photosynthetic activity, resulting in enhanced growth, increased sucrose accumulation, and protection against photobleaching towards the end of the process.

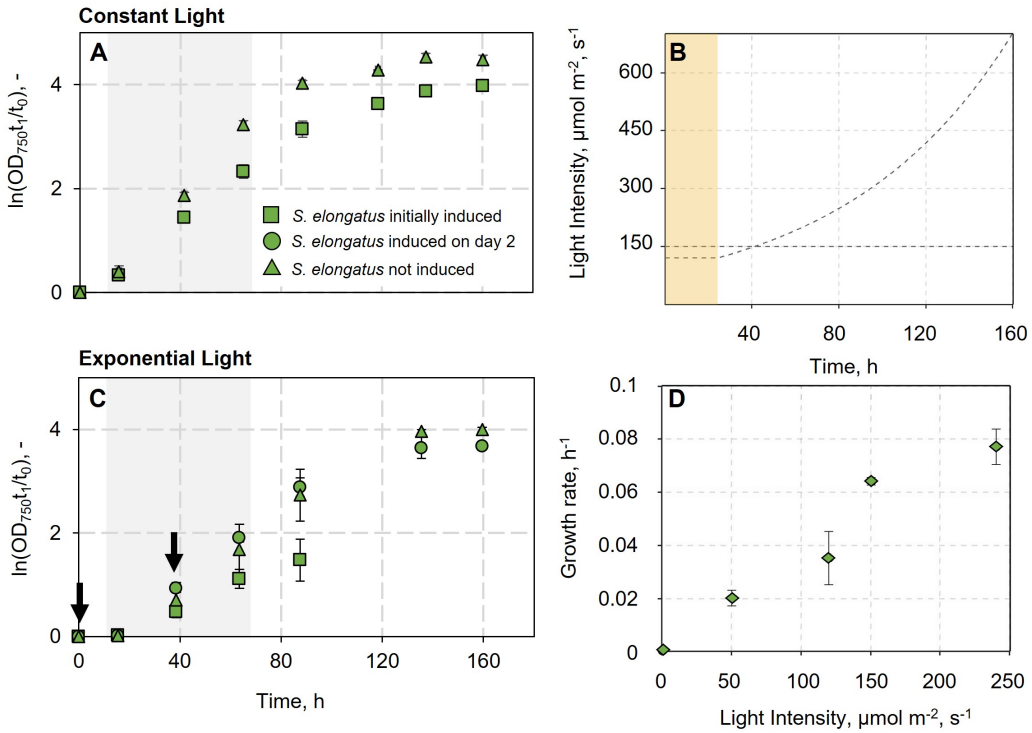

Figure 4.10: **(A)** Growth behavior of *S. elongatus cscB* induced and non-induced at constant light of 150 µmol m^{-2} s^{-1}. **(B)** Light profiles investigated, constant light profile at 150 µmol m^{-2} s^{-1} and a exponential ligth profile (120 µmol m^{-2} s^{-1} for 24 h, t_d = 52 h). **(C)** Growth behavior of *S. elongatus cscB* induced and non-induced at exponential light profile starting from 120 µmol m^{-2} s^{-1} with a doubling time of 52 h. The black arrows indicate the time of induction. **(D)** Growth rates of *S. elongatus cscB* growing at different constant light intensities.

Table 4.5: Growth rates of *S. elongatus cscB* in different light profiles and time of induction.

Growth rate of *S. elongatus cscB*, h^{-1}			
Light	Non-induced	Induced, Initially	Induced, day 2
Exponential	0.038 ± 0.004	0.024 ± 0.004	0.04 ± 0.001
Constant	0.064 ± 0.001	0.036 ± 0.001	n. d

Discussion

The observation made during cultivation of *S. elongatus cscB* induced or non-induced is in line with the literature. The reduced growth of the cyanobacterium was also observed by Ducat et al. [24]. *S. elongatus cscB* cultures grown under constant light exhibited a reduced growth rate of 45% upon induction, compared to non-induced cultures [24]. Further, a decrease in the growth rate led to an increase in photosynthetic capacity when *S. elongatus cscB* was grown under a constant light profile. This was not the case for *S. elongatus cscB* grown under the exponential light profile with initial induction. The total fixed carbon was below the non-induced cyanobacterium after 87.5 h of cultivation. The experiments with the axenic cyanobacterium were highly reproducible even though the temperature cannot be regulated in the 9-fold reactor setup used. The temperature optimum of *S. elongatus* PCC 7942 is between 35-38 °C, which was not reached, especially with a small energy input of low and constant light intensities. Therefore, higher growth rates with rising light intensities are also influenced by higher and consequently more optimal temperatures for the cyanobacterium (see Figure 4.10 **D**).

General reduced growth of the cyanobacterium in the exponential light profile

For *S. elongatus* PCC 7942, light intensities beyond 400 μmol m^{-2} s^{-1} are already considered as "high-light", which is noticeably lower than for other cyanobacteria. High-light intensities can lead to photoinhibition, which has a negative influence on the growth rate [180]. By applying a constant light profile between 0-250 μmol photons m^{-2} s^{-1} a linear increase of the growth rate was observed (see Figure 4.10 **D**). It was recorded that oxidative stress can occur at light intensities as low as 200 μmol m^{-2} s^{-1} in *S. elongatus* PCC 7942 [181], [180]. Let's take a closer look at the two different light profiles: Within the first 40 h, cells growing in the exponential light profile experienced decreased light intensities compared to cells in the constant light profile. Further, within the first 80 h, after the rapid exponential increase in the light intensity, the total time-integrated light intensity of the exponential profile is approx. 70% greater than for the constant light profile. It can be speculated that the reduced growth rate is a combined effect of lower light intensities at the beginning, larger light intensity after 40 h and the adaption to changing illumination conditions. To further describe the light intensity in relation to the produced biomass, the biomass specific light intensity can be calculated as a time-dependent function (see Section A.12) [182].

4.2.3 Co-culture experiments using a 9-fold membrane reactor

In the next step, the findings were transferred to the co-cultivation of *S. elongatus cscB* and *P. putida cscRABY*. Therefore, co-cultures were exposed to different light profiles and compared to the axenic cultures of *S. elongatus cscB* (induced or non-induced). Remarkably, the presence of *P. putida cscRABY* in the co-culture increased the growth rate of the induced *S. elongatus cscB* independent of the light profile chosen and even rescued it from photobleaching in conditions with an exponential light profile (see Figure 4.11 **A**). Besides an overall higher growth rate, the growth behavior of *S. elongatus cscB* in the co-culture resembled that of non-induced cyanobacterial cells. Interestingly, the inoculation time of *P. putida cscRABY* had an influence on the growth behavior and growth rate of *S. elongatus cscB* (see Table 4.6). When *P. putida cscRABY* was added within the first 50 h (compare to Figure 4.11 **B**), it had a positive effect on *S. elongatus cscB*, independently of the light profile. Under an exponential light profile, *S. elongatus cscB* exhibited an increased growth rate by 61% compared to the axenic induced cultures and could be rescued from photobleaching. Inoculating the co-culture on day three (after approximately 65 hours) under the exponential light regime did not fully restore the growth behavior as observed in non-induced *S. elongatus cscB* cells. However, the growth rate in this condition was still elevated by approximately 48% compared to the induced axenic cultures. With constant light, the presence of *P. putida cscRABY* could prevent an early cellular entry into the stationary phase and the growth rate was increased by 64% compared to the non-induced culture and increased by 82% compared to the induced axenic culture. Sucrose accumulated at larger concentration (inoc. day 1, ProcessE1 0.74 $\pm$ 0.12 g L^{-1}) compared to the process where the cyanobacterial cell grew in a constant light regime at 150 µmol m^{-2} s^{-1} (inoc. day1, ProcessC1 0.40 $\pm$ 0.17). The cyanobacterial growth was otherwise as expected. For instance, the growth rate of the cyanobacterium decreased at lower light intensity (see Figure 4.11 **A**). Furthermore, it was observed that the initial induction of axenic *S. elongatus cscB* cultures resulted in halving of the growth rate (see Figure 4.11 at Constant2).

As shown in Figure 4.11 **C**, the ratio between the co-culture partners varies based on the timing of inoculation. When inoculated on day 1 with a ratio of approximately 3:1 (phototroph:heterotroph), the ratio remains nearly constant throughout four days of cultivation. At the end of the experiment, the heterotrophic partner has a share of 72% of the co-culture. In ProcessE2, which was inoculated on day two with the same ratio, the share of *P. putida cscRABY* reaches its maximum between days four and five and decreases to 31% by the end of the experiment.

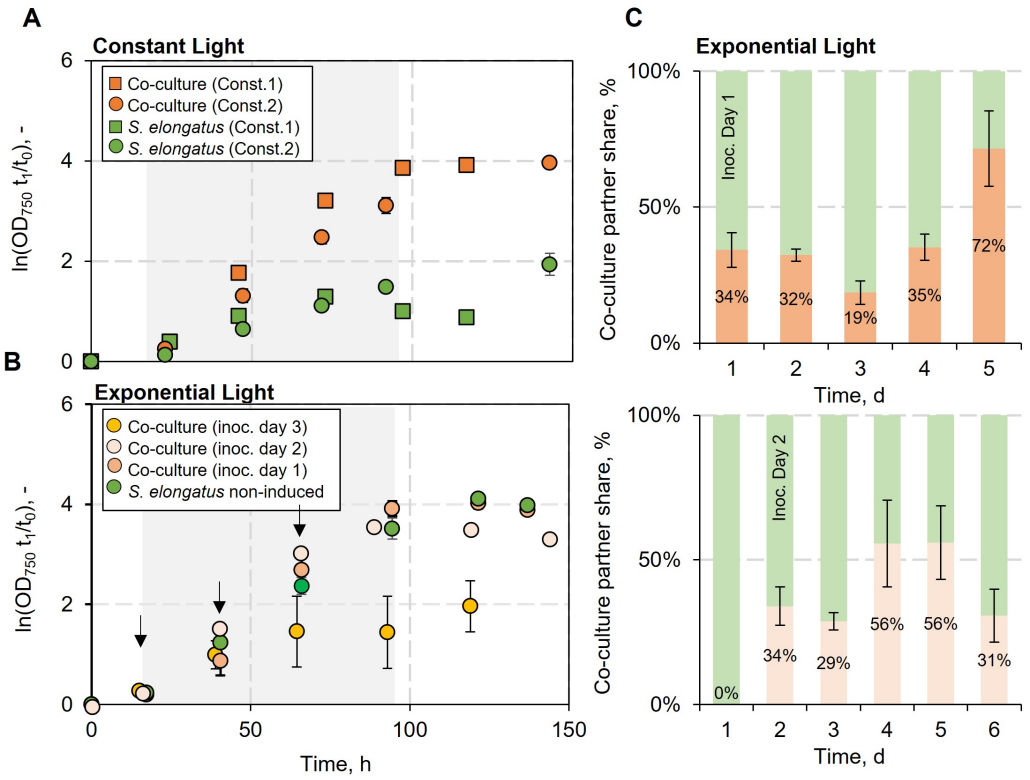

Figure 4.11: **(A)** Growth behaviour of the *S. elongatus* grown in co-culture (orange) and induced axenic *S. elongatus cscB* cultures (green). The gray highlighted data points where used to calculate the growth rates. **(B)** Growth behavior of *S. elongatus* grown in co-culture inoculated with the heterotrophic partner at different times (ProcessE1 = day 1, ProcessE2 = day 2 and ProcessE3 = day 3) and the growth of the non-induced axenic *S. elongatus cscB*. The black arrows indicate inoculation with the heterotrophic partner. **(C)** Ratio of co-culture partner cells for the co-culture inocualted at day one and day two and grown under an exponential light profile. Experimental conditions: 24–37 °C, 2% CO_2, $BG11^+$ supplemented 150 mM NaCl, volume 95 mL; (ProcessC1) Constant1 = 150 µmol m^{-2} s^{-1}, (ProcessC2) Constant2 = 50 µmol m^{-2} s^{-1}, (ProcessE1-E3) Exponential light profile = 120 µmol m^{-2} s^{-1} for 24 h then exponential with t_d = 52 h, N. d. = not determined, Inoc. = Inoculation.

Table 4.6: Growth rates of *S. elongatus cscB* as co-culture or axenic culture grown under different light profiles.

Growth rate of *S. elongatus cscB*, h^{-1}					
Process	Light	Inoc.	non-induced	axenic induced,	co-culture
ProcessE1	Exponential	Day 1	0.057 ± 0.002	0.033 ± 0.001	0.084 ± 0.001
ProcessE2	Exponential	Day 2	0.055 ± 0.002	0.044 ± 0.006	0.066 ± 0.02
ProcessE3	Exponential	Day 3	0.051 ± 0.002	0.031 ± 0.006	0.046 ± 0.002
ProcessC1	Constant1	Day 1	N. d.	0.027 ± 0.006	0.065 ± 0.005
ProcessC2	Constant2	Day 1	0.020 ± 0.003	0.010 ± 0.001	0.056 ± 0.003

Discussion

In summary, the presence of the heterotrophic partner resulted in better growth of the cyanobacterium, which aligns with previous findings of other groups [32], [34], [33] and is also consistent with observations made in smaller scales for the initial growth of the cyanobacterium. The extent of the growth improvement, however, was dependent on the inoculation time and the light profile. From these observations the question arose why the presence of *P. putida cscRABY* has this growth promoting effect on *S. elongatus cscB*. As mentioned above for *S. elongatus* PCC 7942 light intensities beyond 400 µmol m^{-2} s^{-1} are already considered as high-light, which can have negative influence on the growth rate [180]. Therefore, the first hypothesis was that *P. putida cscRABY* prevents the cyanobacterium from harmful illumination due to shading effects. Taken the above experiments into account following counter statements can be made:

- In the experiments with constant light profiles, light intensity of 50 µmol m^{-2} s^{-1} or 150 µmol m^{-2} s^{-1} were applied, thus harmful light intensities should not be reached (see Figure 4.10 **D**). In these conditions an inoculation of the heterotrophic partner should rather increase light limitation due to shading effects and, therefore, should have a negative influence on the growth rate of *S. elongatus cscB*, and not promote growth.
- The inoculation time point of *P. putida cscRABY* had an influence if the cyanobacterial cells were affected negatively or not. The shading effects should be the same independent of the inoculation time.
- The cell ratio phototroph:heterotroph was different during the experiments (see Figure 4.11 **C**), as it adjusted itself over time. Consequently the shading effect varied between the different experiments, but the overall culture behavior was comparable.

Taken together, these observations suggest that the influence on growth cannot be solely attributed to protection from light, indicating the involvement of other factors. Further, the growth influencing effect from *P. putida* seem to be only apparent when *S. elongatus cscB* was already suffering from any other stress, like induced protein expression or suboptimal aeration in 12-well plates (see Section 4.2).

Uncontrolled temperature might affect P. putida cscRABY cell count determination

The heterotrophic partner showed higher cell count fluctuation compared to the cyanobacterium. The high variance of the heterotrophic growth is not surprising as it has a temperature optimum at 30 °C and reacts very sensitively to temperature fluctuations. The uncontrolled temperature can have a severe effect on *P. putida's* growth and can lead to biofilm formation. Biofilm directly impacts the quality of the cell count measurements determined by the flow cytometer.

Different growth modes of cyanobacteria

Studying the growth curve of the cyanobacterial cell count reveals a noticeable distinction. On the one hand, the induced cyanobacteria display linear growth. On the other hand, the non-induced or co-cultured cyanobacteria exhibit exponential growth behavior (see Figure A.13).

4.2.4 Reference Experiment using a 9-fold membrane reactor

To analyze the interplay between *P. putida cscRABY* and *S. elongatus cscB* not only physiologically but also on a transcriptional, proteomic, and metabolomic level, a reference Experiment was established using the 9-fold membrane reactor from CellDeg GmbH, Germany. The exponential light profile was chosen as the condition, as it had a more pronounced effect on the axenically grown cultures. In order to gain insight into the possible origin of the significant increase of the cyanobacterial growth rate in the co-culture, a comparison between the co-culture and respective axenic cultures in biological triplicates should be made (see Figure 4.12 for a schematic representation of the process).

For the heterotrophic partner, comparable growth rates between cells grown in axenic and co-culture should be implemented. To achieve this, an external sucrose feed for axenic *P. putida cscRABY* was adjusted to mimic cyanobacterial sucrose secretion (compare with Chapter 3.7). However, achieving consistency was challenging as the growth rate of *P. putida cscRABY* in the co-culture showed a high variance, assumingly due to temperature variations in the processes. Temperature can be one factor that induces biofilm formation in pseudomonads, which consequently leads to an underestimation of the actual growth rate or sucrose consumption in the process. The sucrose feeding rate was calculated from various co-culture experiments, connecting the biomass formation with the sucrose uptake of the heterotrophic partner (see example calculation Section A.13). In Figure 4.12, the results of two reference Experiments in which the temperature was similar and that were used for the multi-OMIC analysis are depicted. Growth of the phototrophic partner was highly reproducible in the co-culture and axenic culture (see Figure 4.12). As observed before, the growth was reduced in axenic cultures compared to the co-culture and cells showed a loss of chlorophyll after 85 h (see Figure A.14). Cells of *S. elongatus cscB* grown in co-culture had a smaller size, which fits well to the faster specific growth rate (see Figure 4.12 and Appendix for cell size A.15).

Interestingly, the emission between 640-780 nm was higher for the axenic cultures but remained the same during the course of the experiment for the cyanobacteria grown in co-cultures (see Figure A.15). Sucrose was detectable in the supernatant of axenic cultures of *S. elongatus cscB* after 40 h and the sucrose secretion rate was determined to be 0.19 ± 0.022 g L^{-1} d^{-1} which is ∼ 67% of the maximal secretion rate described [27].

The growth of *P. putida cscRABY* depends on the one hand on the cyanobacterial sucrose secretion in the co-culture and on the other hand on sucrose feed in the axenic culture. A growth rate of 0.068 ± 0.005 h^{-1} for *P. putida cscRABY* in the co-culture and of 0.073 ± 0.006 h^{-1} in the axenic cultures in Experiment I was calculated. For Experiment II growth rates were calculated to 0.04 ± 0.003 h^{-1} and 0.043 ± 0.003 h^{-1}, following the same trend as in Experiment I (see Table 4.7). No differences in the cell size of *P. putida cscRABY* in co-cultures or axenic cultures could be observed (see Figure A.15). It was expected that sucrose was the growth limiting factor in both cultures and in fact, in the axenic cultures of *P. putida cscRABY* no sucrose could be detected. However, unexpectedly, an accumulation of sucrose of approx. 0.75 g L^{-1} was observed in the co-cultures after 85 h of Experiment I and even accumulated to 0.91 g L^{-1} in Experiment II, which suggests that the uptake and secretion rate between heterotrophs and phototrophs is unbalanced at later stages. From the data, it cannot differentiate between an increase in the sucrose secretion rate of *S. elongatus cscB* or a decrease in the sucrose uptake rate of *P. putida cscRABY*.

Other medium components, such as citric acid, were monitored during the experiment course. The medium

used contains ∼ 9.4 mg L^{-1} citric acid. Within the first days of the experiment, citric acid was completely metabolized in all cultures, indicating its utilization by both the cyanobacterium *S. elongatus cscB* and *P. putida cscRABY*. Later in the process, the concentration of citric acid increased significantly in the cultures with *P. putida cscRABY*, suggesting its active metabolism and potential contribution to the carbon flux between the co-culture partners (see Figure A.17).

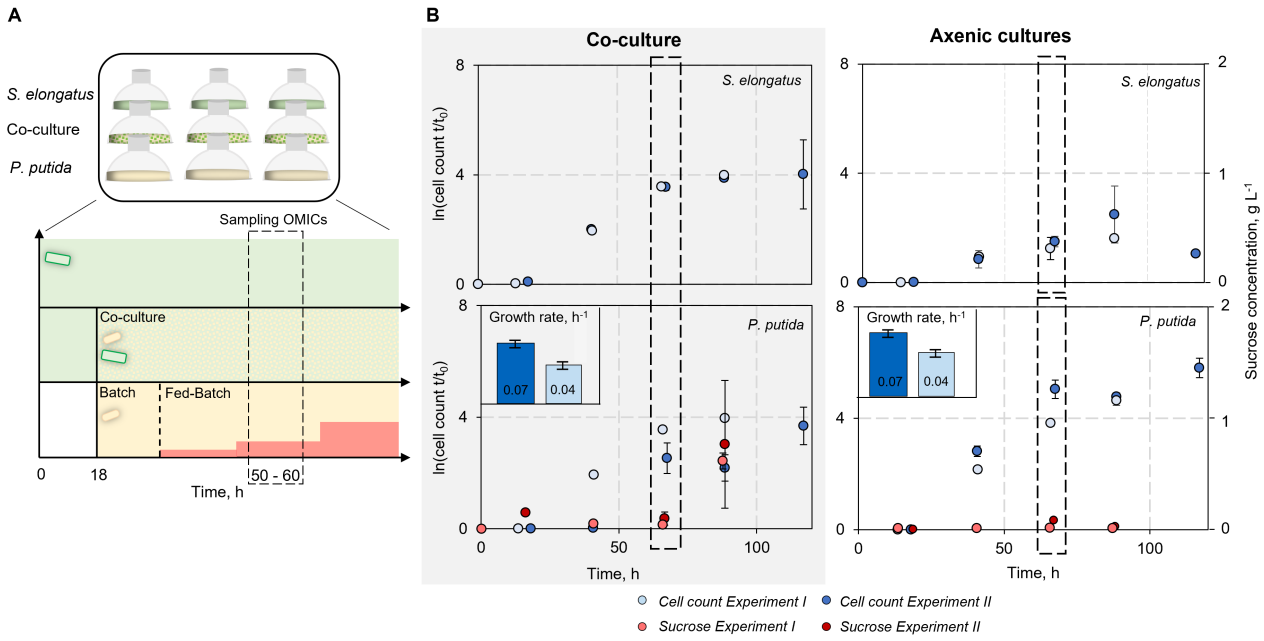

Figure 4.12: **(A)** Schematic visualization of the reference Experiment. **B** Growth of the co-culture and the axenic cultures of *S. elongatus cscB* and *P. putida cscRABY*. The progress of the normed cell count is depicted in blue and sucrose concentration in the supernatant is depicted in red. The co-culture cell count is shown separated for *S. elongatus cscB* and *P. putida cscRABY*. Growth rates from *P. putida cscRABY* in the co-culture and in the axenic culture are represented as small bars chart. Light blue = cell count from Experiment I; Dark blue = cell count from Experiment II and corresponding sucrose concentrations are depicted in light red for Experiment I and dark red for Experiment II. Experimental conditions: 25.0–32 °C, 2% CO_2, 95 mL $BG11^+$ supplemented with 150 mM NaCl, exponential light profile: 24 h constant at 120 µmol m^{-2} s^{-1} and then exponential rising with a doubling time of t_d = 52 h.

Table 4.7: Growth rates of axenic cultures and co-cultures of *S. elongatus cscB* and *P. putida cscRABY*.

	Growth rate of the co-culture partners, h^{-1}			
Experiment	*S. elongatus cscB* Axenic	*S. elongatus cscB* Co-culture	*P. putida cscRABY* Axenic	*P. putida cscRABY* Co-culture
I	0.023 ± 0.003	0.067 ± 0.001	0.073 ± 0.005	0.068 ± 0.006
II	0.030 ± 0.002	0.070 ± 0.002	0.040 ± 0.004	0.043 ± 0.003

Discussion

The literature describes that inducing sucrose secretion alleviates inefficiencies caused by photosynthetic sink limitation, resulting in increased overall CO_2 fixation in *S. elongatus cscB* [24], [100]. In the co-culture, the photosynthetic activity of *S. elongatus cscB* is even higher than in the induced case, as the growth rate surpasses that of the non-induced cells, and heterotrophic growth is supported with sucrose.

The results described in Sections 4.2.2 and 4.2.3 indicate this trend. Following the induction of the sucrose-secreting transporter, biomass accumulation decreased while overall fixed carbon increased due to carbon secretion. Interestingly, the presence of the co-culture partner *P. putida cscRABY* further elevated the total carbon fixation, which can be seen best in the reference Experiments (see Figure 4.12 and Figure 4.13). Notably, an increase in the cyanobacterial growth rate and heterotrophic growth support was observed. Therefore, the total carbon fixed by the cyanobacterium was analyzed in Experiment I.

As visualized in Figure 4.13, significantly more carbon is fixed through the cyanobacterium in the co-culture compared to the axenic culture. The carbon in the co-culture is thereby the sum of the carbon in the form of accumulated biomass of the cyanobacterium, the sucrose necessary to support the biomass accumulation of the heterotrophic partner, and the sucrose measured in the supernatant. For the induced axenic cultures, it is consequently the carbon accumulated in the cyanobacterial biomass and the carbohydrate secreted. Although total carbohydrate fixation increased when *P. putida cscRABY* was added, the sucrose production per cell decreased.

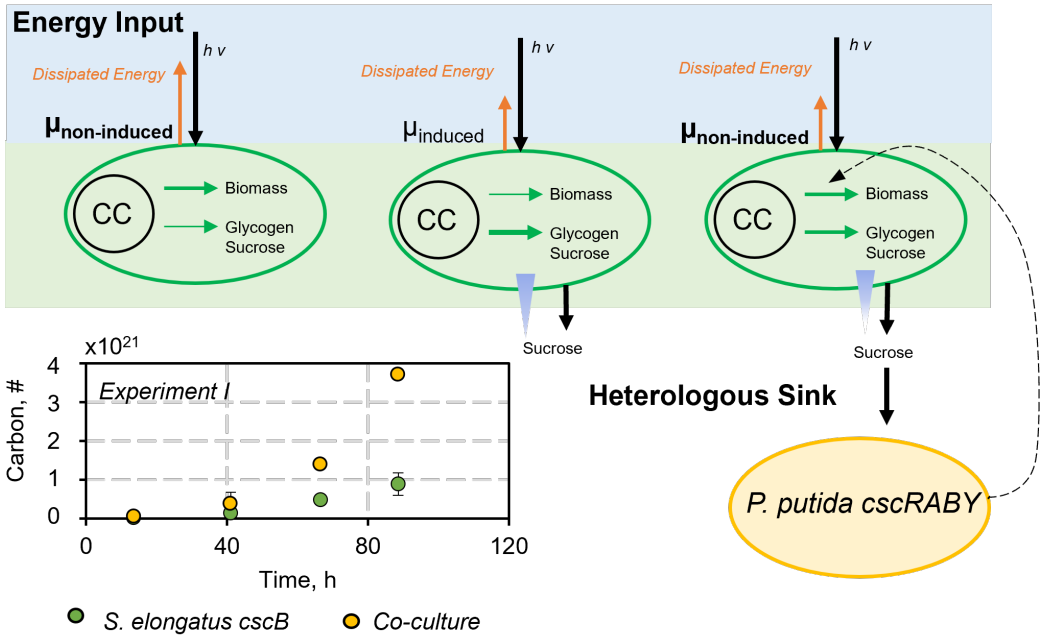

Figure 4.13: Overview of the energy balance in *S. elongatus cscB* under non-induced, induced, and co-culture (induced) conditions. Energy input from light ($h \cdot \nu$) is represented by black arrows, which are balanced by the energy requirements of cellular metabolism (biomass) and glycogen accumulation/sucrose secretion indicated by green arrows in the cells. The thickness of the arrows schematically represents the carbon flux. Excess energy is dissipated through non-photochemical quenching reactions, represented by orange arrows. The length of the arrows schematically represents the amount of energy transferred. The scheme was adapted from [100]. The diagram illustrates the total carbon fixation for *S. elongatus cscB* and the co-culture in Experiment I.

4.2.5 Overview of OMIC results

As described above, the presence of *P. putida cscRABY* in the co-culture has a positive effect on the growth of *S. elongatus cscB*. The next aim was to get an insight into the possible levels of inter-species interaction in the co-culture. This is not only interesting from a fundamental research point of view but will also contribute to a better understanding of the co-culture stability and eventually even to improve the production of value-added products in co-cultures. Omics analyses aimed to provide a detailed understanding of the molecular and biochemical changes occurring in the co-culture system. The time point was chosen to be in the second half of the exponential growth phase before cells entered the stationary phase to have a decent number for the analysis (compare Figure 4.12). OMICs results of the axenic cultures were considered as controls and compared to the co-cultures, which were considered as cases of interest. In all datasets, distinct clusters of the axenic cultures and the co-culture could be identified. Figure 4.14 **A** and 4.14 **B** provide an exemplary illustration of this using the metabolomic data for principal component analysis (PCA) underlining the fact that the cultures differ metabolically from each other. Further, a threshold for differently expressed genes (DEGs) and differently abundant proteins (DAPs) at $|log_2(FC)|$ = 1.0 and a p-value (adjusted, false discovery rate (FDR) corrected) < 0.05 was chosen. For different abundant metabolites, the threshold was an adjusted p-value of 0.05 and a mean difference of 0.3.

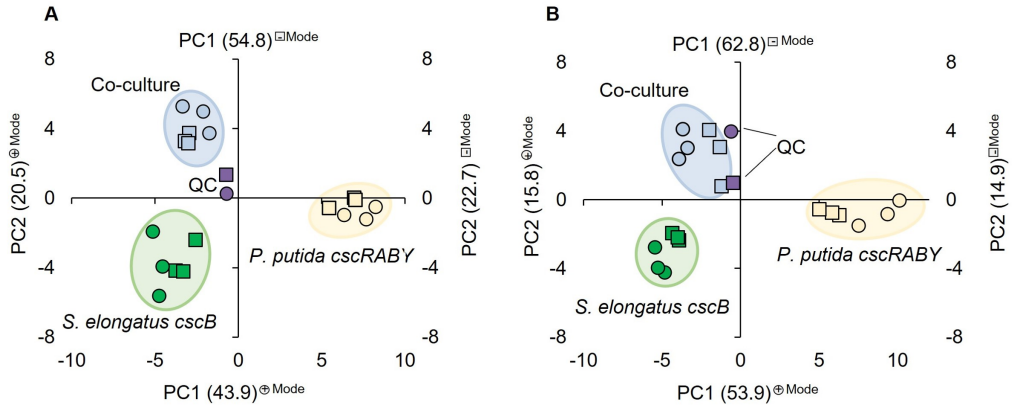

Figure 4.14: Principial component analysis (PCA) for metabolites measured with RP-MS **(A)** and HILIC-MS **(B)**. Positive ionization mode is depicted in circles and the negative ionization mode is depicted in squares. Green = *S. elongatus cscB*, yellow = *P. putida cscRABY* and blue = co-culture.

Transcriptomics analysis:

A total of 2679 genes for the cyanobacterium were identified when comparing the axenic cultures with the co-culture. Further, a total of 5219 genes for the heterotrophic partner were calculated. Comparing the co-culture to the axenic culture, in *P. putida cscRABY* a total of 488 differently expressed genes (DEGs) were identified, of which 303 were up-regulated and 145 were down-regulated (Figure 4.15). In *S. elongatus cscB* a total of 790 DEGs were identified. Of these 324 genes were found to be up-regulated, while 466 were down-regulated in comparison to axenically grown cells (Figure 4D). In *P. putida cscRABY* the majority of the DEGs belong to the category amino acid metabolism and transport and in *S. elongatus cscB* the majority was found in the category translation. The most up-regulated gene for *P. putida cscRABY* grown in co-culture

in comparison to the axenic culture is PP_4604, the most down-regulated is PP_2262 (See Figure 4.15 **A**). When comparing the co-culture with *S. elongatus cscB* the most up-regulated gene is *hilA* and the most down-regulated protein is Synpcc7942_0781 (See Figure 4.15 **B**).

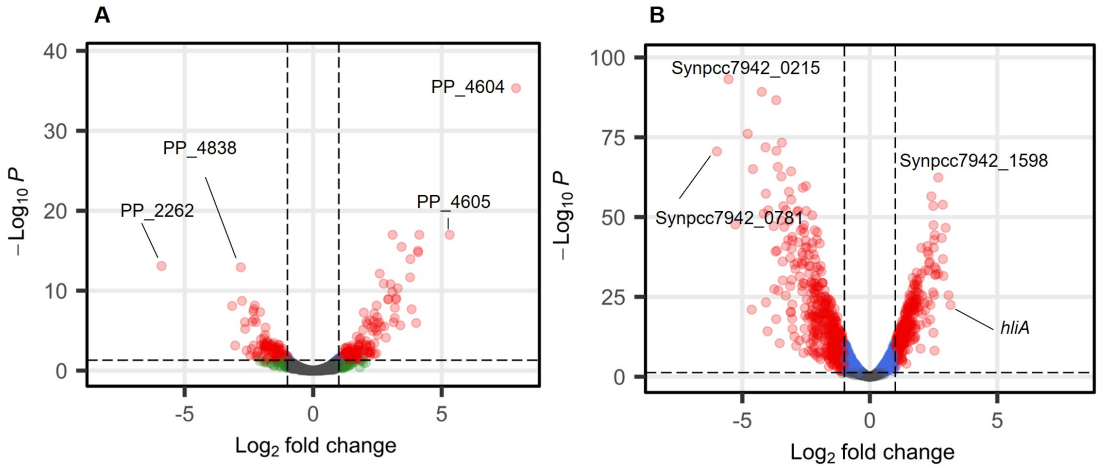

Figure 4.15: Volcano plot of transcriptome data, with $\log_2$-FC change on X-axis and p-value on Y-axis. Threshold: $|log_2(FC)| > 1.0$ and p-value(adjusted) < 0.05. **(A)** Co-culture vs. *P. putida cscRABY*. **(B)** Co-culture vs. *S. elongatus cscB*. Transcripts in red circles meet the threshold for both $\log_2$-fold change ($\log_2$-FC) and p-value. Transcripts depicted in blue fulfill the threshold for the p-value, while transcripts in green meet the threshold for $\log_2$-FC. Transcripts depicted in gray do not meet one of the thresholds.

Table 4.8: Significant transcripts co-culture versus axenic cultures.

	Significant proteins	Annotated
Co-culture vs. *P. putida cscRABY*		
Overall	448	323
Up regulated	303	230
Down regulated	145	119
Co-culture vs. *S. elongatus cscB*		
Overall	790	541
Up regulated	324	228
Down regulated	466	313

Comparative untargeted proteomics analysis:

After applying the threshold, a total of 92 proteins were calculated to be more abundant in *S. elongatus cscB* grown in co-culture, and 91 proteins were less abundant compared to the axenic culture. In *P. putida cscRABY* only 75 proteins were identified to be more abundant, and 22 proteins showed less abundance when compared to the axenic culture (see Figure 4.16 **A**). In *P. putida cscRABY*, most differentially abundant proteins (DAPs) belonged to the category amino acid metabolism and transport, as was already seen in the transcriptomic data. In *S. elongatus cscB*, the majority of proteins identified as DAPs belonged to photosynthesis or the category stress (see Figure 4.16 **B**). The general comparison of collected transcriptomic and proteomic data leads to a correlation between protein and mRNA abundance of only 30-40%. However, this is in the range of what is described as the regular magnitude [183].

Comparative untargeted metabolome analysis of the cell pellet:

In total, 876 features could be identified for HILIC-MS measurements (- and + MS-mode), and 1013 different features were identified with RP-MS (- & + MS-mode). When comparing co-cultures and *P. putida cscRABY* axenic cultures, 336 features for HILIC (- & + MS-mode) and 427 for RP (- & + MS-mode) fulfilled the conditions set. Most features were more abundant in the co-culture than in the respective axenic culture (see Supporting Information A.18 A-D for volcano plots). For the co-culture in comparison to axenically grown *S. elongatus cscB* cells, 143 features fulfilled the threshold set for HILIC-MS measurement (- & + MS-mode), and 254 features fulfilled it for the RP-MS (- & + MS-mode) (see Appendix A.18 E-F for volcano plots). In Figure A.19 **A** (RP) and **B** (HILIC) metabolites identified through reference measurements are depicted in a heatmap comparing their abundance between the co-culture with the two axenic cultures. Most identified metabolites belong chemically to sugars, amino acids, and fatty acid.

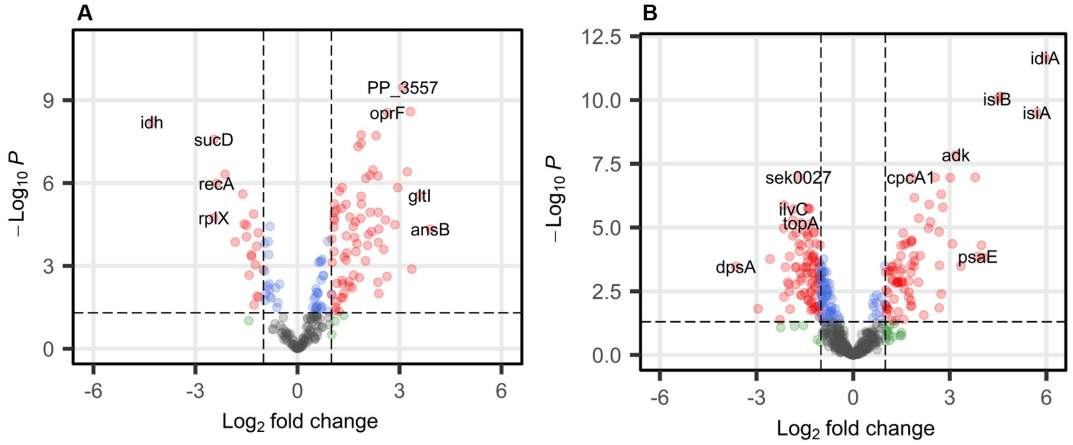

Figure 4.16: Volcano plots of OMICs, with $\log_2$-FC change on the X-axis and p-value on the Y-axis. Threshold: $|log_2(FC)| > 1.0$ and p-value(adjusted) < 0.05. **(A)** Co-culture vs. *P. putida cscRABY*. **(B)** Co-culture vs. *S. elongatus cscB*. Proteins in red circles meet the threshold for both $\log_2$-FC and p-value. Proteins depicted in blue fulfill the threshold for the p-value, while transcripts in green meet the threshold for $\log_2$-FC. Proteins depicted in gray do not meet one of the thresholds.

Table 4.9: Significant proteins co-culture versus axenic cultures.

	Significant proteins	Annotated
Co-culture vs. *P. putida cscRABY*		
Overall	97	
More Abundant	75	All
Less Abundant	22	All
Co-culture vs. *S. elongatus cscB*		
Overall	183	
More Abundant	92	All
Less Abundant	91	All

4.3 Multilevel insights: transciptional, proteomic and metabolic changes

This chapter provides a detailed overview of the obtained data on the transcriptome, proteome, and metabolic levels. It begins by summarizing the data and then discusses the findings, including existing literature[5].

Effects from the co-culture partners on cellular processes

The above-described analysis of the multi-OMICs data provided a large number of genes and proteins that were differentially expressed or abundant (see Section 4.2.5). Additionally, some metabolites were found to be different abundant. To get an overview of the cellular process that were mainly affected by the presence of the respective co-culture partner, the DEGs, DAPs and metabolites were sorted into different groups according to their putative function. In *P. putida cscRABY* the presence of the phototrophic partner led to changes of various cellular processes, namely in the core metabolism, transport of amino acids, nitrogen, small acids, and sugars, but also in the general stress response, detoxification, and degradation (see Figure 4.17). In *S. elongatus cscB* we found that the presence of the heterotrophic partner also had an effect on the core metabolism and on photosynthesis, which was somehow expected as *S. elongatus cscB* exhibited a higher growth rate in the co-culture. Furthermore, other processes connected to stress, detoxification, or transport of sulphur and iron were affected. In the following these processes will be discussed in more detail (see Figure 4.17).

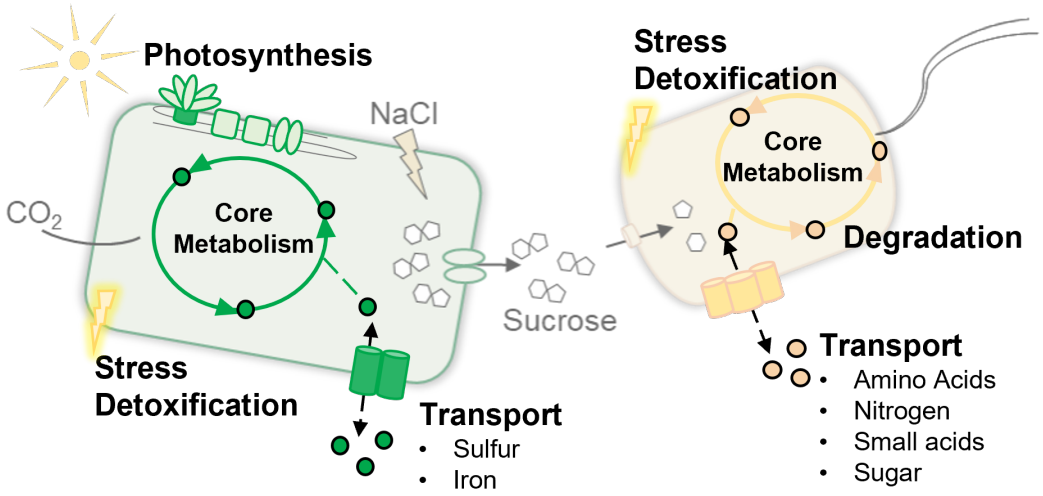

Figure 4.17: Overview of cellular processes affected by the co-culture partners. In *S. elongatus cscB* grown in co-culture, changes were observed in photosynthesis, core metabolism, transportation, stress, and detoxification. Similarly, in *P. putida cscRABY* grown as a co-culture partner, changes were observed in core metabolism, transportation, degradation, stress, and detoxification.

[5]Some of the presented results in this chapter have been summarized in a manuscript with the title "*Pseudomonas putida* as saviour for troubled *Synechococcus elongatus* in a synthetic co-culture – interaction studies based on a multi-OMICs approach" for publication.

4.3.1 Changes in the central metabolism - *P. putida cscRABY*

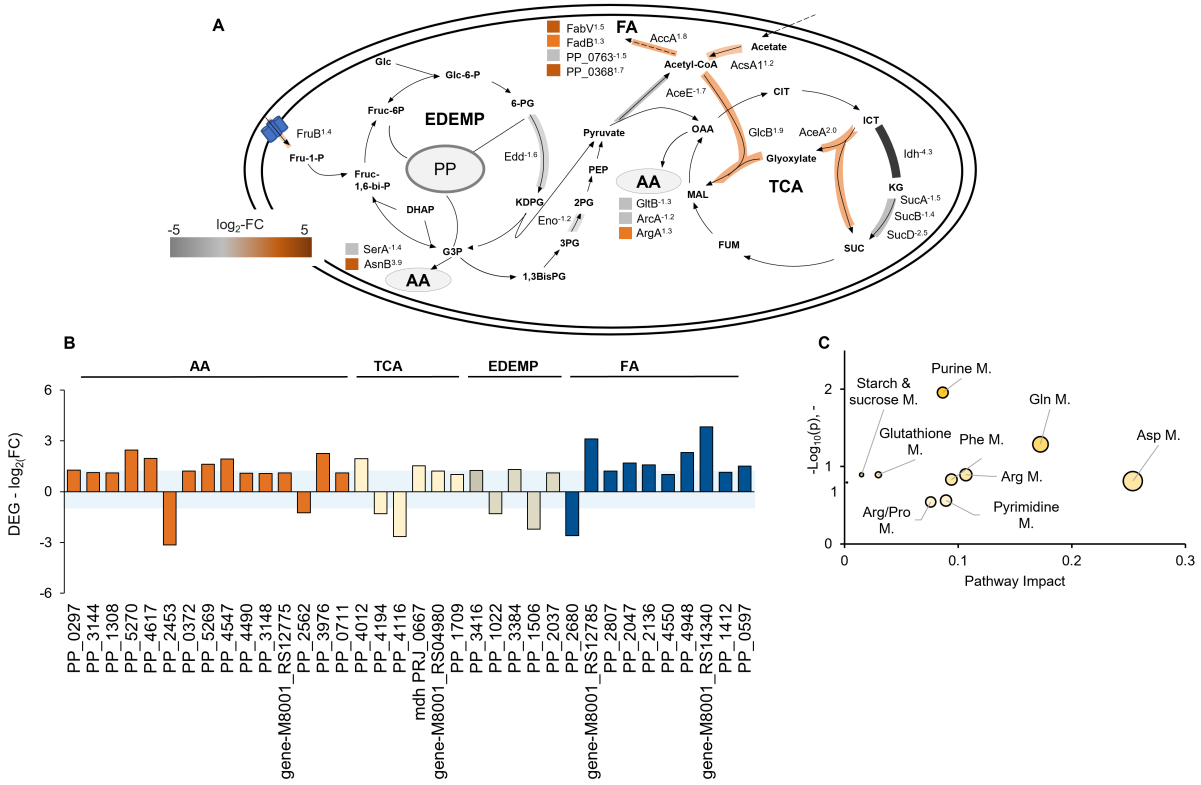

Figure 4.18: Changes in the central carbon metabolism of *P. putida cscRABY*. **(A)** Protein level: DAPs are highlighted in orange (more abundant) or gray (less abundant). **(B)** Transcript level: DEGs were identified that are connected to AA (amino acid) synthesis and degradation, FA (fatty acid) synthesis and degradation, in the EDEMP (Entner-Doudoroff- Embden-Meyerhof-Parnas)-cycle, and in the TCA (tricarboxylic acid)-cycle. The different groups are indicated by different colors of the bars, gene identifiers or names are given blow. The blue area indicates the p-value of 0.05 and the color bar indicates the abundance of the proteins. **(C)** Metabolite level: From reference measurements identified metabolites of the co-culture compared to *P. putida cscRABY* and grouped into pathways through pathway enrichment analysis. Data were obtained by using metabolic pathway analysis of MetaboAnalyst 5.0, 1 = Phe/Tyr-(M) Metabolism, amino acids are abbreviated with three letter code and M stands for metabolism. Gene-M8001_RS12775 locus tag DM483_08080; Gene-M8001_RS04980 locus tag DM483_01605; Gene-M8001_RS12785 locus tag DM483_08090; Gene-M8001_RS14340 locus tag DM483_03170.

Several genes, proteins and metabolites belonging to the core metabolism were identified in *P. putida cscRABY* to be affected by the presence of *S. elongatus cscB* in the co-cultivation. On the protein level, changes were observed with DAPs belonging to the amino acid (AA) synthesis or degradation, the TCA cycle, or to the fatty acid (FA) metabolism (see Figure 4.18 **A**). This was corroborated on transcriptional level, where DEGs putatively involved in the amino acid metabolism, the TCA cycle, the fatty acid synthesis and degradation, or the EDEMP cycle were identified (see Figure 4.18 **B**). Furthermore, differentially abundant metabolites belong mainly to different amino acid metabolisms, such as, alanine, glutamine, and arginine metabolism were identified (see Figure 4.18 **C**).

Changes in the amino acid metabolism

As a rhizobacterium, *P. putida* is specialized for the uptake and metabolization of amino acids [184]. In line with this, it was not surprising that the expression of genes connected to amino acid metabolism was

affected by the presence of the co-culture partner. Most of these genes were up-regulated as can be seen in Figure 4.18 **B**. For instance, five amino acid degrading enzymes, which are also nitrate-generating enzymes (L-serine ammonia lyases (*tdcG-I*, *gltK*), methionine lyase (*mdeA*), and two dehydrogenases (PP_5270 PP_4617)) were up-regulated in the co-culture, which might be connected with the down-regulation of the different nitrogen uptake transporters (see Section 4.3.3). Two other genes, that were identified to be up-regulated, are *dadA2* (PP_5270 $\log_2$-FC 2.5) and *dadX* (PP_5269 $\log_2$-FC 1.6), which are located on the chromosome adjacent to each other, encoding a putative D-amino acid/quinone oxidoreductase and an alanine racemase.

On the protein level, only a few proteins connected to the amino acid metabolism were identified to be differentially abundant (see Figure 4.18 **A**). With the most abundant being AsnB an asparagine synthetase, responsible for the conversion of aspartate into asparagine. The corresponding transcript *asnB* is, however, down-regulated (PP_2453 $\log_2$-FC -3.1). Further, from the metabolomics data it could be extracted that the amino acids pathways for L-phenylalanine, L-glutamic acid, L-aspartic acid and L-glutamine are enriched when the co-culture cell pellets are compared to the axenic *P. putida cscRABY* ones (see Supporting Information A.19 **A** & **B**).

Changes in the TCA cycle

DAPs connected to the TCA cycle are Idh and SucA/B/D and show a decreased abundance, coinciding with a higher abundance of the proteins AceA and GlcB. This suggests a shut-down of the TCA cycle and a redirection of the metabolic flux through the glyoxylate cycle. This can occur when degradation of aromatics or xenobiotics is necessary [119]. The protein Idh is the most negatively affected protein in the co-culture belonging to the core carbon metabolism, with an abundance of -4.3, however, on transcriptional level, the *idh* gene was up-regulated (PP_4012 $\log_2$-FC 1.9) (see Figure 4.18 **A**).

Changes in the synthesis and degradation of fatty acids

Other differentially regulated genes belong to the group related to the synthesis and degradation of fatty acids. Most of them are up-regulated and belong to the β-oxidation. In detail, three genes encoding putative acyl-CoA dehydrogenases are up-regulated (PP_4948, PP_2047, and gene-M8001_RS12785). Up-regulation was also observed for PP_2136 (*fadB* $\log_2$-FC 1.6) and PP_2047 ($\log_2$-FC 1.7). That complements some up-regulated short-chain fatty acid transports as the *atoABC* operon and fits that more abundant proteins belong likewise to the β-oxidation (FabV and FabB).

4.3.2 Changes in the central metabolism - *S. elongatus cscB*

When focusing on the cellular processes affected in *S. elongatus cscB* by the presence of the heterotrophic partner, special attention has to be taken when comparing cells grown in co-culture with those that grew axenically, as the growth rates differ by a factor of about two. It has to be kept in mind that the difference in the amount of transcript or protein can be a consequence of the higher growth rate itself or of the present co-culture partner. However, these effects might also be entangled, as a positive interaction could lead to a higher growth rate. Thus, a differentiation is not always possible. In line with the higher growth rate of *S. elongatus cscB* in the co-culture, growth-associated genes such as ribosomes, tRNAs, and polymerases were mainly up-regulated (see Figure A.20). It is worth noting that the identification of DEGs for ribosomes, tRNA or polymerases in *P. putida cscRABY* was nearly impossible. This observation suggests that the similar growth rates in both axenic and co-culture are reflected by a similar expression pattern of these genes.
Regarding the central carbon metabolism in *S. elongatus cscB*, only a few proteins were identified as differently abundant (see Figure 4.19). For instance, the protein glucose-6-phosphate-1-dehydrogenase (Zwf), linked to ED and PP pathway, was slightly down-regulated. Some isolated proteins acting in the amino acid degradation and synthesis were detected, all less abundant in the co-culture. At the transcriptional level, the regulation was also ambiguous. The most down-regulated gene is Synpcc7942_0781, encoding for a phosphoenolpyruvate synthase ($\log_2$-FC = -6). Further, genes for amino acid synthesis and few transcripts for carbon storage were affected by the presence of the co-culture partner. The genes, which can be grouped to amino acid metabolism, showed ambiguous regulation see Figure A.21 **A**. Interestingly, the heterologously expressed sucrose transport protein CscB was less abundant in *S. elongatus cscB* when grown in co-culture. This observation was unexpected, as its transcription is regulated by the IPTG inducible P_{lacUV5} promoter. Therefore, it should be expressed equally, independent of the presence of the co-culture partner or of the growth rate.

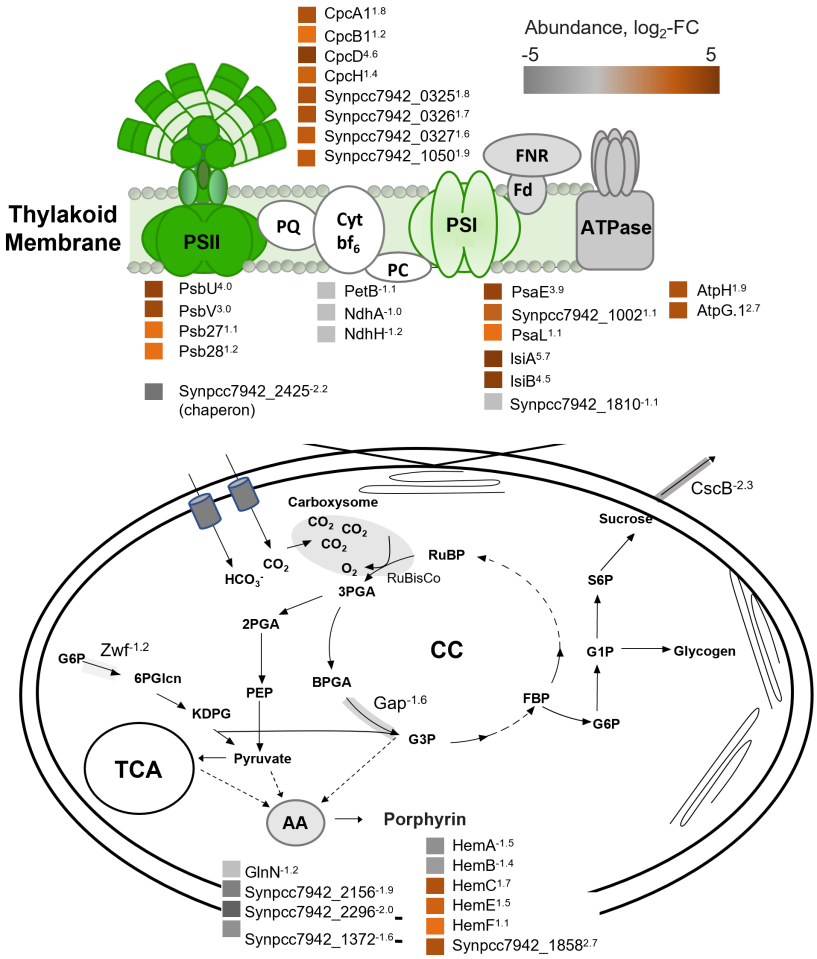

Figure 4.19: Changes in the central carbon metabolism and in the photosynthesis apparatus for *S. elongatus cscB* on protein level. Depicted is a schematic cell of the cyanobacterium with highlighted changes in the amino acid (AA) pool, porphyrin pool/biosynthesis and in the photosynthesis apparatus. TCA = tricarboxylic acid cycle, AA = amino acid, CC = Calvin cycle. Protein abundance in the photosynthesis apparatus consisting of PSII = photosystem II, PSI Photosystem I, Cyt-bf_6 = cytochrome bf_6, PQ = plastoquinone, FNR = ferredoxin-$NADP^+$ reductase and FD = ferredoxin/flavodoxin. The color bar indicates the abundance of the proteins.

Changes in photosynthesis and connected cellular processes

Looking at genes and proteins related to photosynthesis, the effect of the difference in growth rates between *S. elongatus cscB* grown axenically or in co-culture becomes obvious. For instance, the pigment-proteins phycocyanin and allophycocyanin, which are present in the light-harvesting complex, were more abundant (see Figure 4.19). The light-harvesting complexes are involved in photosynthesis and growth, which is why differences were expected. However, only a share of proteins were detected for Photosystem I (PSI), Photosystem II (PSII), and the connecting electron chain consisting of NAD(P)H-dehydrogenase-like complex (NDH) and plastocyanin (PQ), which are all complexes consisting of lots of proteins. Regarding the overall photosynthesis, a tendency towards an increase in proteins for PSI and PSII and a decrease in the abundance of proteins building the NDH/PQ complex could be identifyed. At the transcriptional level, the opposite effect was observed: Genes encoding proteins forming the PSI and PSII and the phycobiliproteins were down-regulated, whereby genes coding for the connecting NDH/PQ complex were up-regulated (see Figure A.21 **B**).

A plausible explanation for the observed difference can be attributed to the different growth rates of the cyanobacteria grown in co-culture or axenically (see Section 4.12). As the experiment control, the induced *S. elongatus cscB* was used, which had decreased growth and showed phenotypically obvious stress effects. Therefore, the comparison is potentially made between different cellular states. On the one hand, *S. elongatus cscB* grown in co-culture shows exponential growth with a constant growth rate in the co-culture, implying an intracellular steady state of transcripts, proteins, and metabolites. On the other hand, the cyanobacterium in the axenic culture exhibits linear growth at the sampling point, indicating a non-constant growth rate and, consequently, a dynamic state of cellular processes. Consequently, transcripts and proteins can be differently affected when the co-culture is compared to the axenic cultures of *S. elongatus cscB*.
Furthermore, in relation to photosynthesis and restructuring of the photosynthetic apparatus, the protein pair IsiA and IsiB showed a significant increase in abundance at the protein level. IsiA is annotated as an iron stress-induced chlorophyll-binding protein, while IsiB is a flavodoxin. This pair is known to provide protection against photooxidative stress in high-light conditions for the PSI and PSII. Considering that these proteins accumulate during iron starvation, along with the higher abundance of other iron starvation proteins, such as IdiA and IrpA, it was assumed that a reduced iron concentration prevails in the co-culture. The decreased iron availability might be the effect of co-culture partner's presence and triggers a sophisticated cellular response to high light stress with IsiA and isiB [185]. Pseudomonads, including *P. putida*, are well-known for their optimized iron scavenging capabilities through the production of siderophores [186]. It is likely that *S. elongatus* is unable to take up the iron when it is bound in such "pseudomonad-siderophores". However, attempts to enhance co-culture growth by increasing the iron concentration by two or 5-fold proved unsuccessful. Only the reduction of iron to a 1/100th of the default concentration led to a reduced growth rate of axenically grown cultures. This high resistance to iron limitation is not surprising considering the poor availability of iron in the natural habitat of microbes (see Figure A.22). Furthermore, measurements of iron concentration after 40 hours (reference Experiment II) did not reveal any differences between the co-culture and axenically grown *S. elongatus cscB* cultures. However, these measurements have limited significance as it is unclear if siderophores can be accurately measured with the assay used.

4.3.3 Transportation changes in the co-culture

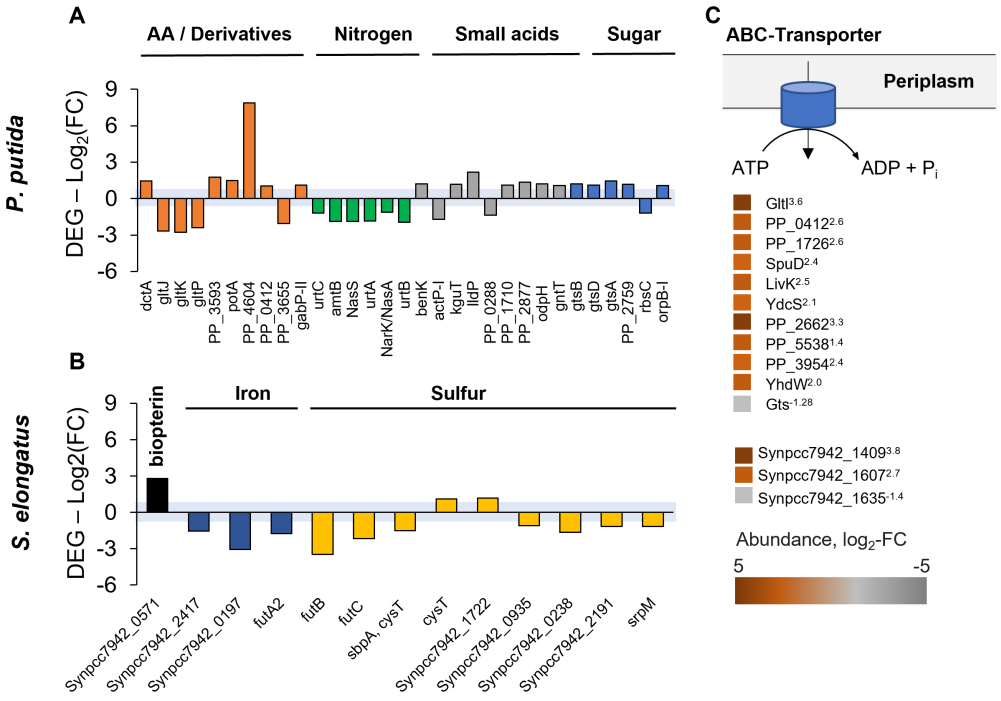

Figure 4.20: **(A)** Selection of DEGs in *P. putida cscRABY*, which can be connected to cell transport. DEGs were classified according to the transported substrate: AA (amino acids), nitrogen, small acids, and sugars. **(B)** Selection of DEGs in *S. elongatus cscB* connected to cell transport. Classification into two groups: Iron and sulfur transporter. **(C)** DAPs in *P. putida cscRABY* (above) and *S. elongatus cscB* (below) for transport. The blue area indicates the p-value of 0.05 and the color bar indicates the abundance of the proteins.

The ability to utilize as many resources as possible can be decisive for microbes in their performance against competitors [187]. Therefore, they have evolved many strategies for the uptake of compounds from the environment. Most interactions between microbes require a form of uptake of substrates, signals in diverse forms, or toxins. In line with this, various transporters for many compounds were differentially expressed in the co-culture versus axenic cultures (see Figure 4.20). In general, it was observed that transporters are more likely up-regulated in *P. putida cscRABY*, whereas the opposite is the case in *S. elongatus cscB* (see Figure 4.20). This might originate in the individual lifestyles of each of the co-culture partners, as a strict autotrophic and anabolic mode needs less transportation of organic carbon compounds compared to a heterotrophic lifestyle.

In *P. putida cscRABY*, the DEGs related to transport are diverse and covering, among others, transporters for amino acids, nitrogen, small acids and sugars (see Figure 4.20 **A**). In the group of amino acid transporters, down- as well as up-regulated genes were identified. For example, the ABC-transporters responsible for uptake of glutamate/aspartate were down-regulated (gltJ (PP_1070) $\log_2$-FC -2.6, gltP (PP_0137) $\log_2$-FC -2.4, and gltK (PP_1069) $\log_2$-FC -2.7), whereas genes connected to transport of other amino acids derivatives, such as putrescine or spermidine (*potA* PP_0411 ATB-binding and *potD* PP_0412 substrate binding with a $\log_2$-FC of 1.5 and 1.0) were up-regulated. On protein level, the latter one, PP_0412, was also

identified to be more abundant. Additionally, the proteins SpuD (PP_5181) and YhdW (PP_1297), annotated as polyamide transporter, were found to be more abundant in *P. putida cscRABY* (see Figure 4.20 **C** and Table 4.10). The most highly up-regulated transcript among all transporters encoding genes was PP_4604, which belongs to the EamA family and might be related to transport of cysteine-derivatives in *E. coli* [188]. This gene, PP_4604, is located downstream of a gene which codes for an AraC-type regulator (PP_4605, $\log_2$-FC 5.3), which is highly up-regulated as well, and a putative connection between these two genes is predicted by the string-database[6]. All DEGs identified in *P. putida cscRABY* encoding transporters connected to nitrogen transport were down-regulated (see Figure 4.20 **A**). These genes encoding proteins responsible for transport of urea (*urtABC*), nitrate (*nasK/nasA*, *nasS*) or ammonia (*amtB*). Additionally, transcripts for urea degradation, encoding for the urease subunits, were down-regulated (*ureABCD*, PP_2842-PP_2845). In line, on protein level, the global regulators NtrB (PP_5047) and NtrC (PP_5048), which are responsible for nitrogen regulation, are less abundant.

Other, through the co-culture induced, genes belong to the group of transporters of small acids. Here, most genes are up-regulated, such as PP_3165, which encodes for an aromatic acid/H^+ symporter (*benK*, PP_3165 $\log_2$-FC 1.2) or PP_4735 coding for a lactate permease PP_4735 ($\log_2$-FC 2.2). Further examples are the putative 2-ketogluconate transporter gene kguT, which is slightly up-regulated and a putative oxalate/formate antiporter gene, which is opposed regulated (PP_0288 $\log_2$-FC -1.4). Among the DEGs grouped to sugar-transport, gtsA/B/D (PP_1015, PP_1016 and PP_1018) encoding a putative transporter for cellobiose/glucose, and *rbsA/C* (PP_2759 and PP_2456), encoding a putative ribose transporter were up-regulated (see Figure 4.20).

On the first glance, it is not intuitive, that *P. putida cscRABY* regulates its transporter differently, since the sole carbon source in the co-culture, neglecting the small amount of citric acid in the $BG11^+$ medium, should be sucrose secreted by the phototrophic partner. However, it has been described that cyanobacteria can secret amino acids and other components. For example, different amino acids, such as tryptophan and phenylalanine were found in the supernatant of *S. elongatus* CCMP 163120. Moreover, *P. putida* can colonize plant roots and was shown to exhibit advanced chemotaxis towards polyamides, which are a component of complex root extrudates [189], [190]. In summary, a clear adaption in transporters seems to be in the presence of the phototrophic co-culture partner. It should be noted that additional changes were observed in genes and proteins encoding proteins connected to the heterotroph's membrane (compare Table 4.10). For instance, the secretion system T6SS K3 was found to be mostly down-regulated (see Figure A.23).

The DEGs identified in *S. elongatus cscB* that belong to the group of transport are dominated by sulfur and iron transport (see Figure 4.20 **B**). Almost all differentially regulated genes belonging to "transport" in the cyanobacterial co-culture partner were down-regulated. One exception was the most highly up-regulated transporter gene Synpcc7942_0197, encoding a putative folate/biopterin family MFS transporter ($\log_2$-FC 2.8). Pterins are ubiquitously occurring molecules that are needed by cyanobacteria for pigment generation, phototaxis, and UV protection [191]. The sulfur/sulfonate transporter *cysT* (Synpcc7942_1682 $\log_2$-FC -2.1) was down-regulated. Another gene Synpcc7942_0935, annotated as a sulfite transporter, was slightly up-regulated. Sulfur is an essential element for microbes and participates as iron-sulfur clusters, a common

[6] https://string-db.org/

cofactor of proteins, in many important physiological processes including photosynthesis, DNA/RNA modification, and purine metabolism [192]. Sulfite is cell toxic and arises from the intracellular breakdown of metabolic products, including sulfur-containing amino acids. Sulphite boosts ROS generation, harms photosynthesis, and decreases growth [193]. This hints towards differences in sulfur homeostasis in *S. elongatus cscB*, when grown in co-culture with *P. putida cscRABY*.

Additionally, the transcription of genes annotated as iron transporters was affected by the presence of *P. putida cscRABY*. Genes for the *futABC*-operon, which is responsible for iron uptake via siderophores, was found to be down-regulated (Synpcc7942_1409 *futA-II* $\log_2$-FC -1.6, Synpcc7942_1407 *futB* $\log_2$-FC -3.1, and Synpcc7942_1406 *futC* $\log_2$-FC -1.74) (compare Figure 4.20 **B**).

Table 4.10: DAPs for transport and membrane in *P. putida cscRABY*.

GeneName	ProteinIDs	$\log_2$-FC	Description
Transport			
gltI	Q88NY2	3.6	ABC-Transporter
PP_0412	Q88QS6	2.6	Polyamine ABC transporter, periplasmic polyamine-binding protein
PP_1726	Q88M48	2.6	ABC transporter, periplasmic binding protein
spuD	Q88CJ9	2.4	Polyamine ABC transporter, periplasmic polyamine-binding protein
livK	Q88NR4	2.5	ABC-Transporter
ydcS	Q88MT2	2.1	Polyamine ABC transporter, periplasmic polyamine-binding protein
yhdW	Q88NB5	2.0	Putative amino-acid ABC transporter-binding protein YhdW
PP_2662	Q88JI7	3.3	Porin_4 domain-containing protein
PP_5538	A0A140FW92	1.4	Putative ABC transporter, substrate-binding protein
gtsA	Q88P38	-1.3	Mannose/glucose ABC transporter, glucose-binding periplasmic protein
PP_3954	Q88FX3	2.4	C4-dicarboxylate ABC transporter
Membrane			
mcpQ	Q88D09	1.7	Methyl-accepting chemotaxis protein McpQ
PP_4332	Q88EX0	1.9	Chemotaxis protein CheW
PP_3089	Q88IB0	2.9	Type VI secretion system tube protein Hcp
fliC	Q88ES5	-1.4	Flagellin
tolC	Q88EE6	1.1	-

4.3.4 Detoxification, degradation and stress in the co-culture

The microbes experience multiple stresses in the co-culture. One challenge is the increased salinity due to high ionic strength (ionic stress) and external osmotic pressure (osmotic stress) [99]. Furthermore, it is known that light exposure can induce oxidative stress, and the adaptation to changing light intensities can also display a burden on organisms. However, these external factors are comparable between the axenic cultures and co-cultures. Therefore, any differences in stress signals, degradation processes, and detoxification mechanisms are regarded to be specific to the presence of the co-culture partner.

The data indicate that several stress-processes in the heterotrophic partner seem to be affected by the presence of *S. elongatus cscB*. More specifically, genes and proteins involved in:

- the degradation of compounds,

- oxidative stress through light,
- efflux of (toxic) substances,
- general stress response and
- regulation of ion detoxification or homeostasis

were identified and will be presented in more detail in the following.

A group of DEGs involved in aromatic degradation, the *ben*- and *cat*-operon were found to be up-regulated (see Figure 4.21 **A**). The transcripts of *benA/B* were up-regulated (see Figure 4.21 **B**; $\log_2$-FC 1.86 and $\log_2$-FC 1.5) and the genes for the degradation of catechol to muconolactone were up-regulated as well (*catA-II, catB, catC*). The gene encoding the AraC-type regulator BenR for the *benABC*-operon, however, was slightly down-regulated ($\log_2$-FC -1.2, refer to Figure 4.21 **B**).

Genes that are light-inducible, such as PP_0741, PP_0742, PP_0738, and PP_0739, the latter one encodes a deoxyribodipyrimidine photolyase, were found to be up-regulated (see Figure 4.21 **B**). Additionally, PP_0740 encodes for a MerR family transcriptional regulator of light-inducible genes, known as PplR1 [194]. The light exposure was similar between the axenic culture of *P. putida cscRABY* and the co-culture. Further, the culture density was even higher in the co-culture, which would imply a lower light intensity per OD_{750} (compare Figure A.12). Therefore, it can be hypothesized that the presence of the co-culture partner is responsible for the changes in the expression of these genes.

Genes linked to the efflux of substances are mostly up-regulated (see Figure 4.21 **C**). Here, multiple resistance-nodulation-division (RND) efflux pumps, such as Mex-RND and TolC-RND, which are responsible for the removal of toxic compounds, were detected (see Figure 4.21 **C**). The multidrug efflux pump PP_2817 ($\log_2$-FC 2.1) and PP_2731 ($\log_2$-FC 3.2) showed the highest activation. As mentioned above, ROS generated from the photosynthesis of the cyanobacterium are believed to be one of the main stress factors for the heterotrophic partners in the co-culture [32]. Consistent with this, the up-regulation of one catalase gene (PP_2887 $\log_2$-FC 1.2) was observed, indicating its role in ROS degradation. At the protein level, one catalase enzyme KatG was found to be more abundant, further supporting ROS detoxification. However, of the two major cellular ROS degrading regulators, only one, SoxR (PP_2060 $\log_2$-FC 1.1), was found to be marginally up-regulated [195], [32] and most of the common genes for the glutathione metabolism, which plays an important role in antioxidant defends, are not differently regulated.

Transcripts connected to the general stress response were mainly up-regulated, as shown in Figure 4.21 **C**. Three of the found transcripts encode for putative universal stress proteins (PP_2132, PP_2187, PP_3156, and the hypothetical protein gene-M8001_RS13900), and four encode for putative heat shock proteins (gene-M8001_RS10375, gene-M8001_RS17415, PP_3313, and PP_3314). At the protein level, two identified stress proteins are less abundant (RecA $\log_2$-FC -2.4 and DnaK $\log_2$-FC -1.1).

The most pronounced up-regulation within the genes related to ion-detoxification belong to the *cop* and *czc*-operon (see Table 4.11 and Figure 4.21 **D**). Copper is an essential ion [196] and can induce oxidative stress like other metals. Therefore, its homeostasis is tightly controlled with the copper-sensing metalloregulator CopR-II (PP_5383 $\log_2$-FC 2.0), which forms a two-component system with CopS. This two-component system is responsible for the activation of transcription of the copper resistance operon *copABCD* (see Figure 4.21 **D**). The transcripts *copA-I/II* (PP_2205 and PP_5380) and *copB-II* (PP_5379) were up-regulated, and

in line with this, the gene encoding the putative copper receptor OrpC (PP_4838, log_2-FC -2.8) was down-regulated (see Table 4.11). Genes of the *czc/cus*-operon were up-regulated as well. It is located downstream of the *cop*-operon and is associated with the cytoplasmic detoxification of copper and silver ions (see Table 4.11). Furthermore, connected transcriptional regulators for ion homeostasis were found to be differently regulated. One encodes a putative MerR-transcriptional regulator (PP_0740) and was found to be highly up-regulated with a log_2-FC of 3.3. Further, one ArsR/SmtB family transcription factor, likewise connected to metal-induced stress, was slightly up-regulated (log_2-FC 1.1). The MerR-transcriptional regulator protein family is connected to the ability to respond to stress by heavy metal-induced toxicity [197]. In summary, these findings indicate that *P. putida cscRABY* experienced a general stress situation, most likely triggered by the cyanobacterium, and responded to it with changes in ion homeostasis.

Table 4.11: Transcritps of the *cop* and *czc*-operon divided in regulator, outer membrane and periplasmic proteins.

Gene Name	Gene function (annotation)	Log_2-FC
Regulator		
PP_5383, *copR-II*	Heavy metal response regulator transcription factor	2.0
Outer membrane proteins		
PP_5385, *czcC*	CzcC family metal RND transporter outer membrane protein	1.4
PP_5379, *copB-II*	Copper resistance protein B	3.0
PP_4828, *orpC*	TonB-dependent copper receptor	-2.8
Periplasmic proteins		
PP_0588, *copZ*	Putative copper-binding chaperone	2.4
PP_2205, *copA-I*	Copper resistance system multicopper oxidase	1.3
PP_5383, *copA-II*	Copper resistance system multicopper oxidase	2.9
PP_5732	Putative metal-binding protein	3.4

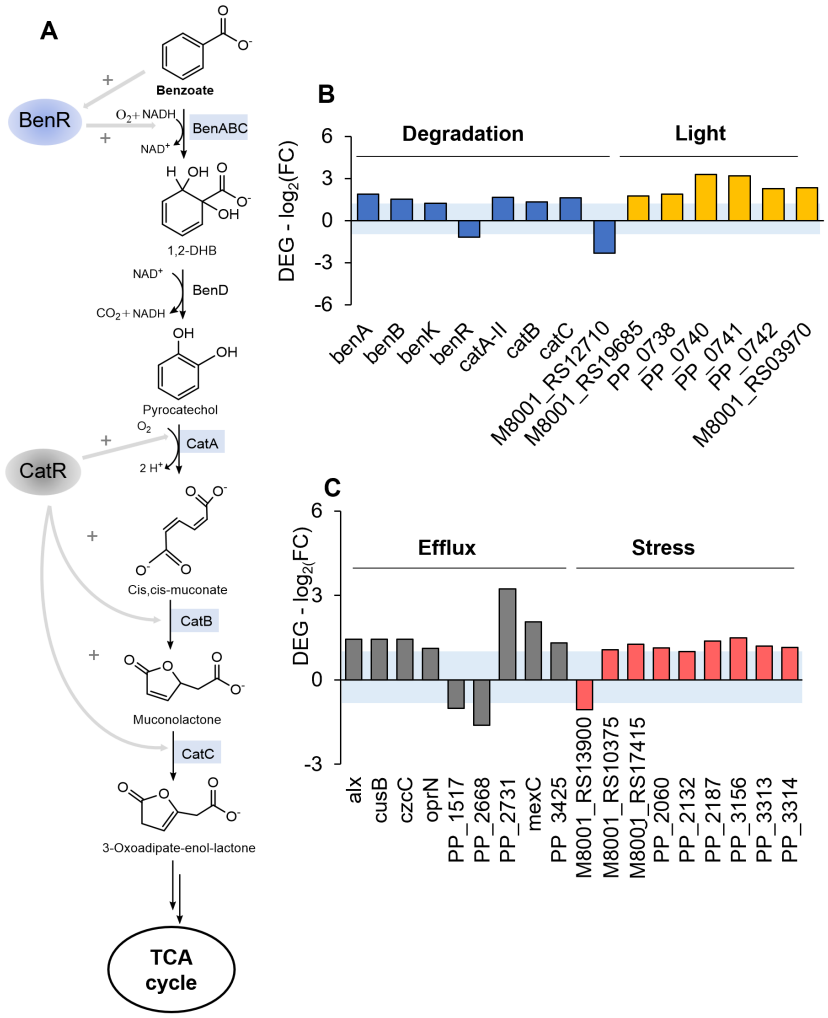

Figure 4.21: Degradation, detoxification, and stress response in *P. putida cscRABY* cells grown in the co-culture compared to axenic cultures. **(A)** Shows a schematic visualization of the degradation of benzoate and assimilation in the Tricarboxylic Acid (TCA)-cycle catalyzed by enzymes from the BenABCD- and CatABC-operon. The transcripts of the enzymes marked in blue show differential regulation. The gray arrows indicate regulations of CatR (not in the data) and BenR. This part of the figure was created with ChemSketch (https://www.acdlabs.com/resources/free-chemistry-software-apps/chemsketch-freeware/) and the KEGG-database (https://www.kegg.jp/pathway/ppu00362+M00551). **(B)** Depicts the DEGs for aromatic degradation and light induced stress. **(C)** Shows the DEGs for efflux of (toxic) substances and DEGs for general stress in *P. putida* grown in co-culture. gene-M8001_RS12710 locus tag DM483_08015; gene-M8001_RS19685 locus tag carboxymuconolactone decarboxylase family protein; gene-M8001_RS03970 locus tag deoxyribodipyrimidine photo-lyase, PP_0739; gene-M8001_RS13900 locus tag DM483_02730; gene-M8001_RS10375 locus tag Hsp20 family protein; gene-M8001_RS17415 locus tag DM483_12495.

Processes involved in redox reactions, efflux, general stress, and ion homeostasis were identified by analyzing the genes, proteins, and metabolites related to the stress response in *S. elongatus cscB*. One of the key compounds to combat redox stress is glutathione, which can exist in its reduced (GSH) and oxidized (GSSG) form 4.22 **A**. GSSG is formed by peroxidases accompanied by the reduction of hydrogen peroxide (H_2O_2) or other damaging ROS. The cycle is closed by the formation of GSH via oxidation of the electron acceptor NADPH by the activity of glutathione reductases 4.22 **A**).

Two glutathione peroxidases (Synpcc7942_0437 and gene-H6G84_RS08920) and one thioredoxin peroxidase *tpxA* (log_2-FC 1.3) were up-regulated in cyanobacterial cells growing in the co-culture (see Fig-

ure 4.22 **B**). One reductase (Synpcc7942_0842 $\log_2$-FC 1.6) was up-regulated, that might be responsible for the reduction of GSSG. Proteins of this family are generally handled as glutathione degrading enzymes in *E. coli* [198]. Fittingly, the metabolites oxidized glutathione (GSSG), L-glutamate, and γ-glutamylglutamic acid are more abundant in the co-culture compared to both axenic cultures. This circumstance might be connected to oxidative stress in cyanobacteria growing in the co-culture (see Figure 4.22 **C**). Oxidative stress can also be faced by a glutathione-independent degradation of H_2O_2, performed enzymatically by catalases, peroxidases, and superoxide dismutase. The transcript of the catalase KatG was highly down-regulated with a $\log_2$-FC -5.4 in the co-culture growing cyanobacterium. A superoxide dismutase SodB, however, was found to be up-regulated with a $\log_2$-FC 1.5 in *S. elongatus* grown in co-culture.

As observed for the heterotrophic partner, some DEGs encoding for different types of efflux transporters were mainly found to be up-regulated in the co-culture. Two examples are HlyD-family efflux transporters (Synpcc7942_1224) or RND efflux transporters (Synpcc7942_1869, Synpcc7942_1870).

Other genes identified as differentially expressed and connected to general stress in the co-culture are annotated to be involved in DNA repair (RecN gene-H6G84_RS04095 $\log_2$-FC 1.5), iron stress (Synpcc7942_1542 $\log_2$-FC -1.1) (see Figure 4.22 **D**). Under various exogenous stresses and already under moderate light intensity, the high-light-inducible proteins (Hlip) are expressed [199], [200]. Two of them were found to be up-regulated in the co-culture grown *S. elongatus cscB* (Synpcc7942_1997 $\log_2$-FC 3.1 and Synpcc7942_1120 $\log_2$-FC 2.5) (see Figure 4.22 **D**). Three FtsH proteases, responsible for protein homeostasis of the thylakoid membrane in photooxidative stress situations, are up-regulated (Synpcc7942_1820, Synpcc7942_0998, and Synpcc7942_0942) on a transcriptional level but on a protein level the proteins *ftsH*, *ftsH.1*, and *ftsH.3* (Synpcc7942_0297, Synpcc7942_0942, and Synpcc7942_0998) are less abundant in the co-culture (see Table 4.12).

Balancing ion homeostasis in the co-culture seems also to be important task for the cyanobacterium *S. elongatus cscB*. In respect to this, differential expression of genes annotated as metalloregulatory transcriptional repressors of the SmtB/ArsR family, which might repress operons linked to stress response induced via heavy metals, was identified. Two other genes encoding putative metallo-regulators were also up-regulated (Synpcc7942_1739, $\log_2$-FC 1.5 and Synpcc7942_0938, $\log_2$-FC 1.1) and another gene, *smtB*, which is annotated to function mainly as Zn(II) responsive repressor, was down-regulated (Synpcc7942_1291 $\log_2$-FC -2.3) [201]. On the protein level, two bacterioferritins were more abundant in the co-culture *S. elongatus cscB* cells (Synpcc7942_2180 and Synpcc7942_1942) (see Table 4.12). This finding aligns with the observed differences in ion homeostasis, as cytoplasmic free iron is tightly regulated through such storage molecules.

Both co-culture partners show differently regulated genes connected to various stresses, detoxification, and degradation when grown together. Despite *S. elongatus cscB* showing reduced growth in the axenic culture, the detected DEGs for stress in the cyanobacterium are mainly up-regulated in the co-culture, not vice versa. At a protein level, general stress proteins were less abundant in the cyanobacteria cells grown in co-culture (see Table 4.12).

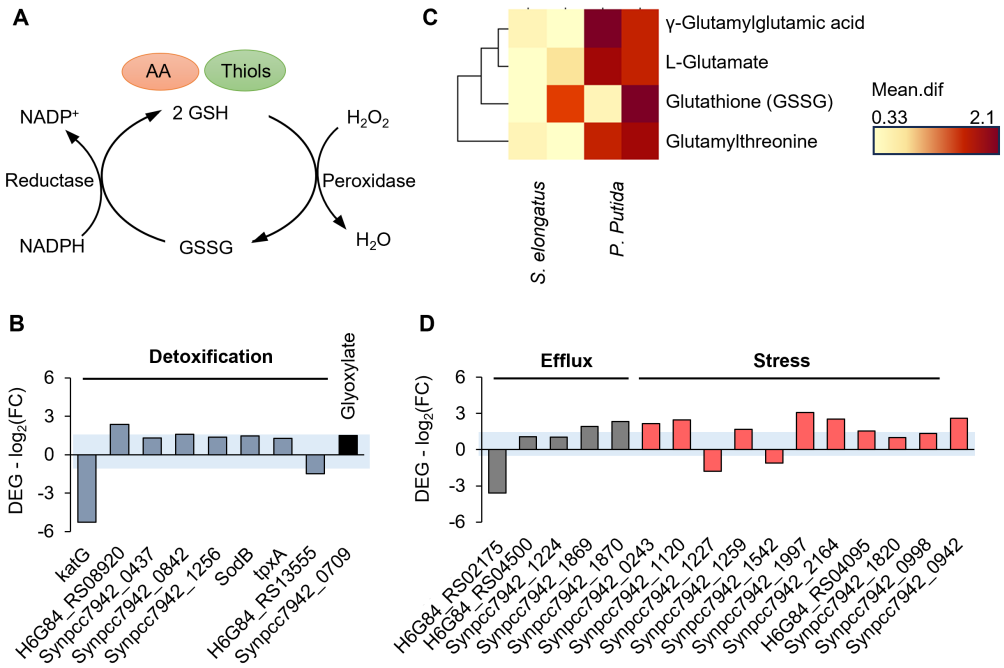

Figure 4.22: DEGs involved in H_2O_2 detoxification, efflux of substances, and stress response identified in *S. elongatus cscB* cells grown in co-culture compared to axenically grown cyanobacterial cells. **(A)** Schematic representation of the glutathione cycle with GSH = glutathione reduced and GSSG = glutathione oxidized. H_2O_2 = hydrogen peroxide, H_2O = water, $NADP^+$ (oxidized) and NADPH (reduced). Indicated are the two main pools of glutathione (GSH), namely the amino acid pool (AA) and the pool of thiols. **(B)** Depicted are DEGs for ROS and glyoxylate degradation/detoxification of *S. elongatus cscB*. **(C)** Depicted is a heat map (Mean difference) for metabolites measured with HILIC in positive and negative ionization modes. The metabolites are compared between co-culture and the axenic cultures of *S. elongatus cscB* and to *P. putida cscRABY*. Figure **(D)** visualizes the DEGs for efflux and stress of the phototrophic co-culture partner. gene-H6G84_RS08920 glutathione peroxidase, gene-H6G84_RS13555 locus tag srpE Synpcc7942_B2624 anL50, gene-H6G84_RS02175 HlyD family efflux transporter periplasmic adaptor subunit; gene-H6G84_RS04500 MATE family efflux transporter; gene-H6G84_RS04095 DNA repair protein RecN.

Table 4.12: Different abundant proteins related to stress in *S. elongatus cscB* grown in co-culture.

Locus Tag (Protein name)	Gene function (annotation)	Abundance
Iron related stress proteins		
Synpcc7942_2180	Bacterioferritin comigratory protein	2.0
Synpcc7942_1942	Bacterioferritin comigratory protein-like	2.1
IdiA, Q5N0R0	Iron deficiency-induced protein A	6.0
Synpcc7942_1462, IrpA	Iron-regulated protein A	1.9
Redox related proteins		
Synpcc7942_0109	DNA-binding ferritin-like protein (Oxidative damage protectant)-like	1.2
Synpcc7942_2449	1-Cys peroxiredoxin	2.4
Synpcc7942_0842	Glutathione reductase	1.8
General stress proteins		
Synpcc7942_2468	Putative copper-binding chaperone	-1.2
DpsA, Q9R6T3	DNA protection during starvation protein	-3.6
Synpcc7942_0877	Elongator protein 3/MiaB/NifB	-1.8
FusA, Q31PV4	Elongation factor G	-1.7
Synpcc7942_0297	ATP-dependent zinc metalloprotease FtsH	-1.4
Synpcc7942_0942	ATP-dependent zinc metalloprotease FtsH	-1.4
Synpcc7942_0998	ATP-dependent zinc metalloprotease FtsH	-1.1

Discussion

Natural communities of heterotrophs and phototrophs are omnipresent, and phototrophs often can not be cultivated without heterotropic partners. Further, an increase in biomass is generated when heterotrophic partners are available (see Section 2.1.2). The synthetic co-culture of *P. putida cscRABY* and *S. elongatus cscB* showed multi-layered changes on a molecular and metabolic level in comparision to the respective axenic cultures.

The heterotrophic partner shows a differently regulated metabolism, transportation and reacts to stress situations when cultivated together with *S. elongatus cscB*. The highest up-regulated gene in *P. putida cscRABY* is PP_4604, which encodes a protein of the EamA family transporter. Further, the second most up-related gene is the adjacent PP_4605, which encodes for an AraC family transcriptional regulator protein. The biochemical functionality of the transporter is not yet described in *P. putida*. In *E. coli* it might be involved in the transport of cysteine or its derivatives [188]. As several minor changes were observed in the group of amino acid transport and metabolism, it could serve as starting point for investigating targeted exchange reactions between the co-culture partners. Additionally, it was found that the most down-regulated gene in the heterotrophic cells grown in the co-culture was PP_2662, which encodes for a not-well annotated porin. This observation further supports the notion that transportation processes are influenced in the presence of the cyanobacterium. In line with this, the transcriptomic data indicate that *P. putida cscRABY* degrades aromatic substances. In subsequent experiments, it is necessary to validate whether the observed intracellular degradation of aromatic compounds in *P. putida cscRABY* was a result of limited nutrients or stress, or if it was due to the presence of compounds derived from the co-culture partner. If the aromatic compounds originated from the cyanobacterium, further investigations are required to determine whether this is a direct response to the co-culture partner or an indirect release of substances, as observed in *S. elongatus* CCMP 163120 [189]. Both partners did not evolve together, thus, natural and unspecific signals to one another are expected. At the protein level, strong evidence for the shutdown of the TCA was observed in combination with increased flux through the glyoxylate shunt for *P. putida cscRABY* grown in the co-culture. This finding is consistent with a previous study that demonstrated a similar effect in *P. putida* KT2440 during mixotrophic growth with glucose

and benzoate, supporting the hypothesis of the uptake of compounds other than sucrose in the co-culture [135]. Further, the metabolism of the co-culture partner could be investigated in detail with isotope-labeled $13CO_2$ pulses and subsequent flux analysis. The carbon distribution in the core metabolism in the co-culture would be an interesting new opportunity in studying the co-culture. As reactive oxygen species (ROS) have been described as highly invasive to co-culture partners grown with *S. elongatus cscB*, it is intriguing to observe only minor changes in the degradation processes of such species at a transcriptomic and proteomic level in the co-culture with *P. putida cscRABY*.

The phototrophic partner shows better growth with *P. putida cscRABY* as co-culture partner, particularly when conditions are suboptimal (see Section 4.2). However, it also shows differential regulation of transcripts and proteins related to the core metabolism, transportation, and stress in the co-culture. Differentiating between the effects of the co-culture partner and the consequences of enhanced growth on a transcriptional or proteomic level can be challenging. For instance, distinguishing specific changes in the photosynthesis apparatus becomes difficult to classify. Nevertheless, since the increased growth is a response to the co-culture partner, changes in the photosynthesis apparatus can be considered a logical effect of the co-culture. The highest up-regulated gene Synpcc7942_1997 encodes a high light-inducible protein [202], [199], which is unexpected because the light intensity per OD_{750} should be higher in the axenic cultures. It needs to be further validated if this protein might be induced due to other stresses. Stress factors were mainly up-regulated in the co-culture growing *S. elongatus cscB*, in spite of the phenomenological obvious stressed axenic cyanobacterial cells, this fact has to be further pursued. Here, integrating dynamic analysis, would provide a valuable insight.

From the data, it became evident that the interaction between the co-culture partners operates on multiple levels, including competition for medium components such as citrate and various salts like PO_4^{3-} and SO_4^{2-} or iron compounds. The interplay with iron was experimentally investigated, but neither an increase in iron concentration nor a decrease had a significant effect on the cyanobacterium as long as it remained above 1/100th of the default concentration. This observation suggests that iron availability may not be a limiting factor influencing the growth of the co-culture. One possible explanation for this is the overall limited accessibility of iron in the natural habitats of the co-culture partners. The biggest constraint for the heterotrophic growth was, however, the slow sucrose secretion of the partner, which results in a carbon-limited regime.

5 Summary and Conclusion

A light-driven synthetic co-culture was investigated, in which the cyanobacterium *Synechococcus elongatus* PCC 7942 *cscB* provides the feedstock for the heterotrophic partner, a genetically engineered derivative of the gram-negative *Pseudomonas putida* [24], [25]. Three variants of *P. putida* were investigated in the co-culture process for medium chain length polyhydroxyalkanoate (mcl-PHA) accumulation. The strains carry the operon *cscRABY* derived from *Pseudomonas protengens* Pf-5 [27], which allows uptake and metabolization of the disaccharide sucrose. In the co-culture between *P. puitda cscRABY* and *S. elongatus cscB*, a PHA accumulation of 256 mg L^{-1} with a rate of 9 mg L^{-1} d^{-1} was observed. The growth rate of both co-culture partners could be monitored at the cell count level through a new flow cytometer method.

A separation of nitrogen sources was possible by applying the "nitrate-blind" strain *P. putida cscRABY* Δ*nasT* [30]. It allowed for the implementation of a defined carbon-to-nitrogen ratio ($\frac{r_{mol_C}}{r_{mol_N}}$), a key-value for PHA accumulation, in the co-cultivation processes. First, it was confirmed that *S. elongatus cscB* cannot metabolize urea, unlike *P. putida*. Subsequently, the growth rate of *P. putida cscRABY* Δ*nasT* could be manipulated independently of the cyanobacterial partner by adjusting the provided nitrogen amount with different urea feeds. Finally, a maximum PHA titer of 393 mg L^{-1} with a rate of 42.1 mg L^{-1} d^{-1} was recorded, when a $\frac{r_{mol_C}}{r_{mol_N}}$-ratio of 25.8 was applied. Calculating the ratio was performed with a simple model of the carbon provided by the cyanobacterium and consumed by the heterotrophic partner. With this process, it's probable that the physiological maximum of PHA accumulation in the heterotrophic partner has been reached. This implies that further increase of the PHA titer in the co-cultivation needs genetic manipulation of the PHA metabolism or a significant increase in the cell density of *P. putida cscRABY*.

The new derivative *P. putida cscRABY* Δ*gcd* was generated by introducing the *cscRABY* operon into the strain *P. putida* KT2440 Δ*gcd*. The strain's periplasmatic glucose oxidation is hindered by the deletion of *gcd*, which encodes a glucose dehydrogenase [110]. The newly constructed strain showed a minor increase in PHA accumulation when using glucose compared to *P. putida cscRABY*, but this increase was not observed with sucrose. This fact highlights the changed glucose uptake capabilities by the introduced sucrose operon. In the matter of PHA accumulation, the strain exhibited similar behavior to *P. putida cscRABY* in the co-culture process.

Interactions were previously observed between *S. elongatus cscB* and different co-culture partners, such as *Escherichia coli*. Thus, the co-culture with *P. putida cscRABY* was investigated towards potential interactions [32], [33], [34]. At a physiological level *P. putida cscRABY* had a positive or neutral effect on the cyanobacterial growth. The fact that the growth of the heterotrophic partner was not negatively affected in the co-culture at small scales highlights its potential as an ideal co-culture partner for the phototroph *S. elongatus cscB*. This might be a consequence of its high capability for efflux and degradation of harmful substances such as ROS.

A reproducible experiment in a 9-fold membrane reactor was set up to investigate the interaction within the co-culture. Initially, *S. elongatus cscB* was studied as an axenic culture induced and non-induced to understand its growth behavior under different conditions. Induction had a notable impact on the cyanobacterial growth, leading to a decreased growth rate by $\sim$ 50% upon induction (0.1 mM IPTG, constant or exponential light). Subsequently, the co-culture between *S. elongatus cscB* and *P. putida cscRABY* was examined. A significant growth-promoting effect from the heterotrophic partner on the cyanobacteria was observed. The growth rate increased with a maximum of 85% compared to the non-induced axenic cultures. The cyanobacterial cells supported heterotrophic growth and additionally showed increased biomass production. Consequently, the overall carbon fixation of the cyanobacterium was elevated when growing in the co-culture.

The integration of a feed for *P. putida cscRABY* provided a controlled environment for nutrient supply and allowed *in situ* sampling for the axenic cultures. Thus, it became possible to compare the performance of axenic *P. putida cscRABY* to the cells growing in the co-culture. Triplicates of axenic *P. putida cscRABY* cultures fed with external sucrose, axenic *S. elongatus cscB* cultures and the co-culture, all growing under an exponential light profile, were used for the OMICs analysis.

The analysis at a transcriptomic, proteomic, and metabolomic level of the co-culture revealed multi-layered signals of small changes. When cultivated alongside *S. elongatus cscB*, the heterotrophic partner exhibited up-regulated transport strategies, differentially expressed degradation operons, and responsive behavior to stress. Thus, in addition to the synthetic connection by sucrose, more processes have to be integrated into the mechanistic model of the co-culture. The competition for common resources, such as medium components including citric acid and various salts should be integrated into the new co-culture model. Furthermore, in both organisms, the ion homeostasis was unbalanced, which might indicate limitations or reduced accessibility through advanced scavenging strategies of the respective co-culture partner. This highlights the requirement for careful medium optimization in co-cultures in general.

The up-regulation of transport processes, particularly for amino acids and degradation of aromatic compounds in *P. putida cscRABY*, suggests the exchange of molecules belonging to these groups. This exchange is unlikely to be attributed to intended signaling, as both organisms have not evolved together. However, cyanobacteria and heterotrophic bacteria have a shared history; therefore, further studies should be directed to analyze the supernatant in order to determine whether amino acids or other compounds are accumulated, which was previously reported to occur in growing cultures of *S. elongatus* CCMP 1631 [189]. Furthermore, the co-culture partners responded to the presence of their respective counterparts by altering processes related to stress and detoxification. These two connections, therefore, should also be included in the mechanistic model of the co-culture.

Stress factors were mainly up-regulated in the co-culture growing *S. elongatus cscB*, in spite of the phenomenological obvious stressed axenic cyanobacterial cells, this fact has to be further pursued. Further, the presence of the heterotrophic partner affected the growth of *S. elongatus cscB*, leading to alterations in the photosynthetic apparatus at a protein and transcript level.

The findings indicate that the interactions between the two organisms are happening at multiple levels and are highly complex. A precise mechanistic model of co-cultures contributes to better controllability and stability in multi-species processes.

Outlook

The newly designed *P. putida cscRABY* [27] and *P. putida cscRABY ΔnasT* [30] derivatives were used to improve the co-cultivation process in terms of controllability and production of the bioplastic mcl-PHA. PHA is accumulated in unbalanced nutrient conditions, such as a state of carbon excess combined with a limitation of essential nutrients, for instance, nitrogen [28]. The physiological maximum of PHA accumulation seems already to be reached with both *P. putida* derivatives. Thus, further improvements of the synthetic consortium in terms of PHA production rely on other strategies. One such is to achieve higher cell densities by employing other cyanobacterial strains with higher growth rates and increased sucrose production rates. It might be suitable to apply the fast-growing *S. elongatus* UTEX 2973, which recently was equipped with the gene *cscB* for sucrose secretion [154]. It was reported that the derivative accumulates a maximum of 9 g L^{-1} sucrose, which would increase heterotrophic biomass and thus PHA accumulation by a factor of three in the co-culture. Another strategy would be to utilize derivatives of *P. putida* that have been metabolically engineered to enhance the accumulation of polyhydroxyalkanoates (PHAs), particularly when using substrates that are not structurally related to PHAs. One example of such a genetic improvement is the overexpression of the gene encoding the pyruvate dehydrogenase subunit *acoA* [126]. Another option is to focus on the 3-hydroxyalkanoate (HA) monomer production. The monomers leave the cell due to their chemical properties [172] and might be custom polymerized after purification so that the polymer meets the physical and chemical properties needed (see section A.2). Furthermore, the co-culture process could be optimized by employing the strain *P. putida* EM371 [179], after equipping it with the sucrose metabolizing operon *cscRABY*, to prevent biofilm formation under suboptimal conditions.

Process engineering techniques could step in to enhance biomass accumulation or prevent the sucrose secretion rate from decreasing. One example could be a continuous cultivation process with biomass skimming of the phototroph, which could lead to increased sucrose yields. However, it is essential to consider the impact of high cell densities of the heterotroph, as shading effects can have negative consequences for the cyanobacterium. Careful optimization of the cultivation conditions and parameters is necessary to ensure growth and metabolic activities of both organisms in the co-culture system.

In principle, the co-culture can be considered a biotechnology platform utilizing two powerful workhorses. Through introducing a suitable transfer plasmid carrying the desired genes, a wide range of potential products could be synthesized from light and CO_2. *P. putida* is a highly capable organism that has been utilized for the production of various value-added products, including terpenoids and amino acid derivatives [134], [136]. These strains can be readily equipped with the sucrose-operon and then employed in co-cultivation. Newly gained understanding of the unique aspects of the metabolism of *P. putida cscRABY*, particularly regarding glucose uptake with the *cscRABY*-operon, should be incorporated into well-established metabolic core models of the bacterium. Additionally, the metabolic model of the heterotroph can be connected with that of the phototroph to investigate their interactions and dependencies at a community level. To obtain a more comprehensive understanding of the metabolic fluxes within the co-culture system, flux analysis experiments can be conducted using isotopically labeled CO_2 or nitrate. By pulsing these labeled compounds, it becomes possible to track their incorporation into different metabolic pathways and determine the flux rates. For instance, the flux through the TCA cycle and the connected glyoxylate shunt could be investigated comparing the co-culture and the axenic cultures. This analysis is particularly interesting considering the

observed differences in protein abundance between the two culture conditions.

Microbial interactions in co-cultures are omnipresent, and especially the connection between phototrophic and heterotrophic organisms is widespread in nature [31]. The substantial positive impact of *P. putida cscRABY* on cyanobacterial growth could be a result of the targeted degradation of harmful substances by the heterotrophic partner. It is worth investigating the supernatant of the co-culture for the presence of potential toxins or harmful compounds that could be detrimental to the cyanobacterium. As genes for transportation and for the membrane in *P. putida cscRABY* showed major changes, analyzing the highest up-regulated transporter (PP_4604) and the possibly connected transcriptional regulator (PP_4605) would be one step to prove the direct exchange of molecules between the partners. Additionally, time-dependent analysis of targeted metabolites in the supernatant, such as amino acids, would be a suitable complementation. Considering that interactions in the co-culture system may rely on physical contact and separating the co-culture partners can provide valuable insights into their behavior (see section A.1).

The dynamic of the co-culture between *S. elongatus cscB* and *P. putida cscRABY* has been extensively investigated. However, it is equally important to comprehend how the co-culture responds when the equilibrium between the partners is disrupted due to the presence of contaminants. It is interesting from two perspectives: First, in future scenarios, the co-culture might be cultivated in open ponds, which would require it to be resistant to various contaminants or potential competitors. Second, the fundamental understanding of how the dynamic changes in co-cultures with three or more partners could be increased. To investigate potential contaminants, it would be necessary to explore various salt-resistant microbes with diverse phylogenetic relationships compared to the co-culture partners. This analysis might be expanded to the single-cell level as well. Additionally, targeted competitions between two different strains of *P. putida* enabled for sucrose metabolization could provide valuable insights into the co-culture dynamics. Understanding and describing the dynamic of competition between different strains mathematically might enable further optimization of the co-culture.

The combination of phototrophic and heterotrophic organisms holds great potential for biotechnological applications, as it combines different metabolic regimes and thus links the capability of CO_2-fixation to diverse metabolic traits.

List of Figures

List of Tables

Bibliography

[1] N. Lane, „The unseen world: reflections on Leeuwenhoek (1677) 'Concerning little animals'.“ *Philosophical transactions of the Royal Society of London. Series B, Biological sciences*, vol. 370, no. 1666, 2015, DOI: 10.1098/rstb.2014.0344.

[2] S. M. Blevins and M. S. Bronze, „Robert Koch and the 'golden age' of bacteriology,“ *International Journal of Infectious Diseases*, vol. 14, no. 9, e744–e751, 2010, DOI: https://doi.org/10.1016/j.ijid.2009.12.003. Available: https://www.sciencedirect.com/science/article/pii/S1201971210023143.

[3] S. M. Opal. „*A Brief History of Microbiology and Immunology.*“ eng. Nov. 2009. DOI: 10.1007/978-1-4419-1108-7{_}3.

[4] S. H. E. Kaufmann, „Robert Koch, the Nobel Prize, and the ongoing threat of tuberculosis.“ *The New England journal of medicine*, vol. 353, no. 23, pp. 2423–2426, 2005, DOI: 10.1056/NEJMp058131.

[5] K. Govender et al., „A novel and more efficient biosynthesis approach for human insulin production in Escherichia coli (E. coli),“ *AMB Express*, vol. 10, no. 1, p. 43, 2020, DOI: 10.1186/s13568-020-00969-w. Available: https://doi.org/10.1186/s13568-020-00969-w.

[6] I. Vecchio et al., „The Discovery of Insulin: An Important Milestone in the History of Medicine,“ *Frontiers in Endocrinology*, vol. 9, 2018, DOI: 10.3389/fendo.2018.00613. Available: https://www.frontiersin.org/articles/10.3389/fendo.2018.00613.

[7] C. C. Quianzon and I. Cheikh, „History of insulin.“ *Journal of community hospital internal medicine perspectives*, vol. 2, no. 2, 2012, DOI: 10.3402/jchimp.v2i2.18701.

[8] J. D. WATSON and F. H. CRICK, „Molecular structure of nucleic acids; a structure for deoxyribose nucleic acid.“ *Nature*, vol. 171, no. 4356, pp. 737–738, 1953, DOI: 10.1038/171737a0.

[9] F. CRICK, „Central Dogma of Molecular Biology,“ *Nature*, vol. 227, no. 5258, pp. 561–563, 1970, DOI: 10.1038/227561a0. Available: https://doi.org/10.1038/227561a0.

[10] J. M. Heather and B. Chain, „The sequence of sequencers: The history of sequencing DNA.“ *Genomics*, vol. 107, no. 1, pp. 1–8, 2016, DOI: 10.1016/j.ygeno.2015.11.003.

[11] F. S. Collins and L. Fink, „The Human Genome Project.“ *Alcohol health and research world*, vol. 19, no. 3, pp. 190–195, 1995.

[12] J. M. S. Bartlett and D. Stirling, „A Short History of the Polymerase Chain Reaction,“ in *PCR Protocols*, J. M. S. Bartlett and D. Stirling, ed. Totowa, NJ: Humana Press, 2003, pp. 3–6, ISBN: 978-1-59259-384-2. DOI: 10.1385/1-59259-384-4:3. Available: https://doi.org/10.1385/1-59259-384-4:3.

[13] J. Jumper et al., „Highly accurate protein structure prediction with AlphaFold," *Nature*, vol. 596, no. 7873, pp. 583–589, 2021, DOI: 10.1038/s41586-021-03819-2. Available: https://doi.org/10.1038/s41586-021-03819-2.

[14] V. D'Argenio, „The High-Throughput Analyses Era: Are We Ready for the Data Struggle?," *High-throughput*, vol. 7, no. 1, 2018, DOI: 10.3390/ht7010008.

[15] R. Shute and N. Lynch, „The Next Big Developments – The Lab of the Future," in *Digital Transformation of the Laboratory* John Wiley & Sons, Ltd, 2021, pp. 3–31, ISBN: 9783527825042. DOI: https://doi.org/10.1002/9783527825042.ch1. Available: https://onlinelibrary.wiley.com/doi/abs/10.1002/9783527825042.ch1.

[16] C. Bai et al., „Industry 4.0 technologies assessment: A sustainability perspective," *International Journal of Production Economics*, vol. 229, p. 107776, 2020, DOI: https://doi.org/10.1016/j.ijpe.2020.107776. Available: https://www.sciencedirect.com/science/article/pii/S0925527320301559.

[17] E. Dolgin, „The tangled history of mRNA vaccines," *Nature*, vol. 597, 2021. Available: doi:%20https://doi.org/10.1038/d41586-021-02483-w.

[18] T. Stein. „*Greenhouse gases continued to increase rapidly in 2022*," Available: https://www.noaa.gov/news-release/greenhouse-gases-continued-to-increase-rapidly-in-2022.

[19] „. *The Paris Agreement*," Available: https://unfccc.int/process-and-meetings/the-paris-agreement.

[20] T. Schwander et al., „A synthetic pathway for the fixation of carbon dioxide in vitro." *Science (New York, N.Y.)*, vol. 354, no. 6314, pp. 900–904, 2016, DOI: 10.1126/science.aah5237.

[21] M. Srikanth et al., „Biodegradation of plastic polymers by fungi: a brief review," *Bioresources and Bioprocessing*, vol. 9, no. 1, p. 42, 2022, DOI: 10.1186/s40643-022-00532-4. Available: https://doi.org/10.1186/s40643-022-00532-4.

[22] C. Jerves et al., „Reaction Mechanism of the PET Degrading Enzyme PETase Studied with DFT/MM Molecular Dynamics Simulations," *ACS Catalysis*, vol. 11, no. 18, pp. 11626–11638, 2021, DOI: 10.1021/acscatal.1c03700. Available: https://doi.org/10.1021/acscatal.1c03700.

[23] J.-G. Rosenboom, R. Langer and G. Traverso, „Bioplastics for a circular economy," *Nature Reviews Materials*, vol. 7, no. 2, pp. 117–137, 2022, DOI: 10.1038/s41578-021-00407-8. Available: https://doi.org/10.1038/s41578-021-00407-8.

[24] D. C. Ducat et al., „Rerouting carbon flux to enhance photosynthetic productivity." *Applied and environmental microbiology*, vol. 78, no. 8, pp. 2660–2668, 2012, DOI: 10.1128/AEM.07901-11.

[25] H. Löwe et al., „Photoautotrophic production of polyhydroxyalkanoates in a synthetic mixed culture of Synechococcus elongatus cscB and Pseudomonas putida cscAB," *Biotechnology for Biofuels*, vol. 10, no. 1, p. 190, 2017, DOI: 10.1186/s13068-017-0875-0. Available: https://doi.org/10.1186/s13068-017-0875-0.

[26] H. Löwe et al., „Metabolic engineering to expand the substrate spectrum of Pseudomonas putida toward sucrose." *MicrobiologyOpen*, vol. 6, no. 4, 2017, DOI: 10.1002/mbo3.473.

[27] H. Löwe et al., „Engineering sucrose metabolism in Pseudomonas putida highlights the importance of porins.“ *Microbial biotechnology*, vol. 13, no. 1, pp. 97–106, 2020, DOI: 10.1111/1751-7915.13283.

[28] M. P. Mezzina et al., „Engineering Native and Synthetic Pathways in Pseudomonas putida for the Production of Tailored Polyhydroxyalkanoates,“ *Biotechnology Journal*, vol. 16, no. 3, p. 2000165, 2021.

[29] I. Poblete-Castro et al., „The metabolic response of P. putida KT2442 producing high levels of polyhydroxyalkanoate under single- and multiple-nutrient-limited growth: Highlights from a multi-level omics approach,“ *Microbial Cell Factories*, vol. 11, no. 1, p. 34, 2012, DOI: 10.1186/1475-2859-11-34. Available: https://doi.org/10.1186/1475-2859-11-34.

[30] K. Hobmeier et al., „A Nitrate-Blind P. putida Strain Boosts PHA Production in a Synthetic Mixed Culture,“ *Frontiers in Bioengineering and Biotechnology*, vol. 8, 2020, DOI: 10.3389/fbioe.2020.00486. Available: https://www.frontiersin.org/articles/10.3389/fbioe.2020.00486.

[31] L. J. Stal and N. Noffke, „Microbial Mats,“ in *Encyclopedia of Astrobiology*, M. Gargaud et al., ed. Berlin, Heidelberg: Springer Berlin Heidelberg, 2011, pp. 1042–1045, ISBN: 978-3-642-11274-4. DOI: 10.1007/978-3-642-11274-4{_}986. Available: https://doi.org/10.1007/978-3-642-11274-4_986.

[32] S. G. Hays et al., „Synthetic photosynthetic consortia define interactions leading to robustness and photoproduction,“ *Journal of Biological Engineering*, vol. 11, no. 1, p. 4, 2017, DOI: 10.1186/s13036-017-0048-5. Available: https://doi.org/10.1186/s13036-017-0048-5.

[33] J. Ma et al., „Cross-feeding between cyanobacterium Synechococcus and Escherichia coli in an artificial autotrophic-heterotrophic coculture system revealed by integrated omics analysis.“ *Biotechnology for biofuels and bioproducts*, vol. 15, no. 1, p. 69, 2022, DOI: 10.1186/s13068-022-02163-5.

[34] H. Liu et al., „Study on the isoprene-producing co-culture system of Synechococcus elongates–Escherichia coli through omics analysis,“ *Microbial Cell Factories*, vol. 20, no. 1, p. 6, 2021, DOI: 10.1186/s12934-020-01498-8. Available: https://doi.org/10.1186/s12934-020-01498-8.

[35] C. Nai and V. Meyer, „From Axenic to Mixed Cultures: Technological Advances Accelerating a Paradigm Shift in Microbiology.“ *Trends in microbiology*, vol. 26, no. 6, pp. 538–554, 2018, DOI: 10.1016/j.tim.2017.11.004.

[36] X.-Y. Peng et al., „Co-culture: stimulate the metabolic potential and explore the molecular diversity of natural products from microorganisms.“ *Marine life science & technology*, vol. 3, no. 3, pp. 363–374, 2021, DOI: 10.1007/s42995-020-00077-5.

[37] G. Rosero-Chasoy et al., „Microbial co-culturing strategies for the production high value compounds, a reliable framework towards sustainable biorefinery implementation – an overview,“ *Bioresource Technology*, vol. 321, p. 124458, 2021, DOI: https://doi.org/10.1016/j.biortech.2020.124458. Available: https://www.sciencedirect.com/science/article/pii/S0960852420317326.

[38] K. G. Jarvis et al., „Microbiomes Associated With Foods From Plant and Animal Sources,“ *Frontiers in Microbiology*, vol. 9, 2018, DOI: 10.3389/fmicb.2018.02540. Available: https://www.frontiersin.org/articles/10.3389/fmicb.2018.02540.

[39] J. Falardeau et al., „Farm-to-fork profiling of bacterial communities associated with an artisan cheese production facility," *Food Microbiology*, vol. 83, pp. 48–58, 2019, DOI: https://doi.org/10.1016/j.fm.2019.04.002. Available: https://www.sciencedirect.com/science/article/pii/S074000201831044X.

[40] A. Hakansson and G. Molin, „Gut microbiota and inflammation." *Nutrients*, vol. 3, no. 6, pp. 637–682, 2011, DOI: 10.3390/nu3060637.

[41] H.-C. Flemming and J. Wingender, „The biofilm matrix," *Nature Reviews Microbiology*, vol. 8, no. 9, pp. 623–633, 2010, DOI: 10.1038/nrmicro2415. Available: https://doi.org/10.1038/nrmicro2415.

[42] L.-L. Jiang et al., „Advances in industrial microbiome based on microbial consortium for biorefinery," *Bioresources and Bioprocessing*, vol. 4, no. 1, p. 11, 2017, DOI: 10.1186/s40643-017-0141-0. Available: https://doi.org/10.1186/s40643-017-0141-0.

[43] G. Ghoshal, „Chapter 2 - Biotechnology in Food Processing and Preservation: An Overview," in *Advances in Biotechnology for Food Industry* (Handbook of Food Bioengineering), A. M. Holban and A. M. Grumezescu, ed. Academic Press, 2018, pp. 27–54, ISBN: 978-0-12-811443-8. DOI: https://doi.org/10.1016/B978-0-12-811443-8.00002-5. Available: https://www.sciencedirect.com/science/article/pii/B9780128114438000025.

[44] X. Dai and L. Shen, „Advances and Trends in Omics Technology Development," *Frontiers in Medicine*, vol. 9, 2022, DOI: 10.3389/fmed.2022.911861. Available: https://www.frontiersin.org/articles/10.3389/fmed.2022.911861.

[45] J. Lu and S. L. Salzberg, „Ultrafast and accurate 16S rRNA microbial community analysis using Kraken 2," *Microbiome*, vol. 8, no. 1, p. 124, 2020, DOI: 10.1186/s40168-020-00900-2. Available: https://doi.org/10.1186/s40168-020-00900-2.

[46] J. Bengtsson-Palme, „Microbial model communities: To understand complexity, harness the power of simplicity." *Computational and structural biotechnology journal*, vol. 18, pp. 3987–4001, 2020, DOI: 10.1016/j.csbj.2020.11.043.

[47] X. Shan et al., „Annotation-free discovery of functional groups in microbial communities," *Nature Ecology & Evolution*, 2023, DOI: 10.1038/s41559-023-02021-z. Available: https://doi.org/10.1038/s41559-023-02021-z.

[48] F. A. B. von Meijenfeldt, P. Hogeweg and B. E. Dutilh, „A social niche breadth score reveals niche range strategies of generalists and specialists," *Nature Ecology & Evolution*, 2023, DOI: 10.1038/s41559-023-02027-7. Available: https://doi.org/10.1038/s41559-023-02027-7.

[49] P. N. Deo and R. Deshmukh, „Oral microbiome: Unveiling the fundamentals." *Journal of oral and maxillofacial pathology : JOMFP*, vol. 23, no. 1, pp. 122–128, 2019, DOI: 10.4103/jomfp.JOMFP{_}304{_}18.

[50] X. Li et al., „The Oral Microbiota: Community Composition, Influencing Factors, Pathogenesis, and Interventions," *Frontiers in Microbiology*, vol. 13, 2022, DOI: 10.3389/fmicb.2022.895537. Available: https://www.frontiersin.org/articles/10.3389/fmicb.2022.895537.

[51] E. M. Bik et al., „Bacterial diversity in the oral cavity of 10 healthy individuals," *The ISME Journal*, vol. 4, no. 8, pp. 962–974, 2010, DOI: 10.1038/ismej.2010.30. Available: https://doi.org/10.1038/ismej.2010.30.

[52] R. E. Blankenship et al., „Comparing Photosynthetic and Photovoltaic Efficiencies and Recognizing the Potential for Improvement," *Science*, vol. 332, no. 6031, pp. 805–809, 2011, DOI: 10.1126/science.1200165. Available: https://www.science.org/doi/abs/10.1126/science.1200165.

[53] F. Kirsch, S. Klähn and M. Hagemann, „Salt-Regulated Accumulation of the Compatible Solutes Sucrose and Glucosylglycerol in Cyanobacteria and Its Biotechnological Potential," *Frontiers in Microbiology*, vol. 10, 2019, DOI: 10.3389/fmicb.2019.02139. Available: https://www.frontiersin.org/articles/10.3389/fmicb.2019.02139.

[54] G. C. Dismukes et al., „The origin of atmospheric oxygen on Earth: The innovation of oxygenic photosynthesis," *PNAS*, vol. 98, no. 5, pp. 2170–2175, 2001.

[55] C. M. Prieto-Barajas, E. Valencia-Cantero and G. Santoyo, „Microbial mat ecosystems: Structure types, functional diversity, and biotechnological application," *Electronic Journal of Biotechnology*, vol. 31, pp. 48–56, 2018, DOI: https://doi.org/10.1016/j.ejbt.2017.11.001. Available: https://www.sciencedirect.com/science/article/pii/S0717345817300738.

[56] R. M. Ram et al., „Chapter 22 - Use of microbial consortia for broad spectrum protection of plant pathogens: regulatory hurdles, present status and future prospects," in *Biopesticides* (Advances in Bio-inoculant Science), A. Rakshit et al., ed. Woodhead Publishing, 2022, pp. 319–335, ISBN: 978-0-12-823355-9. DOI: https://doi.org/10.1016/B978-0-12-823355-9.00017-1. Available: https://www.sciencedirect.com/science/article/pii/B9780128233559000171.

[57] M. B. Miller and B. L. Bassler, „Quorum Sensing in Bacteria," *Annual Review of Microbiology*, vol. 55, no. 1, pp. 165–199, 2001, DOI: 10.1146/annurev.micro.55.1.165. Available: https://doi.org/10.1146/annurev.micro.55.1.165.

[58] L. Tanet et al., „Bacterial Bioluminescence: Light Emission in Photobacterium phosphoreum Is Not Under Quorum-Sensing Control," *Frontiers in Microbiology*, vol. 10, 2019, DOI: 10.3389/fmicb.2019.00365. Available: https://www.frontiersin.org/articles/10.3389/fmicb.2019.00365.

[59] S. Schauder et al., „The LuxS family of bacterial autoinducers: biosynthesis of a novel quorum-sensing signal molecule," *moecular microbiology*, vol. 41, no. 2, pp. 463–476, 2001.

[60] L. Zhang et al., „Sensing of autoinducer-2 by functionally distinct receptors in prokaryotes," *Nature Communications*, vol. 11, no. 1, p. 5371, 2020, DOI: 10.1038/s41467-020-19243-5. Available: https://doi.org/10.1038/s41467-020-19243-5.

[61] T. Gibbs, S. A. Levin and J. M. Levine, „Coexistence in diverse communities with higher-order interactions," *Proceedings of the National Academy of Sciences*, vol. 119, no. 43, e2205063119, 2022, DOI: 10.1073/pnas.2205063119. Available: https://www.pnas.org/doi/abs/10.1073/pnas.2205063119.

[62] A. R. Pacheco, M. Moel and D. Segrè, „Costless metabolic secretions as drivers of interspecies interactions in microbial ecosystems," *Nature Communications*, vol. 10, no. 1, p. 103, 2019, DOI: 10.1038/s41467-018-07946-9. Available: https://doi.org/10.1038/s41467-018-07946-9.

[63] D.-H. Kim et al., „Effects of Co-culture on Improved Productivity and Bioresource for Microalgal Biomass Using the Floc-Forming Bacteria Melaminivora Jejuensis," *Frontiers in Bioengineering and Biotechnology*, vol. 8, 2020, DOI: 10.3389/fbioe.2020.588210. Available: https://www.frontiersin.org/articles/10.3389/fbioe.2020.588210.

[64] J. A. Baker, M. S. Ferguson and C. TenBroeck, „Growth of Platyfish (Platypoecilus maculatus) Free from Bacteria and Other Micro'organisms," *Proceedings of the Society for Experimental Biology and Medicine*, vol. 51, no. 1, pp. 116–119, 1942, DOI: 10.3181/00379727-51-13854. Available: https://doi.org/10.3181/00379727-51-13854.

[65] D. Preussger et al., „Reciprocal Fitness Feedbacks Promote the Evolution of Mutualistic Cooperation," *Current Biology*, vol. 30, no. 18, pp. 3580–3590, 2020, DOI: 10.1016/j.cub.2020.06.100. Available: https://doi.org/10.1016/j.cub.2020.06.100.

[66] S. Schito et al., „Communities of Niche-optimized Strains (CoNoS) – Design and creation of stable, genome-reduced co-cultures," *Metabolic Engineering*, vol. 73, pp. 91–103, 2022, DOI: https://doi.org/10.1016/j.ymben.2022.06.004. Available: https://www.sciencedirect.com/science/article/pii/S1096717622000866.

[67] M. Diender, I. Parera Olm and D. Z. Sousa, „Synthetic co-cultures: novel avenues for bio-based processes," *Current Opinion in Biotechnology*, vol. 67, pp. 72–79, 2021, DOI: https://doi.org/10.1016/j.copbio.2021.01.006. Available: https://www.sciencedirect.com/science/article/pii/S0958166921000112.

[68] L. Pokorny et al., „How to Verify Non-Presence-The Challenge of Axenic Algae Cultivation." *Cells*, vol. 11, no. 16, 2022, DOI: 10.3390/cells11162594.

[69] K. E. Duncker, Z. A. Holmes and L. You, „Engineered microbial consortia: strategies and applications," *Microbial Cell Factories*, vol. 20, no. 1, p. 211, 2021, DOI: 10.1186/s12934-021-01699-9. Available: https://doi.org/10.1186/s12934-021-01699-9.

[70] K. Stephens et al., „Bacterial co-culture with cell signaling translator and growth controller modules for autonomously regulated culture composition," *Nature Communications*, vol. 10, no. 1, p. 4129, 2019, DOI: 10.1038/s41467-019-12027-6. Available: https://doi.org/10.1038/s41467-019-12027-6.

[71] F. K. Balagaddé et al., „A synthetic Escherichia coli predator-prey ecosystem." *Molecular systems biology*, vol. 4, p. 187, 2008, DOI: 10.1038/msb.2008.24.

[72] A. Khare, „Experimental systems biology approaches reveal interaction mechanisms in model multispecies communities." *Trends in microbiology*, vol. 29, no. 12, pp. 1083–1094, 2021, DOI: 10.1016/j.tim.2021.03.012.

[73] T. S. Tshikantwa et al., „Current Trends and Potential Applications of Microbial Interactions for Human Welfare," *Frontiers in Microbiology*, vol. 9, 2018, DOI: 10.3389/fmicb.2018.01156. Available: https://www.frontiersin.org/articles/10.3389/fmicb.2018.01156.

[74] L. Sun et al., „The microbial community structure in industrial biogas plants influences the degradation rate of straw and cellulose in batch tests," *Biotechnology for Biofuels*, vol. 9, no. 1, p. 128, 2016, DOI: 10.1186/s13068-016-0543-9. Available: https://doi.org/10.1186/s13068-016-0543-9.

[75] F. Salimi and R. Mahadevan, „Characterizing metabolic interactions in a clostridial co-culture for consolidated bioprocessing,“ *BMC Biotechnology*, vol. 13, no. 1, p. 95, 2013, DOI: 10.1186/1472-6750-13-95. Available: https://doi.org/10.1186/1472-6750-13-95.

[76] S. K. Bhatia et al., „Engineering of artificial microbial consortia of Ralstonia eutropha and Bacillus subtilis for poly(3-hydroxybutyrate-co-3-hydroxyvalerate) copolymer production from sugarcane sugar without precursor feeding,“ *Bioresource Technology*, vol. 257, pp. 92–101, 2018, DOI: https://doi.org/10.1016/j.biortech.2018.02.056. Available: https://www.sciencedirect.com/science/article/pii/S0960852418302499.

[77] J. Kehe et al., „Positive interactions are common among culturable bacteria.“ *Science advances*, vol. 7, no. 45, eabi7159, 2021, DOI: 10.1126/sciadv.abi7159.

[78] K. Zengler and L. S. Zaramela, „The social network of microorganisms — how auxotrophies shape complex communities,“ *Nature Reviews Microbiology*, vol. 16, no. 6, pp. 383–390, 2018, DOI: 10.1038/s41579-018-0004-5. Available: https://doi.org/10.1038/s41579-018-0004-5.

[79] P. Xu, „Dynamics of microbial competition, commensalism, and cooperation and its implications for coculture and microbiome engineering,“ *Biotechnology and Bioengineering*, vol. 118, no. 1, pp. 199–209, 2021, DOI: https://doi.org/10.1002/bit.27562. Available: https://onlinelibrary.wiley.com/doi/abs/10.1002/bit.27562.

[80] G. Laloux, „Shedding Light on the Cell Biology of the Predatory Bacterium Bdellovibrio bacteriovorus,“ *Frontiers in Microbiology*, vol. 10, 2020, DOI: 10.3389/fmicb.2019.03136. Available: https://www.frontiersin.org/articles/10.3389/fmicb.2019.03136.

[81] S. Thiery and C. Kaimer, „The Predation Strategy of Myxococcus xanthus,“ *Frontiers in Microbiology*, vol. 11, 2020, DOI: 10.3389/fmicb.2020.00002. Available: https://www.frontiersin.org/articles/10.3389/fmicb.2020.00002.

[82] K. R. Foster and T. Bell, „Competition, Not Cooperation, Dominates Interactions among Culturable Microbial Species,“ *Current Biology*, vol. 22, no. 19, pp. 1845–1850, 2012, DOI: https://doi.org/10.1016/j.cub.2012.08.005. Available: https://www.sciencedirect.com/science/article/pii/S0960982212009335.

[83] J. Monod, „THE GROWTH OF BACTERIAL CULTURES,“ *Annual Review of Microbiology*, vol. 3, no. 1, pp. 371–394, 1949, DOI: 10.1146/annurev.mi.03.100149.002103. Available: https://doi.org/10.1146/annurev.mi.03.100149.002103.

[84] D. Weuster-Botz and R. Takors, „Wachstumskinetik,“ in *Bioprozesstechnik*, H. Chmiel, R. Takors and D. Weuster-Botz, ed. Berlin, Heidelberg: Springer Berlin Heidelberg, 2018, pp. 45–70, ISBN: 978-3-662-54042-8. DOI: 10.1007/978-3-662-54042-8{_}2. Available: https://doi.org/10.1007/978-3-662-54042-8_2.

[85] J. K. Sakkos et al., „Predicting partner fitness based on spatial structuring in a light-driven microbial community,“ *PLOS Computational Biology*, vol. 19, no. 5, pp. 1–20, 2023, DOI: 10.1371/journal.pcbi.1011045. Available: https://doi.org/10.1371/journal.pcbi.1011045.

[86] B. Shorrocks, „Competition, Interspecific,“ in *Encyclopedia of Biodiversity (Second Edition)*, S. A. Levin, ed. Waltham: Academic Press, 2001, pp. 177–191, ISBN: 978-0-12-384720-1. DOI: https://doi.org/10.1016/B978-0-12-384719-5.00027-7. Available: https://www.sciencedirect.com/science/article/pii/B9780123847195000277.

[87] C. Gu et al., „Current status and applications of genome-scale metabolic models,“ *Genome Biology*, vol. 20, no. 1, p. 121, 2019, DOI: 10.1186/s13059-019-1730-3. Available: https://doi.org/10.1186/s13059-019-1730-3.

[88] J. D. Orth, R. M. T. Fleming and B. Ø. Palsson, „Reconstruction and Use of Microbial Metabolic Networks: the Core Escherichia coli Metabolic Model as an Educational Guide,“ *EcoSal Plus*, vol. 4, no. 1, 10.1128/ecosalplus.10.2.1, 2010, DOI: 10.1128/ecosalplus.10.2.1. Available: https://journals.asm.org/doi/abs/10.1128/ecosalplus.10.2.1.

[89] B. Ø. Palsson, „The Stoichiometric Matrix,“ in *Systems Biology: Constraint-based Reconstruction and Analysis* Cambridge University Press, 2015, pp. 151–171, DOI: 10.1017/CBO9781139854610.012.

[90] B. Ø. Palsson, „Mathematical Properties of Reconstructed Networks,“ in *Systems Biology: Constraint-based Reconstruction and Analysis* Cambridge University Press, 2015, pp. 149–150, DOI: 10.1017/CBO9781139854610.011.

[91] J.-C. Lachance et al., „BOFdat: Generating biomass objective functions for genome-scale metabolic models from experimental data,“ *PLOS Computational Biology*, vol. 15, no. 4, pp. 1–20, 2019, DOI: 10.1371/journal.pcbi.1006971. Available: https://doi.org/10.1371/journal.pcbi.1006971.

[92] J. Hidde de et al., „Mathematical modelling of microbes: metabolism, gene expression and growth,“ *Journal of The Royal Society Interface*, vol. 14, no. 136, 2017.

[93] J. M. Monk et al., „iML1515, a knowledgebase that computes Escherichia coli traits,“ *Nature Biotechnology*, vol. 35, no. 10, pp. 904–908, 2017, DOI: 10.1038/nbt.3956. Available: https://doi.org/10.1038/nbt.3956.

[94] K. Schoppel et al., „Metabolic control analysis enables rational improvement of E. coli l-tryptophan producers but methylglyoxal formation limits glycerol-based production,“ *Microbial Cell Factories*, vol. 21, no. 1, p. 201, 2022, DOI: 10.1186/s12934-022-01930-1. Available: https://doi.org/10.1186/s12934-022-01930-1.

[95] J. T. Broddrick et al., „Unique attributes of cyanobacterial metabolism revealed by improved genome-scale metabolic modeling and essential gene analysis.“ *Proceedings of the National Academy of Sciences of the United States of America*, vol. 113, no. 51, E8344–E8353, 2016, DOI: 10.1073/pnas.1613446113.

[96] Y.-K. Oh et al., „Genome-scale reconstruction of metabolic network in Bacillus subtilis based on high-throughput phenotyping and gene essentiality data.“ *The Journal of biological chemistry*, vol. 282, no. 39, pp. 28791–28799, 2007, DOI: 10.1074/jbc.M703759200.

[97] C. Zuñiga et al., „Synthetic microbial communities of heterotrophs and phototrophs facilitate sustainable growth,“ *Nature Communications*, vol. 11, no. 1, p. 3803, 2020, DOI: 10.1038/s41467-020-17612-8. Available: https://doi.org/10.1038/s41467-020-17612-8.

[98] J. Heo et al., „Genome-wide exploration of Escherichia coli genes to promote Chlorella vulgaris growth," *Algal Research*, vol. 38, p. 101390, 2019, DOI: https://doi.org/10.1016/j.algal.2018.101390. Available: https://www.sciencedirect.com/science/article/pii/S2211926418307495.

[99] Y. Liang et al., „Freshwater Cyanobacterium Synechococcus elongatus PCC 7942 Adapts to an Environment with Salt Stress via Ion-Induced Enzymatic Balance of Compatible Solutes," *Applied and Environmental Microbiology*, vol. 86, no. 7, pp. 02904–19, 2020, DOI: 10.1128/AEM.02904-19. Available: https://journals.asm.org/doi/abs/10.1128/AEM.02904-19.

[100] B. W. Abramson et al., „Increased Photochemical Efficiency in Cyanobacteria via an Engineered Sucrose Sink." *Plant & cell physiology*, vol. 57, no. 12, pp. 2451–2460, 2016, DOI: 10.1093/pcp/pcw169.

[101] K. Jahreis et al., „Adaptation of sucrose metabolism in the Escherichia coli wild-type strain EC3132." *Journal of bacteriology*, vol. 184, no. 19, pp. 5307–5316, 2002, DOI: 10.1128/JB.184.19.5307-5316.2002.

[102] V. de Lorenzo et al., „Mini-Tn5 transposon derivatives for insertion mutagenesis, promoter probing, and chromosomal insertion of cloned DNA in gram-negative eubacteria," *Journal of Bacteriology*, vol. 172, no. 11, pp. 6568–6572, 1990, DOI: 10.1128/jb.172.11.6568-6572.1990. Available: https://journals.asm.org/doi/abs/10.1128/jb.172.11.6568-6572.1990.

[103] M. Chavarría et al., „Regulatory tasks of the phosphoenolpyruvate-phosphotransferase system of Pseudomonas putida in central carbon metabolism." *mBio*, vol. 3, no. 2, 2012, DOI: 10.1128/mBio.00028-12.

[104] A. Weimer et al., „Industrial biotechnology of Pseudomonas putida: advances and prospects." *Applied microbiology and biotechnology*, vol. 104, no. 18, pp. 7745–7766, 2020, DOI: 10.1007/s00253-020-10811-9.

[105] R. Silva-Rocha et al., „The Standard European Vector Architecture (SEVA): a coherent platform for the analysis and deployment of complex prokaryotic phenotypes." *Nucleic acids research*, vol. 41, no. Database issue, pp. 666–75, 2013, DOI: 10.1093/nar/gks1119.

[106] V. de Lorenzo, „Genetic engineering strategies for environmental applications," *Current Opinion in Biotechnology*, vol. 3, no. 3, pp. 227–231, 1992, DOI: https://doi.org/10.1016/0958-1669(92)90097-3. Available: https://www.sciencedirect.com/science/article/pii/0958166992900973.

[107] S. Zobel et al., „Tn7-Based Device for Calibrated Heterologous Gene Expression in Pseudomonas putida," *ACS Synthetic Biology*, vol. 4, no. 12, pp. 1341–1351, 2015, DOI: 10.1021/acssynbio.5b00058. Available: https://doi.org/10.1021/acssynbio.5b00058.

[108] S. S. Sasnow, H. Wei and L. Aristilde, „Bypasses in intracellular glucose metabolism in iron-limited Pseudomonas putida," *micobiologyOpen*, vol. 5, no. 1, pp. 3–20, 2016.

[109] J. Nogales et al., „High-quality genome-scale metabolic modelling of Pseudomonas putida highlights its broad metabolic capabilities." *Environmental microbiology*, vol. 22, no. 1, pp. 255–269, 2020, DOI: 10.1111/1462-2920.14843.

[110] I. Poblete-Castro et al., „In-silico-driven metabolic engineering of Pseudomonas putida for enhanced production of poly-hydroxyalkanoates," *Metabolic Engineering*, vol. 15, pp. 113–123, 2013, DOI: https://doi.org/10.1016/j.ymben.2012.10.004. Available: https://www.sciencedirect.com/science/article/pii/S1096717612001164.

[111] P. I. Nikel et al., „Reconfiguration of metabolic fluxes in Pseudomonas putida as a response to sub-lethal oxidative stress." *The ISME journal*, vol. 15, no. 6, pp. 1751–1766, 2021, DOI: 10.1038/s41396-020-00884-9.

[112] E. Kozaeva et al., „Model-guided dynamic control of essential metabolic nodes boosts acetyl-coenzyme A–dependent bioproduction in rewired Pseudomonas putida," *Metabolic Engineering*, vol. 67, pp. 373–386, 2021, DOI: https://doi.org/10.1016/j.ymben.2021.07.014. Available: https://www.sciencedirect.com/science/article/pii/S1096717621001245.

[113] L. Molina et al., „Pseudomonas putida KT2440 metabolism undergoes sequential modifications during exponential growth in a complete medium as compounds are gradually consumed." *Environmental microbiology*, vol. 21, no. 7, pp. 2375–2390, 2019, DOI: 10.1111/1462-2920.14622.

[114] X. Liu et al., „Reactive oxygen species are involved in plant defense against a gall midge." *Plant physiology*, vol. 152, no. 2, pp. 985–999, 2010, DOI: 10.1104/pp.109.150656.

[115] P. I. Nikel and V. de Lorenzo, „Pseudomonas putida as a functional chassis for industrial biocatalysis: From native biochemistry to trans-metabolism," *Metabolic Engineering*, vol. 50, pp. 142–155, 2018, DOI: https://doi.org/10.1016/j.ymben.2018.05.005. Available: https://www.sciencedirect.com/science/article/pii/S1096717618301502.

[116] P. I. Nikel et al., „Pseudomonas putida KT2440 Strain Metabolizes Glucose through a Cycle Formed by Enzymes of the Entner-Doudoroff, Embden-Meyerhof-Parnas, and Pentose Phosphate Pathways*," *Journal of Biological Chemistry*, vol. 290, no. 43, pp. 25920–25932, 2015, DOI: https://doi.org/10.1074/jbc.M115.687749. Available: https://www.sciencedirect.com/science/article/pii/S0021925820495730.

[117] M. Kohlstedt and C. Wittmann, „GC-MS-based 13C metabolic flux analysis resolves the parallel and cyclic glucose metabolism of Pseudomonas putida KT2440 and Pseudomonas aeruginosa PAO1," *Metabolic Engineering*, vol. 54, pp. 35–53, 2019, DOI: https://doi.org/10.1016/j.ymben.2019.01.008. Available: https://www.sciencedirect.com/science/article/pii/S1096717618304725.

[118] S. Ahn et al., „Role of Glyoxylate Shunt in Oxidative Stress Response." *The Journal of biological chemistry*, vol. 291, no. 22, pp. 11928–11938, 2016, DOI: 10.1074/jbc.M115.708149.

[119] M. A. Kukurugya et al., „Multi-omics analysis unravels a segregated metabolic flux network that tunes co-utilization of sugar and aromatic carbons in Pseudomonas putida." *The Journal of biological chemistry*, vol. 294, no. 21, pp. 8464–8479, 2019, DOI: 10.1074/jbc.RA119.007885.

[120] S. Taguchi and K. Matsumoto, „Evolution of polyhydroxyalkanoate synthesizing systems toward a sustainable plastic industry," *Polymer Journal*, vol. 53, no. 1, pp. 67–79, 2021, DOI: 10.1038/s41428-020-00420-8. Available: https://doi.org/10.1038/s41428-020-00420-8.

[121] G. Licciardello, A. F. Catara and V. Catara, „Production of Polyhydroxyalkanoates and Extracellular Products Using Pseudomonas Corrugata and P. Mediterranea: A Review,“ *Bioengineering*, vol. 6, no. 4, 2019, DOI: 10.3390/bioengineering6040105. Available: https://www.mdpi.com/2306-5354/6/4/105.

[122] Y.-W. Cui, Y.-P. Shi and X.-Y. Gong, „Effects of C/N in the substrate on the simultaneous production of polyhydroxyalkanoates and extracellular polymeric substances by Haloferax mediterranei via kinetic model analysis,“ *RSC Adv.*, vol. 7, no. 31, pp. 18953–18961, 2017, DOI: 10.1039/C7RA02131C. Available: http://dx.doi.org/10.1039/C7RA02131C.

[123] R. Sehgal and R. Gupta, „Polyhydroxyalkanoate and its efficient production: an eco-friendly approach towards development.“ *3 Biotech*, vol. 10, no. 12, p. 549, 2020, DOI: 10.1007/s13205-020-02550-5.

[124] M. Ishii-Hyakutake, S. Mizuno and T. Tsuge, „Biosynthesis and Characteristics of Aromatic Polyhydroxyalkanoates.“ *Polymers*, vol. 10, no. 11, 2018, DOI: 10.3390/polym10111267.

[125] T. Fukui, N. Shiomi and Y. Doi, „Expression and Characterization of (R)-Specific Enoyl Coenzyme A Hydratase Involved in Polyhydroxyalkanoate Biosynthesis by Aeromonas caviae,“ *Journal of Bacteriology*, vol. 180, no. 3, pp. 667–673, 1998, DOI: 10.1128/JB.180.3.667-673.1998. Available: https://journals.asm.org/doi/abs/10.1128/JB.180.3.667-673.1998.

[126] J. M. Borrero-de Acuña et al., „Production of medium chain length polyhydroxyalkanoate in metabolic flux optimized Pseudomonas putida.“ *Microbial cell factories*, vol. 13, p. 88, 2014, DOI: 10.1186/1475-2859-13-88.

[127] Y. Fujita, H. Matsuoka and K. Hirooka, „Regulation of fatty acid metabolism in bacteria,“ *molecular micobiology*, vol. 66, no. 4, pp. 829–839, 2007.

[128] I. Poblete-Castro et al., „Comparison of mcl-Poly(3-hydroxyalkanoates) synthesis by different Pseudomonas putida strains from crude glycerol: citrate accumulates at high titer under PHA-producing conditions,“ *BMC Biotechnology*, vol. 14, no. 1, p. 962, 2014, DOI: 10.1186/s12896-014-0110-z. Available: https://doi.org/10.1186/s12896-014-0110-z.

[129] F. Kratzl, K. Andreas and K. Pflüger-Grau, „Streamlining of a synthetic co-culture towards an individually controllable one-pot process for polyhydroxyalkanoate production from light and CO2,“ *Engineering in Life Science*, vol. 23, no. 1, 2023.

[130] Z. Xu et al., „Understanding of bacterial lignin extracellular degradation mechanisms by Pseudomonas putida KT2440 via secretomic analysis,“ *Biotechnology for Biofuels and Bioproducts*, vol. 15, no. 1, p. 117, 2022, DOI: 10.1186/s13068-022-02214-x. Available: https://doi.org/10.1186/s13068-022-02214-x.

[131] G. J. Kim et al., „Enhanced yield and a high production of medium-chain-length poly(3-hydroxyalkanoates) in a two-step fed-batch cultivation of Pseudomonas putida by combined use of glucose and octanoate,“ *Enzyme and Microbial Technology*, vol. 20, no. 7, pp. 500–505, 1997, DOI: https://doi.org/10.1016/S0141-0229(96)00179-2. Available: https://www.sciencedirect.com/science/article/pii/S0141022996001792.

[132] P. Dvořák and V. de Lorenzo, „Refactoring the upper sugar metabolism of Pseudomonas putida for co-utilization of cellobiose, xylose, and glucose.“ *Metabolic engineering*, vol. 48, pp. 94–108, 2018, DOI: 10.1016/j.ymben.2018.05.019.

[133] C. Roma-Rodrigues et al., „Response of Pseudomonas putida KT2440 to phenol at the level of membrane proteome.“ *Journal of proteomics*, vol. 73, no. 8, pp. 1461–1478, 2010, DOI: 10.1016/j.jprot.2010.02.003.

[134] A. Loeschcke and S. Thies, „Pseudomonas putida-a versatile host for the production of natural products.“ *Applied microbiology and biotechnology*, vol. 99, no. 15, pp. 6197–6214, 2015, DOI: 10.1007/s00253-015-6745-4.

[135] S. Sudarsan et al., „Dynamics of benzoate metabolism in Pseudomonas putida KT2440,“ *Metabolic Engineering Communications*, vol. 3, pp. 97–110, 2016, DOI: https://doi.org/10.1016/j.meteno.2016.03.005. Available: https://www.sciencedirect.com/science/article/pii/S2214030116300086.

[136] L. Benninghaus et al., „Metabolic Engineering of Pseudomonas putida for Fermentative Production of l-Theanine,“ *Journal of Agricultural and Food Chemistry*, vol. 69, no. 34, pp. 9849–9858, 2021, DOI: 10.1021/acs.jafc.1c03240. Available: https://doi.org/10.1021/acs.jafc.1c03240.

[137] I. Poblete-Castro et al., „Industrial biotechnology of Pseudomonas putida and related species,“ *Applied Microbiology and Biotechnology*, vol. 93, no. 6, pp. 2279–2290, 2012, DOI: 10.1007/s00253-012-3928-0. Available: https://doi.org/10.1007/s00253-012-3928-0.

[138] R. Davis et al., „High cell density cultivation of Pseudomonas putida KT2440 using glucose without the need for oxygen enriched air supply,“ *Biotechnology and Bioengineering*, vol. 112, no. 4, pp. 725–733, 2015, DOI: https://doi.org/10.1002/bit.25474. Available: https://onlinelibrary.wiley.com/doi/abs/10.1002/bit.25474.

[139] A. Ankenbauer et al., „Pseudomonas putida KT2440 is naturally endowed to withstand industrial-scale stress conditions,“ *Microbial Biotechnology*, vol. 13, no. 4, pp. 1145–1161, 2020, DOI: https://doi.org/10.1111/1751-7915.13571. Available: https://ami-journals.onlinelibrary.wiley.com/doi/abs/10.1111/1751-7915.13571.

[140] P. Demling et al., „Pseudomonas putida KT2440 endures temporary oxygen limitations,“ *Biotechnology and Bioengineering*, vol. 118, no. 12, pp. 4735–4750, 2021, DOI: https://doi.org/10.1002/bit.27938. Available: https://onlinelibrary.wiley.com/doi/abs/10.1002/bit.27938.

[141] A. M. Ruffing, T. J. Jensen and L. M. Strickland, „Genetic tools for advancement of Synechococcus sp. PCC 7002 as a cyanobacterial chassis,“ *Microbial Cell Factories*, vol. 15, no. 1, p. 190, 2016, DOI: 10.1186/s12934-016-0584-6. Available: https://doi.org/10.1186/s12934-016-0584-6.

[142] D. G. Welkie et al., „A Hard Days Night: Cyanobacteria in Diel Cycles,“ *Trends in microbiology*, vol. 27, no. 3, pp. 231–242, 2018.

[143] A. Taton et al., „The circadian clock and darkness control natural competence in cyanobacteria,“ *Nature Communications*, vol. 11, no. 1, p. 1688, 2020, DOI: 10.1038/s41467-020-15384-9. Available: https://doi.org/10.1038/s41467-020-15384-9.

[144] R. Azevedo et al., „Synechococcus elongatus as a model of photosynthetic bioreactor for expression of recombinant β-glucosidases," *Biotechnology for Biofuels*, vol. 12, no. 1, p. 174, 2019, DOI: 10.1186/s13068-019-1505-9. Available: https://doi.org/10.1186/s13068-019-1505-9.

[145] M. Adomako et al., „Comparative Genomics of Synechococcus elongatus Explains the Phenotypic Diversity of the Strains," *mBio*, vol. 13, no. 3, pp. 00862–22, 2022, DOI: 10.1128/mbio.00862-22. Available: https://journals.asm.org/doi/abs/10.1128/mbio.00862-22.

[146] M. Santos-Merino et al., „Highlighting the potential of Synechococcus elongatus PCC 7942 as platform to produce α-linolenic acid through an updated genome-scale metabolic modeling," *Frontiers in Microbiology*, vol. 14, 2023, DOI: 10.3389/fmicb.2023.1126030. Available: https://www.frontiersin.org/articles/10.3389/fmicb.2023.1126030.

[147] S. Y. Choi et al., „Transcriptome landscape of Synechococcus elongatus PCC 7942 for nitrogen starvation responses using RNA-seq," *Scientific Reports*, vol. 6, no. 1, p. 30584, 2016, DOI: 10.1038/srep30584. Available: https://doi.org/10.1038/srep30584.

[148] C. J. Knoot et al., „Cyanobacteria: Promising biocatalysts for sustainable chemical production." *The Journal of biological chemistry*, vol. 293, no. 14, pp. 5044–5052, 2018, DOI: 10.1074/jbc.R117.815886.

[149] S. Shinde et al., „Glycogen Metabolism Supports Photosynthesis Start through the Oxidative Pentose Phosphate Pathway in Cyanobacteria." *Plant physiology*, vol. 182, no. 1, pp. 507–517, 2020, DOI: 10.1104/pp.19.01184.

[150] Y. Dan et al., „Manipulating the Expression of Glycogen Phosphorylase in Synechococcus elongatus PCC 7942 to Mobilize Glycogen Storage for Sucrose Synthesis," *Frontiers in Bioengineering and Biotechnology*, vol. 10, 2022, DOI: 10.3389/fbioe.2022.925311. Available: https://www.frontiersin.org/articles/10.3389/fbioe.2022.925311.

[151] M. Cano et al., „Glycogen Synthesis and Metabolite Overflow Contribute to Energy Balancing in Cyanobacteria." *Cell reports*, vol. 23, no. 3, pp. 667–672, 2018, DOI: 10.1016/j.celrep.2018.03.083.

[152] M. Santos-Merino, L. Yun and D. C. Ducat, „Cyanobacteria as cell factories for the photosynthetic production of sucrose." *Frontiers in microbiology*, vol. 14, p. 1126032, 2023, DOI: 10.3389/fmicb.2023.1126032.

[153] S. G. Hays and D. C. Ducat, „Engineering cyanobacteria as photosynthetic feedstock factories." *Photosynthesis research*, vol. 123, no. 3, pp. 285–295, 2015, DOI: 10.1007/s11120-014-9980-0.

[154] P.-C. Lin, F. Zhang and H. B. Pakrasi, „Enhanced production of sucrose in the fast-growing cyanobacterium Synechococcus elongatus UTEX 2973," *Scientific Reports*, vol. 10, no. 1, p. 390, 2020, DOI: 10.1038/s41598-019-57319-5. Available: https://doi.org/10.1038/s41598-019-57319-5.

[155] L. González-Resendiz et al., „Photoautotrophic poly(3-hydroxybutyrate) production by a wild-type Synechococcus elongatus isolated from an extreme environment," *Bioresource Technology*, vol. 337, p. 125508, 2021, DOI: https://doi.org/10.1016/j.biortech.2021.125508. Available: https://www.sciencedirect.com/science/article/pii/S0960852421008488.

[156] M. Koch et al., „On the Role and Production of Polyhydroxybutyrate (PHB) in the Cyanobacterium Synechocystis sp. PCC 6803.“ *Life (Basel, Switzerland)*, vol. 10, no. 4, 2020, DOI: 10.3390/life10040047.

[157] E. Martínez-García et al., „Freeing Pseudomonas putidaKT2440 of its proviral load strengthens endurance to environmental stresses.“ *Environmental microbiology*, vol. 17, no. 1, pp. 76–90, 2015, DOI: 10.1111/1462-2920.12492.

[158] H. W. Boyer and D. Roulland-dussoix, „A complementation analysis of the restriction and modification of DNA in Escherichia coli,“ *Journal of Molecular Biology*, vol. 41, no. 3, pp. 459–472, 1969, DOI: https://doi.org/10.1016/0022-2836(69)90288-5. Available: https://www.sciencedirect.com/science/article/pii/0022283669902885.

[159] K.-H. Choi et al., „A Tn7-based broad-range bacterial cloning and expression system,“ *Nature Methods*, vol. 2, no. 6, pp. 443–448, 2005, DOI: 10.1038/nmeth765. Available: https://doi.org/10.1038/nmeth765.

[160] H. Chmiel and D. Weuster-Botz, „Bioreaktoren,“ in *Bioprozesstechnik*, H. Chmiel, R. Takors and D. Weuster-Botz, ed. Berlin, Heidelberg: Springer Berlin Heidelberg, 2018, pp. 157–229, ISBN: 978-3-662-54042-8. DOI: 10.1007/978-3-662-54042-8{_}6. Available: https://doi.org/10.1007/978-3-662-54042-8_6.

[161] R. L. Clark et al., „Light-optimized growth of cyanobacterial cultures: Growth phases and productivity of biomass and secreted molecules in light-limited batch growth.“ *Metabolic engineering*, vol. 47, pp. 230–242, 2018, DOI: 10.1016/j.ymben.2018.03.017.

[162] K. M. McKinnon, „Flow Cytometry: An Overview.“ *Current protocols in immunology*, vol. 120, pp. 1–5, 2018, DOI: 10.1002/cpim.40.

[163] M. Díaz et al., „2.71 - Flow Cytometry: A High-Throughput Technique for Microbial Bioprocess Characterization,“ in *Comprehensive Biotechnology (Second Edition)*, M. Moo-Young, ed. Burlington: Academic Press, 2011, pp. 967–981, ISBN: 978-0-08-088504-9. DOI: https://doi.org/10.1016/B978-0-08-088504-9.00448-7. Available: https://www.sciencedirect.com/science/article/pii/B9780080885049004487.

[164] „Instrumentation: Into the Black Box,“ in *Flow Cytometry: First Principles* John Wiley & Sons, Ltd, 2001, pp. 15–39, ISBN: 9780471223948. DOI: https://doi.org/10.1002/0471223948.ch3. Available: https://onlinelibrary.wiley.com/doi/abs/10.1002/0471223948.ch3.

[165] A. Cossarizza et al., „Guidelines for the use of flow cytometry and cell sorting in immunological studies (third edition),“ *European Journal of Immunology*, vol. 51, no. 12, pp. 2708–3145, 2021, DOI: https://doi.org/10.1002/eji.202170126. Available: https://onlinelibrary.wiley.com/doi/abs/10.1002/eji.202170126.

[166] G.-Y. A. Tan et al., „Start a Research on Biopolymer Polyhydroxyalkanoate (PHA): A Review,“ *Polymers*, vol. 6, no. 3, pp. 706–754, 2014, DOI: 10.3390/polym6030706. Available: https://www.mdpi.com/2073-4360/6/3/706.

[167] J.-Y. de Saint Laumer et al., „Quantification in Gas Chromatography: Prediction of Flame Ionization Detector Response Factors from Combustion Enthalpies and Molecular Structures," *Analytical Chemistry*, vol. 82, no. 15, pp. 6457–6462, 2010, DOI: 10.1021/ac1006574. Available: https://doi.org/10.1021/ac1006574.

[168] J.-Y. de Saint Laumer et al., „Prediction of response factors for gas chromatography with flame ionization detection: Algorithm improvement, extension to silylated compounds, and application to the quantification of metabolites." *Journal of separation science*, vol. 38, no. 18, pp. 3209–3217, 2015, DOI: 10.1002/jssc.201500106.

[169] M. Mõttus et al., „Photosynthetically Active Radiation: Measurementphotosynthesis/photosynthetic(ally)active radiation (PAR)measurementand Modelingphotosynthesis/photosynthetic(ally)active radiation (PAR)modeling," in *Encyclopedia of Sustainability Science and Technology*, R. A. Meyers, ed. New York, NY: Springer New York, 2012, pp. 7902–7932, ISBN: 978-1-4419-0851-3. DOI: 10.1007/978-1-4419-0851-3{_}451. Available: https://doi.org/10.1007/978-1-4419-0851-3_451.

[170] S. G. Bowden and C. Honsberg. „*Photovoltaics Education Website*," 2019. Available: www.pveducation.org.

[171] Y. K. Leong et al., „Economic and environmental analysis of PHAs production process," *Clean Technologies and Environmental Policy*, vol. 19, no. 7, pp. 1941–1953, 2017, DOI: 10.1007/s10098-017-1377-2. Available: https://doi.org/10.1007/s10098-017-1377-2.

[172] M.-Q. Yuan et al., „Microbial production of medium-chain-length 3-hydroxyalkanoic acids by recombinant Pseudomonas putida KT2442 harboring genes fadL, fadD and phaZ," *FEMS Microbiology Letters*, vol. 283, no. 2, pp. 167–175, 2008, DOI: 10.1111/j.1574-6968.2008.01164.x. Available: https://doi.org/10.1111/j.1574-6968.2008.01164.x.

[173] M. Schmidt et al., „Nitrogen Metabolism in Pseudomonas putida: Functional Analysis Using Random Barcode Transposon Sequencing." *Applied and environmental microbiology*, vol. 88, no. 7, e0243021, 2022, DOI: 10.1128/aem.02430-21.

[174] S. C. Galusnyak et al., „Environmental impact assessment of green ammoniacoupled with urea and ammonium nitrate production," *Journal of Environmental Management*, vol. 343, p. 118215, 2023, DOI: https://doi.org/10.1016/j.jenvman.2023.118215. Available: https://www.sciencedirect.com/science/article/pii/S0301479723010034.

[175] I. P.-C. ^{1 and 2*}, „Improved Production of Medium-Chain-Length Polyhydroxyalkanoates in Glucose-Based Fed-Batch Cultivations of Metabolically Engineered Pseudomonas putida Strains," *Journal of Microbiology and Biotechnology*, vol. 24, no. 1, pp. 59–69, 2014, DOI: 10.4014/jmb.1308.08052. Available: http://jmb.or.kr/journal/view.html?doi=10.4014/jmb.1308.08052.

[176] J. Cole et al., „Phototrophic biofilm assembly in microbial-mat-derived unicyanobacterial consortia: model systems for the study of autotroph-heterotroph interactions," *Frontiers in Microbiology*, vol. 5, 2014, DOI: 10.3389/fmicb.2014.00109. Available: https://www.frontiersin.org/articles/10.3389/fmicb.2014.00109.

[177] R. Simkovsky et al., „Transcriptomic and Phenomic Investigations Reveal Elements in Biofilm Repression and Formation in the Cyanobacterium Synechococcus elongatus PCC 7942.“ *Frontiers in microbiology*, vol. 13, p. 899150, 2022, DOI: 10.3389/fmicb.2022.899150.

[178] A. López-Sánchez et al., „Biofilm formation-defective mutants in Pseudomonas putida,“ *FEMS Microbiology Letters*, vol. 363, no. 13, 2016, DOI: 10.1093/femsle/fnw127. Available: https://doi.org/10.1093/femsle/fnw127.

[179] E. Martínez-García et al., „Naked Bacterium: Emerging Properties of a Surfome-Streamlined Pseudomonas putida Strain,“ *ACS Synthetic Biology*, vol. 9, no. 9, pp. 2477–2492, 2020, DOI: 10.1021/acssynbio.0c00272. Available: https://doi.org/10.1021/acssynbio.0c00272.

[180] K. Kojima et al., „High-Light-Induced Stress Activates Lipid Deacylation at the Sn-2 Position in the Cyanobacterium Synechocystis Sp. PCC 6803.“ *Plant & cell physiology*, vol. 63, no. 1, pp. 82–91, 2022, DOI: 10.1093/pcp/pcab147.

[181] T. Stork et al., „Bioinformatic analysis of the genomes of the cyanobacteria Synechocystis sp. PCC 6803 and Synechococcus elongatus PCC 7942 for the presence of peroxiredoxins and their transcript regulation under stress,“ *Journal of Experimental Botany*, vol. 56, no. 422, pp. 3193–3206, 2005, DOI: 10.1093/jxb/eri316. Available: https://doi.org/10.1093/jxb/eri316.

[182] W. Du et al., „Photonfluxostat: A method for light-limited batch cultivation of cyanobacteria at different, yet constant, growth rates,“ *Algal Research*, vol. 20, pp. 118–125, 2016, DOI: https://doi.org/10.1016/j.algal.2016.10.004. Available: https://www.sciencedirect.com/science/article/pii/S2211926416304908.

[183] M. Zapalska-Sozoniuk et al., „Is it useful to use several “omics” for obtaining valuable results?,“ *Molecular Biology Reports*, vol. 46, no. 3, pp. 3597–3606, 2019, DOI: 10.1007/s11033-019-04793-9. Available: https://doi.org/10.1007/s11033-019-04793-9.

[184] M. Espinosa-Urgel and J. L. Ramos, „Expression of a Pseudomonas putida aminotransferase involved in lysine catabolism is induced in the rhizosphere.“ *Applied and environmental microbiology*, vol. 67, no. 11, pp. 5219–5224, 2001, DOI: 10.1128/AEM.67.11.5219-5224.2001.

[185] A. Jia et al., „Regulation and Functional Complexity of the Chlorophyll-Binding Protein IsiA,“ *Frontiers in Microbiology*, vol. 12, 2021, DOI: 10.3389/fmicb.2021.774107. Available: https://www.frontiersin.org/articles/10.3389/fmicb.2021.774107.

[186] C. M. Mendonca et al., „Hierarchical routing in carbon metabolism favors iron-scavenging strategy in iron-deficient soil Pseudomonas species,“ *Proceedings of the National Academy of Sciences*, vol. 117, no. 51, pp. 32358–32369, 2020, DOI: 10.1073/pnas.2016380117. Available: https://www.pnas.org/doi/abs/10.1073/pnas.2016380117.

[187] S. A. Rice, „Interaction between microbial community members,“ *Environmental microbiology*, vol. 9, no. 5, pp. 471–473, 2017.

[188] I. Franke et al., „YfiK from Escherichia coli promotes export of O-acetylserine and cysteine.“ *Journal of bacteriology*, vol. 185, no. 4, pp. 1161–1166, 2003, DOI: 10.1128/JB.185.4.1161-1166.2003.

[189] C. L. Fiore et al., „Release of ecologically relevant metabolites by the cyanobacterium Synechococcus elongates CCMP 1631.“ *Environmental microbiology*, vol. 17, no. 10, pp. 3949–63, 2015, DOI: 10.1111/1462-2920.12899.

[190] J. M. Luengo and E. R. Olivera, „Catabolism of biogenic amines in Pseudomonas species,“ *Applied Microbiology international*, vol. 22, no. 4, pp. 1174–1192, 2020.

[191] N. Feirer and C. Fuqua, „Pterin function in bacteria,“ vol. 28, no. 1, pp. 23–36, 2017, DOI: doi: 10.1515/pterid-2016-0012. Available: https://doi.org/10.1515/pterid-2016-0012.

[192] F. Gao, „Iron–Sulfur Cluster Biogenesis and Iron Homeostasis in Cyanobacteria,“ *Frontiers in Microbiology*, vol. 11, 2020, DOI: 10.3389/fmicb.2020.00165. Available: https://www.frontiersin.org/articles/10.3389/fmicb.2020.00165.

[193] S. Kobayashi, M. Tsuzuki and N. Sato, „Sulfite-stress induced functional and structural changes in the complexes of photosystems I and II in a cyanobacterium, Synechococcus elongatus PCC 7942,“ *Plant and Cell Physiology*, vol. 56, no. 8, pp. 1521–1532, 2015, DOI: 10.1093/pcp/pcv073. Available: https://doi.org/10.1093/pcp/pcv073.

[194] S. Sumi et al., „Light Response of Pseudomonas putida KT2440 Mediated by Class II LitR, a Photosensor Homolog.“ *Journal of bacteriology*, vol. 202, no. 20, 2020, DOI: 10.1128/JB.00146-20.

[195] V. Méndez et al., „The OxyR and SoxR transcriptional regulators are involved in a broad oxidative stress response in Paraburkholderia xenovorans LB400,“ *Biological Research*, vol. 55, no. 1, p. 7, 2022, DOI: 10.1186/s40659-022-00373-7. Available: https://doi.org/10.1186/s40659-022-00373-7.

[196] C. Miller et al., „Copper and cadmium:responses in Pseudomonas putida KT2440,“ *Letters in Applied Microbiology*, vol. 49, no. 6, pp. 775–783, 2009.

[197] N. L. Brown et al., „The MerR family of transcriptional regulators.“ *FEMS microbiology reviews*, vol. 27, no. 2-3, pp. 145–163, 2003, DOI: 10.1016/S0168-6445(03)00051-2.

[198] M. Saini et al., „Bacterial Gamma-Glutamyl Transpeptidase, an Emerging Biocatalyst: Insights Into Structure-Function Relationship and Its Biotechnological Applications.“ *Frontiers in microbiology*, vol. 12, p. 641251, 2021, DOI: 10.3389/fmicb.2021.641251.

[199] M. M. Konert et al., „High-light-inducible proteins HliA and HliB: pigment binding and protein–protein interactions,“ *Photosynthesis Research*, vol. 152, no. 3, pp. 317–332, 2022, DOI: 10.1007/s11120-022-00904-z. Available: https://doi.org/10.1007/s11120-022-00904-z.

[200] K. S. Mironov et al., „Universal Molecular Triggers of Stress Responses in Cyanobacterium Synechocystis.“ *Life (Basel, Switzerland)*, vol. 9, no. 3, 2019, DOI: 10.3390/life9030067.

[201] L. S. Busenlehner, M. A. Pennella and D. P. Giedroc, „The SmtB/ArsR family of metalloregulatory transcriptional repressors: structural insights into prokaryotic metal resistance,“ *FEMS Microbiology Reviews*, vol. 27, no. 2-3, pp. 131–143, 2003, DOI: 10.1016/S0168-6445(03)00054-8. Available: https://doi.org/10.1016/S0168-6445(03)00054-8.

[202] K. Salem and L. G. van Waasbergen, „Light control of hliA transcription and transcript stability in the cyanobacterium Synechococcus elongatus strain PCC 7942.“ *Journal of bacteriology*, vol. 186, no. 6, pp. 1729–1736, 2004, DOI: 10.1128/JB.186.6.1729-1736.2004.

[203] P. Bernal et al., „The Pseudomonas putida T6SS is a plant warden against phytopathogens.“ *The ISME journal*, vol. 11, no. 4, pp. 972–987, 2017, DOI: 10.1038/ismej.2016.169.

[204] C. Jo et al., „A co-culture microplate for real-time measurement of microbial interactions,“ *bioRxiv*, 2021, DOI: 10.1101/2021.01.07.425753. Available: https://www.biorxiv.org/content/early/2021/01/08/2021.01.07.425753.

[205] V. Nurmikko, „Microbiological Determination of Vitamins and Amino Acids Produced by Microorganisms, Using the Dialysis Cell,“ *Applied Microbiology*, vol. 5, no. 3, pp. 160–165, 1957, DOI: 10.1128/am.5.3.160-165.1957. Available: https://journals.asm.org/doi/abs/10.1128/am.5.3.160-165.1957.

[206] S. Pande et al., „Metabolic cross-feeding via intercellular nanotubes among bacteria,“ *Nature Communications*, vol. 6, no. 1, p. 6238, 2015, DOI: 10.1038/ncomms7238. Available: https://doi.org/10.1038/ncomms7238.

[207] M. G. Thompson et al., „Fatty Acid and Alcohol Metabolism in Pseudomonas putida: Functional Analysis Using Random Barcode Transposon Sequencing,“ *Applied and Environmental Microbiology*, vol. 86, no. 21, pp. 01665–20, 2020, DOI: 10.1128/AEM.01665-20. Available: https://journals.asm.org/doi/abs/10.1128/AEM.01665-20.

Appendix

A Appendix

A.1 Compartmentalization - Physical contact as interaction

This section briefly discusses how physical contact may influence the co-culture partners. As explained in Section 2.2.1, microbes show different types of interaction. On the one hand, physical interactions in microbial systems involve cell-cell contact and can occur through various mechanisms. One such mechanism is bacterial conjugation, which allows DNA transfer between cells. Another example is the recently discovered T6SS system in pseudomonads, in which the K1 cluster potentially operates as contact-dependent defense mechanisms against other bacteria [203]. On the other hand, microbes can also interact through diffusion-mediated mechanisms. For instance, quorum sensing relies on the diffusion of signaling molecules to coordinate behaviors of cells or toxin production as a defense strategy (see Section 2.2 for more details). Considering these modes of interaction, it was investigated whether physical separation has an impact on the growth of the co-culture partners *Synechococcus elongatus* PCC 7942 *cscB* and *Pseudomonas putida* EM178 *cscRABY*.

To investigate the physical contact, small-scale compartmentalized bioreactors with a working volume of 10 mL were designed and 3D-printed (see Figure A.1 **A** - **C**). This design enabled the axenic growth of *S. elongatus cscB* and *P. putida cscRABY*. The cyanobacterium showed two-phased growth with different rates. At the beginning, a rate of 1.1 ± 0.02 d^{-1} was calculated and after 50 h, a rate of 0.26 ± 0.03 d^{-1} could be monitored. *P. putida cscRABY* grew with a rate of 0.3 ± 0.02 h^{-1}. Further, the bioreactors allowed repeated compartmentalization of the two co-culture partners by separating them with a cellulose acetate filter with a cut-off of 0.2 µm. The design could effectively prevent contamination between the compartments and allowed physically separated growth of the partners.

In initial co-culture experiments, the cyanobacterium exhibited a growth rate of 0.51 ± 0.037 d^{-1} when the two partners were physically separated, while a growth rate of 0.56 ± 0.047 d^{-1} was observed when the partner grew together. Further, the growth rate of the non-compartmentalized heterotroph was determined to be 0.082 ± 0.006 h^{-1}, whereas, for *P. putida cscRABY* growing in physically separated from the partner, a growth rate of 0.099 ± 0.005 h^{-1} was determined.

In summary, the preliminary experiments showed a slight effect on the growth of the heterotrophic co-culture partner. However, no significant difference was observed in the growth behavior of the cyanobacterium. The overall reduced growth, especially from the axenic *P. putida cscRABY*, suggest that in the reactors prevail a limitation of the gas supply. Moreover, experiments have shown that this separation method influences biofilm or presumably cluster formation. The formation was repeatedly observed when *P. putida cscRABY* was added in higher concentrations than the co-culture partner (see section A.8). Therefore, further experiments

are necessary to confirm these results, which might go in hand with optimizing the reactors. One potential approach would be to transfer the design from the current setup to glass bioreactors, which would help to optimize the gas transfer during the cultivation. Another recently presented strategy for the separation of co-culture partners utilized a custom 96-well plate, separating the partners at a smaller scale that makes it easy to investigate the dynamics between different co-cultures or conditions [204]. If the setup is suitable for phototrophic organisms has to be evaluated. Furthermore, encapsulation of the co-culture partners in agar beads can be employed for compartmentalization. In this approach, the cells are embedded within agar, forming individual beads that act as separate compartments. This technique might allow for the encapsulation of one co-culture partner while the other is cultivated in the liquid medium.

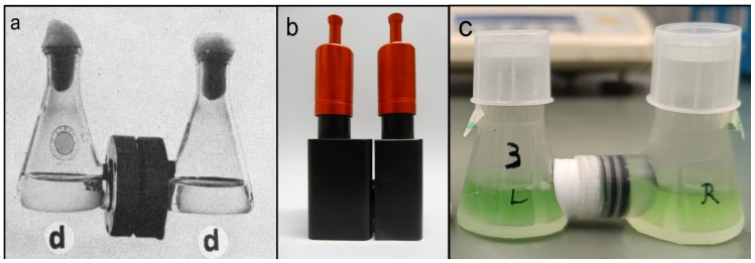

Figure A.1: Different designs of compartimentalized bioreactors to investigate co-cultures consisting of two partners. **(A)** The "Numikko Cell" [205]. This design, proposed by Veikko Nurmikko, provides a compartmentalized bioreactor system suitable for co-culture experiments. **(B)** This modified version of the Numikko Cell focused on investigating nanotube interactions among microorganisms in co-cultures [206]. **(C)** Compartmentalizable bioreactor design of this study: The design aims to investigate the growth behavior of co-culture partners under physically separated and non-separated conditions.

A.2 Strategies for diversifying the co-culture's product spectrum

This section discusses how to broaden the product spectrum of the co-culture, which is an important step towards further enhancing the co-culture system. One intriguing aspect involves producing not just the PHA polymer but also the monomers. Since PHA is present in intracellular, insoluble granules, purification and quantification of PHA poses a challenge (see Section 2.3.1). PHA is considered a medium to low value-added product, indicating that any planned downstream process should aim to minimize labor and cost as much as possible. One possibility to overcome the issue of PHA recovery is by focusing on producing the monomers of mcl-PHAs. These monomers, as mentioned in Section 2.3.1, are R-enantiomerically pure chemicals and can pass through the bacterial cell membrane, which would simplify the recovery and quantification process. Moreover, these monomers can be utilized to synthesize customized polymers, offering additional flexibility in product development.

In the literature, it has been demonstrated that the overexpression of the PHA depolymerase PhaZ can lead to the secretion of monomers when *P. putida* is grown on PHA structurally similar substrates [172]. Therefore, the strain *P. putida* EM178 *cscRABY* was equipped with a plasmid containing the depolymerase PhaZ from *P. protengens* Pf-5 or from *P. putida* KT2440, resulting in two *P. putida cscRABY* (pSEVA221_*phaZ*) derivatives (see Table A.1 and Table A.2). Growth experiments conducted under PHA-producing conditions revealed that 3-HA monomer production was achievable when the carbon source was octanoic acid but not when glucose was used as the carbon source (see Figure A.2). Little to no PHA accumulation was observed in the cell pellet, regardless of the carbon source utilized when *phaZ* was over expressed (see Figure A.2). A potential explanation for the observed outcomes could be attributed to the distinct metabolic pathways associated with the different carbon sources. Glucose differs structurally from PHA. As a result, the monomers must be synthesized through the fatty acid *de novo* synthesis pathway, whereas octanoate requires minimal transformation carried out in the β-oxidation to form PHA monomers (refer to Section 2.3.1). Two approaches were followed:

Firstly, it was hypothesized that the produced monomers might be incorporated into the β-oxidation pathway and subsequently degraded. To test this hypothesis, the β-oxidation pathway was down-regulated by a clean deleting of the gene *fadD* (PP_4549) encoding for a long-chain-fatty acid-CoA ligase. The resulting derivative confirmed that disruption of this gene leads to a loss of fitness when grown on fatty acids but not on other substrates such as sodium citrate, sucrose, and glucose [207]. However, it is worth noting that the mutant strain was still able to grow on octanoate with a rate of 0.3 h^{-1}. Further, no extracellular monomer accumulation was observed when the cells were cultivated in PHA-production conditions (C-source: unlimited glucose and N-source: limited ammonium) and overexpressed *phaZ* gene.

Secondly, Flux balance analysis (FBA) with the metabolic model iJN1462 of *P. putida* [109] suggested that other overflow metabolites than the PHA-monomers are secreted. To investigate this, the supernatant was analyzed using HPLC, which revealed a significant accumulation of citrate when *P. putida cscRABY* (pSEVA221_*KT_phaZ*) was grown under PHA-forming conditions with glucose as a carbon source. These results suggest that the carbon metabolism in the mutant strain reaches a bottleneck in the central metabolism,

leading to an overflow of citrate. Thus, a further investigation involving metabolic engineering should be conducted to explore the possibility of redistributing the carbon flux and alleviating this bottleneck.

Table A.1: Primer for *phaZ* overexpression. Cutting sites for restriction enzymes are depicted in italics.

Name	**Sequence (5'-3')**	**Note**
Fw_5UTR_AvrII_012	TAT *CCT AGG* TTT GAA TGA CTT GCA GAC	Forward primer to amplify *phaZ* from *P. protegens* Pf-5 with native 5'UTR region with restriction side of AvrII
Rw_5UTREcoRI_011	CT GCG *GAA TTC* CTA CGA CGC TCC GTT G	Reverse primer to amplify *phaZ* from *P. protegens* Pf-5 with native 5'UTR region with restriction side of EcoRI
Fw_syn_5UTR_Kt_AvrII_013	CG TAT*GAA TTC* AAG TAC TAA GGA GGT TTT TTA TGC CGC AAC CCT ATA TTT TCA GG	Forward primer to amplify *phaZ* from *P. putida* KT2440 with synthetic ribosomal binding side. The primer introduces the restriction side AvrII
Fw_syn_5UTR_Pf_EcoRI_014	CG TAT*GAA TTC* AAG TAC TAA GGA GGT TTT TTA TGC CAC ACT CAT TCA TAT TC	Reverse primer to amplify *phaZ* from *P. putida* KT2440 with synthetic ribosomal binding side. the primer introduces the restriction side EcoRI.

Table A.2: Strains produced during this study.

Strain name	Description	Function
P. putida EM178 *att*Tn7::*cscRABY* (pSEVA221_*KT_phaZ)*	Sucrose metabolising strain *P. putida* EM178 *cscRABY* carring the plasmid pSEVA221_ *KT_phaZ*. The PHA polymerase PhaZ originates from the strain *P. putida* KT2440.	Investigation for 3-HA monomer production in PHA accumulating conditions.
P. putida EM178 *att*Tn7::*cscRABY* (pSEVA221_*Pf_phaZ)*	Sucrose metabolising strain *P. putida* EM178 *cscRABY* carring the plasmid pSEVA221_ *Pf_phaZ*. The PHA polymerase PhaZ originates from the strain *P. protegens* Pf-5.	Investigation for 3-HA monomer production in PHA accumulating conditions.
P. putida EM178 *att*Tn7::*cscRABY* (pSEVA221_*KT_phaZ)*	Sucrose metabolising strain *P. putida* EM178 *cscRABY* carring the plasmid pSEVA221_*KT_phaZ* and deletion of the *fadD* gene (PP_4549) encoding a long-chain-fatty acid-CoA ligase	Investigation for 3-HA monomer production in PHA accumulating conditions with reduced β-oxidation.
P. putida EM178 *att*Tn7::*cscRABY* (pSEVA221_ *Pf_phaZ)*	Sucrose metabolising strain *P. putida* EM178 *cscRABY* carring the plasmid pSEVA221_*Pf_phaZ* and deletion of the *fadD* gene (PP_4549) encoding a long-chain-fatty acid-CoA ligase	Investigation for 3-HA monomer production in PHA accumulating conditions with reduced β-oxidation.

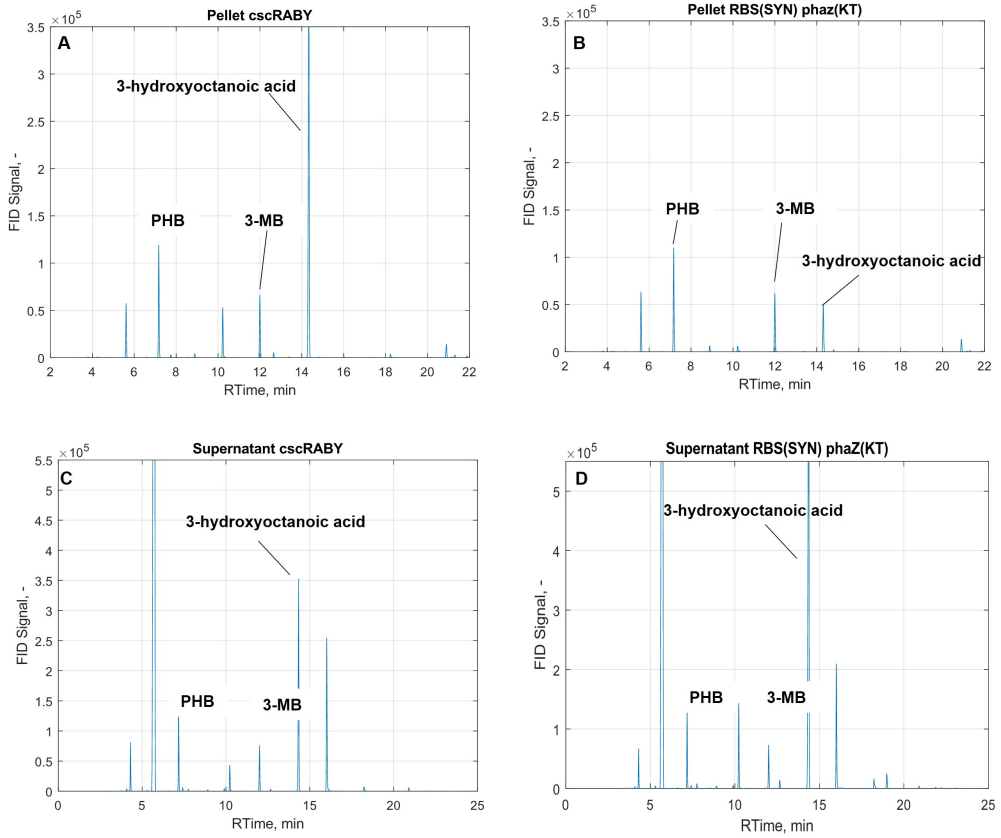

Figure A.2: PHA or 3-HA accumulation in cell pellets and supernatant with octanoate as a carbon source. **(A)** Chromatogram of *P. putida cscRABY's* cell pellet to analyze PHA accumulation. **(B)** Chromatogram of the pellet from *P. putida cscRABY* carrying the plasmid pSEVA221_*KT_phaZ*. **(C)** Chromatogram of the supernatant from *P. putida cscRABY*. **(D)** Chromatogram of the supernatant from *P. putida cscRABY* carrying the plasmid pSEVA221_*KT_phaZ* for monomer accumulation. Experimental conditions: PHA accumulation in M9 medium with nitrogen-limited conditions of 8 g L^1 octanoate with 0.1 g L^1 NH_4Cl as nitrogen source, 30 ℃, 220 rpm (MaxQ 8000 from Thermo Scientific, USA). Gas chromatographic analysis details in Section 3.6.4, optical density was adjusted to OD_{600} = 0.5 and 1 mL supernatant per culture was used monomer quantification. PHB = polyhydroxybutyrate, 3-MB = 3-methylbenzoate, RBS = ribosomal binding site, SYN = synthetic (RBS), *phaZ* = PHA depolymerase gene, KT = indicates *phaZ* derives from *P. putida* KT2440

As seen above, expanding the product spectrum of the synthetic co-culture on the heterotrophic side may require the expression of heterologous genes or the overexpression of homologous ones. To achieve this, a commonly employed approach is the use of plasmids. These plasmids carry the gene of interest along with a selectable marker, typically an antibiotic resistance gene. The presence of this marker enables the bacteria to proliferate in a selective medium containing the specific antibiotic, allowing for the identification and maintenance of the genetically engineered strains. In the co-culture system described, the use of antibiotics is limited due to the presence of only a chloramphenicol resistance gene in *S. elongatus cscB* resulting from the genomic integration of the *cscB* transporter gene. To overcome this limitation and enable the integration of genes of interest into the co-culture system, the design of a universal transfer plasmid would be advantageous. One potential option is to utilize the *cscRABY* operon as a plasmid selection marker. This approach would provide a flexible and antibiotic-free strategy for introducing genetic modifications and expanding the capabilities of the co-culture.

Therefore, a transfer plasmid was designed based on the pSEVA424 *acoA* plasmid, which was constructed to

overexpress the *acoA* gene and increase PHA accumulation [126] (see Section 4.1.4). The sucrose operon *cscRABY* with its native promoters and ribosomal binding sites (RBS) was integrated by the HiFi DNA Assembly method upstream of the streptomycin gene[1]. The plasmid's functionality was demonstrated through successful growth in both axenic cultures and co-culture settings with sucrose as the sole carbon source. *P. putida* carrying the sucrose operon plasmid-based showed a slightly decreased growth rate of 0.3 ± 0.04 h^{-1} which can be compared in Table A.4. The heterotroph in the co-culture expressing the sucrose operon plasmid-based showed increased cell counts and growth in comparison to *P. putida* EM178 *att*Tn7::*cscRABY*. However, it should be noted that this plasmid was developed as a proof of concept, and further improvements are necessary to enhance and verify its performance in the co-culture system. These improvements may include size reduction of the plasmid, ensuring compatibility and stability within the co-culture, and optimizing the expression of genes of interest. Subsequent investigations should also integrate the comparison with the derivative carrying the sucrose-operon genomically integrated.

Table A.3: Growth rate of transfer plasmid carrying strain.

Strain name	Sequence (5'-3')	Note
FW_A	CCCCAATAATTACGATTTACGTATTTATTGGCTAACACGACTCACG	Forward primer to amplify *cscRABY* with overlapping region of pSEVA424.
FW_C	GGTACAGATGGAAACCTGGTAAATGAACCTTGACCGAAC	Forward primer to amplify the backbone pSEVA424 with overlapping the *cscRABY* operon.
FW_B	CGTGAGTCGTGTTAGCCAATAAATACGTAAATCGTAATTATTGGGG	Reverse primer to amplify the backbone pSEVA424 with overlapping the *cscRABY* operon.
FW_D	GTTCGGTCAAGGTTCATTTACCAGGTTTCCATCTGTACC	Reverse primer to amplify *cscRABY* with overlapping region of pSEVA424.

Table A.4: Primer for NEB high fidelity assembly for the integration of *cscRABY* operon into pSEVA424.

Name	Growth rate	Note
P. putida EM178 *att*Tn7::*cscRABY*	0.46 ± 0.08	Strain with genomic integrated sucrose operon, growing on sucrose.
P. putida EM178 (pSEVA424*acoA_cscRABY*)	0.32 ± 0.04	Strain carrying the new transfer plasmid grown on sucrose.
P. putida EM178 (pSEVA424*acoA_cscRABY*)	0.31 ± 0.04	Strain carrying the new transfer plasmid grown on sucrose with addition of streptomicin.

[1]The protocol of NEB was strictly followed. Link: https://international.neb.com/protocols/2014/11/26/nebuilder-hifi-dna-assembly-reaction-protocol

A.3 Gas chromatography

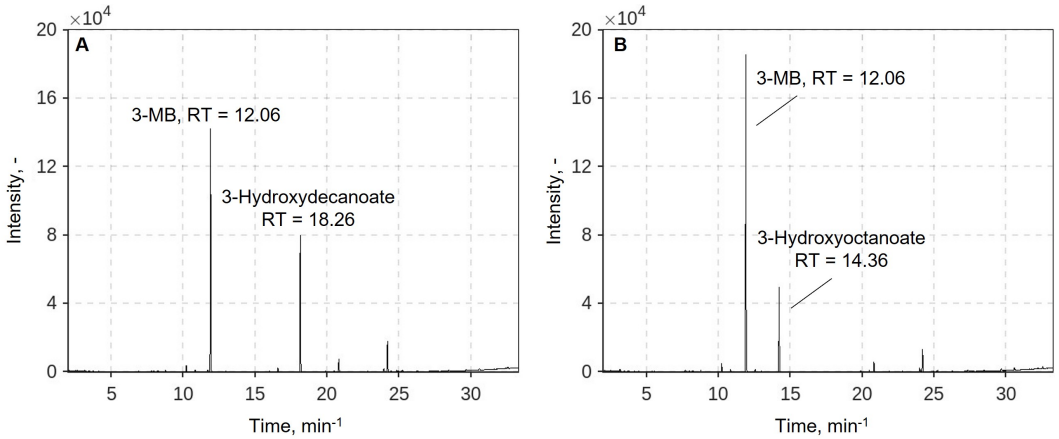

Figure A.3: Example of a chromatogram with the propylesters of 3-methylbenzoate (3-MB, 130 mg mL^{-1}) and 3-hydroxydecanoate (0.109 mg mL^{-1}) in **(A)** and 3-MB (140 mg mL^{-1}) together with 3-hydroxyoctanoate (0.06 mg mL^{-1}) in **(B)**. RT = retention time, 3-MB = 3-methylbenzoate.

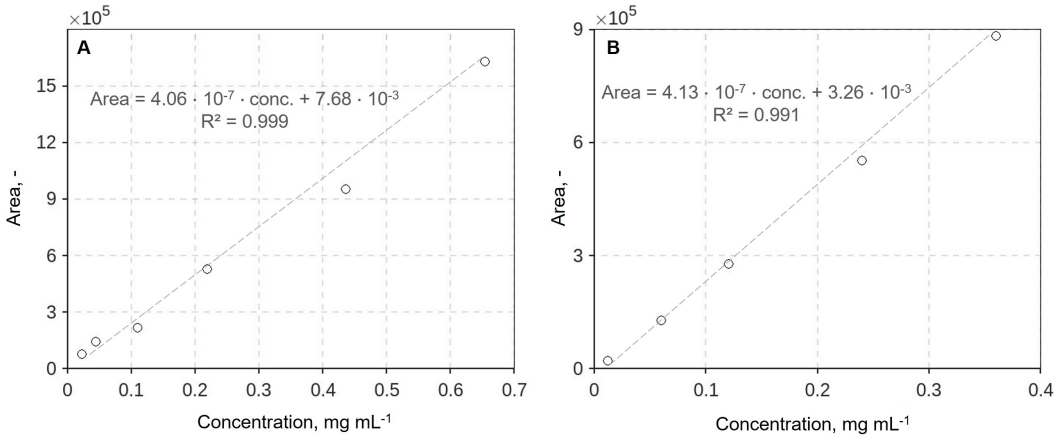

Figure A.4: Example regression of the propylesters from the standards 3-hydroxydecanoate **(A)** and 3-hydroxyoctanoate **(B)**. Concentrations range: standard 3-hydroxydecanoate [0.0218; 0.0438; 0.109; 0.218; 0.436; 0.654] in mg mL^{-1} and 3-Hydroxyoctanoate [0.012; 0.06; 0.12; 0.24; 0.36] in mg mL^{-1}. RT = retention time, 3-MB = 3-methylbenzoate.

A.4 Conversion of irradiance

The total power density function is defined as:

$$H_T^E(\lambda) = \int_{\lambda min}^{\lambda max} \frac{\phi^m \cdot E_p}{\lambda} = \frac{1}{N_A \cdot h \cdot c} \cdot \int_{\lambda min}^{\lambda max} \lambda \cdot I(\lambda) d\lambda. \tag{A.1}$$

Here, N_A stands for the Avogodro's number ($6.022 \cdot 10^{17}$ µmol photons). The h stands for the Planck's constant ($6.63 \cdot 10^{-37}$ J s) and c stand for the velocity of light ($3 \cdot 10^{8}$ m s^{-1}). The integral $\int_{\lambda max}^{\lambda min} \lambda \cdot I(\lambda) d\lambda$ was determined in the photosynthetically active radiation (PAR 400-700 nm) range of the LED light source (CellDEG 400-RX LED). The spectrum in a range of 400-750 nm of the light source (CellDEG 400-RX LED) is depicted in Figure A.5.

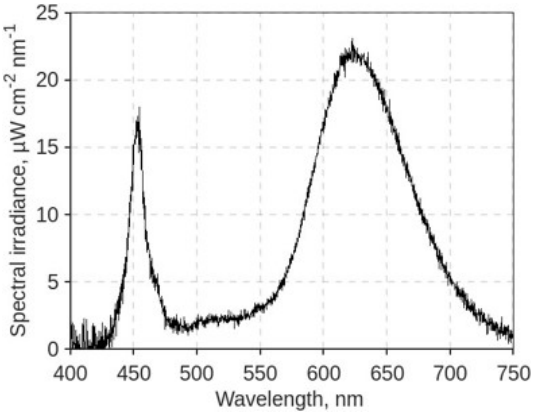

Figure A.5: Spectrum of the LED lamp (CellDEG RX-400 LED) used in the cultivation chamber of the CellDeg Device. The spectrum was measured with a miniature spectrometer Flame-T, Ocean Optics Inc., Florida, USA.

A conversion from energy in quantum units needs to consider that photons decrease in energy with increasing wavelength. Consequently, to achieve the same power, a greater number of photons is required at longer wavelengths compared to shorter wavelengths. In other words, the higher the wavelength, the more photons are necessary to maintain the same power level. To find a universal conversion factor independent of the wavelength, formula A.3 was used [169], which represents the ratio between the total power density $H_T^Q(PAR)$ in quantum units and $H_T^E(PAR)$ in energy units.

$$\frac{H_T^Q(PAR)}{H_T^E(PAR)} = \frac{1}{N_A \cdot h \cdot c} \cdot \frac{\int_{400}^{700} \lambda \cdot I(\lambda) d\lambda}{\int_{400}^{700} \cdot I(\lambda) d\lambda} \tag{A.2}$$

After conversion to the term $H_T^Q(PAR)$, Equation A.3 follows:

$$H_T^Q(PAR) = H_T^E(PAR) \cdot \frac{1}{N_A \cdot h \cdot c} \cdot \frac{\int_{400}^{700} \lambda \cdot H(\lambda) d\lambda}{\int_{400}^{700} \cdot H(\lambda) d\lambda} = H_T^E(PAR) \cdot \frac{1}{119.8 \frac{W \cdot s \cdot nm}{\mu mol}} \cdot \frac{1.561 \cdot 10^6 \frac{W \cdot nm}{m^2}}{2.58 \cdot 10^3 \frac{W}{m^2}} \tag{A.3}$$

It follows as written in Chapter 3.7 an universal conversion term for the LED spectrum used:

$$H_T^Q(PAR) = H_T^E(PAR) \cdot 5.05 \tag{A.4}$$

The values $1.56 \times 10^6 \frac{W \cdot nm}{m^2}$ and $2.58 \times 10^3 \frac{W}{m^2}$ were obtained by integration in the PAR-range.

A.5 The design of the membrane reactor cap

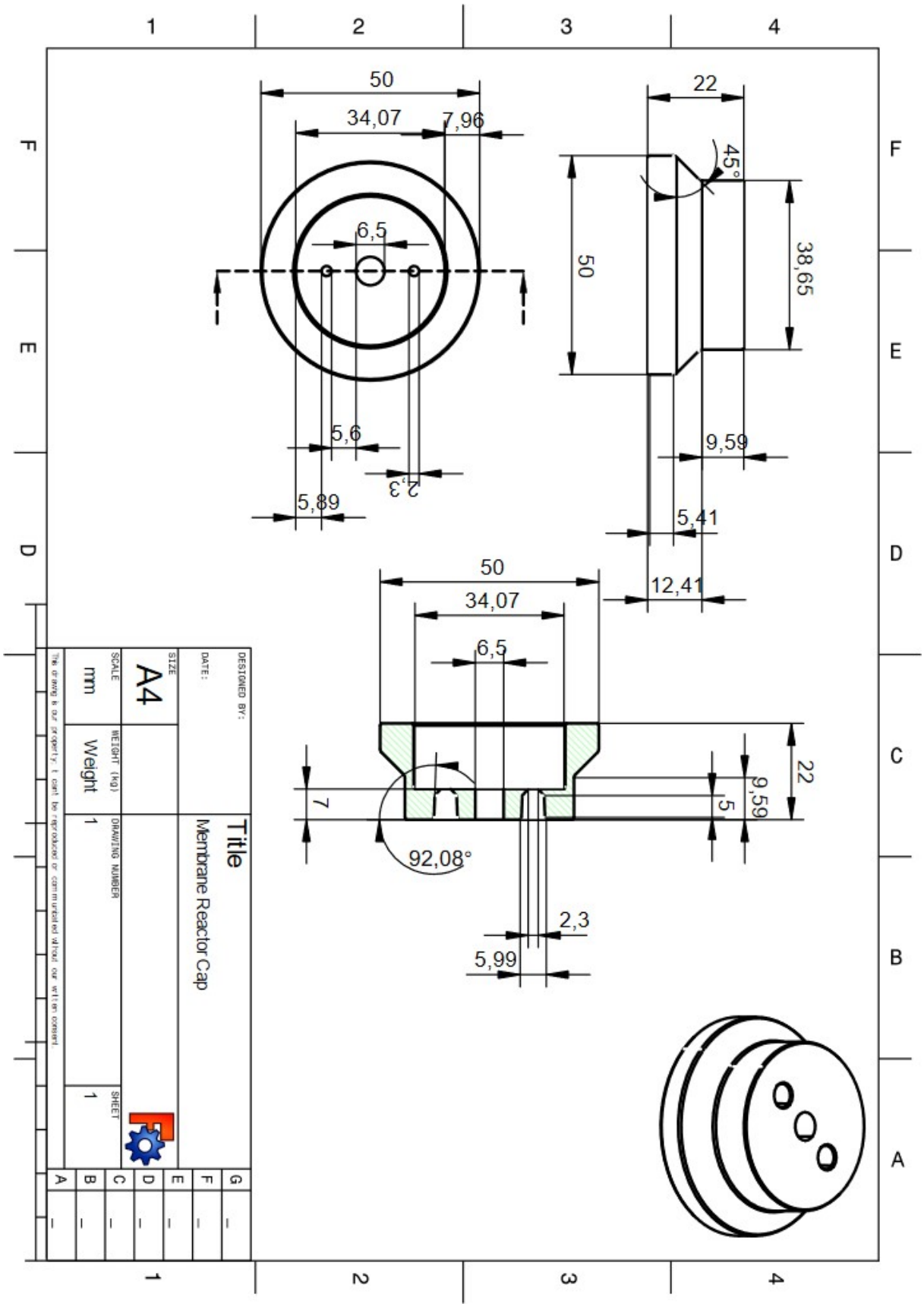

Figure A.6: Technical drawing created with freeCAD (https://www.freecad.org/) of the membrane reactor cap. The values are given in nm with a comma as decimal separator.

A.6 Exploring diverse nitrogen sources in the co-culture

In a co-culture experiment of *P. putida cscRABY* and *S. elongatus cscB*, urea was utilized as the sole nitrogen source to investigate the potential nitrogen cross-feeding from the heterotroph. The heterotrophic partner is capable of urea degradation, but the cyanobacterium lacks essential genes for its metabolization. In the experiment, the cyanobacterium showed limited growth, unable to sustain growth beyond two days. However, it retained its green color even after 300 hours of co-cultivation which indicates a stable and healthy state. In contrast, the axenic cultures, where *P. putida cscRABY* was absent, exhibited a yellowish color, and demonstrated signs of cell precipitation. This observation suggests that the co-culture system provides advantages in terms of stability and viability compared to the axenic cultures when urea is the sole nitrogen source (see Figure A.7 **A**). No accelerating effect in terms of growth was observed when the co-culture was supplied with both urea and nitrate, as shown in Figure A.7 **B**.

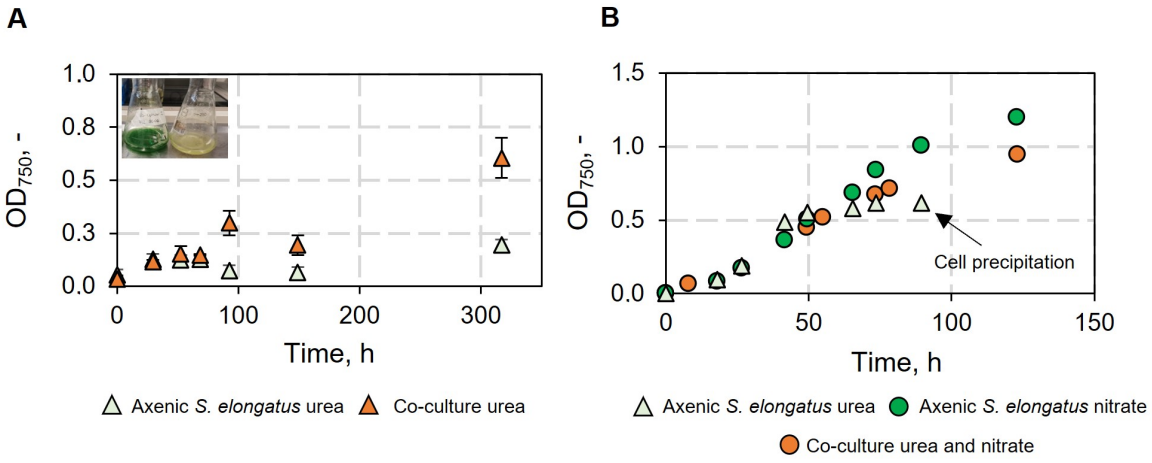

Figure A.7: **(A)** Co-culture of *P. putida cscRABY* and *S. elongatus cscB* and the axenic culture with urea as sole nitrogen source. The co-culture remained green even after 300 h, whereas the axenic cultures turned yellow and showed cell precipitation. Experimental conditions: Shake flask experiment with 20 mL BG11^{+} medium supplemented with 150 mM NaCl and 13.8 mmol urea at 25 °C, 120 rpm, 20 µmol photons s^{-1} m^{-2} in a Multitron Pro from Infors HT orbital shaker. The CscB permease was induced with 0.1 mM IPTG at the beginning of the experiment and the co-culture was inoculated after 24 h with and OD_{600} of 0.1. **(B)** Growth of *S. elongatus cscB* axenically with urea and nitrate and in a co-culture with *P. putida cscRABY* in which both nitrogen sources where added. Cell precipitation an loss of chlorophyll occurred for the axenic culture grown with urea as sole nitrogen source. Experimental conditions: Shake flask experiment with 20 mL BG11^{+} medium supplemented with 150 mM NaCl and 13.8 mmol, or nitrate 27.6 mmol at 25 °C, 120 rpm, 20 µmol photons s^{-1} m^{-2} in a Multitron Pro from Infors HT orbital shaker. The CscB permease was induced with 0.1 mM IPTG to begin of the experiment and the co-culture was immediately started with a inoculation density of 0.15 at 600 nm.

A.7 Mass fraction of PHA monomers

Table A.5: Mass fraction of PHA monomers accumulated in co-culture processes.

Chain length	6	8	10	12/12:1
Massfraction Process with *P. putida cscRABY*, (%)	2.4 ± 0.93	23.1 ± 2.7	62.2 ± 1.9	12.2 ± 0.7
Massfraction Process I with *P. putida cscRABY* Δ*nasT* 1, (%)	2.4 ± 0.35	19.6 ± 2.2	64.3 ± 1.0	13.7 ± 1.5
Massfraction Process II with *P. putida cscRABY* Δ*nasT* 2, (%)	2.4 ± 0.31	19.9 ± 2.0	65.3 ± 5.1	12.4 ± 7.0
Massfraction Process III with *P. putida cscRABY* Δ*nasT* 3, (%)	2.9 ± 0.60	24.1 ± 6.5	60.1 ± 9.1	12.8 ± 9.1

A.8 Cluster formation: When *P. putida cscRABY* dominates the co-culture

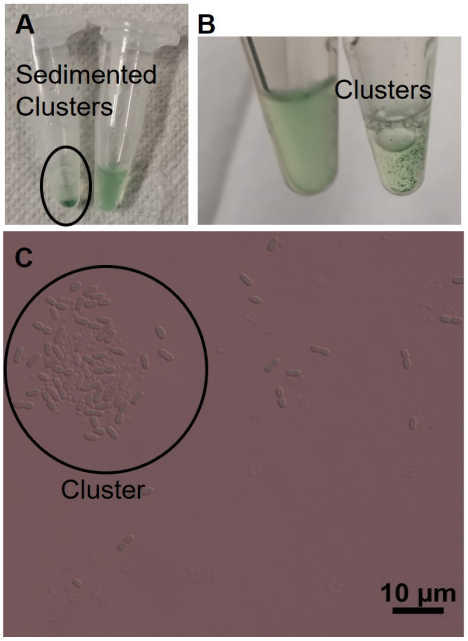

Figure A.8: Sample from a shake flask co-culture experiment with a ratio of 1:10 (*S. elongatus cscB* to *P. putida cscRABY*) were cluster formed and in comparison to a co-culture of $1{:}10^{-2}$ (*S. elongatus cscB* to *P. putida cscRABY*). **(A)** Sedimented clusters of *S. elongatus cscB* and *P. putida cscRABY*. **(B)** Clusters during sedimentation after mixing. **(C)** Cluster formation of the two co-culture partners under the microscope using a 100X magnification objective.

A.9 Co-cultivation with *P. putida cscRABY* Δ*gcd*

Co-cultivation of *S. elongatus cscB* and *P. putida cscRABY* Δ*gcd* was performed at a 1.8 L scale. Figure A.9 **A** illustrates a schematic depiction of the co-culture process. Initially, a biomass production phase was carried out for the phototrophic partner, using a batch nitrate concentration of 50 mg L^{-1}, followed by a subsequent nitrate feed with a rate of 76 mg L^{-1} d^{-1}. The inoculation of the heterotrophic partner was accompanied by the addition of a urea batch with a concentration of 0.36 g L^{-1}. During the heterotrophic biomass production phase, the addition of urea significantly enhanced the growth of *P. putida cscRABY* Δ*gcd*. After metabolizing the urea batch, the growth rate of *P. putida cscRABY* Δ*gcd* slowed down, and PHA accumulation commenced, reaching a maximum of 208 mg L^{-1}. However, it is important to note that the likely maximal PHA titer was not determined as the process was shut down before PHA accumulation could reach a steady-state level (see Figure A.9 **B**). In the end of the process approximately 1 g L^{-1} sucrose were accumulated in the culture supernatant which was secreted with a maximal rate of 0.2 g L^{-1} d^{-1}.

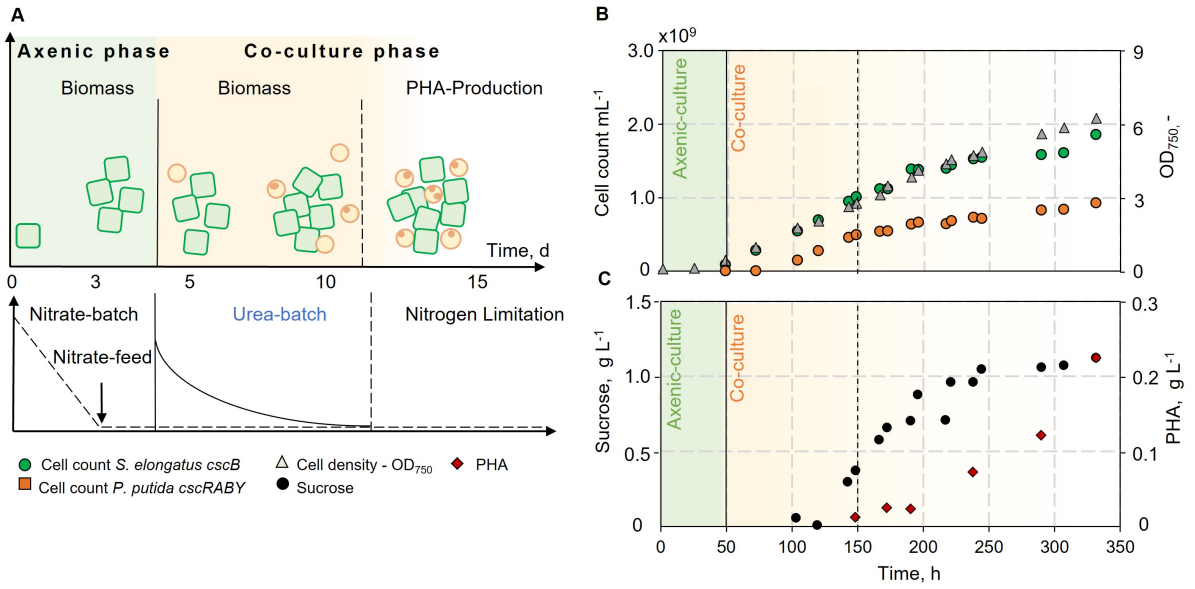

Figure A.9: **(A)** Graphical overview of the co-cultivation process with *P. putida cscRABY* Δ*gcd*. **(B)** Growth of the co-culture partners represented in cell count and OD_{750}. The numbers given are the mean of technical triplicates, and the error bars represent the standard deviation. **(C)** PHA accumulation in the heterotrophic cells and sucrose titer in the reactor. Sucrose and PHA measurements were performed in single or double measurements. Co-cultivation was conducted in a 1.8 L Labfors Lux 5 flat panel photo-bioreactor in $BG11^+$ medium supplemented with 150 mM NaCl and 50 mg mL^{-1} batch $NaNO_3$. After the additional batch phase, a feed $NaNO_3$ with 75.6 mg d^{-1} was started. Secretion of sucrose into the medium was induced one day thereafter with 0.1 mM IPTG. Inoculation with *P. putida cscRABY* Δ*gcd* followed another 30 hours later (solid line).

A.10 The influence of external sucrose

To investigate if sucrose accumulation in the normal range in the co-culture (up to 3 g L^{-1}) influences the growth behavior of *S. elongatus cscB*, experiments were conducted with varying sucrose concentrations. A negative effect on the growth rate was only observed when adding 50 g L^{-1} of sucrose (data not shown), a concentration significantly higher than what is typically achieved in the co-culture.

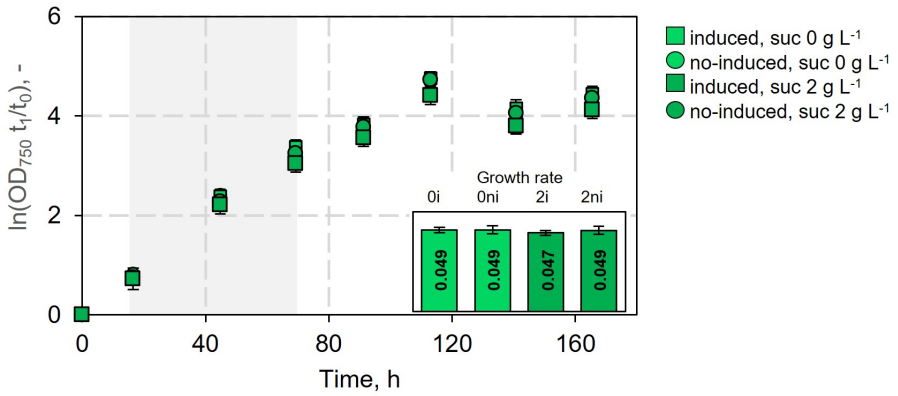

Figure A.10: *S. elongatus cscB* axenic cultures with or without IPTG induction and with 0 or 2 g L^{-1} sucrose were performed in biological duplicates. Cultivation at 30 ℃ at a constant photon flux density of 22 µmol photons m^{-2} s^{-1} in a Multitron Pro from Infors HT orbital shaker. Initial IPTG-induction (0.1 mM IPTG) to induce the sucrose secretion to the medium. Cultivation was performed one week with daily sampling. OD_{750} measurement was performed for the biological duplicates. Logarithmic plot of the OD_{750} values, normalized to the initial OD_{750}. 0i = no sucrose, induced; 0ni = no sucrose, not induced; 2i = 2 g L^{-1} sucrose induced; 2ni = 2 g L^{-1} not induced. Growth was performed in shake flasks in a final volume of 25 mL BG-11^{+} medium supplemented with 150 mM NaCl.

A.11 Cell counts and temperature in CellDeg experiments

As an example, the cell count and temperature profiles of two cultivations in the CellDeg system are shown below. In the presence of an exponentially increasing light profile, the temperature gradually increases from approximately 25 to 35 °C during the process, as indicated by the dotted line in Figure A.13 **A** and **B**. Figure A.13 **C** and **D** illustrate the exponential growth of the heterotrophic partner and the cyanobacterium in co-culture or in the non-induced case.

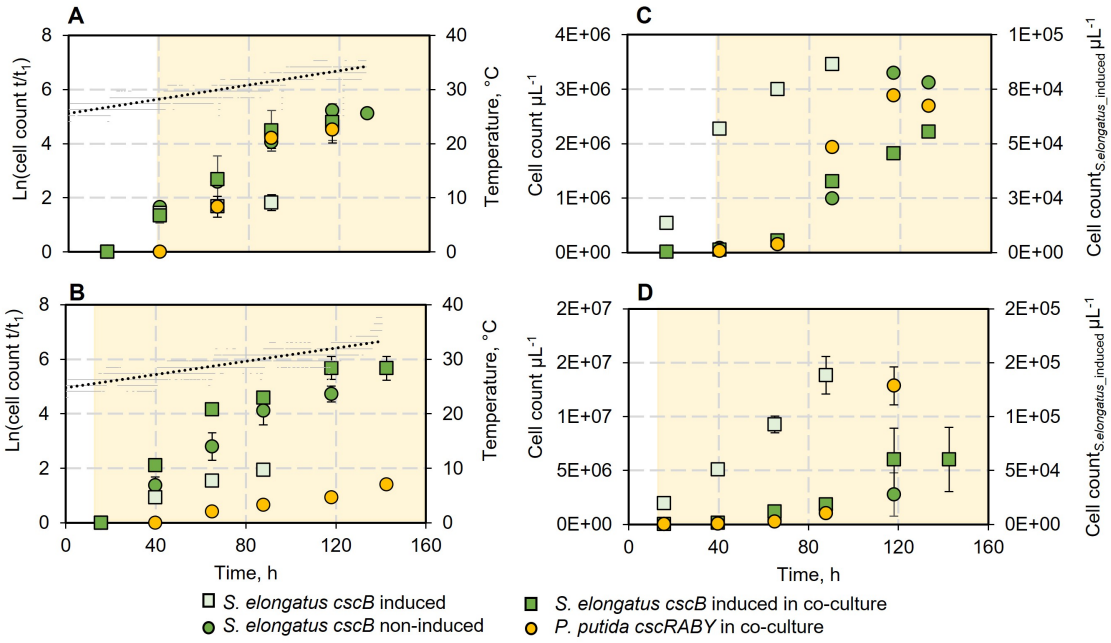

Figure A.11: Logarithmic cell count of *P. putida cscRABY* grown in co-culture and *S. elongatus cscB* in co-culture and axenic culture induced or non-induced and temperature during the process. **(A)** Inoculation at day two and **(B)** inoculation at day one of the co-culture partner. Co-culture phase is indicated through yellow background. Temperature rises linearly during both processes: **(A)** Temperature = 0.066 $\frac{C}{h}$ · Time + 25.58 °C and **(B)** y = 0.061 $\frac{C}{h}$ · Time + 24.76 °C. Absolute cell count of the process with inoculation of the co-culture at day 2 **(C)** and day one **(D)**. Experimental conditions: 2 % CO_2, $BG11^+$ + 150 mM NaCl, volume 95 mL; Exponential light profile = 120 m^{-2} s^{-1} for 24 h then exponential with t_d = 52 h.

A.12 Biomass specific light intensity

To further analyse the different light profiles the biomass specific light intensity can be calculated as follows:

$$\frac{H_T^Q(PAR)}{X}(t) = \frac{\text{Light profile}}{\text{Biomass accumulation}} \tag{A.5}$$

For this, an exponential growth for the cyanobacterium was assumed throughout the entire process (140 h).

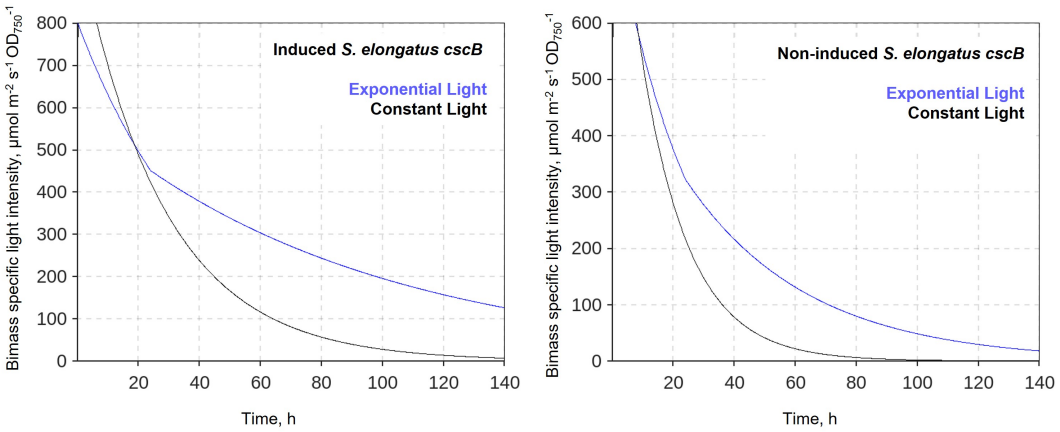

Figure A.12: Left: Constant light 150 µmol m^{-2} s^{-1}. Right: Exponential light starting with constant 120 µmol m^{-2} s^{-1} for 24 h and then exponential course with t_d=52 h.

A.13 Reference Experiment: Example calculation of sucrose feed

In order to obtain a similar growth rate for *P. putida cscRABY* in axenic culture and in the co-culture the external sucrose-feed was adjusted based on beforehand cultivated co-cultures. With the following correlation, a conversion from optical density to cell dry weight is possible (compare with section 3.7).

$$C_X = 2.2 \cdot 10^9 \cdot OD_{600} \tag{A.6}$$

C_X in $[\frac{\text{cells}}{\text{mL}}]$ stands for the biomass of the heterotrophic partner in cells per mL and the expression C_{Xcdw} in $[\frac{\text{g}}{\text{L}}]$ stands for the biomass of the heterotrophic partner.

$$C_{Xcdw}[\frac{g}{L}] = \frac{C_X}{2.2 \cdot 10^9} \cdot 0.256 \tag{A.7}$$

With the biomass yield coefficient $Y_{Xsuc} = 0.23\frac{g}{g}$, an estimation of the produced sucrose of the cyanobacterium in the co-culture is possible or the non-specific sucrose production rate $\frac{dC_{suc}}{dt}$ $[\frac{\text{g}}{\text{L·d}}]$ can be calculated.

$$\frac{dC_{suc}}{dt} = \frac{\frac{d_{Xcdw}}{dt}}{Y_{Xsuc}} \tag{A.8}$$

The term $\frac{dC_{Xcdw}}{dt}$ can be substituted with $\mu \cdot c_{Xcdw}$, which leads to formula below. Here, μ $[h^{-1}]$ stands for the maximal growth rate in the exponential phase.

$$\frac{dC_{suc}}{dt} = \frac{\frac{C_X}{2.2 \cdot 10^9} \cdot 0.256 \cdot \mu}{Y_{Xsuc}} \tag{A.9}$$

The calculation is shown from one example process. It should be noted that the *P. putida cscRABY* cell count had a high variability and, therefore, adjustments were carried out during different processes. Within 24 h a non-specific rate of $\frac{C_X}{dt} = 0.192 \cdot 10^9$ $[\frac{\text{cells}}{\text{mL·d}}]$ was determined through linear regression (see Table A.6). This leads to a constant feed rate of:

$$\frac{dC_{suc}}{dt} = \frac{\frac{0.192 \cdot 10^9}{2.2 \cdot 10^9} \cdot 0.256}{0.23} = 0.096 \simeq 0.1 \tag{A.10}$$

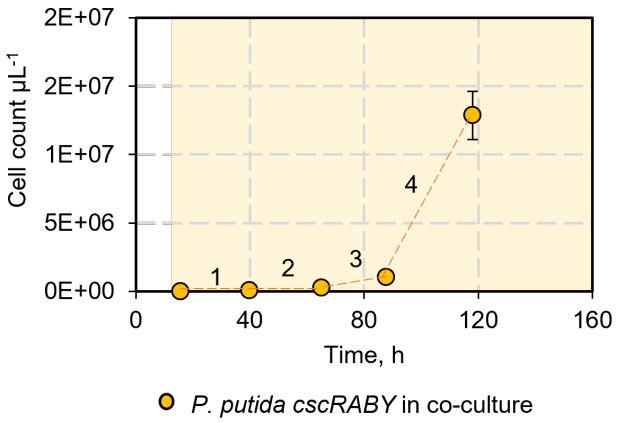

Figure A.13: Cell count of *P. putida cscRABY* in co-cultivation with *S. elongatus cscB*. 1-4 linear regression to obtain the estimated non-specific growth rate of $\frac{C_X}{dt}$ (see Table A.6).

Table A.6: Example estimation of sucrose feed.

	1	**2**	**3**	**4**
Slope $[\frac{cells}{\mu L \cdot h}]$	$2.7 \cdot 10^3$	$8.01 \cdot 10^3$	$3.3 \cdot 10^4$	$4.7 \cdot 10^5$
Sucrose-Feed $[\frac{g}{L \cdot d}]$	0.03	0.1	0.4	0.6

A.14 OD_{750} of *S. elongatus cscB* - Reference Experiments

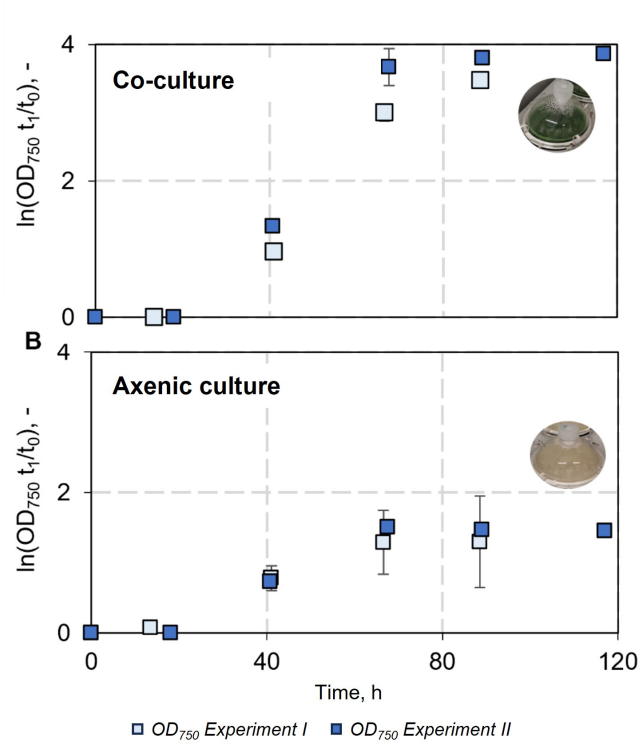

Figure A.14: Light blue represents reference Experiment I, and dark blue represents reference Experiment II. Both are shown for the co-culture (depicted as circles) and the axenically grown *S. elongatus cscB* cells. There was a noticeable photobleaching effect, or loss of chlorophyll observed towards the end of the process. The OD values are normalized to the initial inoculation density of 0.1, and standard deviations are calculated from biological triplicates.

A.15 Cell size and chlorophyll fluorescence - Reference Experiment II

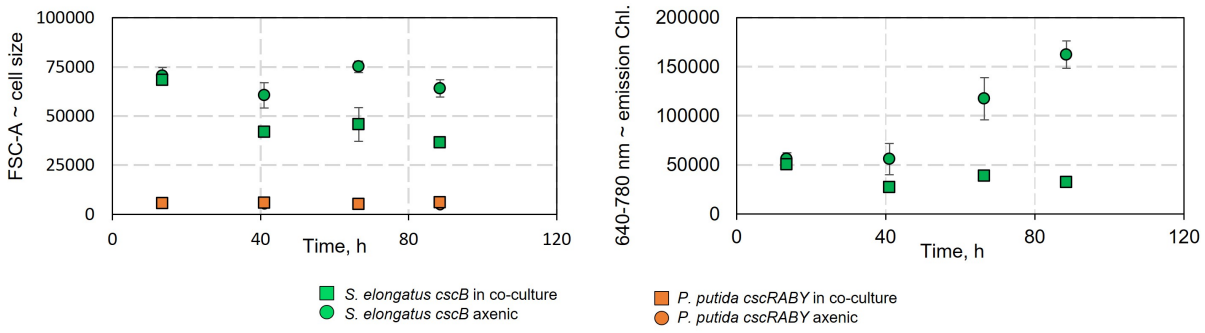

Figure A.15: Median of cell populations (heterotrophic and phototrophic partner) and median chlorophyll (Chl.) emission at the wavelength band 640-780 nm.

A.16 Temperature and real light - Reference Experiments

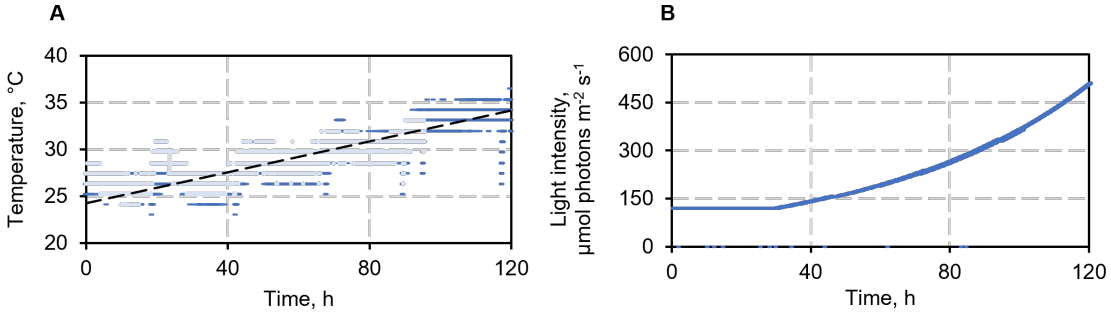

Figure A.16: Light and temperature of reference Experiment I and II. **(A)** Temperature profile of reference Experiment I (light blue) and experiment II (dark blue). **(B)** Light profile of experiment I and II (no difference).

A.17 Medium components - Reference Experiment II

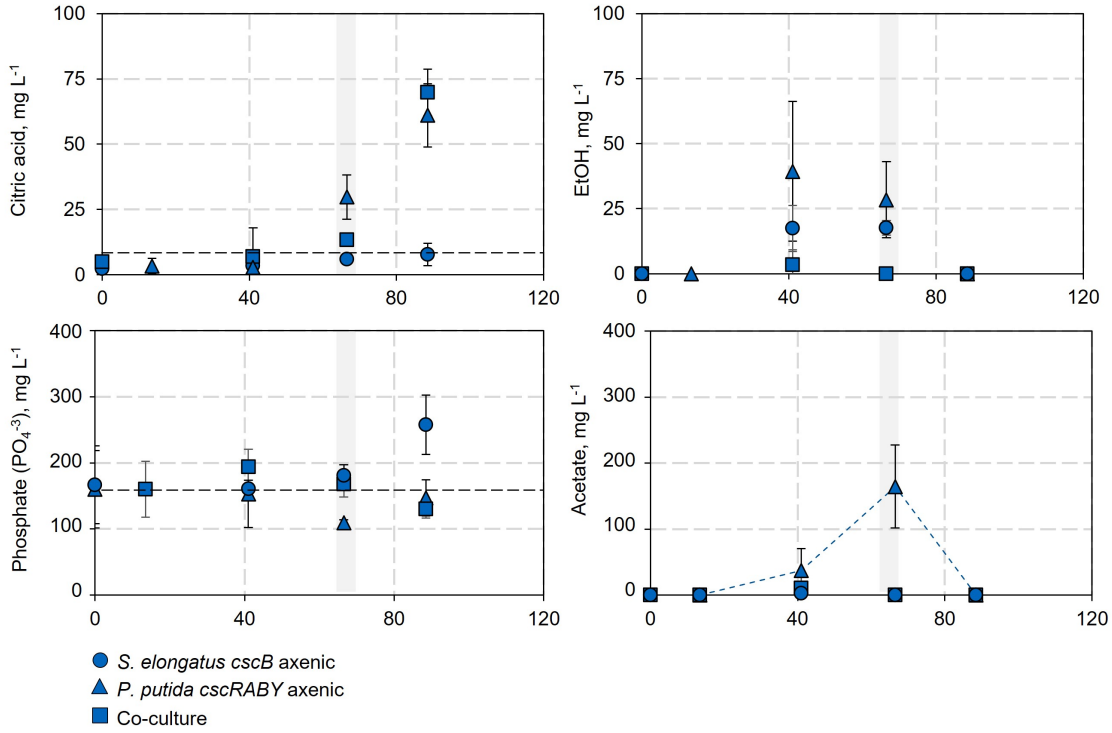

Figure A.17: Medium components citric acid and phosphat as well as potential overflow metabolits acetate and EtOH. Dashed line represents concentration in the medium $BG11^{+}$ and gray area represents sampling points for OMICs. Experimental condition can be found in Section 3.7 and details for analytics can be found in Section 3.6.3

A.18 Volcano plots - Metabolomic data

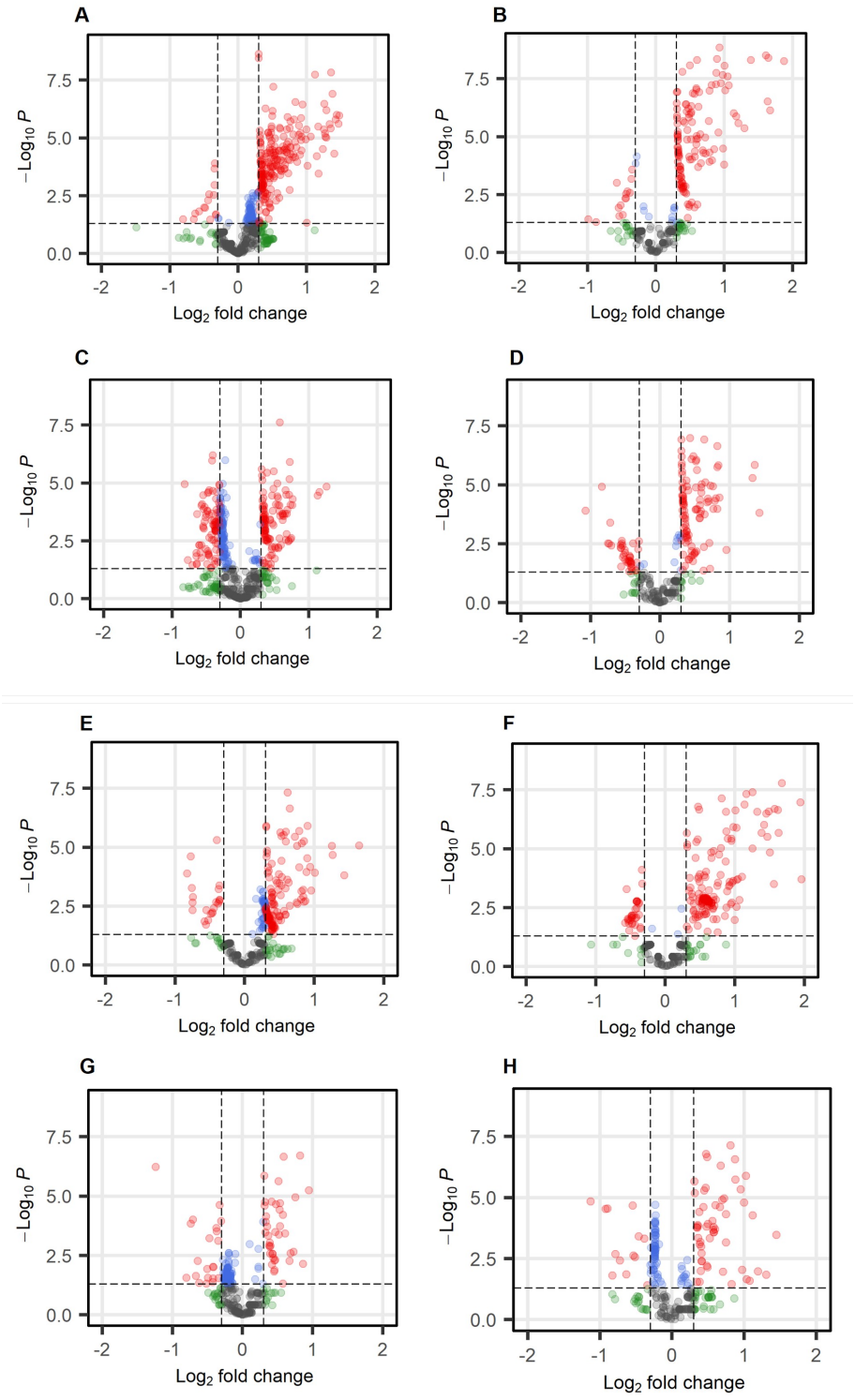

Figure A.18: Volcano plots of the metabolomic data. Reverse Phase (RP) and positive ionization mode of MS: **(A)** Comparing the heterotroph in the co-culture with axenic *P. putida cscRABY*. **(C)** Comparing the cyanobacterium in the co-culture with the axenic *S. elongatus cscB*. RP and negative ionization mode of MS: **(B)** Comparing the cyanobacterium in the co-culture with the axenic *S. elongatus cscB*. **(D)** Comparing the heterotroph in the co-culture with axenic *P. putida cscRABY*. Hydrophilic Interaction (HILIC) and positive ionization mode of MS: **(E)** Comparing the heterotroph in the co-culture with axenic *P. putida cscRABY*. **(F)** Comparing the cyanobacterium in the co-culture with the axenic *S. elongatus cscB*. HILIC and positive ionization mode of MS: **(G)** Comparing the cyanobacterium in the co-culture with the axenic *S. elongatus cscB*. **(H)** Comparing the heterotroph in the co-culture with axenic *P. putida cscRABY*.

A.19 Heat Maps: Metabolites identified through reference measurements

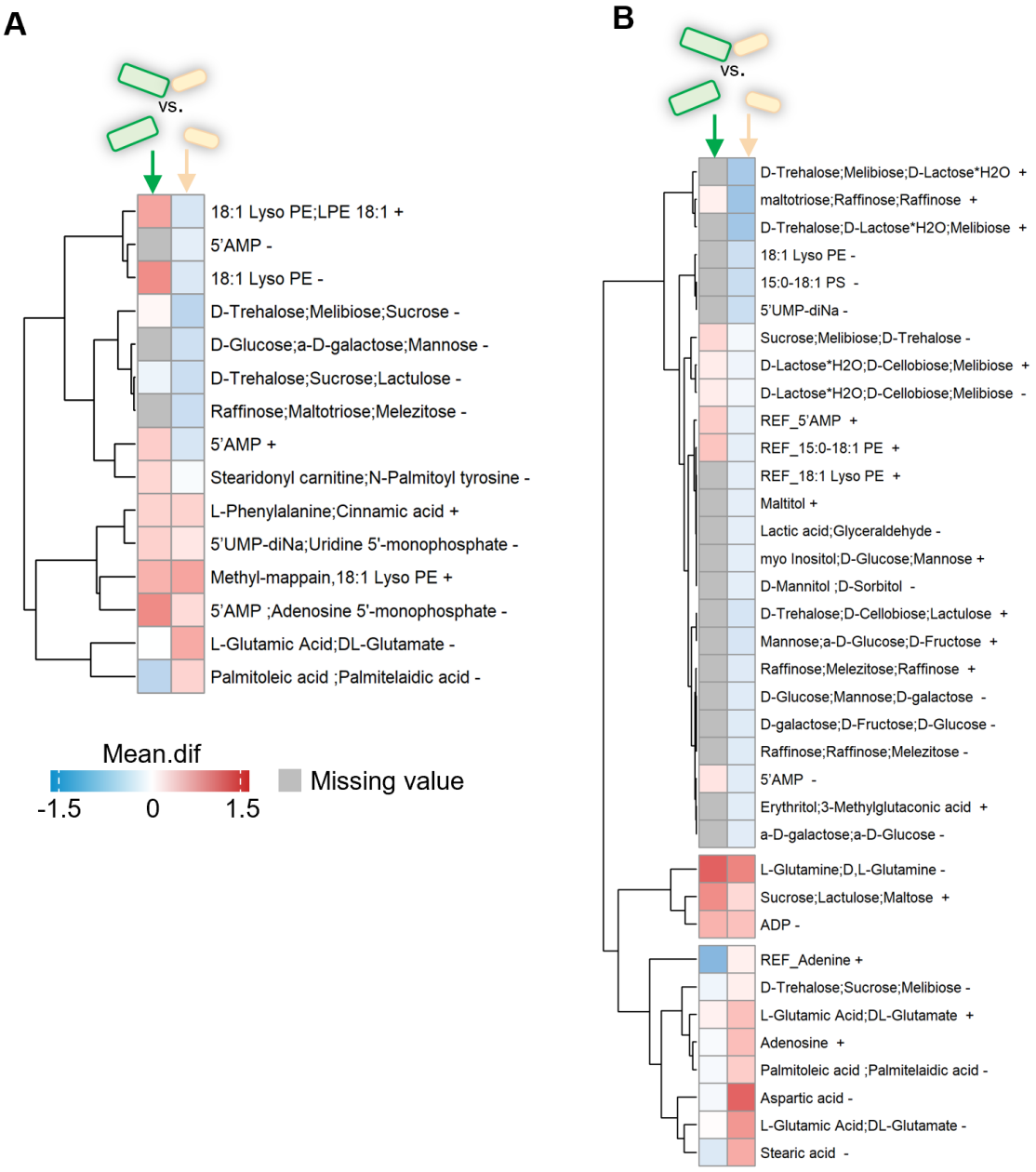

Figure A.19: Metabolites identified through reference measurements different abundant in the co-culture compared to *S. elongatus cscB* or *P. putida cscRABY*. **(A)** Shows comparison for reverse phase (RP) and **(B)** shows it for Hydrophilic interaction (HILIC) chromatography; the plus (+) or minus (-) indicate the ionization mode of the mass spectrometer (MS).

A.20 DEGs associated with ribosomes and tRNA - *S. elongatus cscB*

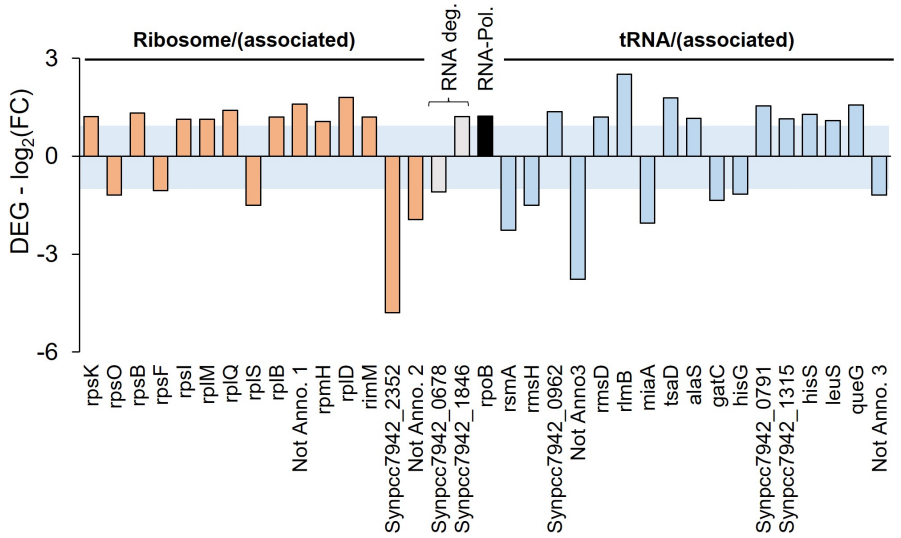

Figure A.20: DEGs grouped into ribosome associated and tRNA associated of *S. elongatus cscB* grown in co-culture vs. grown axenically. The blue area marks the threshold of p-value = 0.05. Not Anno. 1 = WP_199290541.1, not Anno. 2 = WP_011377886.1 and not Anno. 3 = WP_242021706.1.

A.21 DEGs of the core metabolism and photosynthesis - *S. elongatus cscB*

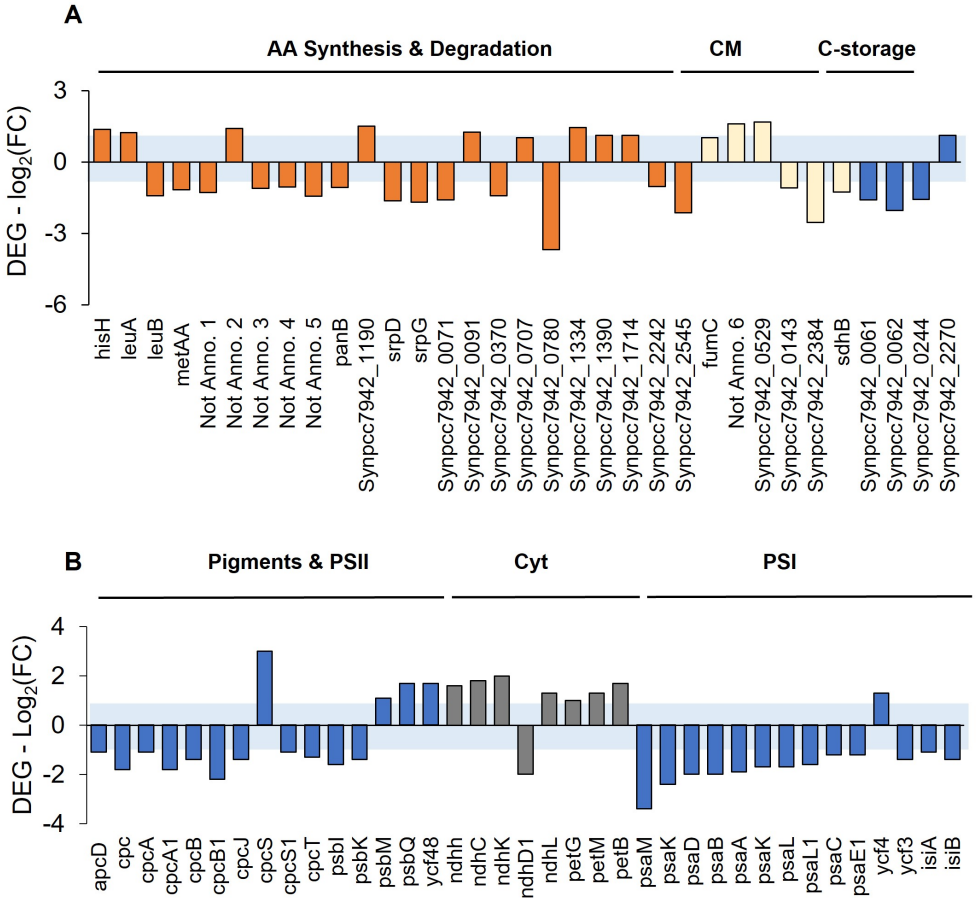

Figure A.21: **(A)** DEGs grouped into amino acid (AA) synthesis and degradation, central metabolism (CM; single DEGs belonging to Calvin cycle or the pentose phosphate pathway) and carbon (C)-storage of *S. elongatus cscB* grown in co-culture vs. grown axenically. **(B)** DEGs belonging to photosynthesis in *S. elongatus cscB* grown in co-culture vs. grown axenically. The blue area marks the threshold of p-value = 0.05. Not Anno. 1 = WP_039756002.1, not Anno. 2 = WP_199290702.1, not Anno. 3 = WP_173282540.1, not Anno. 4 = WP_039755494.1, not Anno. 5 = WP_199290793.1 and not Anno. 6 = W_199290796.1.

A.22 Cultivation with different iron concentrations

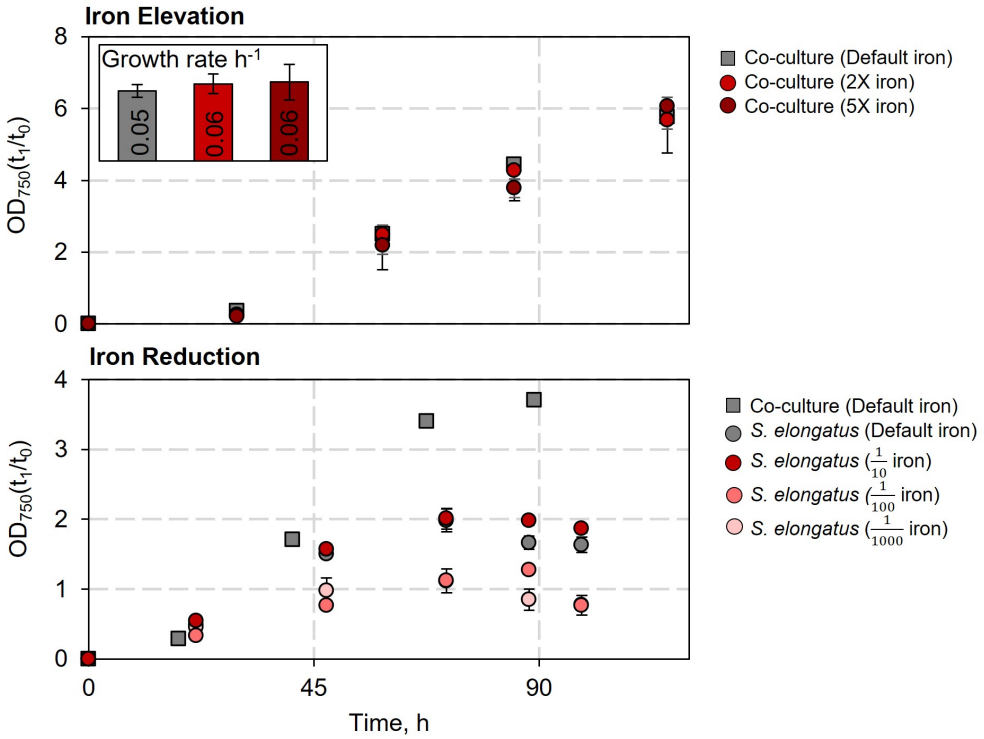

Figure A.22: Cultivations of axenic *S. elongatus cscB* and the co-culture were conducted with either elevated or reduced iron concentrations. Experimental conditions: 25–30 °C, 2 % CO_2, 95 mL $BG11^+$ supplemented 150 mM NaCl, exponential light profile: 24 h constant at 120 µmol m^2 s^1 and then exponential rising with a doubling time of t_d = 52 h.

A.23 DEGs associated with the membrane - *P. puitda cscRABY*

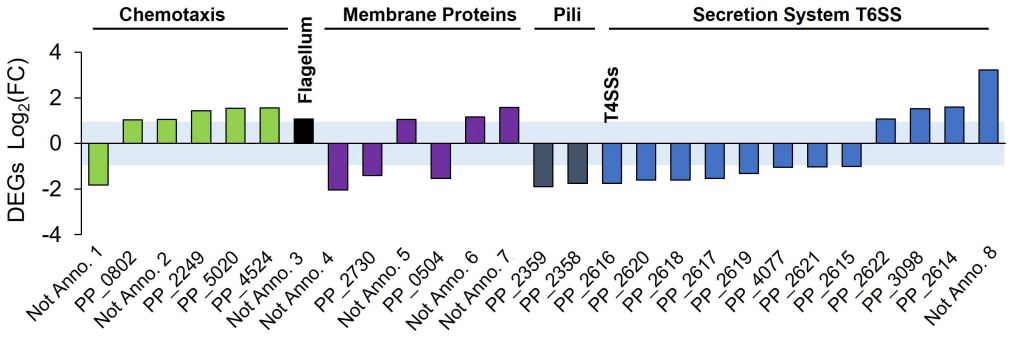

Figure A.23: DEGs which can be connected to the membrane and membrane structures in *P. putida cscRABY* grown in co-culture compared to the mono-culture. The DEGs were categorized into groups including chemotaxis, membrane proteins, pili, and the secretion system T6SS. The blue area marks the threshold of p-value = 0.05. Not Anno. 1 = WP_049587741.1, Not Anno. 2, = WP_257766427.1 , Not Anno. 3 = WP_003253671.1, Not Anno. 4 = WP_003253030.1, Not Anno. 5 = WP_003249613.1, Not Anno. 6 = WP_010951793.1, Not Anno. 7 = WP_049588514.1 and Not Anno. 8 = WP_079732571.1.